

Analysis of Conformational Behaviour Exhibited by Dihydrofolate Reductase During Catalysis

*Submitted in fulfilment of the requirement for the degree of doctor of
philosophy (PhD)*



*By
Robert Lloyd Hughes*

*School of Chemistry, Cardiff University
2018*

Declaration

This work has not been submitted in substance for any other degree or award at this or any other university or place of learning, nor is being submitted concurrently in candidature for any degree or other award.

Signed.....(candidate) Date.....

Statement 1

This thesis is being submitted in partial fulfilment of the requirements for the degree of Doctor of Philosophy (PhD).

Signed.....(candidate) Date.....

Statement 2

This thesis is the result of my own independent work/investigation, except where otherwise stated, and the thesis has not been edited by a third part beyond what is permitted by Cardiff university's policy on the use of third party Editors by Research Degree Students. Other sources are acknowledged by explicit references. The views expressed are my own.

Signed.....(candidate) Date.....

Statement 3

I hereby give consent for my thesis, if accepted, to be available online in the university's open access repository and for inter-library loan, and for the title and summary to be made available to outside organisations.

Signed.....(candidate) Date.....

Statement 4: Previously approved bar on access

I hereby give consent for my thesis, if accepted, to be available online in the University's Open Access repository and for inter-library loans **after expiry of a bar on access previously approved by the Academic Standards & Quality Committee.**

Signed.....(candidate) Date.....

Acknowledgements

First and foremost, I would like to thank Professor Rudolf Allemann for the opportunity to study for a PhD in his research group and the help and guidance he has given me over the last four years. Secondly, I would like to thank Dr. Joel Loveridge and Dr. Louis Luk for their guidance, training, suggestions and proof reading of my work. Thank you also to Dr. Alan Scott and Dr. Enas Behiry for your help with respect to kinetics and general advice. Thank you to Dr. Luke Johnson for your guidance in helping me in understanding the intricacies of protein NMR. I would also like to thank Dr. Robert Mart and Dr. Veronica Gonzalez for their help in the laboratory during my studies. Thanks to all members of the Allemann group, past and present, who have helped make my own experience an enjoyable one. I would also like to thank Thomas Williams and Dr. Robert Jenkins for their help with mass spectrometry and NMR spectroscopy.

I would also like to thank my family for their help and encouragement over the years. Last, but not least, I would like to thank my wife, Sarah.

Abstract

Protein motions, which occur on a multitude of timescales, are known to be central to enzyme catalysis. However, between enzyme variants there exists diversity in the influence such motions have. Understanding why apparently similar enzymes that have similar primary sequences, tertiary structures and rate constants utilize different motions is therefore of great interest. Dihydrofolate reductase (DHFR) has been used extensively as a model to study such relationships between protein motions and catalysis. Firstly, we have probed conformational behaviour exhibited by different DHFR variants by a simplified, cost-effective NMR based approach utilizing selective ^{13}C labelling of methionine and tryptophan sidechains. Before this work, DHFR from *Escherichia coli* (EcDHFR) was the only known DHFR to adopt an occluded conformation following the chemical step. ^{13}C labelling of methionine and tryptophan sidechains is shown to be sufficient to probe such conformational behaviour in EcDHFR, with clear chemical shift perturbations observed between the two conformational states. No such chemical shift perturbations are observed in spectra relating to DHFR from *Thermotoga maritima* (TmDHFR) or DHFR from *Moritella profunda* (MpDHFR), where an occluded conformation is not adopted following the chemical step. Through amino acid sequence analysis DHFR from *Salmonella enterica* (SeDHFR) was identified as conserving a key hydrogen bonding interaction known to stabilise an occluded conformation in EcDHFR. By analysing chemical shift perturbations of ^{13}C labelled methionine and tryptophan sidechains, it has been confirmed SeDHFR exhibits similar conformational behaviour to EcDHFR. The second part of this work aimed to further explore the contribution of femtosecond dynamics acting upon the chemical step of catalysis in SeDHFR. The role of such motions coupling to the chemical step is hugely controversial. Our work, with SeDHFR, aligns with previous reports that the influence of dynamic coupling to the chemical step is minimised in catalysis by DHFR. To further explore the role of dynamic coupling to the chemical step in other enzyme families, L-lactate dehydrogenase-1 from *Staphylococcus aureus* (SaLDH) was studied. Initial findings align with work done with DHFR variants and reports the dynamic coupling to the chemical step is minimised at close to physiological conditions.

List of Abbreviations

<i>A</i>	Arrhenius pre-exponential factor
ADP	Adenosine diphosphate
ATCC	American type culture collection
ATP	Adenosine triphosphate
BaDHFR	Dihydrofolate reductase from <i>Bacillus anthracis</i>
β ME	2-mercaptoethanol
BSA	Bovine serum albumin
BsDHFR	Dihydrofolate reductase from <i>Geobacillus stearothermophilus</i>
BsLDH	LDH from <i>Bacillus stearothermophilus</i>
CD	Circular dichroism
CHAPS	3-[(3-cholamidopropyl)dimethylammonio]-1-propanesulfonate
CPMG	Carr-Purcell-Meiboom-Gill NMR relaxation
CSP	Chemical shift perturbation
DAD	Donor-acceptor distance
DHF	Dihydrofolate
DHFR	Dihydrofolate reductase
DNA	Deoxyribonucleic acid
dTMP	Deoxythymidine monophosphate
dUMP	Deoxyuridine monophosphate
E	Energy
[E]	Enzyme
E_a	Activation energy
[EP]	Enzyme-Product complex
EcDHFR	Dihydrofolate reductase from <i>Escherichia coli</i>
ECT	Electron transport chain
EDTA	Ethylenediaminetetraacetic acid
[ES]	Enzyme-substrate complex
ESI-MS	Electrospray ionising mass spectroscopy
FPLC	Fast protein liquid chromatography
FRET	Förster resonance energy transfer
fs	Femtosecond

G	Probability of barrier crossing
GS	Ground state
h	Plancks constant = 6.626×10^{-34} J s
HsDHFR	Dihydrofolate reductase from <i>Homo sapiens</i>
HsLDH	LDH from <i>Homo Sapiens</i>
HSQC	Heteronuclear single quantum coherence spectroscopy
IPTG	Isopropyl β -D-1-thiogalactopyranoside
κ	Transmission coefficient
k	Rate constant
k_B	Boltzmann constant = $1.38064852 \times 10^{-23}$ J K ⁻¹
k_{cat}	Steady state rate constant
k_f	Force constant
KIE	Kinetic isotope effect
K_m	Michaelis constant
k_{obs}	Observed rate constant
LB	Luria Bertani (media)
LDH	Lactate dehydrogenase
LcDHFR	Dihydrofolate reductase from <i>Lactobacillus casei</i>
M9	Minimal media
MD	Molecular dynamics
MES	2-(<i>N</i> -morpholino)ethanesulfonic acid
MpDHFR	Dihydrofolate reductase from <i>Moritella profunda</i>
MmDHFR	Dihydrofolate reductase from <i>Mus musculus</i>
MRE	Mean residue ellipticity
ms	Millisecond
MtDHFR	Dihydrofolate reductase from <i>Mycobacterium tuberculosis</i>
MTEN	Mes tris ethanolamine sodium chloride
MWCO	Molecular weight cut-off
m_x	Atomic mass
MyDHFR	Dihydrofolate reductase from <i>Moritella yayanosii</i>
NAD ⁺	Oxidised nicotinamide adenine dinucleotide
NADD	4R ² H Reduced nicotinamide adenine dinucleotide
NADH	Reduced nicotinamide adenine dinucleotide

NADP ⁺	Oxidised nicotinamide adenine dinucleotide phosphate
NADPD	4R ² H Reduced nicotinamide adenine dinucleotide phosphate
NADPH	Reduced nicotinamide adenine dinucleotide phosphate
NMR	Nuclear magnetic resonance
NOESY	Nuclear Overhauser effect spectroscopy
ns	Nanosecond
[P]	Product
PCR	Polymerase chain reaction
PNP	Purine nucleoside phosphorylase
ps	Picosecond
Q _t	Bells tunnelling correction
R	Gas constant = 8.314 J mol ⁻¹ K ⁻¹
s	Second
[S]	Substrate
SaLDH	LDH from <i>Staphylococcus aureus</i>
SeDHFR	Dihydrofolate reductase from <i>Salmonella enterica</i>
Γ	Correcting factor
T	Temperature
TAE	Tris-acetate-EDTA
TEMED	Tetramethylethylenediamine
TCEP	(Tris(2-Carboxyethyl)phosphine
TEV	Tobacco etch virus
THF	Tetrahydrofolate
TmDHFR	Dihydrofolate reductase from <i>Thermotoga maritima</i>
TOCSY	Total correlation spectroscopy
TRIS	Tris(hydroxymethyl)aminomethane
TROSY	Transverse relaxation optimized spectroscopy
TS	Transition state
TST	Transition state theory
μ	Reduced mass
VTST	Variational transition state theory
V _o	Velocity of the reaction
V _{max}	Maximal velocity for the reaction

W	Energy of a particle
WT	Wild type
ZPE	Zero point energy
γ	Dynamic recrossing coefficient
ΔG^\ddagger	Gibbs free energy of activation
ΔH^\ddagger	Gibbs free enthalpy of activation
ΔS^\ddagger	Gibbs free entropy of activation
μs	Microsecond

Amino Acid	1 letter code	3 letter code
Alanine	A	Ala
Cysteine	C	Cys
Aspartic acid	D	Asp
Glutamic acid	E	Glu
Phenylalanine	F	Phe
Glycine	G	Gly
Histidine	H	His
Isoleucine	I	Ile
Lysine	K	Lys
Leucine	L	Leu
Methionine	M	Met
Asparagine	N	Asn
Proline	P	Pro
Glutamine	Q	Gln
Arginine	R	Arg
Serine	S	Ser
Threonine	T	Thr
Valine	V	Val
Tryptophan	W	Trp
Tyrosine	Y	Tyr

Table of contents

Declaration	i
Acknowledgement	iii
Abstract	iv
List of Abbreviations	v
Table of Contents	ix
List of figures	xiii
List of tables	xxii

1 Introduction

1.1 Enzymes as catalysts	2
1.2 Steady state kinetics and Michaelis-Menten	4
1.3 Transition state theory and KIE	6
1.4 Tunnelling in enzymatic reactions	10
1.5 Pre-steady state kinetics	15
<i>1.5.1 Study of fast dynamics by stopped-flow</i>	16
1.6 Dihydrofolate reductase (DHFR)	17
1.7 The physical structure of DHFR with a focus on EcDHFR	19
1.8 The chemical step in EcDHFR	20
1.9 The catalytic cycle of EcDHFR	22
1.10 Motions involved in enzyme catalysis	23
1.11 Conformational behaviour and catalysis in DHFR	24
1.12 Role of fast dynamics in catalysis	29
1.13 Enzyme KIE	32

2 Materials & methods

2.1 Materials	36
2.2 Media and buffers	36
2.2.1 Lysogeny Broth (LB)	36
2.2.2 M9 minimal media	36
<i>2.2.2.1 Preparation of 1M MgSO₄ solution</i>	36
<i>2.2.2.2 Preparation of 1M CaCl₂ solution</i>	36
<i>2.2.2.3 Preparation of (100x) trace elements solution</i>	37

2.2.3 Use of ampicillin (Antibiotic)	37
2.2.4 Preparation of Sterile solutions	37
2.2.5 Buffers used	38
2.2.5.1 <i>P1 re-suspension buffer</i>	39
2.2.5.2 <i>P2 lysis buffer</i>	39
2.2.5.3 <i>N3 neutralisation buffer</i>	39
2.2.5.4 <i>PE wash buffer</i>	39
2.3 Methods	39
2.3.1 <i>E.coli</i> strains used	39
2.3.1.1 <i>Preparation of calcium competent cells</i>	39
2.3.1.2 <i>Expression strains</i>	39
2.3.1.3 <i>Cloning strains</i>	39
2.3.2 Transformation protocol for chemically competent cells	40
2.3.3 Plasmid purification	41
2.3.4 PCR protocol	41
2.3.4.1 <i>Primer design</i>	42
2.3.5 DNA sequencing	42
2.3.6 Protein production	42
2.3.7 Protein purification	42
2.3.7.1 <i>Purification via Ni-NTA agarose affinity column</i>	43
2.3.7.2 <i>Purification via Q-sepharose anion exchange</i>	43
2.3.7.3 <i>Purification via BSD75 size exclusion</i>	44
2.3.8 Enzyme concentration	44
2.3.8.1 <i>Concentration from Bradford assay</i>	44
2.3.8.2 <i>Concentration from UV</i>	45
2.3.9 Preparation of 12% SDS-PAGE gel	45
2.3.10 1% agarose gel	46
2.3.11 Synthesis of dihydrofolate	46
2.3.12 Synthesis of NADPD	46
2.3.13 Synthesis of NADD	46
2.3.14 Synthesis of NADPD and NADD	46
2.3.15 Kinetic assays	47
2.3.15.1 <i>Pre-steady state kinetics</i>	47

2.3.15.2 Kinetics involving heavy enzymes	47
2.3.15.3 Steady state Kinetics	47
2.3.15.4 Measurements involving pH dependency	48
2.3.15.5 Measuring K_M (Michaelis constant)	48
2.3.15.6 Calculation of activation energies (E_a) and Arrhenius pre-exponential factors (A)	48
2.3.16 Sidechain NMR experiments	48
2.3.16.1 Preparation of ligand stocks	49
2.3.16.2 Calculation of weighted chemical shifts	49
2.3.17 Circular Dichroism spectroscopy	50
2.3.17.1 Calculation of melting temperature (T_m)	50
2.3.18 Calculation of errors and propagation of errors	50
3 Rapid analysis of conformational behaviour in DHFR variants	
3.1 Variations in conformational behaviour in DHFRs	53
3.2 NMR assignment of TmDHFR	54
3.3 Introduction to chemical shift mapping	64
3.4 Sidechain labelling to probe conformational behaviour	65
3.5 Sidechain NMR experiments	70
3.6 Summary and conclusions	89
4 Hydride transfer and catalysis by <i>salmonella enterica</i> DHFR	
4.1 Introduction	92
4.2 Expression and purification of ^{13}C & ^{15}N SeDHFR	93
4.3 Circular dichroism analysis and thermal unfolding of SeDHFR	96
4.4 Steady state kinetics of SeDHFR	98
4.5 Effect of temperature on steady state kinetics of SeDHFR	99
4.6 Effect of pH on steady state kinetics of SeDHFR	102
4.7 Product inhibition in SeDHFR	104
4.8 Hydride transfer in SeDHFR	105
4.9 Enzyme KIE and dynamics in SeDHFR	114
4.10 Summary and conclusions	121
5 Catalysis by <i>Staphylococcus aureus</i> Lactate Dehydrogenase	
5.1 Introduction	124

5.2 Lactate dehydrogenase biochemistry	124
5.3 Lactate dehydrogenase physical chemistry	125
5.4 Lactate dehydrogenase from <i>Staphylococcus aureus</i>	128
5.5 Expression and purification of SaLDH	130
5.6 Pre-steady state measurements	131
5.7 pH dependency of steady state kinetics in SaLDH	132
5.8 Examination of hydride transfer through steady state kinetics	135
5.9 pH dependence of the steady state enzyme KIE	138
5.10 Temperature dependence of the steady state heavy enzyme KIE	141
5.11 Promiscuity in catalysis by SaLDH	144
5.12 Summary and conclusions	146
6 Summary and general conclusions	149
7 References	155

List of Figures

Figure 1.1	Initially the rate of reaction is first order and linearly dependent on substrate concentration. As the enzyme becomes saturated it becomes independent of substrate concentration.	5
Figure 1.2	Graphical representation of how enzymes lower the ΔG^\ddagger of the reaction, (red) with enzyme, (blue) without enzyme. ES, ES^\ddagger , and EP represent the enzyme-substrate complex, the transition state complex and the enzyme-product complex respectfully.	6
Figure 1.3	Difference in Z.P.E. in a reaction involving breaking of a carbon-hydrogen bond compared to a carbon-deuterium bond.	9
Figure 1.4	Graphical representation of Bells correction for tunnelling, note how quantum tunnelling has a larger effect on the lighter molecule.	11
Figure 1.5	Graphical representation of an Arrhenius plot for a H transfer reaction with Bells tunnelling correction, adapted from reference.	12
Figure 1.6	Graphical representation of the Marcus-like model. In this model there are two orthogonal co-ordinates. The gating term describes fluctuations in the donor-acceptor distance (DAD) and the Marcus term has the energy wells for both the reactant and product as well as the energy of the transition state.	14
Figure 1.7	Curve showing transient phase of enzymatic reaction (red) as well as when the system has reached steady state conditions (blue), continuation of the steady state slope to the y axis (hashed line) gives an approximate concentration of enzyme in the experiment as at this point the system each single enzyme has completed one reaction.	16
Figure 1.8	Simplified diagram of a stopped-flow spectrometer. Small amounts of solution are rapidly mixed <i>via</i> the application of force to the drive syringes. A sensor on the stopping syringe triggers the system to observe the reaction-taking place in the observation cell.	17
Figure 1.9	Reaction catalysed by DHFR, DHF is reduced to THF in the presence of NADPH. The structural parts of DHF are highlighted; pterin ring (blue), <i>P</i> -aminobenzoate (green) and glutamate (red).	17

Figure 1.10	Redox transitions between various forms of tetrahydrofolate. The reaction catalysed by DHFR is highlighted in red, figure adapted from reference.	19
Figure 1.11	Two cartoon representations of EcDHFR (1RX2), both in complex with folate (pink) and NADP ⁺ (yellow). A. The Three main domains are highlighted: Substrate binding domain (green), Adenosine binding domain (red) and the loop domain (blue). B. Highlighted are the important secondary structural elements: β -sheet (green), α -helices (red) and loops (blue).	20
Figure 1.12	Proposed Keto-enol tautomerisation mechanism for protonation of the DHF N5 position, Asp27 indirectly protonates the N5 position.	21
Figure 1.13	The two possible positions of water molecules inside the active site of DHFR respective to DHF. Site A is highlighted in red and site B highlighted in blue.	21
Figure 1.14	Kinetic scheme of catalysis by EcDHFR as determined by Benkovic <i>et al.</i>	23
Figure 1.15	Timescale of protein motions.	23
Figure 1.16	Cartoon representation of EcDHFR with the M20 loop highlighted in different structural conformations (Green = open/disordered, Blue = closed, Red = Occluded).	25
Figure 1.17	Catalytic cycle of EcDHFR with each of the five kinetic intermediates highlighted with respect to the structural conformation adopted by EcDHFR (Green = open/disordered, Blue = closed, Red = Occluded).	25
Figure 1.18	Cartoon representation of EcDHFR in the occluded (red), E:NADPH:THF complex rapidly probing a structural conformation similar to that of the closed (blue), E:NADPH complex to facilitate release of THF. NADPH is highlighted in green and folate derivatives in orange. The middle complex highlights how steric clash between substrates may lower binding affinities. The original rate measured by Benkovic <i>et al</i> is shown on top.	26
Figure 1.19	The network of promoting motions proposed in EcDHFR, highlighted in red are the partaking residues, ASP122, GLY15, LLE14, TYR100 and PHE31 and NADPH (green) and DHF (orange) as proposed by Agarwal <i>et.al</i> .	31

Figure 1.20	Graph showing the enzyme KIE of various DHFR variants over a temperature range. EcDHFR = Blue, MpDHFR = green and BsDHFR = red. Values taken from references.	34
Figure 3.1	Cartoon representation of TmDHFR (PDB entry 1D1G). NADPH (yellow) and methotrexate (pink) are highlighted as well as important secondary structural elements: β -sheet (green), α -helices (red) and loops (blue). One monomer is highlighted in orange for clarity.	53
Figure 3.2	(Top) mass spectrum of natural abundance TmDHFR, Mw = 19235.5 +/- 0.5. (Middle) mass spectrum of triply labelled TmDHFR (^2H , ^{13}C & ^{15}N), Mw = 21289.0 +/- 12.0, corresponding to 99.4% enrichment of non-exchangeable atoms. (Bottom) mass spectrum of triply labelled TmDHFR (^2H , ^{13}C & ^{15}N) grown in 70 % D_2O , Mw = 21053.7 +/- 7.9, corresponding to ~59 % deuteration.	56
Figure 3.3	1D ^1H spectra of TmDHFR complexed with NADP^+ and folate, a reasonable signal to noise ratio was achieved after 16 scans and the dispersion of chemical shifts at low and high fields is indicative of the protein being folded.	57
Figure 3.4	^1H - ^{15}N HSQC of TmDHFR complexed with NADP^+ and folate, spectra was acquired at 800 MHz.	58
Figure 3.5	Top: HNCA, magnetization is evolved on the amide proton before being passed to ^{15}N and then onto the alpha carbon <i>via</i> J coupling, before being returned by the same pathway for detection. Chemical shifts are gained for all three isotopes involved (^1H , ^{13}C & ^{15}N) producing 3D spectra. Bottom: HN(CO)CA, is very similar to HNCA experiment except magnetisation is passed onto the immediate carbonyl ^{13}C before the alpha carbon. Again chemical shifts are evolved for the amide ^1H and ^{15}N and the alpha carbon but not for the carbonyl ^{13}C . As the HN(CO)CA experiment only selects for the previous alpha carbon sequential assignment becomes possible.	61
Figure 3.6	^1H - ^{15}N spectra of ^{15}N labelled TmDHFR recorded after 4 days at 60 °C incubation in buffer containing 99 % D_2O .	63
Figure 3.7	Cartoon representation of TmDHFR, Spin systems that have been assigned have been highlighted in red, approximately 30 %.	64
Figure 3.8	Primary sequence of TmDHFR, highlighted in yellow are residues we found possible to assign.	64

- Figure 3.9** Cartoon representation of three DHFR variants discussed in this work; EcDHFR (PDB entry 1RX2, light blue), TmDHFR (PDB entry 1D1G, green) and MpDHFR (PDB entry 3IA5, red). The M20 loop in the closed position in EcDHFR and MpDHFR and open position in TmDHFR is highlighted in yellow. The M20 loop in the occluded position is highlighted in black in EcDHFR. The positions of methionine (blue) and tryptophan (purple) residues are also highlighted. 67
- Figure 3.10** Alignment of the amino acid sequences of DHFR orthologues, showing methionine and tryptophan residues in DHFR variants. DHFR alignments comprise *Thermotoga maritima* (TmDHFR), Human (hDHFR), *Mus musculus* (mouse, MmDHFR), *Lactobacillus casei* (LcDHFR), *Mycobacterium tuberculosis* (MtDHFR), *Escherichia coli* (EcDHFR), *Salmonella enterica* (SeDHFR), *Moritella profunda* (MpDHFR), *Moritella yayanosii* (MyDHFR), *Staphylococcus aureus* (SaDHFR), *Geobacillus stearothermophilus* (BsDHFR) and *Bacillus anthracis* (BaDHFR). 68
- Figure 3.11** Deconvoluted ESI mass spectrum of TmDHFR wherein the methyl group of each methionine residue has been systematically labelled with ^{13}C . The calculated mass is 19,370.0 and following cleavage of Met1 by aminopeptidase is 19,239.0. As can be observed the majority of Met1 has been cleaved but a significant amount of TmDHFR with Met1 still remains. 69
- Figure 3.12** Reaction catalysed by Tryptophan synthase. Serine forms a Schiff base with pyridoxal phosphate (PLP) held within the active site which reacts with indole to form tryptophan. 70
- Figure 3.13** ^1H - ^{13}C HSQC spectra of ^{13}C -labelled EcDHFR complexes. (A) [*methyl*- ^{13}C]methionine-labelled EcDHFR with no ligands. (B) [δ_1 - ^{13}C] tryptophan-labelled EcDHFR with no ligands. (C) [*methyl*- ^{13}C]methionine-labelled EcDHFR in the Michaelis complex. (D) [δ_1 - ^{13}C] tryptophan-labelled EcDHFR in the Michaelis complex. (E) [*methyl*- ^{13}C]methionine-labelled EcDHFR in the product complex. (F) [δ_1 - ^{13}C] tryptophan-labelled EcDHFR in the product complex. 72
- Figure 3.14** ^1H - ^{13}C HSQC spectra of ^{13}C -labelled EcDHFR complexes, Apo (green), E:NADP $^+$:folate (closed conformation in EcDHFR) (blue) and E:NADP $^+$:THF (occluded conformation in EcDHFR) (red). (G and I) [*methyl*- ^{13}C]methionine-labelled EcDHFR (H and J) [δ_1 - ^{13}C] tryptophan-labelled EcDHFR. 73

- Figure 3.15** ^1H - ^{13}C HSQC spectra of ^{13}C -labelled MpDHFR complexes. (A) $[\text{methyl-}^{13}\text{C}]$ methionine-labelled MpDHFR with no ligands. (B) $[\delta_1\text{-}^{13}\text{C}]$ tryptophan-labelled MpDHFR with no ligands. (C) $[\text{methyl-}^{13}\text{C}]$ methionine-labelled MpDHFR in the Michaelis complex. (D) $[\delta_1\text{-}^{13}\text{C}]$ tryptophan-labelled MpDHFR in the Michaelis complex. (E) $[\text{methyl-}^{13}\text{C}]$ methionine-labelled MpDHFR in the product complex. (F) $[\delta_1\text{-}^{13}\text{C}]$ tryptophan-labelled MpDHFR in the product complex. 75
- Figure 3.16** ^1H - ^{13}C HSQC spectra of ^{13}C -labelled MpDHFR complexes, Apo (green), E:NADP⁺:folate (closed conformation in EcDHFR) (blue) and E:NADP⁺:THF (occluded conformation in EcDHFR) (red). (G and I) $[\text{methyl-}^{13}\text{C}]$ methionine-labelled MpDHFR (H and J) $[\delta_1\text{-}^{13}\text{C}]$ tryptophan-labelled MpDHFR. 76
- Figure 3.17** ^1H - ^{13}C HSQC spectra of ^{13}C -labelled TmDHFR complexes. (A) $[\text{methyl-}^{13}\text{C}]$ methionine-labelled TmDHFR with no ligands. (B) $[\delta_1\text{-}^{13}\text{C}]$ tryptophan-labelled TmDHFR with no ligands. (C) $[\text{methyl-}^{13}\text{C}]$ methionine-labelled TmDHFR in the Michaelis complex. (D) $[\delta_1\text{-}^{13}\text{C}]$ tryptophan-labelled TmDHFR in the Michaelis complex. (E) $[\text{methyl-}^{13}\text{C}]$ methionine-labelled TmDHFR in the product complex. (F) $[\delta_1\text{-}^{13}\text{C}]$ tryptophan-labelled TmDHFR in the product complex. 79
- Figure 3.18** ^1H - ^{13}C HSQC spectra of ^{13}C -labelled TmDHFR complexes, Apo (green), E:NADP⁺:folate (closed conformation in EcDHFR) (blue) and E:NADP⁺:THF (occluded conformation in EcDHFR) (red). (G and I) $[\text{methyl-}^{13}\text{C}]$ methionine-labelled TmDHFR (H and J) $[\delta_1\text{-}^{13}\text{C}]$ tryptophan-labelled TmDHFR. 80
- Figure 3.19** ^1H - ^{13}C HSQC spectra of ^{13}C -labelled SeDHFR complexes. (A) $[\text{methyl-}^{13}\text{C}]$ methionine-labelled SeDHFR with no ligands. (B) $[\delta_1\text{-}^{13}\text{C}]$ tryptophan-labelled SeDHFR with no ligands. (C) $[\text{methyl-}^{13}\text{C}]$ methionine-labelled SeDHFR in the Michaelis complex. (D) $[\delta_1\text{-}^{13}\text{C}]$ tryptophan-labelled SeDHFR in the Michaelis complex. (E) $[\text{methyl-}^{13}\text{C}]$ methionine-labelled SeDHFR in the product complex. (F) $[\delta_1\text{-}^{13}\text{C}]$ tryptophan-labelled SeDHFR in the product complex. 82
- Figure 3.20** ^1H - ^{13}C HSQC spectra of ^{13}C -labelled SeDHFR complexes, Apo (green), E:NADP⁺:folate (closed conformation in EcDHFR) (blue) and E:NADP⁺:THF (occluded conformation in EcDHFR) (red). (G and I) $[\text{methyl-}^{13}\text{C}]$ methionine-labelled SeDHFR (H and J) $[\delta_1\text{-}^{13}\text{C}]$ tryptophan-labelled SeDHFR. 83

Figure 3.21	^1H - ^{13}C HSQC spectra of ^{13}C -labelled S150A-SeDHFR complexes. (A) [<i>methyl</i> - ^{13}C]methionine-labelled S150A-SeDHFR with no ligands. (B) [δ_1 - ^{13}C] tryptophan-labelled S150A-SeDHFR with no ligands. (C) [<i>methyl</i> - ^{13}C]methionine-labelled S150A-SeDHFR in the Michaelis complex. (D) [δ_1 - ^{13}C] tryptophan-labelled S150A-SeDHFR in the Michaelis complex. (E) [<i>methyl</i> - ^{13}C]methionine-labelled S150A-SeDHFR in the product complex. (F) [δ_1 - ^{13}C] tryptophan-labelled S150A-SeDHFR in the product complex.	85
Figure 3.22	^1H - ^{13}C HSQC spectra of ^{13}C -labelled S150A-SeDHFR complexes, Apo (green), E:NADP ⁺ :folate (closed conformation in EcDHFR) (blue) and E:NADP ⁺ :THF (occluded conformation in EcDHFR) (red). (G and I) [<i>methyl</i> - ^{13}C]methionine-labelled S150A-SeDHFR (H and J) [δ_1 - ^{13}C] tryptophan-labelled S150A-SeDHFR.	86
Figure 3.23	Two overlaid ^1H - ^{15}N HSQC spectra of ^{15}N labelled SeDHFR in both the Michaelis (blue) and product complexes (red).	88
Figure 4.1	Chromatogram of the elution trace (red) of SeDHFR from the Q-Sepharose column. The salt gradient (% NaCl) is in blue. SeDHFR eluted before the salt gradient (60-120 mL).	94
Figure 4.2	Chromatogram of the elution trace (red) of SeDHFR from the HiLoad Superdex G75 (GE Healthcare). SeDHFR elutes between 210-230 mL.	94
Figure 4.3	SDS-polyacrylamide gel showing; 1) Cell Lysate 2) Combined fractions from Q-Sepharose column 3) After size exclusion chromatography (BSD75). MW of SeDHFR = 18,032.	95
Figure 4.4	Deconvoluted ESI mass spectrum of natural abundance SeDHFR (18036.2 ± 1.6).	95
Figure 4.5	Deconvoluted ESI mass spectrum SeDHFR labelled with ^{13}C and ^{15}N (19031.6 ± 6.0).	96
Figure 4.6	CD spectra of natural abundance (blue) and ^{13}C and ^{15}N labelled (red) SeDHFR, recorded at 20 °C.	97
Figure 4.7	MRE recorded at 208 nm over a temperature range of 5 to 85 °C for natural abundance SeDHFR.	98
Figure 4.8	Effect of temperature (range of 5-40 °C shown only) on the steady state rate constant for five DHFR variants at pH 7.0. SeDHFR (red diamond), EcDHFR (blue square), MpDHFR (green triangle), BsDHFR (orange circle) and TmDHFR (black square).	101

Figure 4.9	Arrhenius plot of the effect of temperature on the steady state rate of SeDHFR.	101
Figure 4.10	The effect of pH on the steady state rate constant in SeDHFR.	103
Figure 4.11	IC ₅₀ curve (μM) for NADP ⁺ inhibition in SeDHFR.	105
Figure 4.12	No crystal structure of SeDHFR exists. Shown is a cartoon representation of EcDHFR (1RX2), highlighted in blue is residue Trp22 that is conserved in nearly all DHFR variants including SeDHFR. Also highlighted is NADPH in cyan, FRET occurs between Trp22 and the nicotinamide ring of NADPH.	106
Figure 4.13	Temperature dependence of the single turnover rate constant for hydride/deuteride transfer in SeDHFR.	107
Figure 4.14	Arrhenius plots of hydride/deuteride transfer in SeDHFR. In both figures blue triangle represent hydride transfer and red squares denote deuteride transfer.	109
Figure 4.15	Temperature dependency of the primary KIE for SeDHFR at pH 7.0	110
Figure 4.16	Temperature dependency of the primary KIE for SeDHFR (red diamond), EcDHFR (blue square), MpDHFR (green triangle) and TmDHFR (black square).	111
Figure 4.17	Temperature dependence of the rate constant for hydride transfer in light SeDHFR (blue triangles) and heavy SeDHFR (red squares).	115
Figure 4.18	Arrhenius plots of hydride transfer in light SeDHFR (blue diamonds) and heavy SeDHFR (red diamonds).	116
Figure 4.19	Temperature dependency of the enzyme KIE (k^{LE}/k^{HE}).	116
Figure 4.20	Temperature dependency of the enzyme KIE in a number of DHFR variants. SeDHFR (red diamond), EcDHFR (blue square), TmDHFR (black square), MpDHFR (green triangle) and BsDHFR (orange square).	119
Figure 5.1	Reaction catalysed by LDH. Pyruvate is reduced to L-lactate using NADH as a cofactor.	125
Figure 5.2	The proposed catalytic cycle of BsLDH (NH = NADH, Pyr = pyruvate, N ⁺ = NAD ⁺ and Lac = Lactate). A blue circle indicates the open conformation and a red circle indicates the closed conformation.	126

Figure 5.3	Cartoon representation of Human heart LDH (1I0Z). The residues reported to be part of the promoting protein network are highlighted in blue and are Gln66, Leu65, Met33, Gly32, Val31 and Arg106 from left to right respectfully. NADH and oxamate are highlighted in red and green respectfully.	127
Figure 5.4	Enzyme KIE of human heart LDH against temperature. Data from reference.	128
Figure 5.5	Cartoon representation of a single monomer of SaLDH (3D4P) complexed with NAD ⁺ (dark green) and pyruvate (light green). Structural elements such as coils (cyan), helix's (orange) and beta sheets (purple) are also highlighted, as well as the catalytically important His179 (red) residue.	129
Figure 5.6	SDS-PAGE of SaLDH purification. L = lysate, F = flow through and W = wash. Fraction 1 was discarded; fractions 2-6 were combined for further use.	131
Figure 5.7	pH dependency on the steady state rate constants for hydride (blue diamond) and deuteride (red square) transfer during catalysis by SaLDH at 20 °C.	134
Figure 5.8	pH dependency on the steady state rate primary NADH/D KIE during catalysis by SaLDH at 20 °C.	134
Figure 5.9	Temperature dependency on the steady state rate constants for hydride (blue diamond) and deuteride (red square) transfer during catalysis by SaLDH.	136
Figure 5.10	Temperature dependency on the steady state rate constants for hydride (blue diamond) and deuteride (red square) transfer during catalysis by SaLDH.	136
Figure 5.11	Temperature dependency on the steady state rate primary KIE during catalysis by SaLDH at pH 7.0.	137
Figure 5.12	pH dependency on the steady state rate constants catalysed by light (blue diamond) and heavy (red square) SaLDH at 20 °C.	139
Figure 5.13	pH dependency on the steady state rate enzyme KIE during catalysis by SaLDH at 20 °C.	139
Figure 5.14	Temperature dependency on the steady state rate constants catalysed by light (blue diamond) and heavy (red square) SaLDH.	141
Figure 5.15	Temperature dependency on the steady state rate enzyme KIE during catalysis by SaLDH.	142

- Figure 5.16** Graph of k_{cat} (s^{-1}) vs. concentration of pyruvate (μM). 145
- Figure 5.17** Pyruvate analogues incubated with SaLDH, differences with respect to pyruvate are highlighted in red. From left to right, top to bottom; (A) pyruvate, (B) 2-ketobutyric acid, (C) oxaloacetate, (D) 2-ketoglutaric acid and (E) 2,3-butanedione. 146

List of Tables

Table 1.1	Enzymatic rate enhancements taken by comparing catalysed and uncatalysed reactions under aqueous conditions, data taken from reference.	3
Table 1.2	IC ₅₀ Values for NADP ⁺ (μM) at 20 °C, taken from reference.	27
Table 2.1	Preparations of buffers used in this work.	38
Table 2.2	Plasmids used in this study.	40
Table 2.3	PCR conditions used.	41
Table 2.4	Concentrations of Imidazole used in the purification of LDH and TEV protease.	43
Table 2.5	Buffer conditions used in the purification of enzymes.	44
Table 2.6	Exact buffer conditions used in the purification of enzymes (BSD-75).	44
Table 2.7	Quantities of reagents used in the making of SDS plates.	45
Table 2.8	Molar coefficients of ligands used.	49
Table 3.1	List of recorded spectra recorded for TmDHFR complexed with NADP ⁺ and folate at pH 7.0.	59
Table 3.2	Weighted chemical shift perturbations (ppm) between ¹ H- ¹³ C HSQC of spectra relating to [<i>methyl</i> - ¹³ C] methionine-labelled EcDHFR.	73
Table 3.3	Weighted chemical shift perturbations (ppm) between ¹ H- ¹³ C HSQC of spectra relating to [δ_1 - ¹³ C] tryptophan-labelled EcDHFR.	74
Table 3.4	Weighted chemical shift perturbations (ppm) between ¹ H- ¹³ C HSQC of spectra relating to [<i>methyl</i> - ¹³ C] methionine-labelled MpDHFR.	76
Table 3.5	Weighted chemical shift perturbations (ppm) between ¹ H- ¹³ C HSQC of spectra relating to [δ_1 - ¹³ C] tryptophan-labelled MpDHFR.	77
Table 3.6	Weighted chemical shift perturbations (ppm) between ¹ H- ¹³ C HSQC of spectra relating to [<i>methyl</i> - ¹³ C] methionine-labelled TmDHFR.	80

Table 3.7	Weighted chemical shift perturbations (ppm) between ^1H - ^{13}C HSQC of spectra relating to $[\delta_1\text{-}^{13}\text{C}]$ tryptophan-labelled TmDHFR.	80
Table 3.8	Weighted chemical shift perturbations (ppm) between ^1H - ^{13}C HSQC of spectra relating to $[\text{methyl-}^{13}\text{C}]$ methionine-labelled SeDHFR.	83
Table 3.9	Weighted chemical shift perturbations (ppm) between ^1H - ^{13}C HSQC of spectra relating to $[\delta_1\text{-}^{13}\text{C}]$ tryptophan-labelled SeDHFR.	83
Table 3.10	Weighted chemical shift perturbations (ppm) between ^1H - ^{13}C HSQC of spectra relating to $[\text{methyl-}^{13}\text{C}]$ methionine-labelled SeDHFR-S150A.	86
Table 3.11	Weighted chemical shift perturbations (ppm) between ^1H - ^{13}C HSQC of spectra relating to $[\delta_1\text{-}^{13}\text{C}]$ tryptophan-labelled SeDHFR-S150A.	87
Table 4.1	Temperature dependence of the catalytic turnover (k_{cat}) on SeDHFR and the DHFR variants EcDHFR, MpDHFR, BsDHFR and TmDHFR at pH 7.0.	100
Table 4.2	Activation parameters for SeDHFR and the DHFR variants EcDHFR, MpDHFR, BsDHFR and TmDHFR at pH 7.0.	102
Table 4.3	pH dependency on k_{cat} for the reaction catalysed by SeDHFR.	104
Table 4.4	IC_{50} values for NADP^+ for a number of DHFR variants at pH 7.0 and 20 °C.	105
Table 4.5	Temperature dependency of hydride transfer in SeDHFR and previously mentioned DHFR variants at pH 7.	108
Table 4.6	Temperature dependency of hydride and deuteride transfer in SeDHFR and the resulting KIE.	110
Table 4.7	Temperature dependency of the primary KIE for hydride and deuteride transfer at pH 7.0 for SeDHFR, MpDHFR, EcDHFR and TmDHFR.	113
Table 4.8	Activation energies (E_a) for the single turnover rate catalysed by SeDHFR and other reported DHFR variants.	113
Table 4.9	Arrhenius pre-factors ($A_{\text{H/D}}$) for the single turnover rate catalysed by SeDHFR and other reported DHFR variants.	114

Table 4.10	Temperature dependence on the rate of hydride transfer in both light and heavy SeDHFR.	117
Table 4.11	Temperature dependence of the enzyme KIE ($k^{\text{LE}}/k^{\text{HE}}$) in the DHFR variants SeDHFR, EcDHFR, MpDHFR, TmDHFR and BsDHFR.	118
Table 5.1	pH dependency on the steady state rate constants for hydride ($k_{\text{cat}}^{\text{H}}$) and deuteride ($k_{\text{cat}}^{\text{D}}$) transfer during catalysis by SaLDH at 20 °C.	135
Table 5.2	pH dependency on the steady state rate primary KIE during catalysis by SaLDH at 20 °C.	135
Table 5.3	Temperature dependency on the steady state rate constants for hydride ($k_{\text{cat}}^{\text{H}}$) and deuteride ($k_{\text{cat}}^{\text{D}}$) transfer during catalysis by SaLDH.	137
Table 5.4	Temperature dependency on the steady state rate primary KIE during catalysis by SaLDH at pH 7.0.	138
Table 5.5	pH dependency on the steady state rate constant for natural abundance ($k_{\text{cat}}^{\text{LE}}$) and heavy enzyme ($k_{\text{cat}}^{\text{HE}}$) catalysis by SaLDH at 20 °C.	140
Table 5.6	pH dependency on the steady state enzyme KIE during catalysis by SaLDH at 20 °C.	140
Table 5.7	Temperature dependency on the steady state rate constant for natural abundance ($k_{\text{cat}}^{\text{LE}}$) and heavy enzyme ($k_{\text{cat}}^{\text{HE}}$) catalysis by SaLDH at 20 °C.	142
Table 5.8	Temperature dependency on the steady state enzyme KIE during catalysis by SaLDH at 20 °C.	143
Table 5.9	Kinetic constants for pyruvate analogues incubated with SaLDH at pH 7.0 and 20 °C.	146

1

Introduction

Introduction.

1.1 Enzymes as catalysts.

Spoiled wine is not often a problem in the modern world but in 1860 it became a national crisis for France.¹ Contrary to the popular beliefs of the time, Louis Pasteur identified that yeast was responsible for converting sugars to alcohol and that bacterial growth resulted in spoiled wine.^{1,2} Following this, Eduard Buchner showed that extracts from yeast were still able to convert sugar into alcohol. This discovery won Buchner the 1907 Nobel Prize in chemistry for cell-free fermentation and proved that living cells were not necessary to catalyse chemical reactions.³

Over the last 150 years, enzymology has identified a huge variety of enzymes that catalyse a wide range of chemical reactions.⁴ Compared to manmade catalysts enzymes exhibit a number of interesting properties. Firstly, enzymes have enormous catalytic power and are able to increase reaction rates up to 10^{17} fold compared to uncatalysed reactions (**Table 1.1**).⁴ In the case of hydrogen peroxide decomposition the enzyme catalase is able to outperform an iron chloride catalyst by 10^6 fold, protecting the host organism from oxidative damage.^{5,6} Secondly, enzymes are both specific to the reaction they catalyse and to the substrate they bind, being able to select specific substrates from a pool of structurally similar compounds. The origin of such specificity arises from the three-dimensional structure of the enzymes active site, which also facilitates the production of stereospecific products.⁷ Thirdly, enzymes can be tightly regulated by small ions or molecules, which bind non-covalently resulting in competitive inhibition, or allosteric effects at a distinct binding site that either perturb the three-dimensional structure of the active site or restrict conformational behaviour resulting in stimulation or inhibition of activity. Enzymes can also be regulated through changes to their covalent structure, such as is the case with reversible phosphorylation that can switch an enzymes activity on or off.⁸ Moreover, some enzymes are susceptible to product inhibition allowing the system to self-regulate, preventing over production of products which may be toxic to the cell.^{4,9} Finally, enzymes are increasingly being used in industrial applications such as laundry detergents and food processing due to their ability to fulfil their function under moderate temperatures and aqueous environments.^{10,11}

Table 1.1: Enzymatic rate enhancements taken by comparing catalysed and uncatalysed reactions under aqueous conditions, data taken from reference. ⁹	
Enzyme	Rate enhancement
Cyclophilin	10^5
Carbonic anhydrase	10^7
Triose phosphate isomerase	10^9
Carboxypeptidase A	10^{11}
Phosphoglucomutase	10^{12}
Succinyl-CoA transferase	10^{13}
Urease	10^{14}
Orotine monophosphate decarboxylase	10^{17}

To explain the mechanism of enzyme catalysis, Emil Fisher in 1894 proposed that enzymes only bind substrates which match the geometry of the enzymes active site, defined as the ‘lock and key’ model.¹² Shortly after, Brown in 1902 provided evidence for an enzyme-substrate complex by showing the enzyme invertase had increased thermal stability in the presence of sugar. Brown also noted that formation of such a complex likely impacted on the overall rate constant for the catalysed reaction.¹³ Observations such as these laid the foundations for Victor Henri in 1903 to release the first realistic mathematical model for the kinetic analysis of enzyme catalysed reactions.^{14,15} A decade later, Leonor Michaelis and Maud Menten built on the work of Henri, adding detail to the mathematical model through better defining of the constants involved.¹⁶

These models, however, did not explain the chemical mechanism or how enzymes were able to achieve such large rate enhancements. Transition state theory (TST), first developed in 1935, by Eyring, Evans and Polanyi, proposed that it is possible to increase reaction rates by reducing the energy of the transition state.¹⁷⁻¹⁹ Koshland added to this theory in 1958 with his theory of ‘induced fit’ wherein enzymes undergo conformational changes upon substrate binding, allowing for residues within the enzyme active site to form intermolecular interactions with the substrate, effectively enhancing the activity of the enzyme.²⁰ Contrary to this it was noted that enzymes could also be inhibited by molecules other than the designated substrate and to address this

Changeux, Monod and Wyman developed the ‘allosteric model’ in 1965, which allows such molecules to bind into allosteric sites, inducing conformational changes which can de-activate or even activate the protein.²¹ However, no single model is yet able to fully explain how enzymes achieve their catalytic power. In particular, the role of conformational behaviour and protein dynamics are still not fully understood. As a result, this Thesis will further investigate the role of such motions and how they impact on catalysis in enzymatic systems.

1.2 Steady state kinetics and Michaelis-Menten.

In order to explain how enzymes convert substrates into product steady state kinetic explanations can be used. One of the most famous is the Michaelis-Menten equation proposed in 1913. In this model the enzyme rapidly and reversibly binds substrate to form an enzyme substrate complex [ES]. In the second step this slowly breaks down into free enzyme [E] and product [P] as described in **Equation 1.1**. The rate of catalysis (V_o) increases with substrate concentration [S] until saturation conditions are reached; at this point the system has reached V_{max} (**Figure 1.1**). In Michaelis-Menten kinetics a number of assumptions are adopted;

1. Almost zero [P] reverts back to starting material [ES].
2. The concentration of intermediates remains constant.
3. The enzyme concentration [E] is much lower than substrate concentration [S].
4. The formation of [P] is much slower than formation of [ES].

Through derivation of **Equation 1.1**, **Equation 1.2** is yielded.^{16,22}

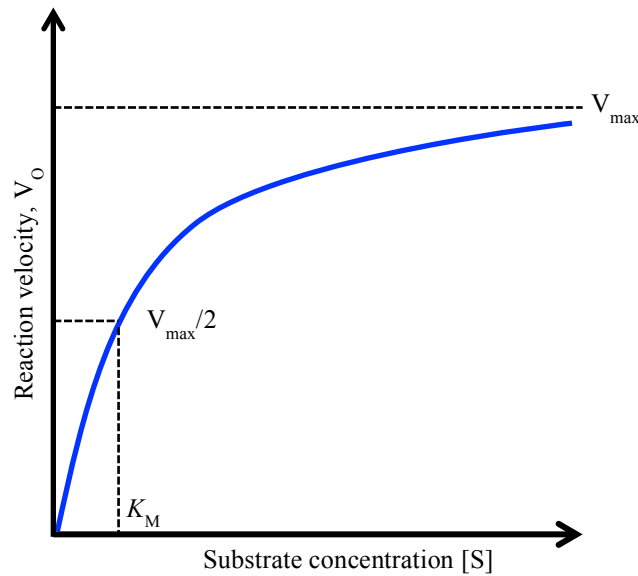
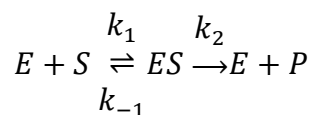


Figure 1.1: Initially the rate of reaction is first order and linearly dependent on substrate concentration. As the enzyme becomes saturated it becomes independent of substrate concentration.



Equation 1.1: A simple equation that accounts for a two-step model of enzyme catalysis.

$$V_o = \frac{V_{max} [S]}{K_M + [S]}$$

Equation 1.2: Michaelis-Menten equation.¹⁶

From **Equation 1.2** we get the Michaelis constant, K_M which has units of concentration and can be described as the concentration of substrate required to achieve half the maximal velocity (V_{max}) of the reaction. Although the value of K_M is affected by pH, temperature and ionic strength of the buffer it is independent of enzyme concentration. Although **Equation 1.1** characterises the formation of product from the enzyme substrate complex as a single step it often involves multiple intermediates. The turnover number, or k_{cat} encompasses all intermediates and describes the total complete conversions an enzyme is capable of in a given timescale. The ratio of k_{cat}/K_M is also known as the specificity constant and reports on the efficiency of an enzyme, the higher the value, the more able the enzyme is to convert substrate to product. The specificity

constant is often used as a measure of enzyme efficiency and is utilised in the identification of the enzymes natural substrate and varies greatly between different enzymes. For example, Hexokinase, phosphorylates a number of hexoses and comparison of the specificity constants allows for the identification of its preferred substrate, glucose.^{4,22,23}

1.3 Transition state theory and KIE.

From a thermodynamic perspective, chemical reactions proceed from reactants to products over a transition state barrier (**Figure 1.2**). The transition state has the highest Gibbs free energy and as such is the lowest populated point along the reaction pathway. Enzymes effectively lower the activation energy barrier without altering the Gibbs free energy of reactants/products, thus not changing the equilibrium constant.⁴

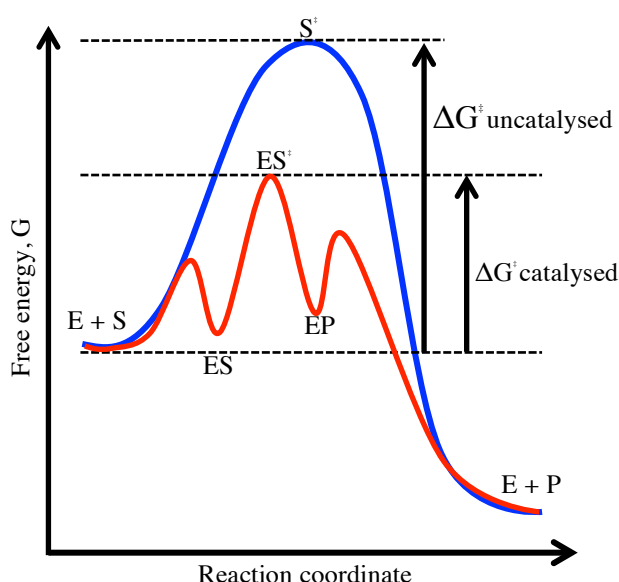


Figure 1.2: Graphical representation of how enzymes lower the ΔG^\ddagger of the reaction, (red) with enzyme, (blue) without enzyme. ES, ES^\ddagger , and EP represent the enzyme-substrate complex, the transition state complex and the enzyme-product complex respectively.^{4,22}

Transition state theory (TST) is based upon assumptions that molecules in the transition state are in quasi-equilibrium with reactants and that the reaction rate is governed by breakdown of the transition state complex. The development of TST is attributed to Eyring, Evans and Polanyi in 1935 and builds upon work done by Arrhenius nearly 50 years earlier.^{17,18,24} The Arrhenius equation (**Equation 1.3**) developed in 1889 was originally used to study reactions in the gas phase and describes the relationship

between the activation energy (E_a), the rate of reaction and the temperature of chemical reactions. Two important observations can be made: firstly, as the activation energy increases, the rate of reaction decreases exponentially, and secondly, with every 10 °C rise in temperature the rate is expected to roughly double.²⁴

$$k = Ae^{-E_a/(RT)}$$

Equation 1.3: The Arrhenius equation. k is the rate constant, E_a is the activation energy, R is the universal gas constant, T is the temperature in Kelvin and A is the pre-exponential factor which is dependent on temperature and describes the number of successful collisions in the correct orientation between molecules and is different for every chemical reaction.²⁴

The Eyring equation (**Equation 1.4**) further developed the Arrhenius equation, which it is notably similar too, except it is derived mathematically from model systems and not from experimental observations. The Eyring equation expands the pre-exponential factor (A) to include the transmission coefficient (κ), which includes a number of correcting factors including solvent friction events and re-crossing of the transition state barrier, which leads to unsuccessful reaction trajectories. Subsequently, the transmission coefficient can deviate greatly from unity in enzyme-catalysed reactions.^{17,22}

$$k = \frac{\kappa k_B T}{h} e^{\frac{\Delta^\ddagger S}{R}} e^{-\frac{\Delta^\ddagger H}{RT}}$$

Equation 1.4: The Eyring equation. Highlighted in green is the enthalpy of activation ($\Delta^\ddagger H$) and this corresponds to the activation energy in the Arrhenius equation. Highlighted in red is the section which corresponds to the pre-exponential factor, A . k_B is the Boltzmann constant, h the Planck's constant, $\Delta^\ddagger S$ the entropy of activation and κ is the transmission coefficient.^{17,22}

The use of kinetic isotope effects (KIE) in the study of reaction mechanisms has become an important tool in understanding mechanisms and is empirically defined by **Equation 1.5**. A KIE is a ratio of the rate constants for reactions involving a light (k_L) and heavy (k_H) isotopes. A primary KIE involves isotopic substitution of the atom that is directly connected to the bond being broken/formed.²⁵

$$KIE = \frac{k_L}{k_H}$$

Equation 1.5: The KIE is the ratio of the rate constant for the reaction with the light isotope (k_L) and the heavy isotope (k_H).²⁶

If we consider a potential energy well from a quantum mechanical perspective we observe discrete energy levels. The lowest energy level is slightly higher than the trough of the potential energy well; this is defined as the zero point energy (ZPE).²⁶ In TST the KIE is primarily thought to derive from a lower zero point energy of the heavier isotope as a result of the greater reduced mass, resulting in a smaller stretching frequency (**Equations 1.6a, b & c**). This effectively increases the free energy needed to overcome the activation energy (**Figure 1.3**).^{26,27}

$$E_0 = \frac{1}{2} \hbar \omega \qquad \omega = \left(\frac{k_f}{\mu}\right)^{\frac{1}{2}} \qquad \mu = \frac{m_1 \times m_2}{m_1 + m_2}$$

Equations 1.6a, b & c (left to right): E_0 equates to the Z.P.E, \hbar is reduced plancks constant, ω is described by equation 1.6b. where k_f is the force constant and μ the reduced mass described by equation 1.6c. m_1 is the mass of the lighter isotope, m_2 the mass of the heavier isotope.²⁶

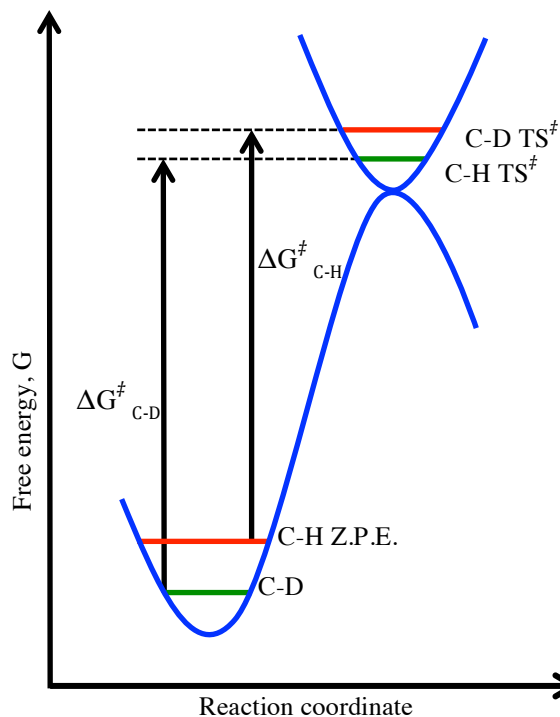


Figure 1.3: Difference in Z.P.E. in a reaction involving breaking of a carbon-hydrogen bond compared to a carbon-deuterium bond.

The difference in Z.P.E. between a C-H and C-D bond is $\sim 4.8 \text{ kJ mol}^{-1}$, with stretching frequencies of $\sim 3000 \text{ cm}^{-1}$ and $\sim 2200 \text{ cm}^{-1}$ respectively.²⁸ When these values are substituted into the Eyring equation (**Equation 1.7**) semi-classical models predict a primary KIE of ~ 6.9 at 298 K, which tends to zero at infinite temperatures as the ratio of pre-exponential factors (A_H/A_D) nears unity. Semi classical models propose the difference in rates arises from these differences in Z.P.E. and does not take into account effects from tunnelling or dynamics. Semi-classical models therefore fail to account for experimentally observed temperature independent KIEs, larger than expected KIEs or even KIEs that are smaller than expected but strongly dependant on temperature.²²

$$KIE = \frac{k_H}{k_D} = \frac{\left(\frac{\kappa K_B T}{h} e^{\frac{\Delta G^\ddagger}{RT}}\right)}{\left(\frac{\kappa K_B T}{h} e^{\frac{\Delta G^\ddagger + 4800}{RT}}\right)} = e^{\frac{4800}{RT}} = 6.9$$

Equation 1.7: Using the Eyring equation to calculate the maximum primary KIE between a C-H and C-D bond.

1.4 Tunnelling in enzymatic reactions.

Semi-classical models do not account for tunnelling contributions in enzymatic reactions. As such semi-classical models fail to explain KIE for a number of enzyme systems including, lipoxygenase-1 from soybean,²⁹ alcohol dehydrogenase from *Bacillus stearothermophilus*,³⁰ flavoprotein pentaerythritol tetranitrate reductase,³¹ and dihydrofolate reductase from *Escherichia coli*.³² In the semi-classical model, KIE are said to arise from differences in Z.P.E of the isotopologues involved, directly altering the activation energies (E_a) classically required for the reaction to occur. Tunnelling allows for a particle to cross a transition state barrier when it classically it does not have enough energy to do so, thereby breaking down the semi-classical models (**Figure 1.4**).^{33,34} Bells modification to the semi-classical model adds a correction factor (Q_t) to the Eyring equation (**Equation 1.8a**) in order to account for effects from tunnelling. The correction factor (Q_t), mathematically calculates the likelihood of a particle tunnelling in a given reaction (**Equation 1.8b**). The variable, G depends strongly on the mass of the particle and as such explains the large difference observed in KIE between reactions involving hydrogen and deuterium. Tunnelling also depends on both the width and height of the potential energy barrier.^{33,34} The addition of Bells tunnelling correction factor to semi-classical models can mathematically explain KIEs that exceed the semi-classical limit of 6.9.³⁴

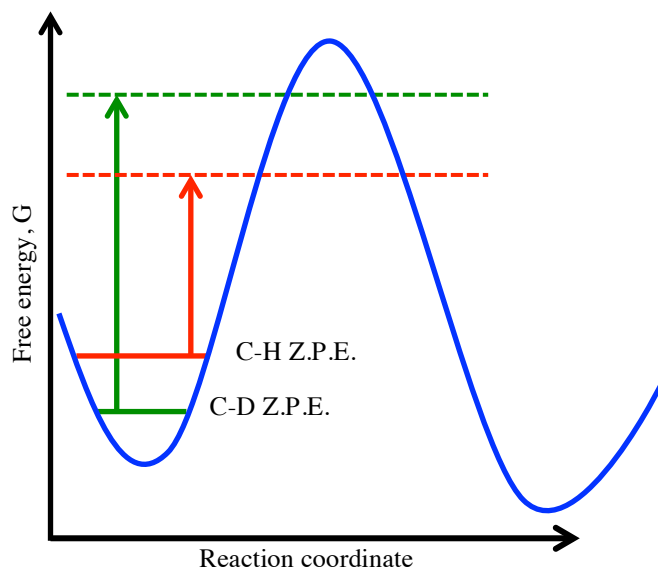


Figure 1.4: Graphical representation of Bell's correction for tunnelling, note how quantum tunnelling has a larger effect on the lighter molecule.

$$k_{obs} = Q_t A e^{\frac{-E_a}{RT}} \quad Q_t = \frac{1}{kT} e^{\frac{-E_a}{k_b t}} \int \frac{G(W)}{kT} e^{\frac{-(E_a - W)}{k_b T}} dW$$

Equations 1.8a & b: Where Q_t is the tunnelling correction factor, G is the probability of barrier crossing and is heavily dependant on the mass of the tunnelling particle, W is the energy of the particle and k_b is the Boltzmann constant

Semi-classical models also fail to effectively model the temperature dependence of the KIE. The semi-classical Arrhenius equation (**Equation 1.3**) shows that the relationship between rate and the activation barrier is exponential; with the KIE simply a ratio of the light and heavy rate constants (**Equation 1.8**).²⁷ At high temperatures the barrier to the reaction becomes negligible, as there is enough thermal energy to overcome it and consequently the contribution from different isotopes also becomes negligible and the ratio between the pre-exponential factors (A_H/A_D) tends to unity. Under these conditions the contribution from tunnelling is also mitigated (**figure 1.5**). At low temperatures the opposite is true, the lack of thermal energy means most molecules do not have the energy required to overcome the potential energy barrier for the reaction. Contributions from tunnelling therefore have a large effect on the rate of reaction, the KIE will be large and the ratio between the pre-exponential factors large ($A_H/A_D > 1$) in respect to measurements at higher temperatures. Between the two temperature extremes the

contribution from tunnelling will be greatest from the lighter isotopologue producing strongly temperature dependant KIE. Therefore if an enzymatic system has a relationship between the ratio of the pre-exponential factors and temperature as described above tunnelling is likely taking place.^{27,35}

$$\frac{K_L}{K_H} = \frac{A_L}{A_H} e^{\frac{\Delta E_{a(H-L)}}{RT}}$$

Equation 1.8: Calculation of KIE *via* the Arrhenius equation.

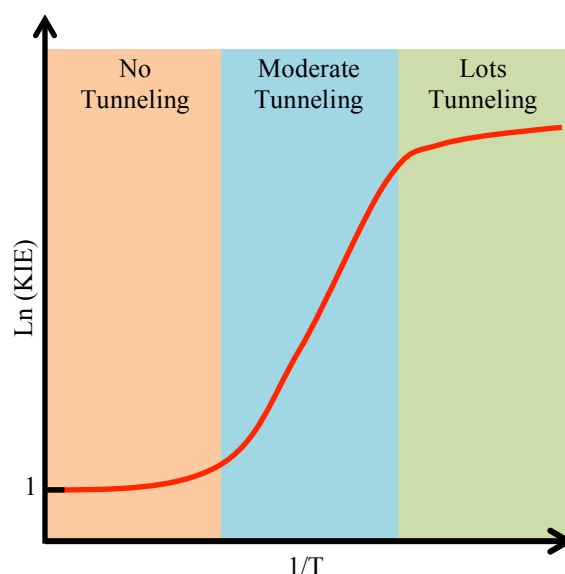


Figure 1.5: Graphical representation of an Arrhenius plot for a H transfer reaction with Bells tunnelling correction, adapted from ref.²⁷

One of the major pit-falls of Bells tunnelling correction and TST theory in general is that it considers the reaction coordinate as rigid and one dimensional and considers only the hydrogen atom being transferred, failing to effectively model contributions from the heavier atoms from which the particle is being transferred too or from. Dihydrofolate reductase, thymidylate synthase and soybean lipoxygenase-1 all represent enzymatic systems that cannot be effectively modelled by semi-classical TST with Bells tunnelling correction due to either larger than expected KIEs, pre-exponential factors (A_H/A_D) that exceed unity and discrepancies in whether temperature independent or dependant KIEs are observed.^{27,29,32,36-38}

To this end Marcus theory was developed as a way to account for discrepancies in TST theory.²⁷ Marcus theory was originally developed to model rates of electron transfer from a donor to acceptor molecule.³⁹ Modified versions of his theory are known as Marcus-like models and replace electron transfer with proton transfer and include parameters to include heavy atom re-organisation and fluctuations in the donor-acceptor distance (DAD).^{27,33} From this model the theory of ‘protein promoting motions’ has its foundations.⁴⁰ Marcus-like models have two main selection rules for efficient tunnelling, a narrow activation barrier and the reactant and product energy levels must be degenerate (**Equation 1.9** describes Marcus like models and graphical representation is shown in **figure 1.6**).^{41,42}

$$k = C e^{-(\Delta G^0 + \lambda)^2 / (4\lambda RT)} \int_{r_0}^{r_\infty} e^{F(m)} e^{-E_{F(m)}/K_b T} dDAD$$

Equation 1.9: Equation describing Marcus like models, where k is the rate constant. The equation can be considered in parts; C is a constant, the first exponential is the Marcus term, the second exponential (F(m)) is the Frank-Condon term and the third exponential is the gating term ($E_{f(m)}$).

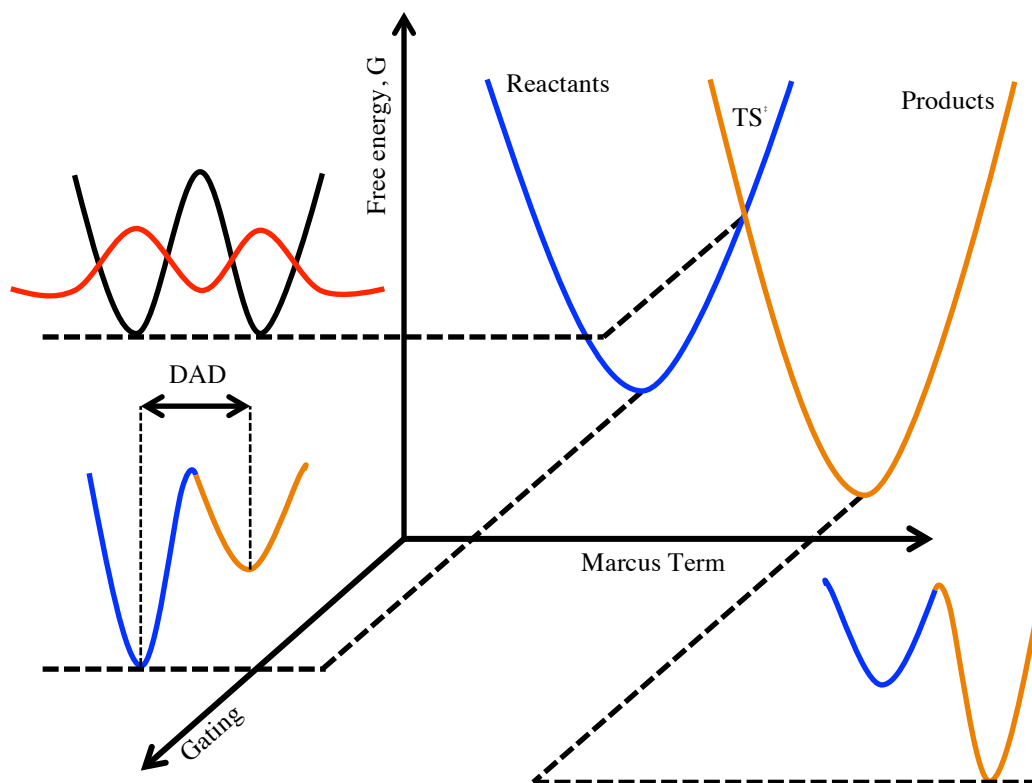


Figure 1.6: Graphical representation of the Marcus-like model. In this model there are two orthogonal co-ordinates. The gating term describes fluctuations in the donor-acceptor distance (DAD) and the Marcus term has the energy wells for both the reactant and product as well as the energy of the transition state.

The equation (**Equation 1.9**) before the integral represents the Marcus term and describes the re-organisation of the wave functions leading to a state where tunnelling is permitted. The term C includes factors relating to reorganisation energy (λ), electronic coupling, reaction driving force (ΔG^0) and the temperature (T) in degrees Kelvin. The C term is also independent with respect to isotope mass. Terms after the integral calculate tunnelling probability once the system has reached a tunnelling ready state and is dependant on both temperature and isotopic mass.^{27,33} Marcus-like models are able to address some of the pitfalls in TST: the formation of the tunnelling ready conformation is independent of temperature and as such is able to account for temperature independent KIEs. Secondly, the equation addresses contributions from the heavier isotopes in the second exponential term and better models donor-acceptor distances.^{27,33}

The most recent debate with respect to the catalytic power of enzymes is how or if protein dynamics influence the rate of reaction by altering the potential energy

landscape.⁴³ Trular and co-workers also developed a variational TST model (VTST) to account for the shortcomings of TST, which is described in section 1.13 of this thesis.⁴⁴ The role of dynamics will be further investigated in this thesis.

1.5 Pre-steady state kinetics.

Steady-state kinetic studies offer limited information regarding the rates of individual steps present in the catalytic cycle. Typically steady-state kinetics using Michaelis Menten provide k_{cat} and K_{M} . This gives a measure of catalytic efficiency with average values of k_{cat} for enzyme catalysis being on the order of 10 s^{-1} , although this varies greatly with the enzyme catalase able to achieve a k_{cat} of 10^7 s^{-1} .^{5,9,22,45} The value of k_{cat} predominantly reports on the slowest step in a catalytic cycle, which often involves a conformational change or ligand binding/release. In order to determine individual rate constants within the reaction coordinate it is necessary to study the enzyme in the transient phase of the enzymatic reaction, before establishment of steady state conditions where the concentration of [ES] reaches equilibrium (**Figure 1.7**). For this purpose it is necessary to study the enzyme under single-turnover conditions and unlike steady state methods the concentration of enzyme [E] is usually greater than concentration of substrate [S].^{22,46}

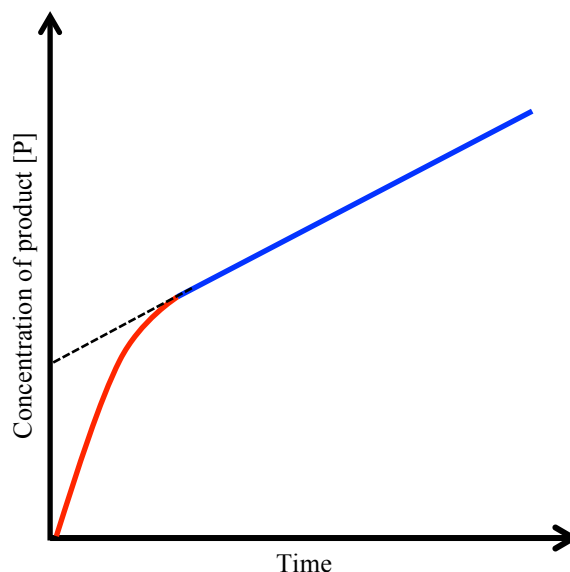


Figure 1.7: Curve showing transient phase of enzymatic reaction (red) as well as when the system has reached steady state conditions (blue), continuation of the steady state slope to the y axis (hashed line) gives an approximate concentration of enzyme in the experiment as at this point the system each single enzyme has completed one reaction.

1.5.1 Study of fast dynamics by stopped-flow.

In order to study KIEs involving the chemical step a method of rapid analysis is necessary. The stopped-flow technique allows for the rapid mixing of solutions for the study of reactions on a timescale of up to a few milli-seconds. This allows for the examination of pre-steady state kinetics in enzymes (**Figure 1.8**).²² In order to study a primary KIE in enzymatic reactions, isotopically labelled substrates need to be prepared.

Recently groups have also been measuring enzyme KIE to gain information on how fast dynamics influence the chemical step of catalysis. Enzymes are produced recombinantly in minimal media containing ‘heavy’ feedstocks such as ^{13}C -glucose. Rates of reaction catalysed by heavy enzymes (labelled with ^1H &/or ^{13}C &/or ^{15}N) can then be compared with the light isotopologue (natural abundance).⁴⁷ Heavy labelling is thought to effect vibrational and rotational motions without altering the electrostatic properties or potential energy surface.^{48,49}

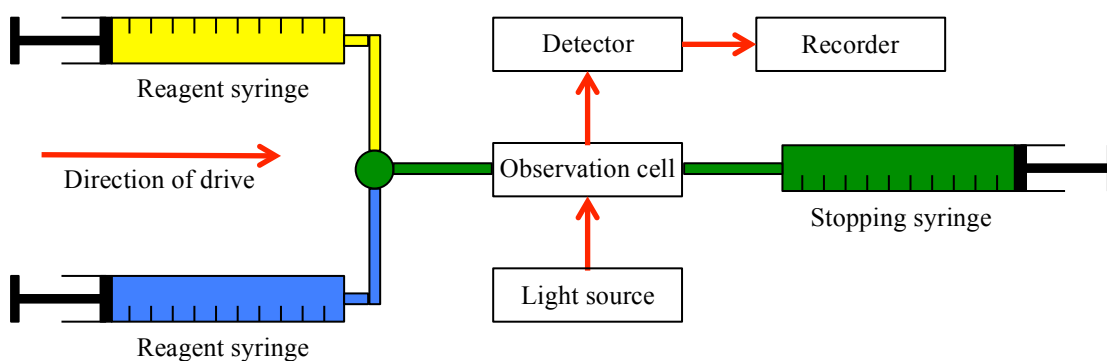


Figure 1.8: Simplified diagram of a stopped-flow spectrometer. Small amounts of solution are rapidly mixed *via* the application of force to the drive syringes. A sensor on the stopping syringe triggers the system to observe the reaction-taking place in the observation cell.

1.6 Dihydrofolate reductase (DHFR).

Dihydrofolate reductase (DHFR) catalyses the transfer of a hydride from the C4 position of NADPH to the C6, *Re* face of DHF, and protonation from water of the N5 position to form THF (**Figure 1.9**).^{50,51} Interestingly, a few DHFR variants are also able to reduce folate to DHF.⁵² DHFR has been used as a model enzyme to study the contribution of protein dynamics and conformational behaviour on catalysis.⁵³

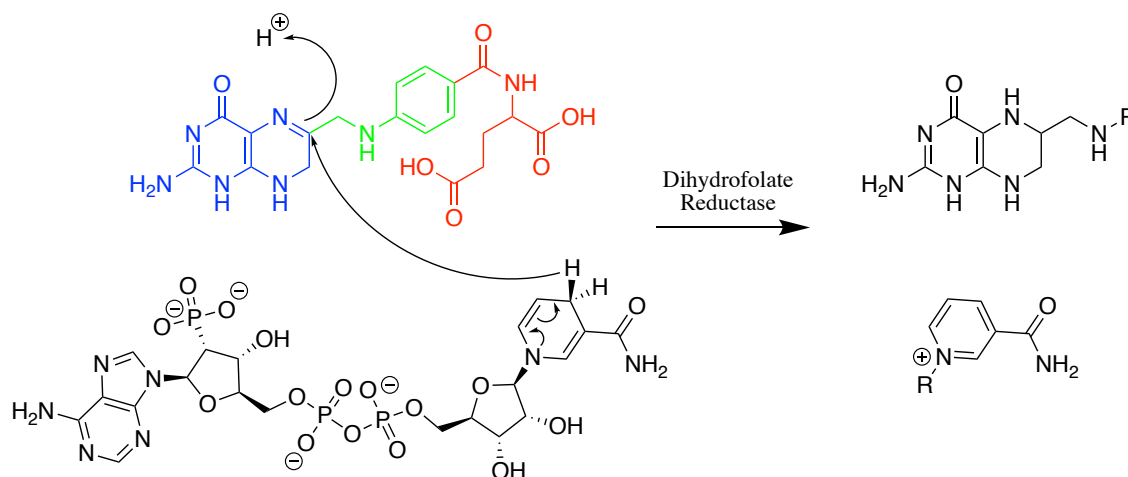


Figure 1.9: Reaction catalysed by DHFR, DHF is reduced to THF in the presence of NADPH. The structural parts of DHF are highlighted; pterin ring (blue), *P*-aminobenzoate (green) and glutamate (red).

THF partakes in a number of vital metabolic reactions as a carrier of activated one carbon units. THF is able to bond one-carbon units in various oxidation states to either

its N5 or N10 position (**Figure. 1.10**).⁹ Serine hydroxymethyltransferase catalyses the reversible transfer of a single carbon unit to THF, forming N^5,N^{10} -Methylene-tetrahydrofolate. Easy inter-conversion between the resulting one-carbon derivatives allows for a stable supply and demand relationship in which THF partakes in over 20 reactions including the systematic synthesis of deoxythymidine monophosphate (dTMP) and deoxyuridine monophosphate (dUMP), used in the synthesis of DNA and hence critical for cell replication.⁹ Consequently, over the last half century a number of drugs targeting DHFR in pathogens have been developed to block replication. These include Methotrexate (Anti-neoplastic), Trimethoprim (Anti-bacterial), Trimetrexate (Anti-fungal) and Proguanil (Anti-malarial).⁵⁴ A lack of dietary folate or Vitamin B9 can cause a range of health problems: neural tube defects in developing foetuses, reduced fertility, depression, anaemia and poor growth to list a few. As a consequence many countries now fortify particular foods with folic acid.⁵⁵⁻⁵⁷

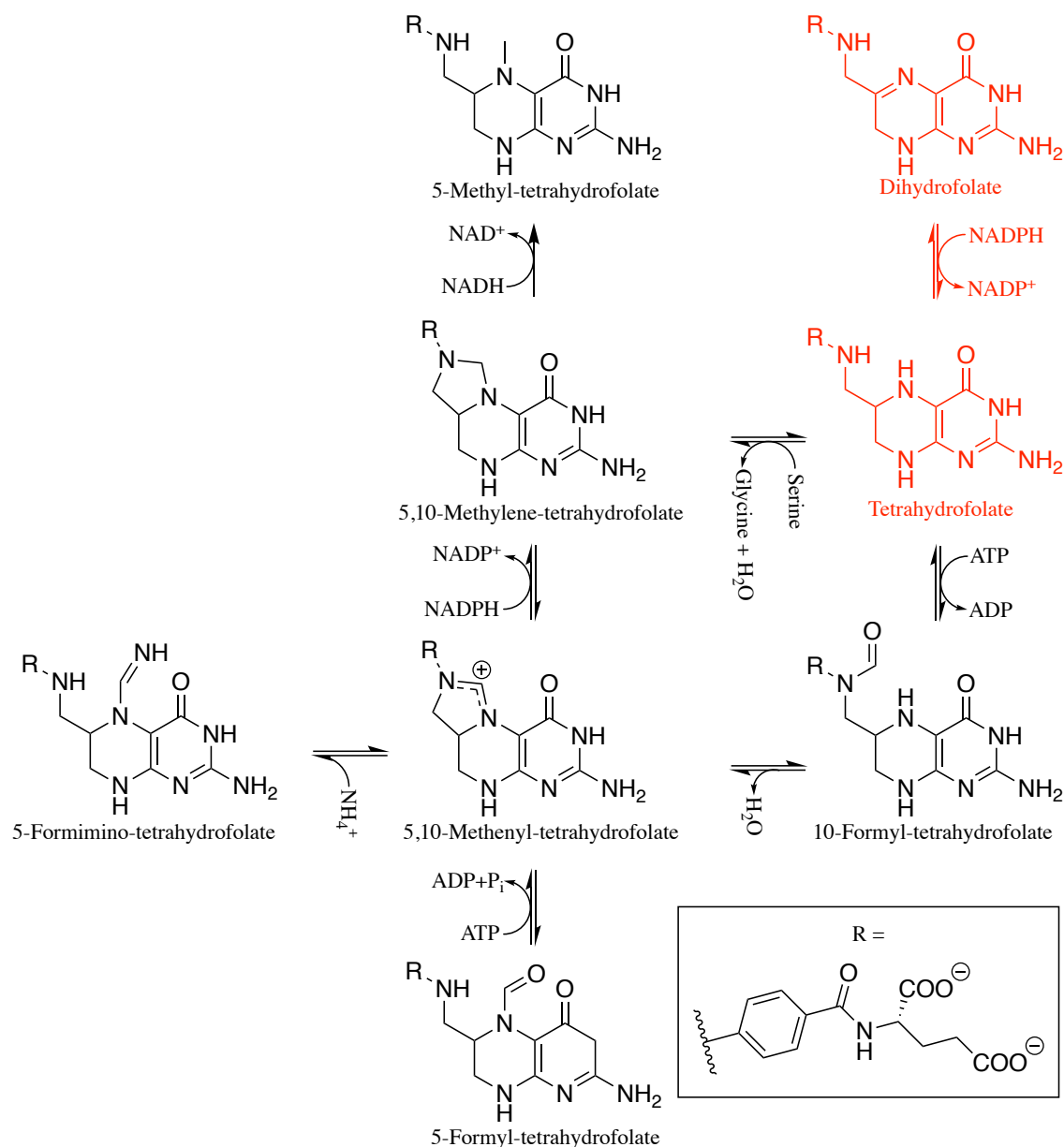


Figure 1.10: Redox transitions between various forms of tetrahydrofolate. The reaction catalysed by DHFR is highlighted in red, figure adapted from reference.⁹

1.7 The physical structure of DHFR with a focus on EcDHFR.

Over 340 structures have been published for various DHFRs with a diverse range of bound ligands (inhibitors, substrates and products) in the protein data bank.^{58,59} DHFRs can be considered as having three main sub-domains: the adenosine binding domain, the loop domain and the substrate-binding domain (**Figure 1.11a**). Dihydrofolate reductase from *Escherichia coli* (EcDHFR) has a core structure of the enzyme consists of an eight-stranded β -sheet; strands β A- β G run in parallel and strand β H is antiparallel and

encompasses the C-terminus. DHFR also contains 4 α -helices (labelled B, C, E and F) and four mobile loops: M20 loop (residues 10-24 with EcDHFR numbering), FG loop (residues 117-131) and the GH loop (residues 146-148) (**Figure 1.11b**).^{60,61} The nicotinamide ring of NADPH sits in a hydrophobic cleft between the β A and β E sheets. Folate and its derivatives bind between the α B and α C helices, the pterin ring is bent perpendicular to its benzoic acid moiety and is coplanar to the nicotinamide ring of NADPH.^{60,62}

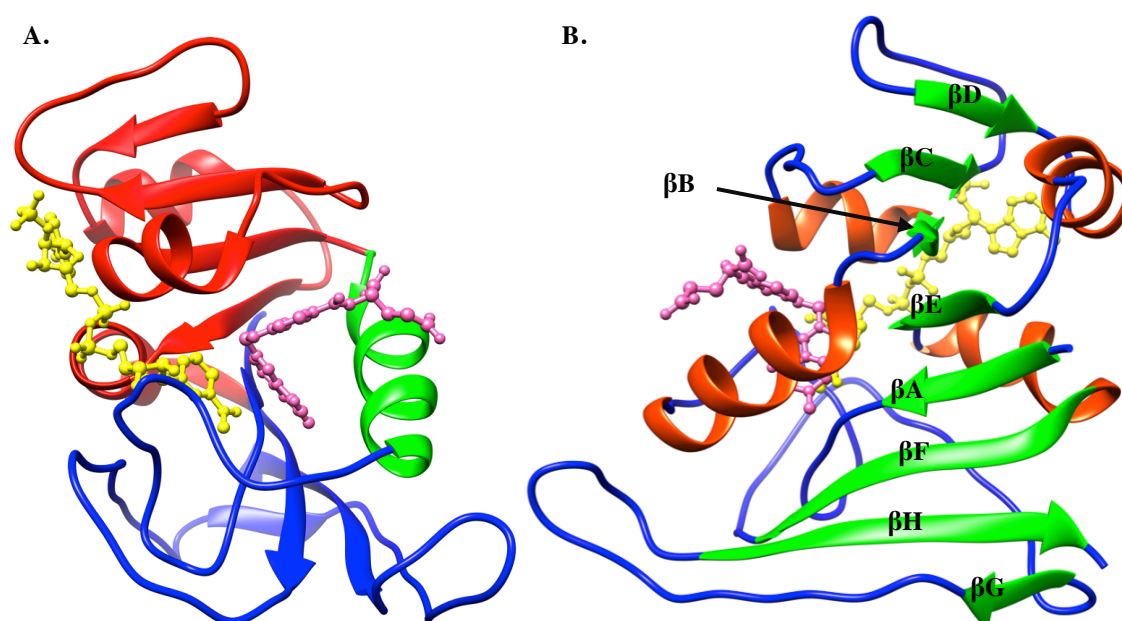


Figure 1.11: Two cartoon representations of EcDHFR (1RX2),⁶¹ both in complex with folate (pink) and NADP⁺ (yellow). **A.** The Three main domains are highlighted: Substrate binding domain (green), Adenosine binding domain (red) and the loop domain (blue). **B.** Highlighted are the important secondary structural elements: β -sheet (green), α -helices (red) and loops (blue).

1.8 The chemical step in EcDHFR.

All known DHFR variants have a single ionisable residue in their active site which is implicated in the protonation of the N5 position of DHF: aspartic acid in bacteria and glutamic acid in vertebrates.^{63,64} Asp27 is the only ionisable residue present in the active site of EcDHFR and as such it was deemed probable that it acts as the proton source in the protonation of the N5 position of DHF. Crystallographic structures however show that Asp27 forms a hydrogen-bonding network to the C2 and N3 position of the pterin ring of DHF, which is over 5 Å away from the N5 position. In order to explain how Asp27 is involved in protonation of the N5 position a number of papers have proposed a

keto-enol tautomerization mechanism. In this theory Asp27 stabilises an enol form of DHF, which in turn allows water held within in the active site to act as a proton source for the N5 position (**Figure 1.12**).^{65–69}

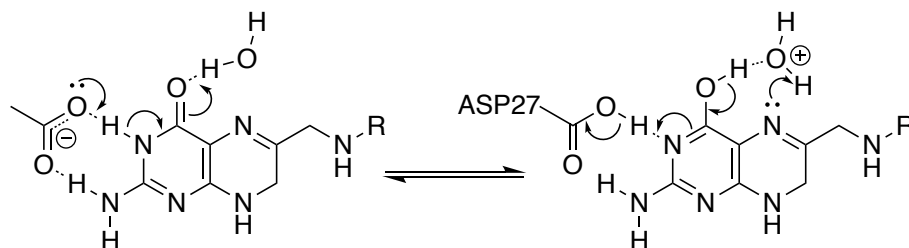


Figure 1.12: Proposed Keto-enol tautomerisation mechanism for protonation of the DHF N5 position, Asp27 indirectly protonates the N5 position.

However, no water molecule was previously observed adjacent to the N5 position of DHF in any crystal structures of the ternary complex (Site B), although a water molecule was observed between Asp27 and Try22 (**Figure 1.13**). A computational study by Shrimpton and Allemann in 2002 proposed that the mechanism involving keto-enol tautomerisation was not viable due to the bond angles and lengths being unfavourable for the protonation of the N5 position. Instead it was proposed rapid, subtle structural rearrangements allowed water trapped within the active site to move closer to the N5 position (site B).^{70,71}

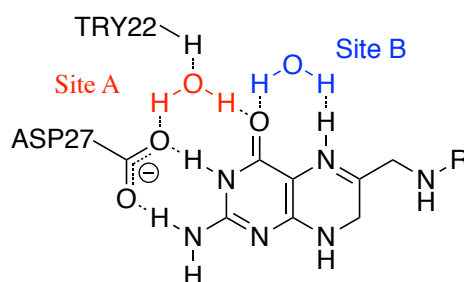


Figure 1.13: The two possible positions of water molecules inside the active site of DHFR relative to DHF. Site A is highlighted in red and site B highlighted in blue.

A high-resolution X-ray structure of EcDHFR in the Michaelis complex was solved by Wan *et al.* in 2014, which revealed the substrate, exists in the keto form with Asp27 carrying a negative charge. Moreover, it was found minor fluctuations in the M20 loop allowed water into site B, allowing for direct protonation of the N5 position of DHF, the

produced hydroxide stabilised by residues in the active site. This direct protonation mechanism means that formation of the enol form is not required.⁷² It is considered EcDHFR facilitates protonation at this position through elevation of the N5 pK_a from 2.6 to 6.5.⁶⁷ Recent work has provided evidence that protonation of the N5 position and hydride transfer from the C4 position of NADPH to the C6 position of DHF proceed independently of one another.⁷³

1.9 The catalytic cycle of EcDHFR.

Using ‘stopped flow’ spectroscopy, Benkovic and co-workers published the kinetic scheme of the catalytic cycle for EcDHFR, which was shown to have five major kinetic intermediates (**Figure 1.14**).⁵¹ The holoenzyme, E:NADPH first binds DHF to form the Michaelis complex E:NADPH:DHF. Following hydride transfer, the product ternary complex, E:NADP⁺:THF, is formed. The maximum measured rate for the chemical step is 950 s⁻¹ at pH 5.0, dropping to 220 s⁻¹ at pH 7.0. Above pH 9 it becomes rate limiting. The enzyme then releases NADP⁺ to form the product binary complex, E:THF. Rebinding of NADPH forms the product release complex, E:NADPH:THF, and precedes the release of THF to reform the holoenzyme E:NADPH. Under close to physiological conditions (pH 7) release of THF is the rate-limiting step (12 s⁻¹). At no point in the catalytic cycle is there any significant quantity of apo-EcDHFR.⁵¹

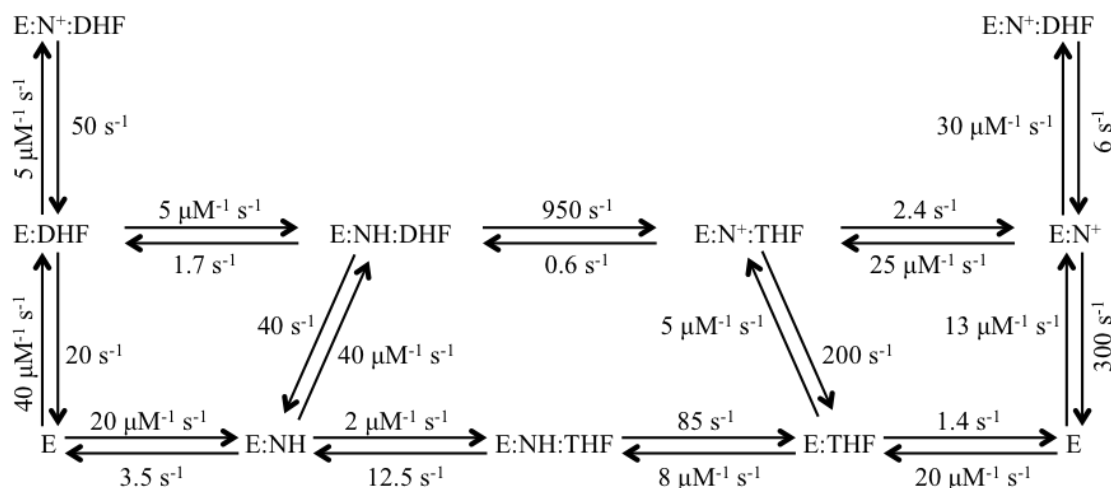


Figure 1.14: Kinetic scheme of catalysis by EcDHFR as determined by Benkovic *et al.*⁵¹

1.10 Motions involved in enzyme catalysis.

Enzymes are found to exhibit motions on massively different timescales. Motions that occur on a second to millisecond (ms) timescale are often considered slow in comparison to the rate of catalysis and largely consist of either large domain movements or loop motion (**Figure 1.15**). Motions, which occur on a nanosecond or lower timescale, are considered fast in comparison to the rate of catalysis and include such things as side-chain rotations. Bond-vibrations, which occur on a femto second timescale (10^{-15} s⁻¹), are dramatically faster than any other observed protein motion. In this thesis the term ‘dynamics’ will refer to motions occurring on a fast, femtosecond timescale.^{74,75}

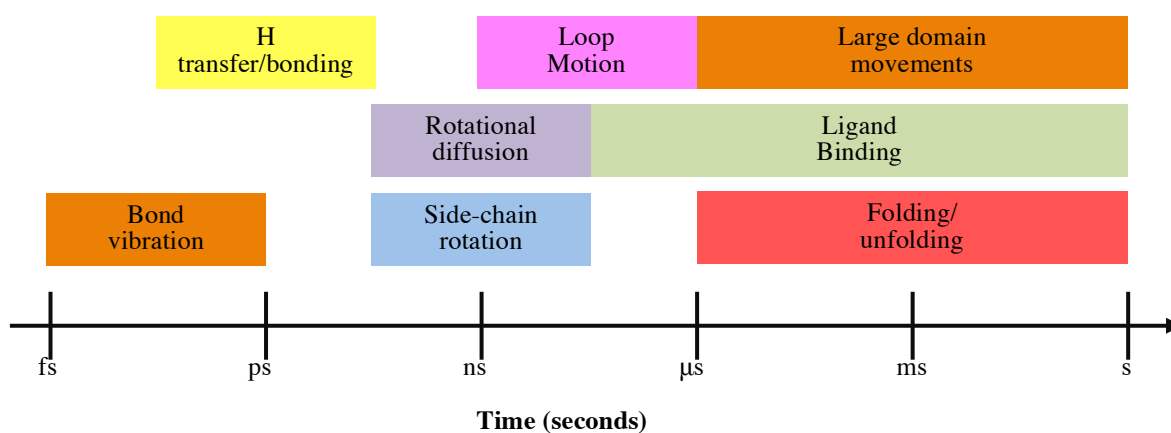
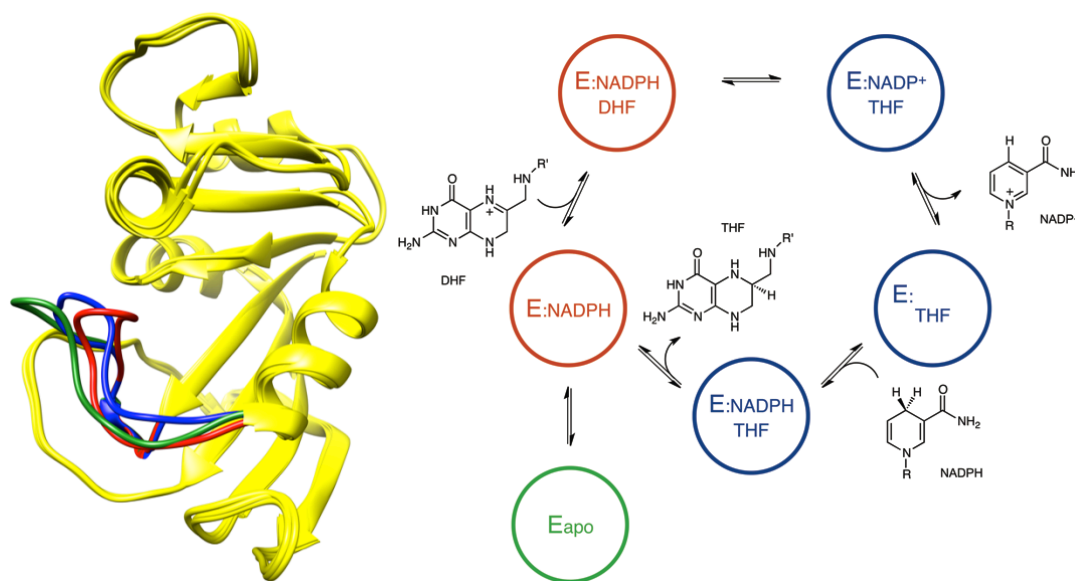


Figure 1.15: Timescale of protein motions.

1.11 Conformational behaviour and catalysis in DHFR.

EcDHFR as has three mobile loops: the FG loop (residues 116-132), the GH loop (142-149) and the M20 loop (9-24).⁶¹ During catalysis EcDHFR cycles predominantly through two main structural conformations, as defined by positions of the M20 loop (**Figure 1.16**).⁶¹ In the E:NADPH and Michaelis complex the enzyme adopts a closed conformation, with the M20 loop closed over the nicotinamide group of NADPH in the active site. Following the chemical step the enzyme switches to an occluded conformation, where residues in the M20 loop protrude into the active site, lowering the binding affinity of the product, NADP⁺.^{61,76} Although free EcDHFR is not observed during catalysis, crystallographic evidence shows the apo form to adopt an open/disordered conformation.^{51,61} Computational simulations propose that relatively small energy barriers separate the different conformational states of EcDHFR, and that binding of different ligands alters their relative stability resulting in conformational changes occurring concurrently with the catalytic cycle. Different conformational states being more or less thermodynamically favourable depending on bound ligands.⁷⁷ In the closed conformation residues in the M20 loop form a hairpin turn and an anti-parallel sheet, stabilised by a hydrogen-bonding network between Asn18 in the M20 loop and His45 in the α C helix. In this conformation Met16 and Glu17 are arranged in such a manner to allow nicotinamide binding.^{61,78} In the occluded conformation these residues move into the active site forcing the nicotinamide group out into solution.^{61,78} In EcDHFR residues Ser148 in the GH loop and Asn23 in the M20 loop stabilise an occluded conformation *via* hydrogen bonding interactions.⁶¹ Only in the closed conformation are the co-factor and substrate close enough to allow hydride transfer.^{79,80} The ability of EcDHFR to adopt an occluded conformation has been shown important for product release and, as such, efficient progress through the catalytic cycle.^{61,81}



Figures 1.16 & 1.17: (1.16) Cartoon representation of EcDHFR with the M20 loop highlighted in different structural conformations (Green = open/disordered, Blue = closed, Red = Occluded) (1.17) catalytic cycle of EcDHFR with each of the five kinetic intermediates highlighted with respect to the structural conformation adopted by EcDHFR (Green = open/disordered, Blue = closed, Red = Occluded).

Using NMR relaxation dispersion experiments Boehr *et al.* proposed an altered catalytic cycle to that shown in **Figure 1.17**. The new model proposed that the major kinetic intermediates, whose structures have all been observed *via* x-ray crystallography sample higher energy intermediates that effectively mimic the conformational structure of the following or past intermediate.⁸¹ Arguably, one of the most interesting findings of the work was that the Michaelis complex closed structure samples the ground state occluded structure of the product complex at a rate of $\sim 1200 \text{ s}^{-1}$. This is comparable to the rate of hydride transfer ($\sim 950 \text{ s}^{-1}$) and it was postulated that k_H and k_{cat} may be governed by physical structural changes.^{51,81} Following on from this, again using Carr-Purcell-Meiboom-Gill (CPMG) NMR relaxation experiments, it was postulated that release of THF from the active site is facilitated by the enzyme in the E:NADPH:THF complex rapidly probing an excited state that mimics the structural conformation of the E:NADPH complex. In this complex the pterin ring of THF is forced out of the active site to avoid steric clash with NADPH in the closed like structure. This in turn lowers the binding affinity facilitating product release (**Figure 1.18**).⁸²

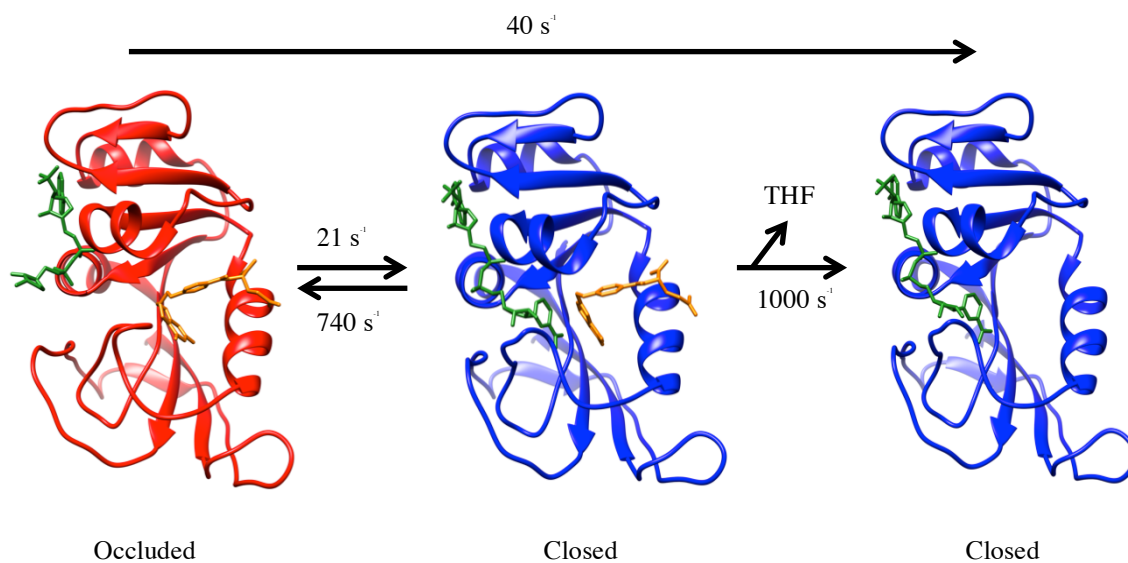


Figure 1.18: Cartoon representation of EcdHFR in the occluded (red), E:NADPH:THF complex rapidly probing a structural conformation similar to that of the closed (blue), E:NADPH complex to facilitate release of THF. NADPH is highlighted in green and folate derivatives in orange. The middle complex highlights how steric clash between substrates may lower binding affinities. The original rate measured by Benkovic *et al* is shown on top.

Conformational behaviour varies greatly between DHFR variants; previously EcdHFR was the only known DHFR variant to adopt an occluded conformation following the chemical step.⁸³ DHFR from *Moritella profunda* (MpDHFR) shares 55% sequence identity to EcdHFR and in terms of tertiary structure is near superimposable (R.M.S.D. of the atomic position of the C_{α} is calculated to be 0.878 Å).^{61,84} Like EcdHFR, the release of THF from the E:NADPH:THF complex is rate limiting at pH 7.0.⁷⁶ Crystallographic and NMR studies have shown that MpDHFR does not adopt an occluded conformation following the chemical step. The Ser148-Asn23 interaction, which stabilises the occluded conformation in EcdHFR, is knocked out in MpDHFR due to the equivalent Ser148 position being replaced with a proline residue.^{76,84} The lack of an occluded conformation is also true for DHFRs from *Lactobacillus casei* and *Bacillus anthracis* that respectively have an alanine and proline residue in place of Ser148.^{85–87} The mutant, EcdHFR-S148P showed no significant change to k_{off} for THF, however the binding affinity for NADP^{+} dramatically increased.⁷⁶ This resulted in the release of THF from the E:NADP⁺:THF complex rather than the E:NADPH:THF complex becoming the rate limiting step. The mutant, MpDHFR-P150S appeared to show evidence of adopting a second conformation and had a much lower binding

affinity for NADP^+ than wild type MpDHFR (**Table 1.2**).⁷⁶ It was concluded an ability to adopt an occluded conformation following the chemical step of catalysis lowered the binding affinity for NADP^+ , allowing for efficient progress through the catalytic cycle in the reaction catalysed by EcDHFR.⁷⁶ However, MpDHFR and EcDHFR exhibit similar K_M values for NADPH and k_{off} values for THF, suggesting MpDHFR does not circumvent the problem of not adopting an occluded conformation by lowering overall binding affinities for substrates. Instead, it is likely additional features in MpDHFR help facilitate release of NADP^+ , this likely explains why the IC_{50} value for NADP^+ for MpDHFR is much larger than for EcDHFR-S148P. Furthermore, EcDHFR and MpDHFR have similar single turnover rates at pH 7, showing that the inability to adopt an occluded does not have a deleterious effect on the overall rate of catalysis.⁷⁶

Enzyme	IC_{50} value for NADP^+ at pH 7
EcDHFR	820 +/- 59
EcDHFR-S148P	40 +/- 1
MpDHFR	170 +/- 11
MpDHFR-P150S	321 +/-12

DHFR from the hyperthermophile *Thermotoga maritima* (TmDHFR) is the only known homodimeric DHFR to exist. The equivalent residues of the FG loop in EcDHFR are locked into the dimer interface in TmDHFR, and as such it was thought TmDHFR remains in a fixed open conformation throughout its catalytic cycle.^{88,89} Restriction of flexibility in the M20 and FG loops in EcDHFR has shown to affect catalysis, and it is theorised that the much lower catalytic activity of TmDHFR can be attributed to its rigidity.⁹⁰ The fixed, open nature of the active site in TmDHFR prevents both modulation of the substrate pK_a by the residues in the M20 loop and expulsion of solvent from the active site during catalysis.^{89,91,92} As such, it is thought that the N5 position of THF is protonated directly from bulk solvent.^{92,93} The addition of CHAPS to the mutant TmDHFR-V11D resulted in formation of monomeric enzyme. Although no significant decrease in k_H was observed between TmDHFR-V11D and the native dimer, a decrease in k_{cat} was observed. It was concluded that the lower rates observed for TmDHFR in comparison to monomeric DHFRs, are not simply a result of increased rigidity but evolutionary pressure to select for modifications to the protein structure, which allow

for greater thermostability.⁹⁴ In order to further study the effects of dimerization, residues from the dimeric interface in TmDHFR were inserted into the equivalent positions in EcDHFR to create the dimeric mutant, Xet-3. Like TmDHFR, Xet-3 had increased thermostability compared to native EcDHFR, and reduced k_H and k_{cat} rate constants. However, unlike TmDHFR, it was concluded that the reduction in rate constants observed for Xet-3 were a consequence of reduced flexibility which facilitates efficient progression through the catalytic cycle in EcDHFR.^{94,95}

Bacterial DHFRs are usually poor in their ability to reduce folate.⁹⁶ Like mammalian variants, TmDHFR is able to reduce folate with a similar catalytic efficiency as DHF, reducing folate to THF without the release of DHF from the active site. It is likely the open nature of TmDHFR facilitates protonated folate.⁵² The specificity for folate can be increased in EcDHFR *via* the addition of avian loop regions, which is believed to restrict loop motion.⁹⁷

Mammalian DHFRs have also been found not to adopt an occluded conformation. Most have a proline rich region at the end of their equivalent M20 loops, decreasing the mobility of the M20 loop in comparison to the bacterial counterparts.⁹⁸⁻¹⁰⁰ DHFR from *Homo sapiens* (HsDHFR) exhibits no significant structural changes between the Michaelis and product complexes, in evidence gained from either crystallographic or NMR experiments.⁹⁹ It has previously been noted that mutants which hinder loop motions in EcDHFR drastically affects the efficiency of the enzyme.⁷⁶ NMR CPMG relaxation experiments also yielded no evidence of conformational behaviour on a millisecond timescale, unlike in EcDHFR where the enzyme rapidly probes structural conformations similar to the next or previous kinetic step.^{81,99} However, motions on the microsecond timescale were revealed and it is thought HsDHFR utilises such motions for ligand binding/release.⁹⁹ Ligand binding is therefore not facilitated by loop motion. Crystallographic evidence suggests movement of the adenosine binding domain closes the active site upon substrate binding. Further evidence of this movement has been found through NMR experiments.⁹⁹ Such hinge movements have also been observed in EcDHFR but accounts for only ~20 % of the movement observed in HsDHFR.^{61,99}

The double mutant EcDHFR-N23PP/S148A was designed to incorporate the proline rich region found in mammalian DHFR and knock out the stabilising effects of the

Ser148-Asn23 interaction.⁹⁸ The mutant reported a significant reduction in k_{cat} as well a change in the rate limiting step from dissociation of THF to dissociation of NADP^+ .⁹⁸ The single mutant, EcDHFR-S148A reported a similar rate for k_{H} but release of THF from the E: NADP^+ :THF product complex became rate limiting rather than release from the E: NADPH :THF mixed ternary complex.⁷⁶ However, further work has shown that the insertion of a single alanine residue into this part of the protein sequence in EcDHFR prevents formation of an occluded conformation and a reduction of motions on an associated timescale. It has been theorised that the extra residues in this region influences millisecond motions more than proline content. In contrast, the extra residues in this position are thought to improve flexibility on a microsecond timescale.⁹⁹

It has been found that the ratio of NADP^+ : NADPH concentrations in mammalian and bacterial cells are significantly different (1:100 and 1:1 respectively).⁹⁹ Furthermore IC_{50} values for inhibition by NADP^+ are much lower in HsDHFR (620 μM) than in EcDHFR (5 mM).⁹⁹ It has, therefore, been postulated that the occluded conformation in EcDHFR may be a mechanism for the enzyme to modulate co-factor binding affinities, allowing for efficient progress through the catalytic cycle by mitigating possible product inhibition effects.^{76,98}

1.12 Role of fast dynamics in catalysis.

Enzymes where the rate-limiting step is substrate diffusion are often regarded as ‘perfect’ enzymes.^{45,101} ‘Perfect’ enzymes such as carbonic anhydrase or catalase have turnover rates as high as 10^6 s^{-1} .⁴⁵ Using unbiased transition path sampling methods the length of transition states has been calculated for DHFR (10^{-15} s), lactate dehydrogenase (LDH) (10^{-15} s) and purine nucleoside phosphorylase (PNP) (10^{-14} s), this is on the same timescale as bond vibrations which occur on a femtosecond timescale.¹⁰² As transition states occur for only small periods of time, direct characterisation of them through experimental observations is essentially impossible, instead computational methods are used to model the transition state structures.^{103,104} It is widely accepted that physical events such as ligand binding/release may in part be controlled by loop or domain motion.^{47,76,81,105,106} However, whether motions on fs-ps timescale couple to the chemical step is still a contentious issue. There have been a number conflicting reports on how or if such motions influence the chemical step of catalysis.⁴⁷

It has been proposed that a network of residues in EcDHFR influence catalysis by forming a network of protein promoting motions (**Figure 1.19**).¹⁰⁷ Mutation of Gly121 in EcDHFR, located ~19 Å away from the active site, results in a drastically diminished rate of hydride transfer (400 fold).^{65,108} MD simulations postulated a disruption in the coupling of backbone dynamics to the rate of hydride transfer, which in turn was claimed to promote barrier crossing.¹⁰⁹ To identify the residues in this proposed network, sequence analysis was performed amongst 36 DHFR variants, which yielded a number of residues that were highly conserved. It was explicit that these residues may be important for catalysis and possibly participate in this proposed network of coupled motions.¹⁰⁹ Mutation of distal residues, Met42 and Gly121 negatively impacted the rate of hydride transfer and, alongside computational analysis, a theory was put forward of promoting protein motions that increase, the rate of hydride transfer by promoting barrier crossing.^{107,109,110}

Stopped-flow experiments have been used extensively to study dynamics in DHFR variants as they are believed to mainly report on hydride transfer. At pH 7.0, however, results can be complicated by small contributions from physical events.¹¹¹ At elevated pH values the rate of hydride transfer becomes rate limiting and as such the small contributions from physical events become lessened.⁵¹ It needs to be considered however, that at elevated pH values the conformational behaviour and protonation states of residues in the protein may be altered.^{111,112} At pH 9.0 the double mutant EcDHFR-G121V/M42W showed a much greater temperature dependence of the KIE than both the single mutants combined. It was proposed this was a synergistic effect that confirmed the theory of promoting motions.³⁶ Through bioinformatics, Phe125 and Trp133 were proposed to also be part of this promoting network.¹¹³ Mutation of Phe125 showed increased temperature dependence with respect to KIE at pH 9.0 and as such it was proposed this residue part of the network that facilitates promoting motions. The EcDHFR-Trp133 mutant on the other hand showed characteristics similar to wild type enzyme so was eliminated.¹¹³

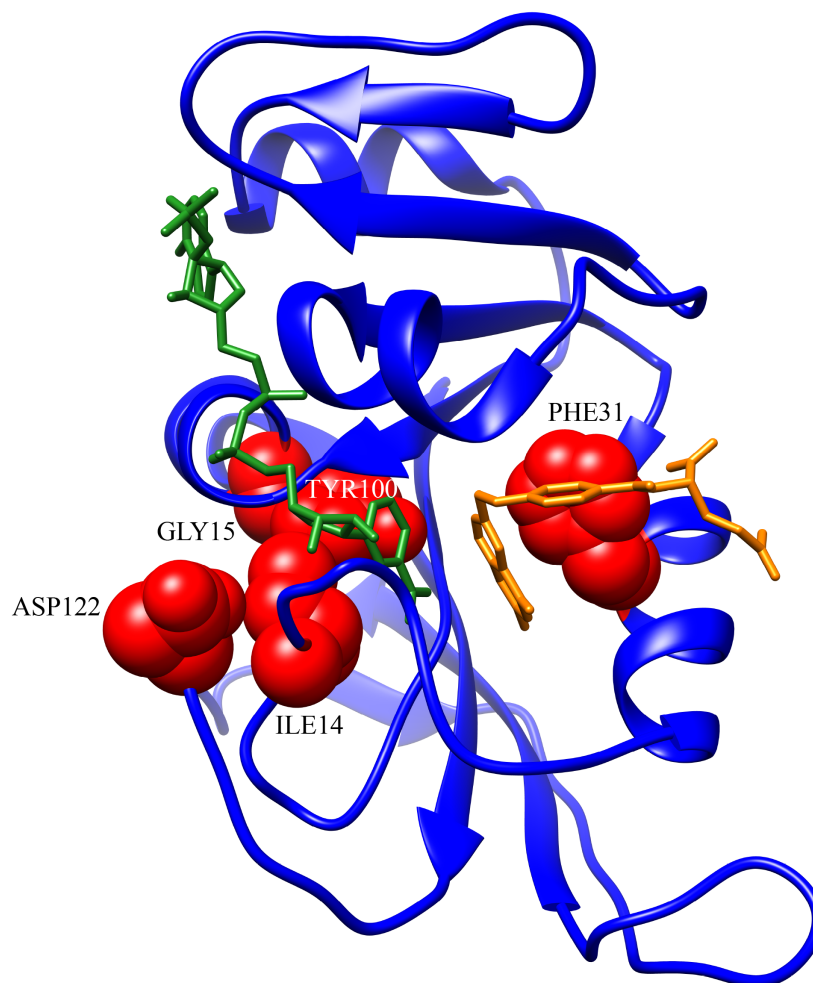


Figure 1.19: The network of promoting motions proposed in EcDHFR, highlighted in red are the partaking residues, ASP122, GLY15, ILE14, TYR100 and PHE31 and NADPH (green) and DHF (orange) as proposed by Agarwal *et.al.*¹⁰⁷

Computational studies of the G121V mutant indeed showed an increase in the energy barrier.¹¹⁴ However, no crystal structure of the G121V mutant existed so the isopropyl side chain was modelled onto the backbone of the original glycine residue.¹¹⁴ Further MD simulations revealed a decrease in stability and folding properties of the enzyme.¹¹⁵ The study implied the massive decrease in the single turnover rate could be explained by diminished stability of the tertiary structure and not by an interruption of long-range coupling.¹¹⁵ This is likely due to the valine side-chain causing steric clash, destabilising the closed conformation as it points into the active site.^{61,115,116}

1.13 Enzyme KIE.

A lot of evidence regarding dynamics in EcDHFR is based upon hydride transfer KIE in either WT or mutant enzymes. Recent work has utilised isotope labelling to create isotopologues of enzymes, which have then been studied *via* stopped flow methodologies to gain insights into enzyme dynamics.^{48,49,53,79,117} By producing enzymes in labelled media (²H₂O, ¹³C, ²H-glucose & ¹⁵N ammonium chloride), it is possible to increase the weight of the enzyme by around 10 % and achieve incorporation rates of up to 98 %. It is generally considered that heavy labelling of enzymes slows the vibrational behaviour of the bond without impairing the electrostatics of the enzyme.^{48,118} Enzyme KIEs are calculated using **Equation 1.10**.

$$Enzyme\ KIE = \frac{k^{LE}}{k^{HE}}$$

Equation 1.10: where k^{LE} and k^{HE} are the rate constants for the light and heavy enzymes respectively.

In order to effectively quantify effects observed in the study of enzyme KIE, analysis of dynamic contributions to the chemical step were calculated using a modified form of variational TST (VTST) developed by Truhlar *et al.*, **Equation 1.11**. The correction factor $\Gamma(T)$ accounts for dynamic and tunnelling effects and can be expressed as in **Equation 1.12**.⁴⁴

$$k = \Gamma(T) \frac{k_B T}{h} e^{\frac{\Delta G_{act}^{QC}}{RT}}$$

Equation 1.11: k_B is Boltzmann's constant, T is temperature in kelvins, R is the gas constant, h is Planck's constant, $\Gamma(T)$ is the correcting factor which accounts for both dynamics and tunnelling effects and is temperature dependant. ΔG_{act}^{QC} is the quasiclassical free energy.

$$\Gamma(T) = \gamma(T) \times \kappa(T)$$

Equation 1.12: Description of the correcting factor $\Gamma(T)$. $\gamma(T)$ is the dynamic recrossing coefficient and accounts for unsuccessful reaction trajectories. $\kappa(T)$ is the contribution from tunnelling.

Initial studies with heavy-EcDHFR reported a slightly inverse $k_{H/D}$ KIE which increased over the measured temperature range to a value of 1.15 near physiological temperatures.⁷⁹ Analysis of this result using models based on VTST developed by Truhlar *et al.* and backed up by computational simulations showed no significant differences in either activation energies or tunnelling contributions between the light and heavy enzymes.^{44,79} This initial study proved controversial as it gave evidence that promoting protein motions may not be significant in driving catalysis at a chemical level.⁷⁹ The mutant EcDHFR-N23PP/S148A has previously been shown to have reduced conformational behaviour in comparison to WT-EcDHFR, resulting in a decrease in the steady state rate constant, k_{cat} . However it was further reported to also lower the rate of k_H and it consequently was claimed as evidence of coupling of large-scale motions to the chemical step.⁹⁸ At pH 7.0 at 25 °C the N23PP/S148A mutant exhibited an enzyme KIE of ~1.33 compared to ~1.13 of the WT enzyme. Although the mutant is known to have diminished flexibility on a millisecond timescale, QM/MM simulations showed residues located in the active site were more mobile in the mutant on a femtosecond timescale. This was the first report which suggested increased coupling of dynamics to the chemical step could be detrimental to the chemical step.^{79,119}

Enzyme KIE was also measured over a temperature range of 5-45 °C for the thermophilic enzyme, *Bacillus stearothermophilus* DHFR (BsDHFR). Interestingly, at near physiological temperatures the KIE was ~1, where at 5°C the KIE had increased to ~1.70. Similarly, variational TST suggested BsDHFR has increased flexibility on timescales associated with the chemical step in comparison to EcDHFR. As in the case of the EcDHFR-N23PP/S148A mutant this lead to increased non-viable reaction trajectories, the heavier isotopologue being more susceptible to dynamic re-crossing events.¹²⁰ Heavy KIE for MpDHFR has also been reported, at 5 °C the KIE is 1.07. As the temperature increases and the enzyme moves away from physiological temperature the KIE increases up to ~1.5.⁴⁷ MpDHFR, EcDHFR and BsDHFR all follow a similar trend with respect to temperature dependence of the enzyme KIE, which approaches unity at near physiological temperatures. It has been suggested that as an enzyme nears physiological temperatures dynamic coupling to the reaction coordinate becomes minimised (**Figure 1.20**).^{53,79,119}

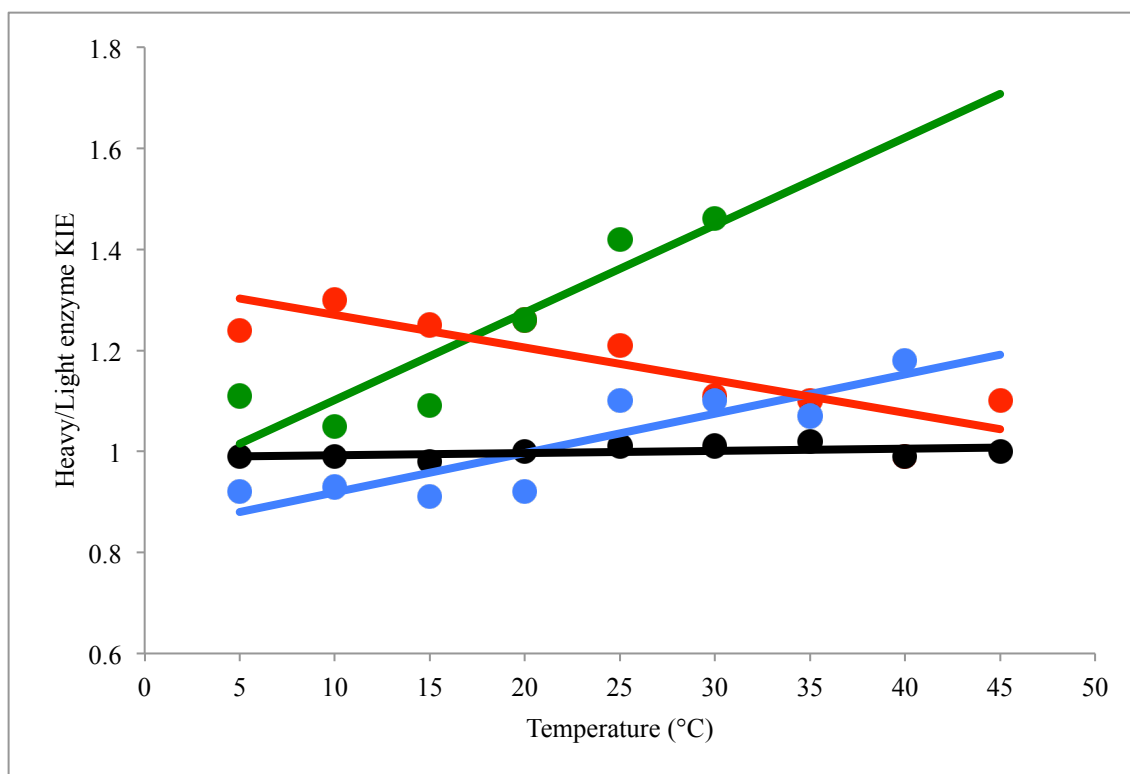


Figure 1.20: Graph showing the enzyme KIE of various DHFR variants over a temperature range. EcDHFR = Blue, MpDHFR = green, BsDHFR = red and TmDHFR = black. Values taken from references.^{47,79,121}

TmDHFR reported a different trend to other DHFR variants with respect to enzyme KIE. No significant KIE was observed between light and heavy TmDHFR with respect to single turnover rate constants across the measured temperature range (5-65 °C). This suggests motions occurring on the timescale of bond-vibrations do not influence the chemical step. Evidence from the EcDHFR-N23PP/S148A mutant suggested dynamics might negatively influence catalysis. Evidence from TmDHFR further suggests evolutionary pressure has minimized active site dynamics in DHFR enzymes to help lower the chances of non-viable reaction trajectories.¹¹⁷

2

Materials & Methods

2.1 Materials

^{13}C glucose, ^{15}N ammonium chloride, D_2O and indole ($2\text{-}^{13}\text{C}$) were purchased from Cambridge Isotope laboratories. L-methionine-(*methyl*- ^{13}C) along with all other reagents were purchased from Sigma-Aldrich.

2.2 Media and buffers

2.2.1 Lysogeny broth (LB)

LB liquid medium was prepared by dissolving tryptone (10 g), yeast extract (5 g) and sodium chloride (10 g) in 1000 ml *ddH*₂O. The media was sterilised by autoclaving at 121 °C for a period of 20 minutes.

LB solid plates were prepared in the same way as LB liquid except for the addition of agar (15 g L⁻¹) prior to autoclaving. Antibiotics, if required, were added to the molten agar solution once it had cooled to approximately 50 °C. The agar solution was then aseptically poured into 100 mm Petri dishes.

2.2.2 M9 minimal media

M9 media was prepared by dissolving Na_2HPO_4 (6.78 g), KH_2PO_4 (3 g) and NaCl (0.84 g) in 800 ml of *ddH*₂O. The pH was adjusted to 7.5 and sterilised by autoclaving at 121 °C for a period of 20 minutes. NH_4Cl (1 g), D-glucose (4 g), 1M MgSO_4 solution (2 ml) (section 2.2.2.1), 1M CaCl_2 solution (100 μL) (section 2.2.2.2) and trace elements solution (section 2.2.2.3) was then added and the final volume made up to 1000 ml with *ddH*₂O.

2.2.2.1 Preparation of 1M MgSO_4 solution

Magnesium sulphate (12.04 g) was dissolved into 100 mL of *ddH*₂O and sterilised by autoclaving at 121 °C for a period of 20 minutes.

2.2.2.2 Preparation of 1M CaCl_2 solution

Calcium chloride (11.10 g) was dissolved into 100 mL of *ddH*₂O and sterilised by autoclaving at 121 °C for a period of 20 minutes.

2.2.2.3 Preparation of (100x) trace elements solution

EDTA (5 g) was dissolved into 800 mL of ddH₂O and the pH adjusted to 7.5 with NaOH. FeCl₃-6H₂O (0.83 g), ZnCl₂ (84 mg), CuCl₂-H₂O (13 mg), CoCl₂-2H₂O (10 mg), H₃BO₃ (10 mg) and MnCl₂-4H₂O (1.6 mg) were then added and the final volume made up to 1000 mL. The solution was then passed through a 0.2 µm filter to sterilise.

2.2.3 Use of Ampicillin (Antibiotic)

Ampicillin (1 g) was dissolved into 10 mL of sterile ddH₂O. 1 mL of this solution was used per 1 L of culture where required.

2.2.4 Preparation of sterile solutions

Buffers/solutions were largely sterilised *via* autoclave (121 °C for 15 minutes). Where this was not suitable solutions were passed through a disposable, sterile bottle top filter (0.2 µM).

2.2.5 Buffers used

Table 2.1: Preparations of buffers used in this work.				
Code Name	Purpose	Buffering Agents	Salt(s)	Reducing agents /other
A	(SDS-PAGE) (Resolving)	1.5 M Tris-HCl, pH 8.8	-	-
B	(SDS-PAGE) (Stacking)	0.5 M Tris-HCl, pH 6.8	-	-
C	Purification (BSD75)	50 mM Trizma, pH 7.0	1 mM NaCl	10 mM β ME
D	Purification (BSD75/QSEPH)	50 mM potassium phosphate, pH7.0	-	15 mM β ME
E	Purification (QSEPH)	50 mM potassium phosphate, pH7.0	1 M NaCl	15 mM β ME
F	Purification (BSD75/QSEPH)	50 mM potassium phosphate, pH 8.0	-	15 mM β ME
G	Purification (QSEPH)	50 mM potassium phosphate, pH 8.0	1 M NaCl	15 mM β ME
H	Purification/ Kinetics/ Exchange buffer	50 mM potassium phosphate, pH 7.0	100 mM NaCl	15 mM β ME
I	Nickel column	50 mM Tris, pH 7.5	-	15 mM β ME, 20 mM Imidazole
J	Nickel column	50 mM Tris, pH 7.5	-	15 mM β ME, 20 mM Imidazole
K	Nickel column	50 mM Tris, pH 7.5	-	15 mM β ME, 20 mM Imidazole
L	Exchange buffer (HIS-TEV)	50 mM Tris, pH 8.0	-	2 mM TCEP
M	Purification (NADH/NADPH)	20 mM Tris, pH 9.0	-	-
N	Purification (NADH/NADPH)	20 mM Tris, pH 9.0	1 M NaCl	-
O	(SDS-PAGE) running buffer	25 mM Tris	-	200 mM glycine, 3.5 mM SDS
P	50x TAE buffer	2 M Tris	50 mM Disodium EDTA	1M glacial acetic acid
Q	MTEN buffer	25 mM Mes, 50 mM Tris, 25 mM ethanolamine	100 mM NaCl	10 mM β ME

2.2.5.1 P1 re-suspension buffer

606 mg of Trizma[®] base (50 mM) and 292 mg of EDTA (10 mM) was dissolved in 100 mL of ddH₂O and the pH adjusted to 8.0 with HCl. 10 mg RNase A was added and the solution stored at 4 °C until needed.

2.2.5.2 P2 lysis buffer

800 mg NaOH (200 mM) and 2.88 g of SDS (100 mM) was dissolved in 100 mL of ddH₂O.

2.2.5.3 N3 neutralisation buffer

40.12 g of guanidine chloride (4.2 M) and 8.83 g of potassium acetate (0.9 M) was dissolved in 100 mL of ddH₂O and the pH adjusted to 4.8.

2.2.5.4 PE wash buffer

121 mg of Trizma[®] base was dissolved in 20 mL 100 mM of ddH₂O and the pH adjusted to 4.8 before the final volume was made up to 100 mL with ethanol.

2.3 Methods

2.3.1 E.coli strains used

2.3.1.1 Preparation of calcium competent cells

Cells from a frozen glycerol stock were streaked out, aseptically, onto an antibiotic free LB agar plate (section 2.2.1) and incubated overnight at 37 °C. A starter culture was prepared from a single colony and grown in 10 mL LB media overnight at 37 °C. LB media (1 L) was then inoculated with starter culture and grown in a shaker at 37 °C until an O.D.₆₀₀ of 0.5 was achieved. The cells were centrifuged (3400 g for 15 minutes at 4 °C). The supernatant was discarded and the cell pellet re-suspended in 100 mL 100mM MgCl₂. The cells were harvested by centrifugation (3400 g for 15 minutes at 4 °C), the supernatant discarded and the cell pellet re-suspended in 200 mL of ice-cold 100 mM CaCl₂. The suspension was incubated on ice for 20 minutes. The cells were harvested by centrifugation (3400 g for 15 minutes at 4 °C) and re-suspended in 2 mL ice-cold 100 mM CaCl₂ and 15% glycerol. The suspension was

then aliquoted (50 μ L) into sterile 1.5 mL micro-centrifuge tubes, flash frozen with N₂ and stored at -80 °C for future use.

2.3.1.2 Expression strains

For large-scale protein expression BL21 Star™ (DE3) chemically competent cells were used (as prepared in section 2.3.1.1)

2.3.1.3 Cloning strains

For expression of plasmid DNA chemically competent XL1-Blue or DH5 α cells (as prepared in section 2.3.1.1)

2.3.2 Transformation protocol for chemically competent cells

A 50 μ L aliquot of chemically competent cells (section 2.3.1) was defrosted on ice. Approximately 50 ng/ μ L plasmid DNA was added (2 μ L) and the cells kept on ice for 30 minutes. The cells were heat shocked (42 °C for 45 seconds) and returned to ice for 30 minutes. Pre-heated LB media (1 mL) was added and the cells incubated for a period of 60 minutes at 37 °C. The cells were spun down (3400g for 10 minutes) and the majority of the supernatant removed. The resulting pellet was then re-suspended in approximately 50 μ L supernatant and plated onto LB-Agar plates containing the appropriate antibiotic.

Name	Vector	Selective marker	Source
WT EcDHFR	pET-28a	Ampicillin	Allemann group plasmid Library
WT MpDHFR	pET-28a	Ampicillin	
WT TmDHFR	pET-28a	Ampicillin	
WT SeDHFR	pET-11b	Ampicillin	Produced for this study
S150A-SeDHFR	pET-11b	Ampicillin	
WT SaLDH	pET-11b	Ampicillin	

2.3.3 Plasmid purification

Plasmid purification was carried out following the methodology detailed by QIAGEN[®]. A single colony from a selective plate was added to 5 mL LB media in a 30 mL Sterilin[™] universal container, and incubated overnight at 37 °C with shaking. The culture was pelleted (3400 g for 10 minutes), and re-suspended in 250 µL P1 buffer. P2 buffer (250 µL) was added and the suspension inverted 6 times to ensure proper mixing. After 3 minutes, 350 µL N3 buffer was added, and the solution again inverted 6 times before being centrifuged (24300 g for 10 minutes). The supernatant was applied to an Econospin[®] all in one mini spin column. The solution was centrifuged (24300 g for 5 minutes), and the flow through was discarded. PE buffer (500 µL) was added and again centrifuged (24300 g for 1 minute), the flow through again discarded. Plasmid DNA was eluted by the addition of 50 µL *ddH*₂O and again centrifuging (24300 g for 1 minute), collecting the solubilised DNA in a sterile 1.5 mL micro-centrifuge tube.

2.3.4 PCR protocol

PCR reactions were performed using Primestar[®] HS (premix) from Takara BIO INC. 25 µL of Primestar[®] HS (premix) was combined with 0.5 µL of forward and reverse primers (diluted to 10 µM), approximately 50 ng template DNA and 23.5 µL *ddH*₂O in a PCR tube. PCR reaction conditions are detailed in **Table 2.3**. The reactions were carried out in a Techne touch gene gradient thermal cycler.

Table 2.3: PCR conditions used		
Step	Temperature (°C)	Time
Initial denaturation	98	2 minutes
30 Cycles	98	10 seconds
	55	15 seconds
	72	1 minute/Kb
Final extension	72	5 minutes
End	4	Hold

PCR products were incubated with 1 μ L FastDigest Dpn1 for 20 minutes at 37°C and directly transformed into suitable cloning strains.

2.3.4.1 Primer design

Below are detailed the primers used, underlined are changes respective to original base pair.

SeDHFR_S150A;

5'-GCGGACGATAAGAACGCGTTATGCGTGCGAGTTTG-3'

5'-CAAACTCGCACGCATACGCGTTCTTATCGTCCGC-3'

2.3.5 DNA sequencing

The concentration of purified DNA from an appropriate cloning strain was measured by NanoDrop 1000 and sent for sequencing to Eurofins genomics.

2.3.6 Protein production

A single colony from a selective plate was used to inoculate 10 mL LB media with the appropriate antibiotic and incubated overnight in a shaker at 37 °C. This was used to inoculate 1000 mL of LB media with antibiotics and incubated in a shaker at 200 rpm at 37 °C until O.D.₆₀₀. Gene expression was induced with IPTG (1 mM) and the culture left at 16 °C overnight with shaking at 200 rpm. Cells were harvested *via* centrifugation (3400 g for 15 minutes at 4 °C). Pelleted cells were either used immediately or stored at -80 °C for future use.

Heavy enzyme (¹³C & ¹⁵N) for use in kinetic experiments was over-produced in the same way except LB was substituted for minimal media (M9). The recipe is described in section 2.2.2 but ¹³C-glucose and ¹⁵N ammonium chloride were substituted in place of natural abundance feedstock.

2.3.7 Protein purification

Pelleted cells were re-suspended in lysis buffer and sonicated for a total of 15 minutes (5 seconds on, 10 seconds off cycle). Cell debris was removed *via* centrifuge (24300 g

for 30 minutes), the supernatant passed through a 0.2 μ M filter and purified by one of the methods below:

2.3.7.1 Purification via Ni-NTA agarose affinity column

LDH was synthesised with 6x histidine tag and a TEV cleavage site on the N-terminus. TEV protease was also synthesised with a 6x histidine tag on the C-terminus. As such they were purified *via* a Ni-NTA affinity column. Protein was prepared as above (section 2.3.2, in buffer I) and loaded onto a pre-charged, 5 mL Ni-NTA agarose column. Protein was eluted using a step-wise gradient as described in (**Table 2.4**). Various concentrations of imidazole in elution buffers were prepared by mixing of buffers I,J and K. TEV protease was used without further purification. The 6x histidine tag on LDH was removed by incubating with TEV protease overnight at 4 °C. LDH was then purified again by Ni-NTA agarose column. Protein purity was confirmed by SDS-PAGE.

Table 2.4: Concentrations of Imidazole used in the purification of LDH and TEV protease.		
Fraction	Conc. Imidazole (mM)	Fraction size (mL)
1	20	100
2	50	10
3	50	10
4	100	10
5	150	10
6	200	10
7	250	10
8	250	10
9	500	10
10	500	100

2.3.7.2 Purification via Q-sepharose anion exchange

Proteins were prepared as in section 2.3.2. The clarified lysate was loaded onto a 70 mL Q-sepharose column. The column was washed with 3 column volumes of low salt buffer (buffer D or E). Protein was eluted with a salt gradient from 0 % NaCl to 100

% NaCl (buffer E or G) over 3 column volumes. Exact buffer conditions for various proteins can be found in (**Table 2.5**). Purity of proteins was determined by SDS-PAGE.

Table 2.5: Buffer conditions used in the purification of enzymes.			
Protein	Lysis buffer	Low salt buffer	High salt buffer
EcDHFR	D	D	E
MpDHFR	D	D	E
SeDHFR WT and S150A	F	F	G

2.3.7.3 Purification via BSD75 size exclusion

Proteins were concentrated in a 50 mL Amicon[®] stirred cell protein concentrator fitted with a 10 MWCO membrane to an approximate volume of 5 mL. The concentrate was loaded onto the column and eluted with an isocratic gradient. The exact buffer conditions are recorded in (**Table 2.6**).

Table 2.6: Exact buffer conditions used in the purification of enzymes (BSD-75).	
Protein	Buffer
EcDHFR, MpDHFR and SeDHFR	D
TmDHFR	C

2.3.8 Enzyme concentration

Enzyme concentration was measured by one of two ways;

2.3.8.1 Concentration from Bradford assay

Bradford reagent was prepared by dissolving 50 mg coomassie brilliant blue G-250 in 50 mL methanol. 100 mL 85 % (w/v) phosphoric acid was added and the total volume made up to 1000 mL with *ddH*₂O. To remove precipitants, the solution was passed through Whatman #1 filter paper. The solution was stored at 4 °C in actinic glass. Known concentrations of BSA solution were incubated with Bradford reagent to create a calibration curve, from which protein of unknown concentrations could be measured.

2.3.8.2 Concentration from UV

20 μL of enzyme solution was added to a 1 mL, 1 cm^{-1} path length quartz cuvette and the absorbance measured at 210 nm, 215 nm and 220 nm on a Shimadzu UV-2600 UV-Vis spectrophotometer. Protein concentration was determined using **Equations 2.1 & 2.2**.

$$\text{Conc (mg/mL)} = \left(\frac{\frac{A_{210}}{\epsilon_{210}} + \frac{A_{215}}{\epsilon_{215}} + \frac{A_{220}}{\epsilon_{2120}}}{3} \right) \times \text{dilution factor}$$

Equation 2.1: Equation used to calculate protein concentration from absorption values.

$$\text{Concentration of enzyme (mM)} = \frac{\text{Concentration mg/mL}}{\text{molecular weight}} \times 1000$$

Equation 2.2: the equation used to convert protein concentrations into molar quantities.

2.3.9 Preparation of 12% SDS-Page gel

Reagents were combined as in (**Table 2.7**). APS 10 % solution and TEMED were added immediately before pouring into casting plates. The resolving gel was first poured into 0.75 mm glass plates (BIO-RAD) leaving a 2 cm gap from the top. This was then overlaid with isopropanol and allowed to set. The isopropanol was then decanted, the stacking gel poured on and a 15 well comb added.

Reagent	Resolving Gel	Stacking Gel
<i>ddH</i> ₂ O	3.4 mL	2.9 mL
40 % Acrylamide/ Bis solution 19:1	2.4 mL	0.75 mL
Buffer	2.0 mL	1.25 mL
10 % SDS solution	80 μL	50 μL
10 % APS solution	80 μL	50 μL
TEMED	8 μL	5 μL

2.3.10 1 % agarose gel

1 g of agarose in 100 mL 1x TAE buffer was microwaved until boiling and all agarose had dissolved. Once cooled, GelRed™ stain was mixed in before being poured and then allowed to set in a casting block. Gels were run at 80 V for 50 minutes in 1x TAE buffer and visualised using a Syngene gene-flash transilluminator.

2.3.11 Synthesis of dihydrofolate

Folic acid (400 mg) was dissolved in 10 % (w/v) ascorbic acid solution, the pH adjusted to 6.0 and stirred on ice for a period of 5 minutes under a N₂ atmosphere. Sodium dithionite (4.4 g) was added followed by the drop wise addition of 1M HCl to pH 2.8. The suspension was centrifuged (24300 g for 5 minutes) and the pellet re-suspended in 10 % (w/v) ascorbic acid solution. The pH was returned to pH 2.8 via the drop wise addition of 1M HCl. Again the suspension was centrifuged (24300 g for 5 minutes). The pellet was washed by sequential re-suspension and centrifuge cycles (2x acetone followed by 1x Diethyl ether). The product was dried under a stream of N₂.¹²²

2.3.12 Synthesis of NADPD

NADPD was synthesised enzymatically from commercially available reagents. 20 mg NAD⁺ was dissolved into 4.8 mL of buffer M along with approximately 2 mg of TbADH (*Thermoanaerobacter brockii*) and 200 µL deuterated *d*₈-2-propanol. Reaction progress was monitored by an increase of UV absorbance at 340 nM.¹¹¹

2.3.13 Synthesis of NADD

NADD was synthesised enzymatically from commercially available reagents. 20 mg NAD⁺ was dissolved into 4.8 mL of buffer M along with approximately 2 mg of ScADH (*Saccharomyces cerevisiae*) and 200 µL deuterated *d*₈-2-propanol. Reaction progress was monitored by an increase of UV absorbance at 340 nM.¹²³

2.3.14 Purification of NADPD and NADD

Both NADPD and NADD were purified by HPLC using an anion exchange column, ProPac™ SAX-10 LC. A gradient from no NaCl (buffer M) to high NaCl (buffer N)

was run over a period of 60 minutes with a flow rate of 5 ml/min. Wavelengths at 260 nM and 340 nM was monitored in order to distinguish between reduced (product) and oxidised (starting material) forms.¹¹¹

2.3.15 Kinetic Assays

2.3.15.1 Pre-steady state kinetics

All stopped flow measurements were carried out on an applied photophysics stopped-flow spectrometer. SeDHFR was pre-incubated with NADPH and rapidly mixed with an excess of DHF to give final concentrations of 20 μ M, 10 μ M and 200 μ M respectively. The enzyme was pre-incubated with NADPH for at least 10 minutes to avoid hysteresis. To study the primary kinetic isotope effect, NADPD was prepared as described in section 2.3.12 and used in the same concentration as NADPH. The reaction was excited at 292 nm and emission measured with a cut-off of 400 nm, which allowed the monitoring of fluorescence energy transfer from residue Trp22 in the active site to NADPH.

2.3.15.2 Kinetics involving heavy enzymes

Heavy enzyme kinetics were performed in an identical manor to section 2.3.15.1 and section 2.3.15.3 with the exception of using ¹³C & ¹⁵N labelled enzymes. Heavy enzymes (labelled ¹³C & ¹⁵N) were prepared as described in section 2.3.6.

2.3.15.3 Steady state kinetics

All measurements were carried out on a JASCO V-660. Rates were monitored under saturating conditions: for SeDHFR (100 μ M DHF and NADPH), for LDH (300 μ M NADH and 2000 μ M pyruvate). Rates were monitored by following the decrease in absorbance at 340 nM. Measurements involving temperature dependence were measured in buffer H and the temperature in the cuvette was monitored immediately before the experiment using a Fisherbrand™ Traceable™ RTD platinum thermometer. Measurements were carried out in triplicate.

2.3.15.4 Measurements involving pH dependency

Steady state measurements involving pH dependency were carried out in MTEN buffer (buffer Q). Measurements involving pH dependency were all carried out at 20°C, the buffer being adjusted at this temperature before every experiment.

2.3.15.5 Measuring K_M (Michaelis constant)

For SeDHFR, the concentration of either NADPH (0.1 μ M -200 μ M) or DHF (0.1 μ M -200 μ M) was varied whilst the other substrate remained fixed with respect to concentration. For LDH, the concentration of NADH was again varied (1 μ M -3000 μ M), as well as pyruvate (0.1 μ M -5000 μ M). For both enzymes, at least seven points were recorded in triplicate. Points were fitted to sigmoidal curve using SigmaPlot 10.

2.3.15.6 Calculation of activation energies (E_a) and Arrhenius pre-exponential factors (A)

Activation energies and Arrhenius pre-exponential factors were calculated by plotting the natural log of the measured rate constants vs. the reciprocal temperature on Microsoft® Excel®, from which a linear trend line could be fitted. The Arrhenius equation was rearranged into **Equation 2.2**, which is in the same form as a typical equation for a straight line, **Equation 2.3**. In this form the Arrhenius pre-exponential factor equates to the y-intercept (highlighted in orange) and the activation energy equates to the slope (highlighted in red).

$$\ln k = \frac{-E_a}{R} \times \frac{1}{T} + \ln A$$

Equation 2.2: Rearranged Arrhenius equation where k is the measured rate constant, R the gas constant, T the temperature in kelvins, E_a the activation energy and A the Arrhenius pre factor.

$$y = mx + b$$

Equation 2.3: Equation of straight line, m equates to the slope and b the y-intercept.

2.3.16 Sidechain NMR experiments

All NMR experiments were carried out on a Bruker AVANCE III 600 MHz (^1H) spectrometer with a QCI-P cryoprobe. Proteins were purified and worked with at

approximate concentrations of 250 μM . MpDHFR, EcDHFR and SeDHFR were recorded in 50 mM potassium phosphate buffer with 1 mM NaCl and 10 mM βME . TmDHFR was recorded in 50 mM Tris with 1 mM NaCl and 10 mM βME . Ligands, if required, were used in a ten-fold excess from pre-prepared stocks (Section 2.3.15.1). For spectra requiring NADP^+ and THF, equimolar concentrations of NADPH and DHF were directly reacted with enzyme in the NMR tube for approximately 30 minutes. The reaction progress was monitored by ^1H NMR. 10 % D_2O was added to each NMR sample and the spectra recorded at 7, 25, 25 and 40 $^\circ\text{C}$ for MpDHFR, EcDHFR, SeDHFR and TmDHFR respectively. NMR spectra were processed with NMRpipe and analysed with CcpNMR Analysis 2.4.1.^{124,125}

2.3.16.1 Preparation of Ligand stocks

Ligand stocks were prepared at concentrations of 100mM in the same buffer as the enzyme for each respective NMR experiment. Concentrations were calculated by reference to molar extinction coefficients (**Table 2.8**).

Table 2.8: Molar coefficients of ligands used.	
Ligand	Molar extinction coefficient ($\text{cm}^{-1} \text{M}^{-1}$)
NADPH	6200 at 339 nm ¹²⁶
NADP^+	18700 at 260 nm ¹²⁷
DHF	28000 at 282 nm ¹²⁸
Folate	28000 at 297 nm ¹²⁹

2.3.16.2 Calculation of weighted chemical shifts

In order to obtain weighted chemical shift perturbations **Equation 2.4** was used.¹³⁰

$$\Delta\delta = \sqrt{\frac{1}{2} \left[\delta_H^2 + \frac{\delta_C^2}{4} \right]}$$

Equation 2.4: where δ_H and δ_C is the change in ppm between the two states in the proton and carbon dimension respectively.

2.3.17 Circular Dichroism spectroscopy

All measurements were performed on a Chirascan™ circular dichroism spectrometer. Measurements were performed in 5 mM potassium phosphate buffer (pH 7) with no salt or reducing agents, using 10 μM of protein. Measurements were taken between 190-400 nm with a 1 nm bandwidth. The mean residue ellipticity (MRE) was calculated using **Equation 2.5**.

$$\Theta_{MRE} = \frac{\Theta}{10 \cdot c \cdot n \cdot l}$$

Equation 2.5: Where Θ is the CD signal in milli-degrees, c is the molar concentration, n is the number of peptide bonds and l is the path-length in cm of the cuvette used.

2.3.17.1 Calculation of melting temperature (T_m)

A series of CD spectra were recorded over a temperature range of 5 to 85 °C with a temperature gradient of 0.5 °C/min. The CD signal at 208 nm was monitored and the fraction of unfolded protein (F_u) at various temperatures calculated using **Equation 2.6**.

$$F_u = \frac{F_o - F}{U_f - F}$$

Equation 2.6: Where F_u is the fraction of unfolded (denatured) protein, F and U_f are extrapolated values of the points where the protein is completely folded and unfolded respectively, and F_o is the value of ellipticity at 208 nm.

2.3.18 Calculation of errors and propagation of errors.

Variation or error in a particular data set were calculated using **Equation 2.7** and expressed as a standard deviation of the mean (σ).

$$\sigma = \sqrt{\frac{\sum_{i=1}^N (x_i - M)^2}{N - 1}}$$

Equation 2.7: where σ is the standard deviation in the sample, N is the number of data points in the sample, M is the mean value of the sample and x_i is the measured values.

Where the error could not be directly calculated, it became necessary to estimate the value of uncertainty *via* the propagation of errors using the equations shown below.

Where $Z = X*Y$ or $Z = X/Y$, **Equation 2.8** was used.

$$\Delta Z = Z \sqrt{\left(\frac{\Delta X}{X}\right)^2 + \left(\frac{\Delta Y}{Y}\right)^2}$$

Equation 2.8: Where ΔZ is the propagated error and Z the value of which the propagated error needs to be calculated for, X and Y are the experimentally measured values and ΔX and ΔY is their associated error.

3

Rapid analysis of conformational behaviour in DHFR Variants

3.1 Variations in conformational behaviour in DHFRs

Discovered off the coast of Italy inhabiting underwater volcanic vents, *Thermotoga maritima* is a hyperthermophilic bacteria with an optimal growth temperature of ~ 80 °C.¹³¹ TmDHFR shares 27% sequence identity with EcDHFR,^{61,132} and with respect to tertiary structure is nearly superimposable.^{61,133} TmDHFR has an extra ninth β -strand, which runs antiparallel to the extended FG loop on the opposing monomer (**Figure 3.1**).¹³³ In contrast, TmDHFR is the only known DHFR to form a thermostable ($T_m = 83$ °C) homo-dimer.⁹⁰ It is believed a reduction in the number of thermo-labile amino acids, a shortening of solvent exposed loops and its dimeric nature all likely contribute to its thermo-stability.^{94,133,134} 66% of the amino acids in the dimer interface of TmDHFR are either aliphatic or aromatic forming a hydrophobic core; in EcDHFR many of these residues are either ionic or polar.^{94,133} Lys129 forms an intermolecular ion-pair with Glu136 and Glu138 in the adjacent monomer.¹³³ Further stabilization comes from hydrogen bonding interactions between the two monomers, with an average of 1.22 interactions per 100 Å² of interface area.¹³³

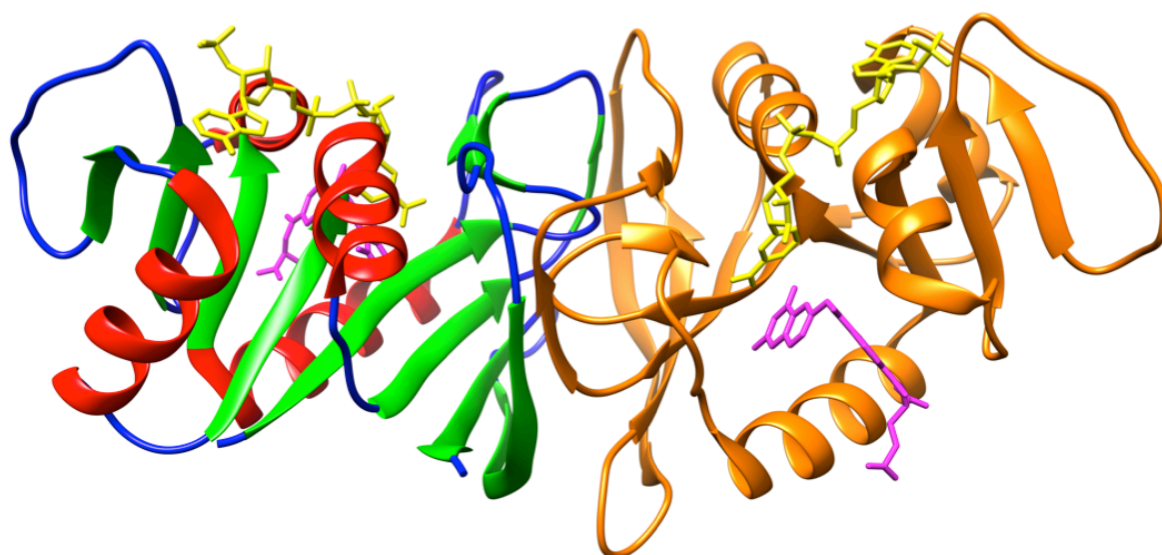


Figure 3.1: Crystal structure of TmDHFR (PDB entry 1D1G)¹³³. NADPH (yellow) and methotrexate (pink) are depicted as sticks. Secondary structural elements are depicted as a cartoon: β -sheet (green), α -helices (red) and loops (blue). One monomer is coloured orange for clarity.⁸⁹

EcDHFR undergoes a catalytic cycle adopting closed and occluded conformations in order to enable efficient catalysis.⁶¹ It has been proposed that the occluded conformation, which is adopted after the chemical step is needed to allow for efficient release of NADP⁺ under intracellular concentrations where NADP⁺ is increased compared to other organisms.⁷⁶ Other DHFR variants have been shown to only adopt a single major conformation throughout the catalytic cycle, equivalent to the closed conformation, even though the tertiary structures and primary sequences are similar to EcDHFR.^{76,85–87} The occluded conformation in EcDHFR is stabilised by a hydrogen bonding interaction between Asn23 in the flexible M20 loop and Ser150 in the GH loop.⁶¹ In MpDHFR the equivalent Ser150 residue is replaced with a proline residue and as such destabilises formation of an occluded conformation.⁷⁶ TmDHFR has a much lower catalytic turnover than EcDHFR (approx. 8-fold) even at their respective physiological temperatures.^{90,135} Mobile loops in EcDHFR, which are critical for efficient progress through the catalytic cycle, are locked into the dimer interface in TmDHFR, greatly reducing protein flexibility and it has been suggested TmDHFR remains in a fixed, open conformation through its catalytic cycle.^{88,90,133}

Although the catalytic cycle of EcDHFR has been well studied, other DHFR variants have been less well characterised. To better understand the role of the occluded conformation, the key amino acid determinants for its formation and how common it is, a more widespread investigation of DHFR variants is needed. TmDHFR represents an interesting variant as the equivalent mobile loops present in EcDHFR are locked within the rigid dimer interface. TmDHFR has been suggested to remain in a single, open conformation throughout the catalytic cycle but no direct evidence has yet been established.^{89,121} Here we investigate the conformational landscape of TmDHFR.

3.2 NMR assignment of TmDHFR

In order to study enzymes by NMR, isotopic enrichment must be employed to improve sensitivity to the experiment.¹³⁶ Protein preparation involves recombinant overproduction in M9 minimal media, which allows natural abundance feedstock to be replaced with ²H, ¹³C and ¹⁵N enriched water, glucose and ammonium chloride respectively. Following overproduction, isotopically enriched protein is purified in buffers that contain natural abundance levels of protium, resulting in nearly all

exchangeable ^2H being replaced with ^1H , which is important for the NMR experiment to work.^{136,137}

In order to characterise TmDHFR further a backbone resonance assignment was needed. ^2H , ^{13}C and ^{15}N isotopically enriched TmDHFR was recombinantly overproduced, purified and concentrated to 400 μL , and placed into a 5 mm borosilicate glass NMR tube. 100 μL of D_2O was added to the sample to act as a lock frequency for the NMR experiment.¹³⁶ In order to align with previous work with EcDHFR and MpDHFR, NADP^+ and folate, which mimic the Michaelis complex, were added so the final concentration of both ligands in the sample was 6 mM and the pH adjusted to 7.0.^{76,138–140} The final concentration of TmDHFR in the NMR sample was calculated to be $\sim 600 \mu\text{M}$. Isotopic enrichment was confirmed *via* mass spectrometry (**Figure 3.2**).

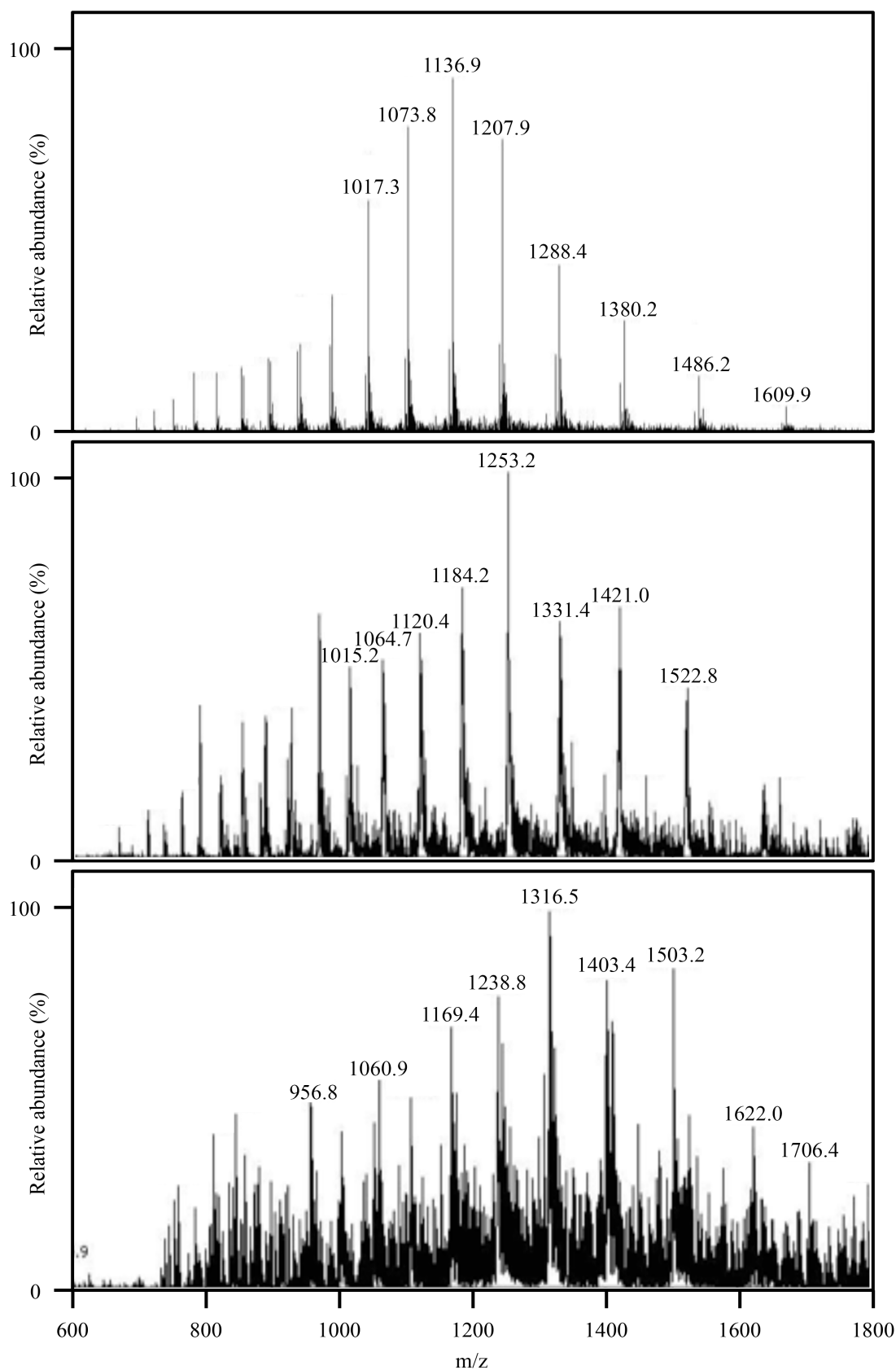


Figure 3.2: (Top) mass spectrum of natural abundance TmDHFR, $M_w = 19235.5 \pm 0.5$. (Middle) mass spectrum of triply labelled TmDHFR (^2H , ^{13}C & ^{15}N), $M_w = 21289.0 \pm 12.0$, corresponding to 99.4% enrichment of non-exchangeable atoms. (Bottom) mass spectrum of triply labelled TmDHFR (^2H , ^{13}C & ^{15}N) grown in 70% D_2O , $M_w = 21053.7 \pm 7.9$, corresponding to ~59% deuteration.

A proton spectrum was acquired but as TmDHFR has ~2750 atoms, the 1D proton spectra exhibits hundreds of overlapping resonances, which are impossible to assign (**Figure 3.3**).^{88,133} The distribution of resonances at high and low field indicates that the protein is folded under these conditions, due to the range of chemical environments found in folded proteins as opposed to an unfolded peptide polymer. A 2D ^1H - ^{15}N HSQC spectra was also acquired and is the primary method of studying proteins by NMR (**Figure 3.4**). This provides a single resonance for each backbone amide. The ^1H - ^{15}N spectrum displayed a large number of resonances with minimal signal diffusion. From this spectrum we assessed it would be feasible to attempt to assign backbone resonances through a multidimensional NMR approach.

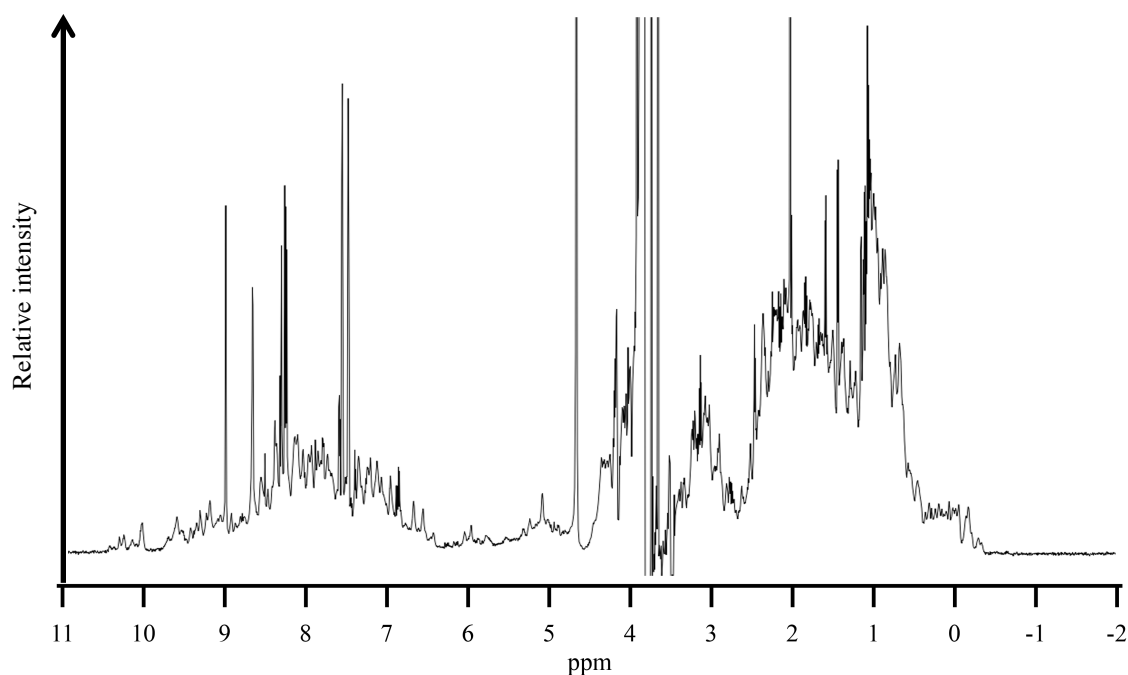


Figure 3.3: 1D ^1H spectra of TmDHFR complexed with NADP^+ and folate, a reasonable signal to noise ratio was achieved after 16 scans and the dispersion of chemical shifts at low and high fields is indicative of the protein being folded.

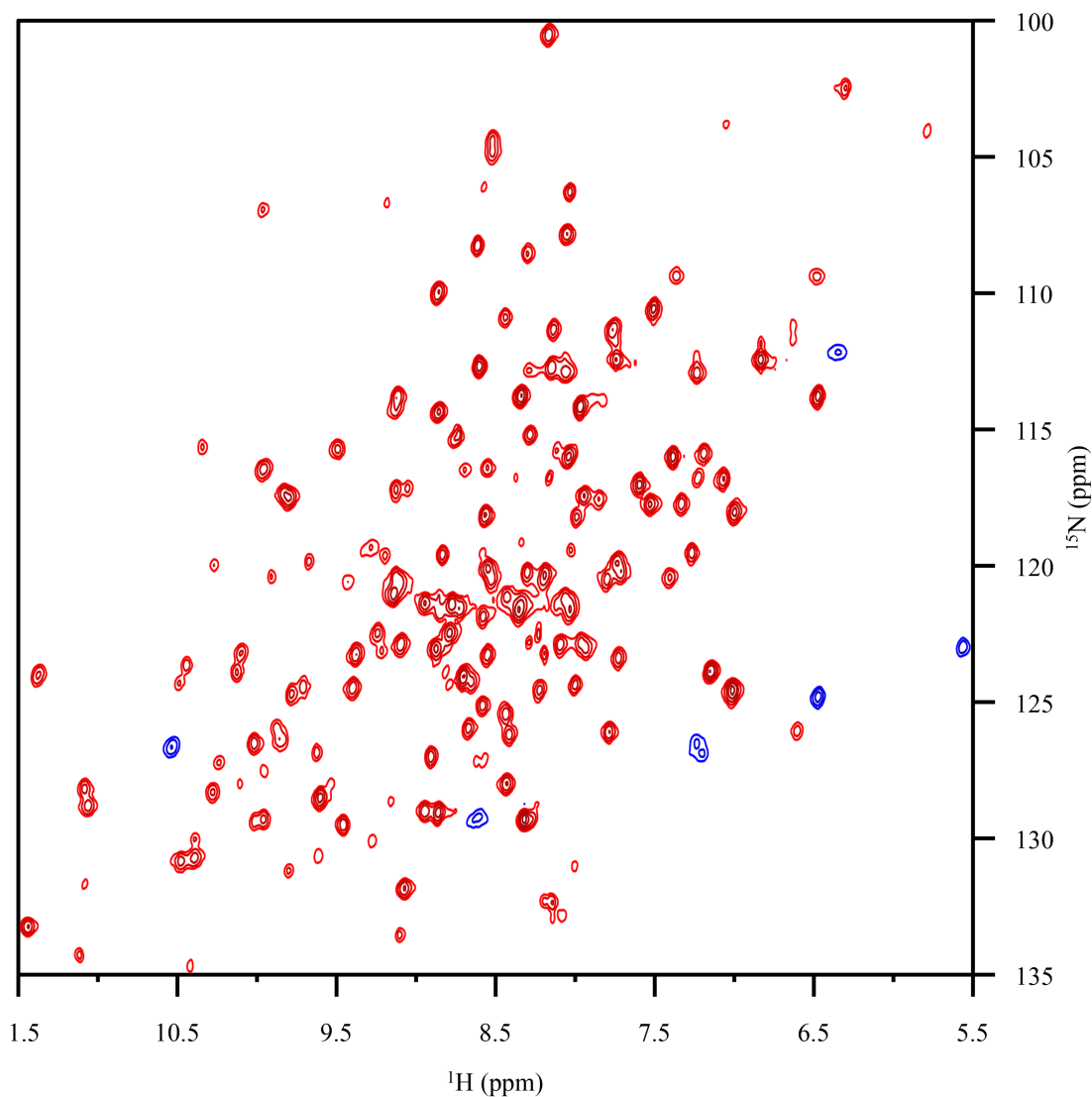


Figure 3.4: ^1H - ^{15}N HSQC of TmDHFR complexed with NADP^+ and folate, spectra was acquired at 800 MHz.

Although 2D ^1H - ^{15}N spectroscopy provides a method to investigate TmDHFR, the information is limited without an assignment of each resonance to the protein sequence. A series of 3D experiments were acquired to assign the backbone resonances in TmDHFR (amide ^1H and ^{15}N , $^{13}\text{C}_\alpha$ and $^{13}\text{C}_\beta$ and the carbonyl ^{13}C) (**Table 3.1**). Each of these experiments is based upon the core ^1H - ^{15}N HSQC and provides specific ^{13}C resonances in a third dimension. The ^{13}C resonances recorded are selected depending on the pulse programme used and experiments are often acquired in pairs such that the resonance can be linked sequentially and the sequence deduced. Using facilities at the National Institute for Medical Research (NIMR) at Mill hill (now the Crick Institute) NMR spectra were recorded at high field strengths (700, 800 MHz). Nearly all NMR

experiments acquired for TmDHFR utilised Transverse Relaxation-Optimised Spectroscopy (TROSY). Large protein molecules have faster transverse relaxation times (T_2) resulting in rapid signal decay and low-resolution spectra. The TROSY pulse sequence was designed for large proteins and mitigates effects from multiple relaxation events resulting in narrower linewidths without adverse effects on sensitivity.¹⁴¹ Some experiments were performed with samples that had only 70 % perdeuteration, this was in an attempt to further improve relaxation issues, details of which will be discussed later on in this chapter.

Table 3.1: List of recorded spectra recorded for TmDHFR complexed with NADP⁺ and folate at pH 7.0.

Experiment	Field Strength (MHz)	Deuteration
¹ H- ¹⁵ N HSQC	800	100 %
¹ H- ¹⁵ N HSQC-TROSY	800	100 %
HNCA-TROSY	800	100 %
HN(CO)CA-TROSY	800	100 %
HNCACB-TROSY	800	100 %
HN(CO)CACB-TROSY	800	100 %
¹ H- ¹⁵ N HSQC	800	70 %
HNCO-TROSY	800	70 %
HN(CO)CA-TROSY	800	70 %
HN(CO)CACB-TROSY	800	70 %
HCCH-TOCSY	700	70 %
hCCH-TOCSY	700	70 %
hC(CO)NH-TOCSY	700	70 %
H(CC)(CO)NH	700	70 %

Multidimensional NMR experiments are designed to take advantage of the repeating polypeptide backbone unit and allow assignment of the backbone resonances (amide ¹H and ¹⁵N, ¹³C_α and ¹³C_β and the carbonyl ¹³C). 3D NMR experiments used to assign protein resonances are often based of the 2D ¹H-¹⁵N HSQC experiment by extending it into the ¹³C dimension. The third dimension further decreases signal overlap and yields extra information crucial for assignment. 3D experiments are often used in pairs to

assign protein resonances such as the HNCA and HN(CO)CA or HNCO and HN(CA)CO experiments (**Figure 3.5**). Using experiments such as these allows for sequential assignment of the protein backbone. During assignment each amino acid residue is considered as its own spin system, experiments such as HNCA and HN(CO)CA allow assignment of the $^{13}\text{C}_\alpha$ in the next (N^{H}_i) and previous ($\text{N}^{\text{H}}_{i-1}$) spin system, thus facilitating sequential assignment of spin systems. Amino acids such as serine, threonine, alanine and glycine have distinctive $^{13}\text{C}_\alpha$ and $^{13}\text{C}_\beta$ chemical shifts, which allows for identification of specific amino acids in the spin system chain and comparison with the amino acid sequence allows for assignment. When ambiguity or further conformation for the correct identification of amino acids is required, side-chain specific experiments such as HCCH-TOCSY and H(CCO)NH can be employed.^{136,137}

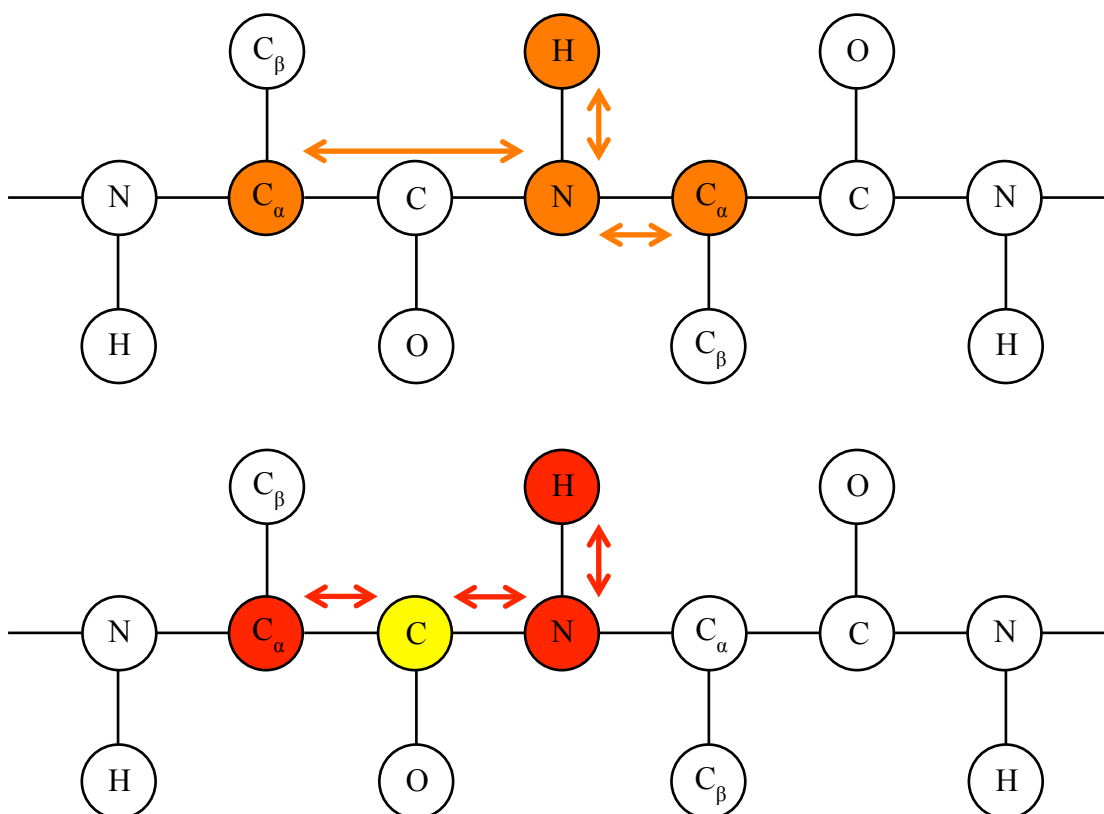


Figure 3.5: Top: HNCA, magnetization is evolved on the amide proton before being passed to ^{15}N and then onto the alpha carbon *via* J coupling, before being returned by the same pathway for detection. Chemical shifts are gained for all three isotopes involved (^1H , ^{13}C & ^{15}N) producing 3D spectra. Bottom: HN(CO)CA, is very similar to HNCA experiment except magnetisation is passed onto the immediate carbonyl ^{13}C before the alpha carbon. Again chemical shifts are evolved for the amide ^1H and ^{15}N and the alpha carbon but not for the carbonyl ^{13}C . As the HN(CO)CA experiment only selects for the previous alpha carbon sequential assignment becomes possible.

Spectra were processed using NMRPipe and resonances picked using CcpNmr analysis.^{124,125} Once a significant number of resonances were picked and spin systems formed it was possible to form linkages and assign resonances to the atoms of the protein sequence. During this process it became apparent that the quality of the spectra for TmDHFR was poorer than expected and that observed for other DHFR orthologues.

A number of factors, which could be negatively impacting the quality of the obtained spectra, were considered. Firstly, increased protein size of TmDHFR leads to slow tumbling in solution, quicker T_2 relaxation and thus poor quality NMR spectra.¹³⁶ TmDHFR is a homodimeric DHFR with a molecular mass of 38472 and an elongated shape, which further impacts tumbling properties, and results in diminished NMR

spectra.^{88,89} However, proteins with a molecular mass of up to 50 kDa should be accessible to the described methodologies with the application of specialised pulse sequences and partial deuteration.¹³⁷ ^1H - ^{13}C dipolar interactions dramatically accelerates relaxation rates of ^{13}C atoms with attached protons, through deuteration these interactions can be minimized, both increasing peak resolution and resonance intensity.¹⁴²⁻¹⁴⁴ Deuteration of the protein therefore often improves relaxation properties.

Secondly, it was noted spin systems located within the core of the protein structure yielded particularly poor, or no signal at all. TmDHFR has a melting temperature of 83 °C and it is thought its structural rigidity facilitates stability at such high physiological temperatures.⁸⁸⁻⁹⁰ This rigidity however is believed to prevent efficient back-exchange of protons in positions that are not solvent exposed, which is necessary for the experiment to work.

In order to assess whether the thermostability of TmDHFR was preventing efficient back exchange of the amide protons, a ^{15}N sample of TmDHFR was expressed and purified. To assess whether the amide backbone exchanged completely the sample was dialysed into 99% D_2O . The sample was incubated for 4 days at 60 °C, spectra being recorded every 24 hours. The aim of this experiment was to increase the flexibility of the protein through increased thermal energy, thus increasing the chance of proton back-exchange in non-solvent exposed residues. If residues in TmDHFR were not accessible to proton back exchange this would result in a persistence of signal in the recorded spectra. A number of cross peaks remained in the ^1H - ^{15}N HSQC spectra after a period of 4 days and incubation at 60 °C (**Figure 3.6**). Also, a number of cross peaks appeared to exhibit no significant decrease with respect to signal intensity.

This result confirmed that a number of residues present in TmDHFR were not accessible to proton back exchange from the bulk solvent, complicating efforts to improve relaxation issues through deuteration. It was suggested that unfolding the protein would expose the non-solvent exposed regions allowing for proton back-exchange. However, previous unfolding and re-folding experiments with TmDHFR in our group suggested proper re-folding of the protein was difficult due in part to the added complexity of the dimer interface.¹⁴⁵

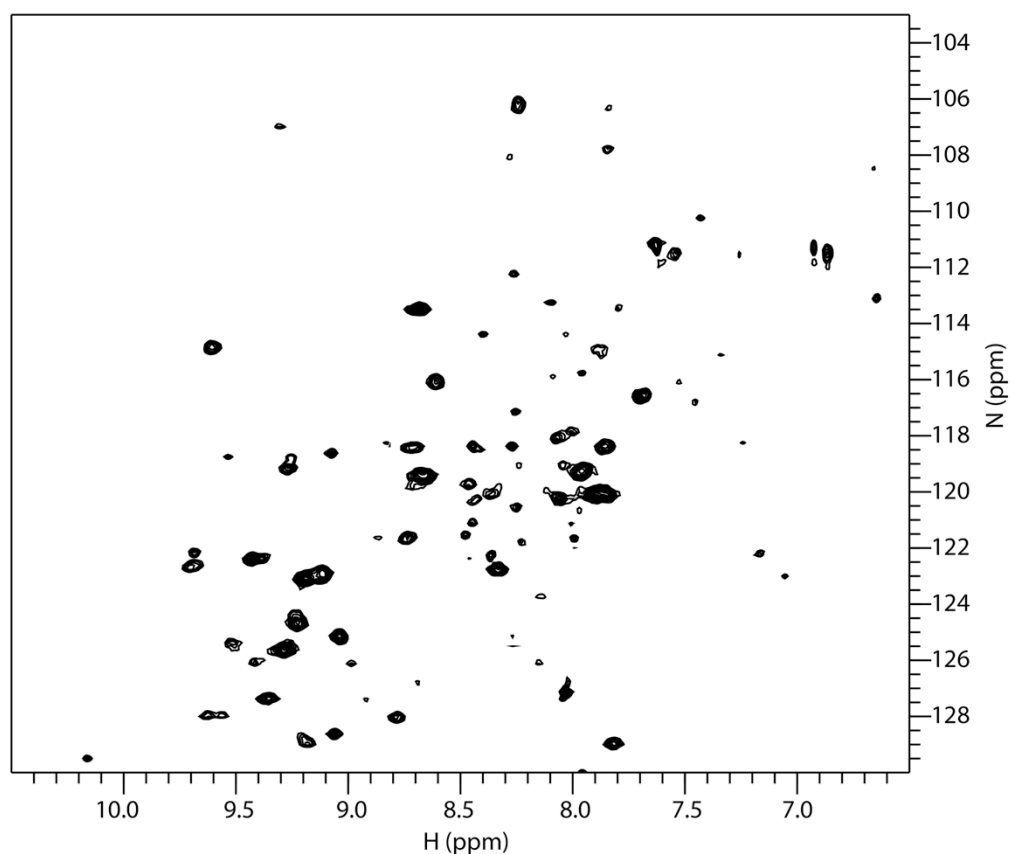


Figure 3.6: ^1H - ^{15}N spectra of ^{15}N labelled TmDHFR recorded after 4 days at 60 °C incubation in buffer containing 99 % D_2O .

Through these methods it was possible to only assign just over ~30% of the protein backbone (**Figure 3.7 and 3.8**), most of the assigned residues residing in solvent exposed regions of the protein structure. As the assigned spin systems do not represent an effective cross section of the different environments in the protein structure it was deemed necessary to attempt a different approach to probe conformational behaviour in TmDHFR.



Figure 3.7: Cartoon representation of TmDHFR, Spin systems that have been assigned have been highlighted in red, approximately 30 %.

AKVIFVLAMDVSGKIASVSVESWSSFEDRKNFRKITTEIGNVVMGRITFEEIGRPLPERL
NVVLTRRPKTSNNPSLVFFNGSPADVVKFLEGKGYERVAVIGGKTVFTEFLREKLVDDEL
FVTVEPYVFGKGIPFFDEFEGYFPLKLLMRRLLNERGTLFLKYSVEKSHR

Figure 3.8: Primary sequence of TmDHFR, highlighted in yellow are residues we found possible to assign.

3.3 Introduction to chemical shift mapping

The backbone assignment of TmDHFR could not be completed due to the adverse properties of the protein; high thermal stability preventing back-exchange after perdeuteration; dimerization giving unsuitable relaxation properties. This prevented the use of conventional NMR methods that rely on the ^1H - ^{15}N HSQC as the fingerprint on which other experiments are based. In order to investigate protein conformational changes for TmDHFR an alternative NMR approach involving sidechain labelling was undertaken. Sidechain labelling provides defined probes within the protein but with low enough populations to enable characterisation without a backbone assignment.

Importantly methyl labelling affords good relaxation properties without the requirement of perdeuteration.

Importantly, using conventional ^1H - ^{15}N approaches for widespread analysis of protein variants from different organisms is impossible due to both the length of time required and simply the number of resonances that provide a complex picture without assignment. Yet it is important to investigate many orthologues to get a picture of the importance of conformational changes to catalysis and to identify key amino acid networks that conserve the mechanism. Therefore we wished to find an alternative method that made analysis of multiple enzymes straightforward.

In order to simplify NMR spectra and optimise we wished to have probes within defined locations of the protein at a low population and with suitable properties. Sidechain labelling affords this.

A search on the protein data bank returns >400 structures relating to DHFR and multiple studies have been conducted with respect to conformational behaviour in DHFR variants.^{58,63} Most of these determined structures are however of the apo enzyme or with DHFR inhibitors such as trimethoprim or methotrexate and as such do not effectively model conformational changes that could occur before and after the chemical step of catalysis. DHFRs from *Lactobacillus casei* and *Bacillus anthracis* have been postulated not to adopt an occluded conformation, however the absence of structural evidence suggesting for an occluded conformation does not imply they cannot adopt such a conformation.⁸⁵⁻⁸⁷

3.4 Sidechain labelling to probe conformational behaviour

The method used in this thesis involves labelling of the enzyme with [*methyl*- ^{13}C]-methionine and [*indole*- δ_1 - ^{13}C] tryptophan.^{146,147} By adding various ligand combinations the different structural conformations such as the Michaelis and product complexes could be probed. This method significantly reduces spectral complexity compared to a ^1H - ^{15}N HSQC and as such allows for the rapid and intuitive probing of conformational behaviour. Further more [*methyl*- ^{13}C]-methionine labelling is very sensitive due to the

three equivalent protons on the ^{13}C labelled methyl group, and will subsequently help to overcome issues caused by relaxation effects in TmDHFR.¹³⁶

As stated in the introduction, evidence of a DHFR enzyme adopting an occluded like conformation following the chemical step has only been found in EcDHFR.^{53,61,76,83} Mutants, which reduce flexibility of the M20 loop, have a diminishing effect on the value of k_{cat} and it is postulated EcDHFR adopts an occluded conformation to reduce product inhibitory effects.^{53,76,98–100} MpDHFR on the other hand, has been shown not to adopt such a conformational change following the chemical step, even though the tertiary structures of EcDHFR and MpDHFR appear to be superimposable.^{61,76,84} To validate side-chain labelling as a method of tracking conformational behaviour in DHFR variants data from EcDHFR and MpDHFR was compared. This identified whether formation of an occluded like conformation could be identified through a simplified chemical shift mapping approach utilizing a limited number of resonances dispersed throughout the protein structure.

Classically chemical shift perturbations have been quantified using **Equation 3.1**.¹⁴⁸ Quantification of chemical shift perturbations allows for a simplified way of identifying significant chemical shift changes, which in this case is likely a result of conformational change. In order to acknowledge the difference in magnetogyric ratios between the proton and carbon atom ($\gamma_{\text{C}}/\gamma_{\text{H}}$) a scaling factor of 0.25 is used to allow chemical shifts of different isotopes to be more comparable.¹⁴⁸

$$\Delta\delta = \left[\frac{1}{2} \left(\delta_{\text{H}}^2 + \frac{\delta_{\text{C}}^2}{4} \right) \right]^{0.5}$$

Equation 3.1: Equation used to calculate weighted chemical shifts ($\Delta\delta$), wherein δ_{H} and δ_{C} is the difference in chemical shifts for each respective atom measured in parts per million (ppm).

Methionine comprises 3.1% of total amino acids in EcDHFR and MpDHFR and 2.4 % in TmDHFR. Similarly tryptophan comprises 3.1% of total amino acids in EcDHFR, 1.9 % in MpDHFR and 0.6 % in TmDHFR (**Figure 3.9**).^{84,88,133,149} Methionine and tryptophan residues are also well dispersed throughout a number of other DHFR

variants (**Figure 3.10**), a number of these residues being highly conserved, allowing for a simplified comparison between data sets from different DHFRs. Trp22, located in the M20 loop has been shown to be important for catalysis in EcDHFR and is highly conserved amongst DHFR variants.¹⁵⁰ Trp133 is also highly conserved and is present in EcDHFR and MpDHFR; all other tryptophan residues are located throughout the enzyme structure. Met42, although distal to the active site is also highly conserved, mutation of this residue in EcDHFR results in diminished k_{cat} and k_m values.¹⁵¹ Met92 and Met42 are also conserved in MpDHFR. Only Met44 is conserved in TmDHFR, the two remaining methionine residues located within the dimer interface. From mass spectrometry we know Met1 usually remains intact on the protein structure, in TmDHFR however aminopeptidase only partially removes this residue (**Figure 3.11**).¹⁵²

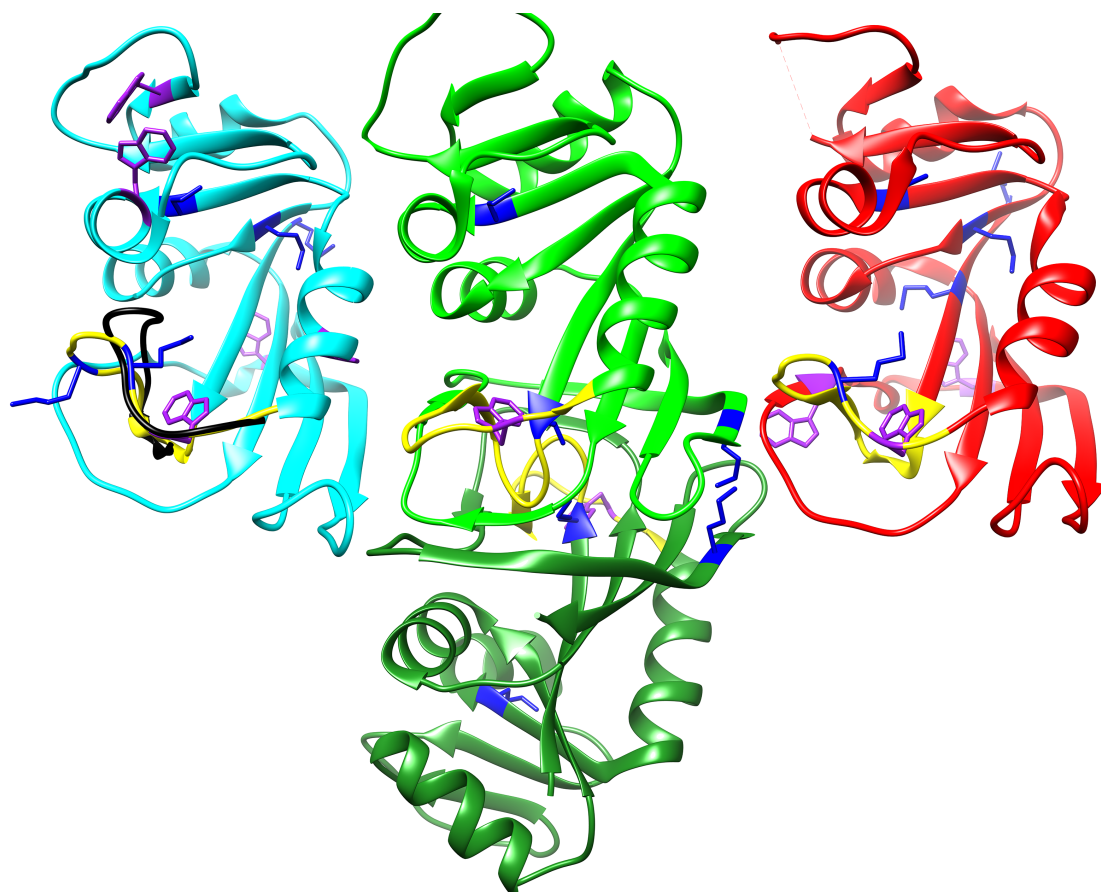


Figure 3.9: Cartoon representation of three DHFR variants discussed in this work; EcDHFR (PDB entry 1RX2⁶¹, light blue), TmDHFR (PDB entry 1D1G⁸⁹, green) and MpDHFR (PDB entry 3IA5¹⁵³, red). The M20 loop in the closed position in EcDHFR and MpDHFR and open position in TmDHFR is highlighted in yellow. The M20 loop in the occluded position is highlighted in black in EcDHFR. The positions of methionine (blue) and tryptophan (purple) residues are also highlighted.

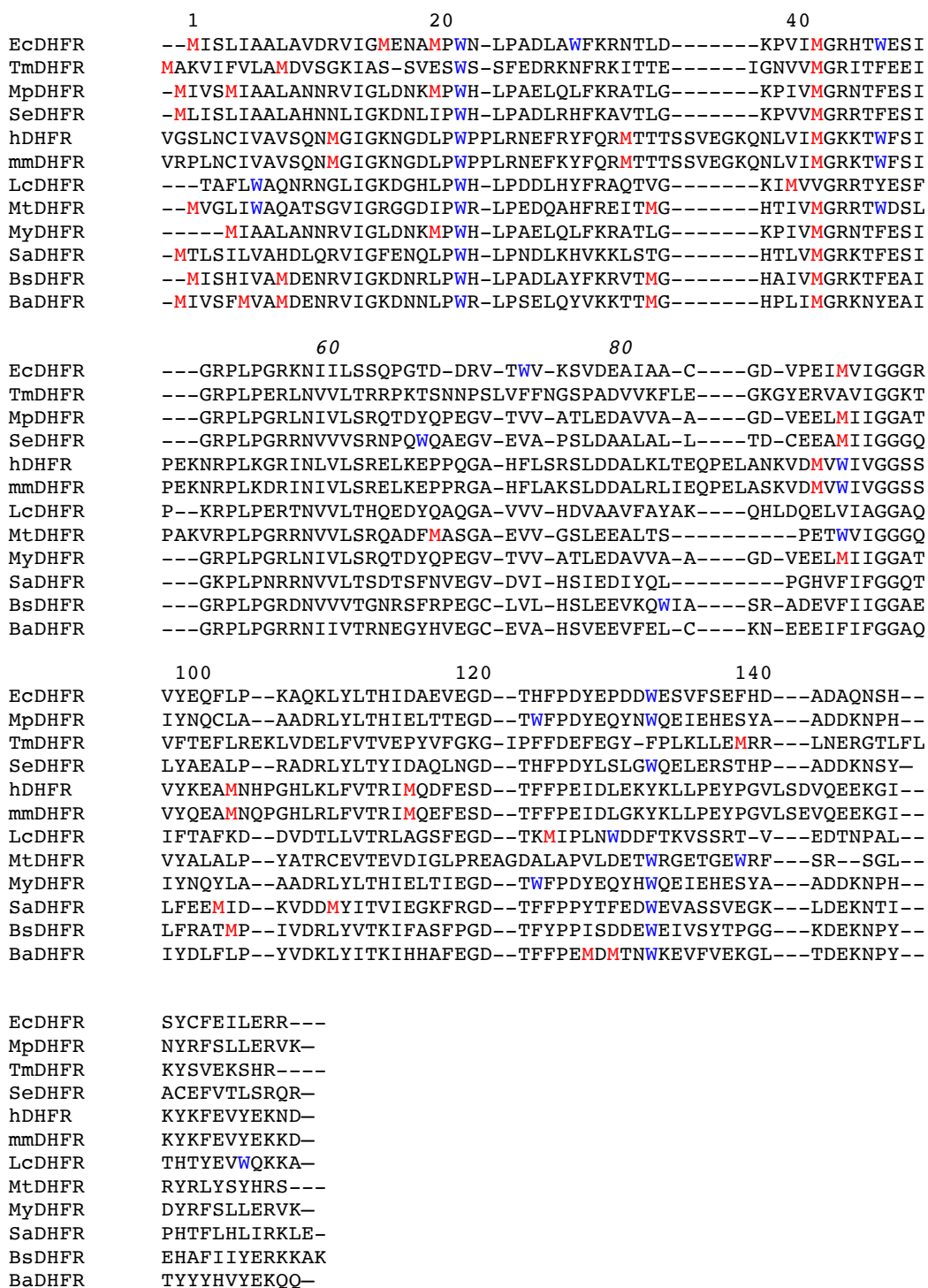


Figure 3.10: Alignment of the amino acid sequences of DHFR orthologues, showing methionine and tryptophan residues in DHFR variants. DHFR alignments comprise *Thermotoga maritima* (TmDHFR), Human (hDHFR), *Mus musculus* (mouse, MmDHFR), *Lactobacillus casei* (LcDHFR), *Mycobacterium tuberculosis* (MtDHFR), *Escherichia coli* (EcDHFR), *Salmonella enterica* (SeDHFR), *Moritella profunda* (MpDHFR), *Moritella yayanosii* (MyDHFR), *Staphylococcus aureus* (SaDHFR), *Geobacillus stearothermophilus* (BsDHFR) and *Bacillus anthracis* (BaDHFR).

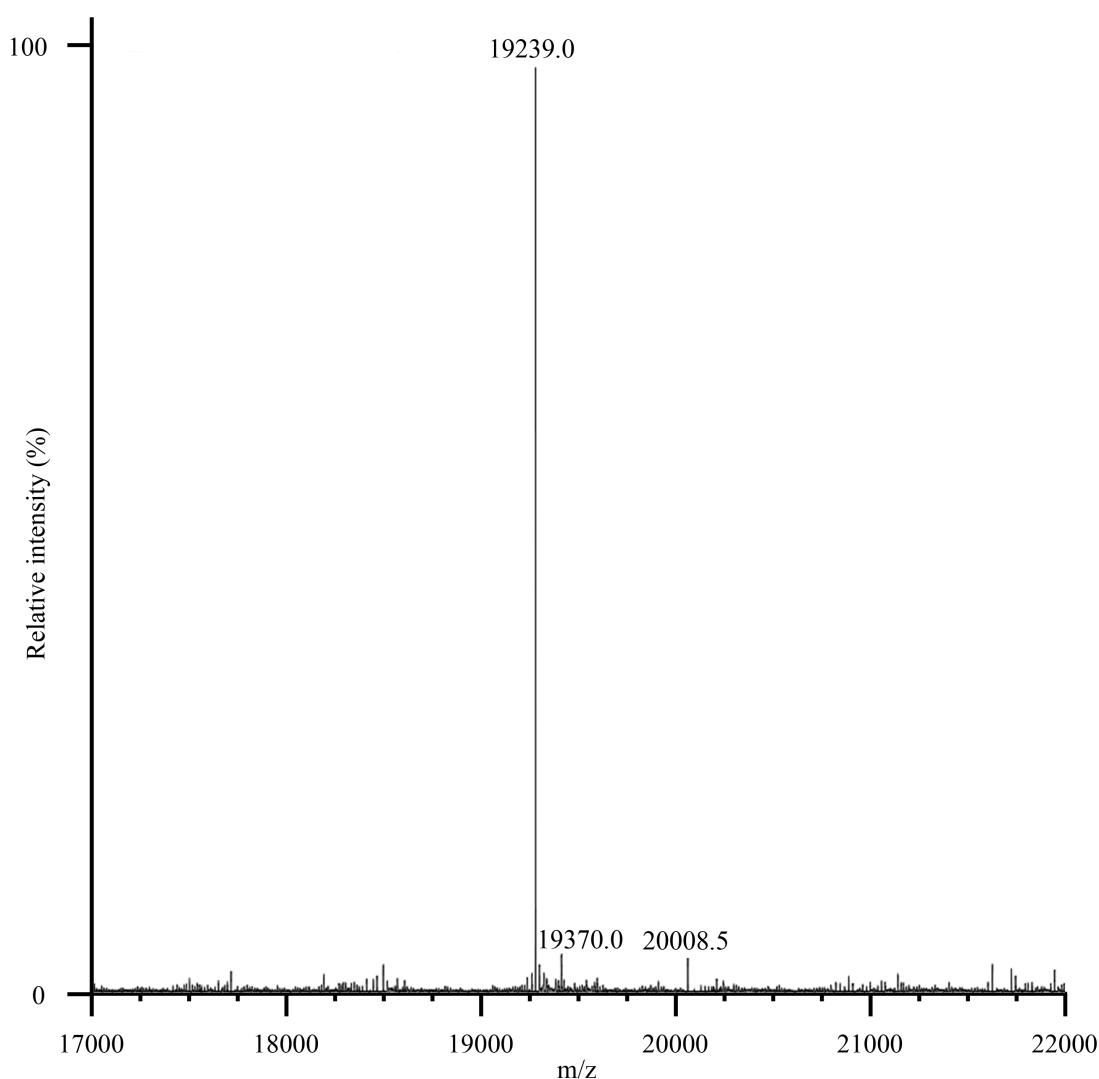


Figure 3.11: Deconvoluted ESI mass spectrum of TmDHFR wherein the methyl group of each methionine residue has been systematically labelled with ^{13}C . The calculated mass is 19,370.0 and following cleavage of Met1 by aminopeptidase is 19,239.0. As can be observed the majority of Met1 has been cleaved but a significant amount of TmDHFR with Met1 still remains.

Sidechain labelling can be achieved by adding various starting materials to the media during recombinant expression. By adding indole, in *E.coli*, tryptophan synthase converts indole-3-glycerol phosphate and serine into tryptophan, passing through an indole intermediate. Indole-(2- ^{13}C) was used to systematically label the C2 position of the indole ring of tryptophan residues, utilizing the tryptophan biosynthetic pathway used by *E.coli* (**Figure 3.12**).^{4,147} Allowing for a cost-effective and simple approach to the labelling of tryptophan residues.¹⁴⁷ For simplicity and reduced label scrambling L-

methionine-(*methyl*- ^{13}C) was used to directly label the methyl groups of methionine residues.¹⁴⁶ Successful labelling being confirmed by mass spectrometry.

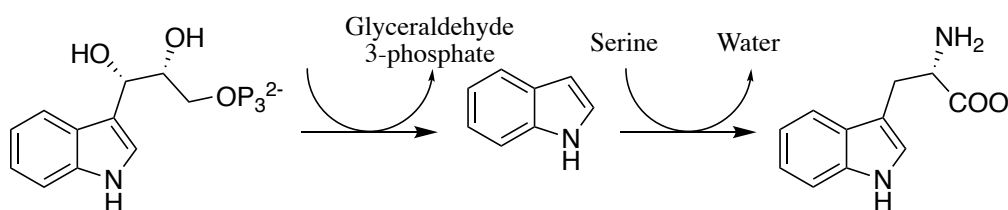


Figure 3.12: Reaction catalysed by Tryptophan synthase. Serine forms a Schiff base with pyridoxal phosphate (PLP) held within the active site which reacts with indole to form tryptophan.^{4,154}

3.5 Sidechain NMR experiments

In order to confirm that sidechain labelling is able to identify the conformational changes that occur with DHFR catalysis, EcDHFR was investigated. ^1H - ^{13}C HSQC spectra of EcDHFR labelled with [*methyl*- ^{13}C]-methionine or [indole- δ_1 - ^{13}C] tryptophan were acquired. Different samples were formed representing the different complexes present in the catalytic cycle. An apo sample was first recorded with no bound ligands in order to gain structural information about the open/disordered state. Direct addition of NADPH and DHF to form the Michaelis complex was not possible due to near immediate product formation. A Michaelis complex was therefore formed using NADP⁺ and folate to prevent turnover, work by Sawaya *et.al.* has shown this complex to adopt a closed conformation in EcDHFR.¹⁴⁹ The ternary product complex was formed by adding equimolar concentrations of NADPH and DHF to DHFR directly in the NMR tube. A period of 20 minutes was allowed for the enzyme to completely turnover all substrates to NADP⁺ and THF, the reaction being monitored by ^1H NMR. A ^1H - ^{13}C HSQC spectrum of the Michaelis and product complexes yielded 5 well-defined cross-peaks in spectra of both [*methyl*- ^{13}C]-methionine and [indole- δ_1 - ^{13}C] tryptophan labelled EcDHFR (**Figure 3.13**). Spectral quality is greatly diminished when studying the enzyme in the apo state, a consequence of conformational heterogeneity, where the enzyme is in slow equilibrium between multiple states.^{138,155} Addition of ligands reduces the number of additional cross peaks and increases resolution as exchange between conformational states is suppressed.¹³⁹

Due to previously published NMR assignments, residues in EcDHFR and MpDHFR were assigned by Stella Matthews and Dr E. Joel Loveridge. For MpDHFR all methionine methyl groups with the exception of Met94 had previously been published which was confirmed through re-evaluation of a previously recorded ^{13}C - ^{15}N edited NOESY.¹³⁸ Tryptophan indole groups were assigned by correlating indole- δ_1 ^1H resonances recorded through [indole- δ_1 - ^{13}C] tryptophan labelling to previously recorded spectra. If not already assigned in spectra relating to EcDHFR, residues were assigned *via* a similar approach and re-evaluation of CCH-TOCSY, HCCH-TOCSY spectra, which was again previously acquired with reference to published material.^{139,140}

Significant differences with respect to chemical shift were observed between the apo, Michaelis and product complexes, indicative of the enzyme undergoing structural conformational changes. It is known that EcDHFR changes from a closed to occluded conformation following the chemical step and as such dramatic changes with respect to chemical shift were witnessed between EcDHFR:NADP⁺:folate and EcDHFR:NADP⁺:THF complexes (**Figure 3.14**). Met16, Met20 and Trp22 located in the flexible M20 loop of EcDHFR showed large chemical shift perturbations (**Table 3.2**). Met42, Met92 and Trp133 although located distal to the active site also exhibited significant chemical shift perturbations (**Table 3.3**).

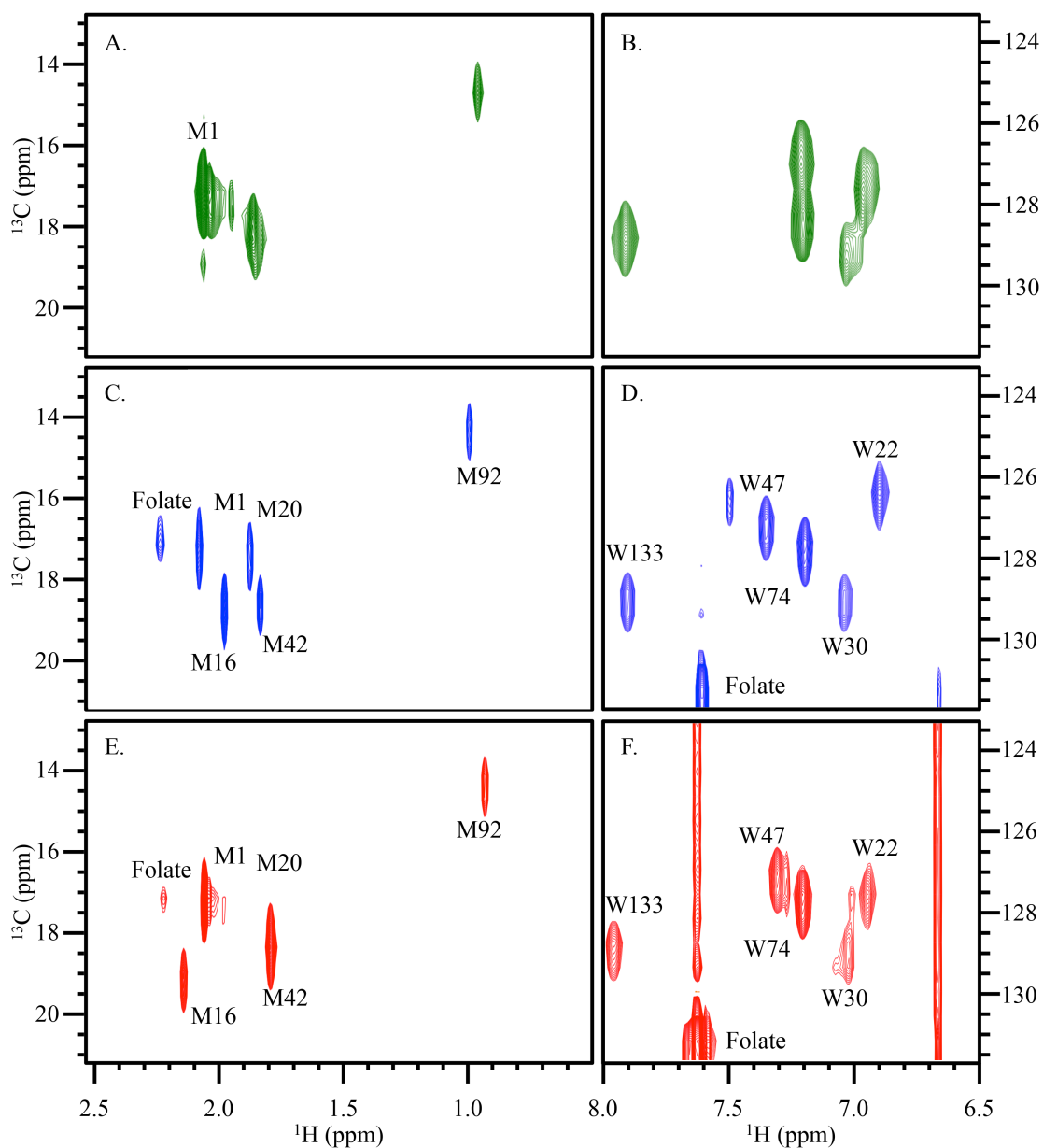


Figure 3.13: ^1H - ^{13}C HSQC spectra of ^{13}C -labelled EcDHFR complexes. (A) [*methyl*- ^{13}C]methionine-labelled EcDHFR with no ligands. (B) [δ_1 - ^{13}C] tryptophan-labelled EcDHFR with no ligands. (C) [*methyl*- ^{13}C]methionine-labelled EcDHFR in the Michaelis complex. (D) [δ_1 - ^{13}C] tryptophan-labelled EcDHFR in the Michaelis complex. (E) [*methyl*- ^{13}C]methionine-labelled EcDHFR in the product complex. (F) [δ_1 - ^{13}C] tryptophan-labelled EcDHFR in the product complex.

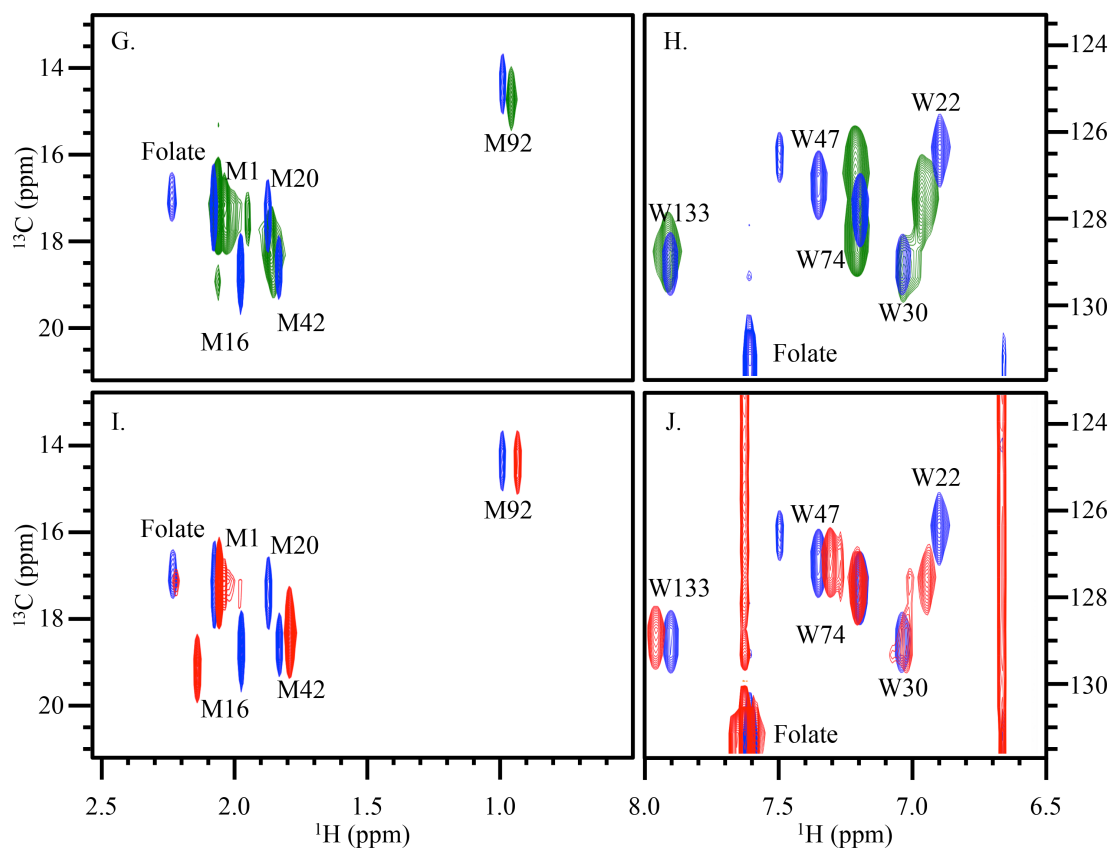


Figure 3.14: ^1H - ^{13}C HSQC spectra of ^{13}C -labelled EcDHFR complexes, Apo (green), E: NADP^+ :folate (closed conformation in EcDHFR) (blue) and E: NADP^+ :THF (occluded conformation in EcDHFR) (red). (G and I) [*methyl*- ^{13}C]methionine-labelled EcDHFR (H and J) [δ - ^{13}C] tryptophan-labelled EcDHFR.

Residue	Apo to Michaelis complex	Michaelis to product complex
Met1	0.012	0.011
Met16	0.062	0.122
Met20	0.100	0.120
Met42	0.032	0.036
Met92	0.107	0.040

Table 3.3: Weighted chemical shift perturbations (ppm) between ^1H - ^{13}C HSQC of spectra relating to $[\delta_1\text{-}^{13}\text{C}]$ tryptophan-labelled EcDHFR.		
Residue	Apo to Michaelis complex	Michaelis to product complex
Trp22	0.233	0.226
Trp30	0.060	0.067
Trp47	0.108	0.046
Trp74	0.129	0.006
Trp133	0.036	0.153

To confirm that chemical shifts observed for EcDHFR are indeed representative of conformational changes and not due to other effects such as ligand binding, MpDHFR was investigated using the same methods. The catalytic cycle of MpDHFR has been previously investigated and shown to progress with a single conformation, alike to the EcDHFR closed conformation. This therefore provides a negative control for the methodology, allowing us to see if we can differentiate between chemical shift perturbations caused by changes in structural conformation or those that are simply an effect of ligand binding.

The spectra for [*methyl*- ^{13}C]-methionine and [*indole*- δ_1 - ^{13}C] tryptophan labelled MpDHFR again showed poor spectral quality in the apo form, likely due to conformational heterogeneity (**Figure 3.15**). When in the Michaelis, MpDHFR:NADP⁺:folate complex, 5 and 3 well defined cross peaks were observed in the methionine and tryptophan labelled spectra respectively as expected. No significant chemical shift perturbations were observed between the MpDHFR:NADP⁺:folate and MpDHFR:NADP⁺:THF complexes (**Figure 3.16 & Table 3.5**). Although small chemical shift perturbations were observed for Met21 and Trp23 this is likely due to their location within the active site and these residues are therefore very susceptible to ligand binding effects. It is very important to be able to differentiate between chemical shift perturbations due to ligand binding effects and those as a result of large-scale conformational changes as observed in EcDHFR.

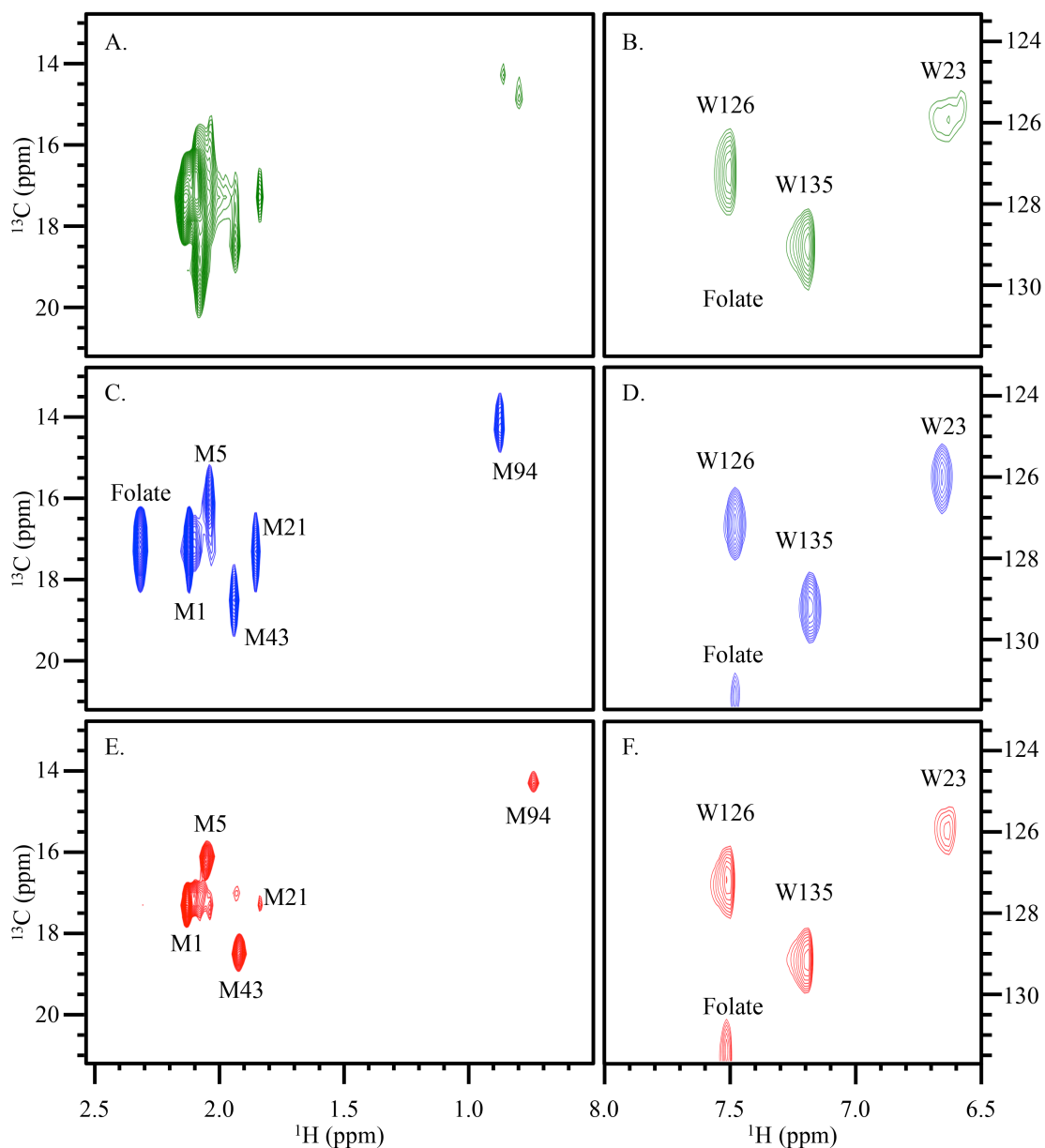


Figure 3.15: ^1H - ^{13}C HSQC spectra of ^{13}C -labelled MpDHFR complexes. (A) [*methyl*- ^{13}C]methionine-labelled MpDHFR with no ligands. (B) [δ_1 - ^{13}C] tryptophan-labelled MpDHFR with no ligands. (C) [*methyl*- ^{13}C]methionine-labelled MpDHFR in the Michaelis complex. (D) [δ_1 - ^{13}C] tryptophan-labelled MpDHFR in the Michaelis complex. (E) [*methyl*- ^{13}C]methionine-labelled MpDHFR in the product complex. (F) [δ_1 - ^{13}C] tryptophan-labelled MpDHFR in the product complex.

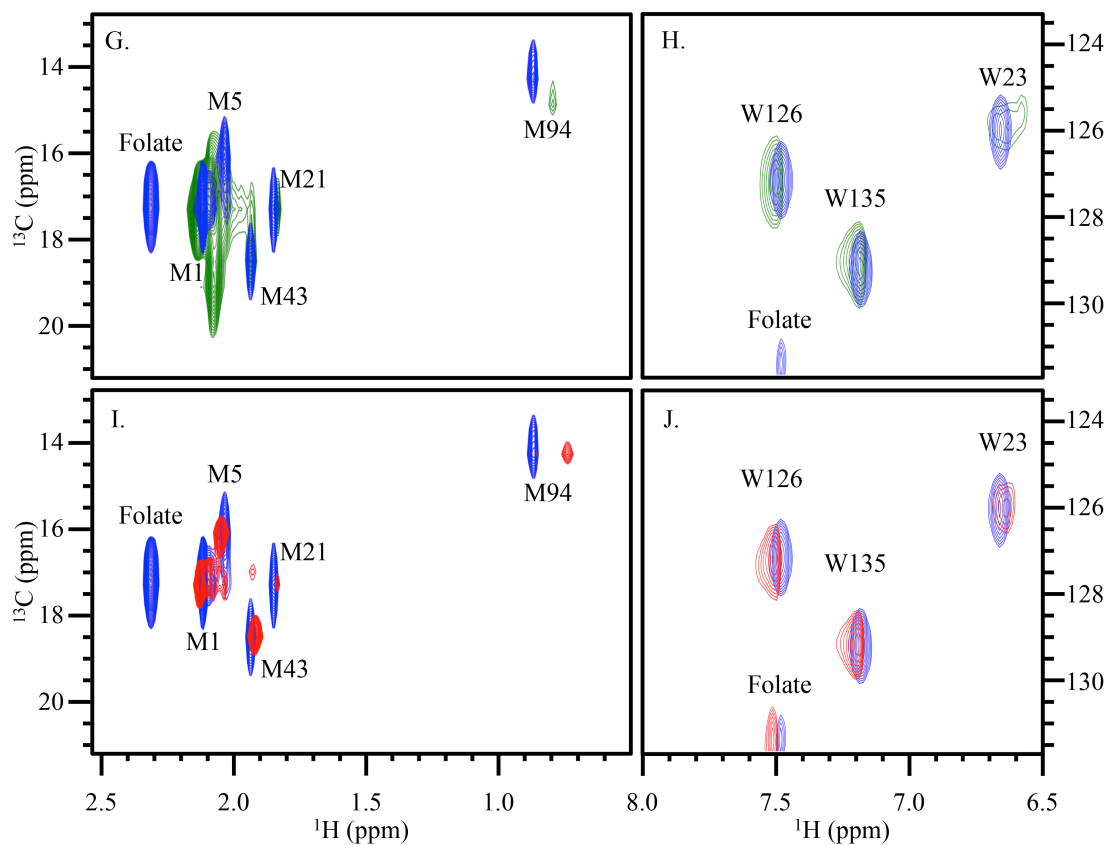


Figure 3.16: ^1H - ^{13}C HSQC spectra of ^{13}C -labelled MpDHFR complexes, Apo (green), E:NADP⁺:folate (closed conformation in EcDHFR) (blue) and E:NADP⁺:THF (occluded conformation in EcDHFR) (red). (G and I) [*methyl*- ^{13}C]methionine-labelled MpDHFR (H and J) [δ_1 - ^{13}C] tryptophan-labelled MpDHFR.

Table 3.4: Weighted chemical shift perturbations (ppm) between ^1H - ^{13}C HSQC of spectra relating to [<i>methyl</i> - ^{13}C] methionine-labelled MpDHFR.		
Residue	Apo to Michaelis complex	Michaelis to product complex
Met1	0.011	0.008
Met5	0.184	0.011
Met21	0.009	0.008
Met43	0.003	0.011
Met94	0.120	0.090

Table 3.5: Weighted chemical shift perturbations (ppm) between ^1H - ^{13}C HSQC of spectra relating to $[\delta_1\text{-}^{13}\text{C}]$ tryptophan-labelled MpDHFR.		
Residue	Apo to Michaelis complex	Michaelis to product complex
Trp23	0.016	0.015
Trp126	0.018	0.020
Trp135	0.024	0.009

Extensive chemical shift perturbations between the Michaelis and product complexes in EcDHFR have also previously been observed with ^{15}N alanine labelled EcDHFR.¹⁵⁶ MpDHFR, which acted as a negative control for this methodology exhibited no significant chemical shift perturbations between the Michaelis and product complexes. These results provide evidence this method of tryptophan and methionine side chain labelling is sufficient for probing large-scale conformational behaviour in DHFR variants. Residues located in the flexible M20 (Met16, Met20 and Trp22) loop exhibit the largest chemical shift perturbations. From crystal structures Met16 points out into bulk solvent in the apo and EcDHFR:NADP⁺:folate complex, wherein the EcDHFR:NADP⁺:THF complex the side chain points directly into the active site, drastically altering the electronic environment around the ^{13}C nucleus.⁶¹ The methyl group of Met20 faces the FG loop in the Michaelis product but becomes increasingly solvent exposed in the product complex, explaining the downfield shift observed.⁶¹ In EcDHFR the majority of methionine and tryptophan side-chains exhibit clear chemical shift perturbations. No such chemical shift perturbations are observed between the MpDHFR:NADP⁺:folate and MpDHFR:NADP⁺:THF complexes, aligning with earlier work which theorised MpDHFR failed to adopt an occluded conformation following the chemical step.⁷⁶ These results further validate our method and allow us to probe other DHFRs for an ability to adopt an occluded conformation.

As our methodology was now validated attention was returned to TmDHFR. Although it has previously been suggested TmDHFR remains in a fixed, open conformation during the catalytic cycle there existed no direct structural evidence for this claim.

As stated earlier in this chapter the elongated shape, increased mass (38 K) and thermal stability of TmDHFR led to poor tumbling and thus fast T_2 relaxation which meant no assigned triple resonance spectra could be achieved for TmDHFR.⁸⁹ Methionine and

tryptophan side-chain labelling has superior sensitivity and relaxation properties compared to traditional NMR based approaches and thus could be applied to explore conformational behaviour in TmDHFR.^{136,148,157} TmDHFR has four methionine residues and a single tryptophan residue (**Figure 3.17**).⁸⁸ Met1 was found to be present in ~10 % of protein, this is due to partial activity of aminopeptidase present in *E.coli*.¹⁵² Due to the decreased cross-peak intensity it was possible to assign Met1. No significant chemical shift perturbations were observed between [*methyl*-¹³C]-methionine labelled spectra in either the Michaelis or product complexes (**Figure 3.18 and Table 3.7**). A proton chemical shift of 0.07 ppm was observed for Trp23 between the Michaelis and product complexes, a similar shift is also observed in MpDHFR. Again this is more than likely due to ligand binding effects and not large scale conformational changes. The apo spectra for TmDHFR shows well resolved cross-peaks and no evidence of conformational heterogeneity (**Figure 3.17**). This evidence suggests TmDHFR remains in a fixed, open conformation during catalysis.

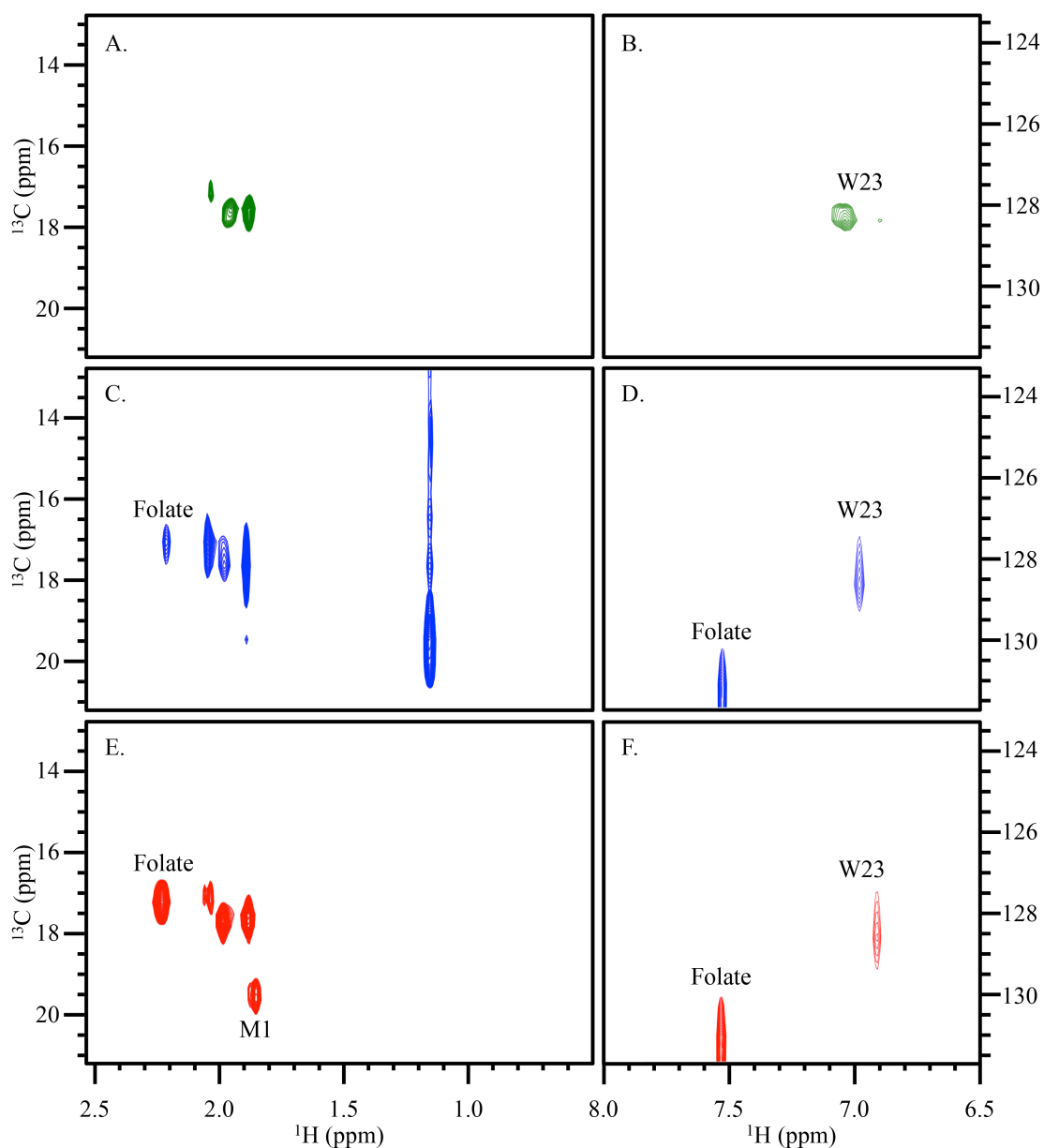


Figure 3.17: ^1H - ^{13}C HSQC spectra of ^{13}C -labelled TmDHFR complexes. (A) [*methyl*- ^{13}C]methionine-labelled TmDHFR with no ligands. (B) [δ_1 - ^{13}C] tryptophan-labelled TmDHFR with no ligands. (C) [*methyl*- ^{13}C]methionine-labelled TmDHFR in the Michaelis complex. (D) [δ_1 - ^{13}C] tryptophan-labelled TmDHFR in the Michaelis complex. (E) [*methyl*- ^{13}C]methionine-labelled TmDHFR in the product complex. (F) [δ_1 - ^{13}C] tryptophan-labelled TmDHFR in the product complex.

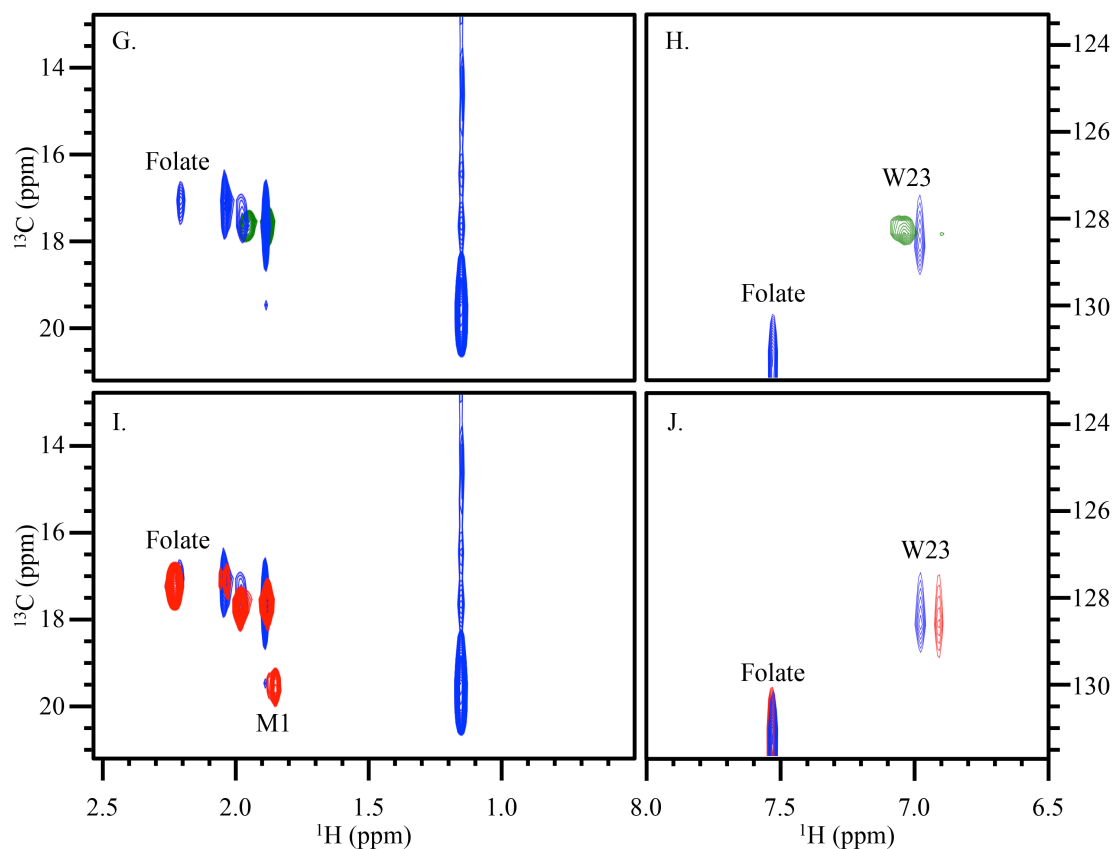


Figure 3.18: ^1H - ^{13}C HSQC spectra of ^{13}C -labelled TmDHFR complexes, Apo (green), E:NADP⁺:folate (closed conformation in EcDHFR) (blue) and E:NADP⁺:THF (occluded conformation in EcDHFR) (red). (G and I) [*methyl*- ^{13}C]methionine-labelled TmDHFR (H and J) [δ_1 - ^{13}C] tryptophan-labelled TmDHFR.

Table 3.6: Weighted chemical shift perturbations (ppm) between ^1H - ^{13}C HSQC of spectra relating to [*methyl*- ^{13}C] methionine-labelled TmDHFR.

Residue	Apo to Michaelis complex	Michaelis to product complex
Met1	0.009	0.041
Unassigned	0.009	0.001
Unassigned	0.006	0.027
Unassigned	0.016	0.013

Table 3.7: Weighted chemical shift perturbations (ppm) between ^1H - ^{13}C HSQC of spectra relating to [δ_1 - ^{13}C] tryptophan-labelled TmDHFR.

Residue	Apo to Michaelis complex	Michaelis to product complex
Trp23	0.069	0.050

To demonstrate the utility of sidechain labelling to rapidly assess the conformational landscape of multiple enzyme variants we wanted to identify a DHFR variant that also formed the occluded conformation. Previously, formation of the occluded conformation following the chemical step had only been observed in EcDHFR.⁹⁹ Although some evidence of conformational behaviour following hydride transfer step has been presented for other DHFRs. The Ser148-Asn23 interaction has previously been shown to be crucial for stabilisation of an occluded conformation.⁷⁶ Amino acid sequence analysis identified DHFR from *Salmonella enterica* (SeDHFR) as having a Ser150 residue in an equivalent position to Ser148 in EcDHFR. In place of Asn23, SeDHFR has His24 but as the hydrogen bonds form to the amide backbone this should not hinder stabilisation of an occluded conformation. No X-ray structures or triple resonance NMR assignment exists for SeDHFR. Details of the expression and purification of SeDHFR is described in chapter 4.

Like in EcDHFR and MpDHFR, the apo spectra of *methyl*-¹³C spectra of methionine labelled SeDHFR was of low quality with multiple additional cross-peaks, indicating the enzyme is in conformational heterogeneity when unbound to ligands (**Figure 3.19**). SeDHFR has 3 methionine residues but unlike EcDHFR and MpDHFR exhibits 6 well defined, equally populated cross peaks in the product complex suggesting the enzyme is in slow equilibrium between two major conformational states (**Figure 3.20**). In the Michaelis complex only 3 cross peaks are observed which match cross peaks present in spectra relating to the product complex. This suggests that in the product complex SeDHFR is in equilibrium between the Michaelis conformation and a second, uncharacterised conformation.

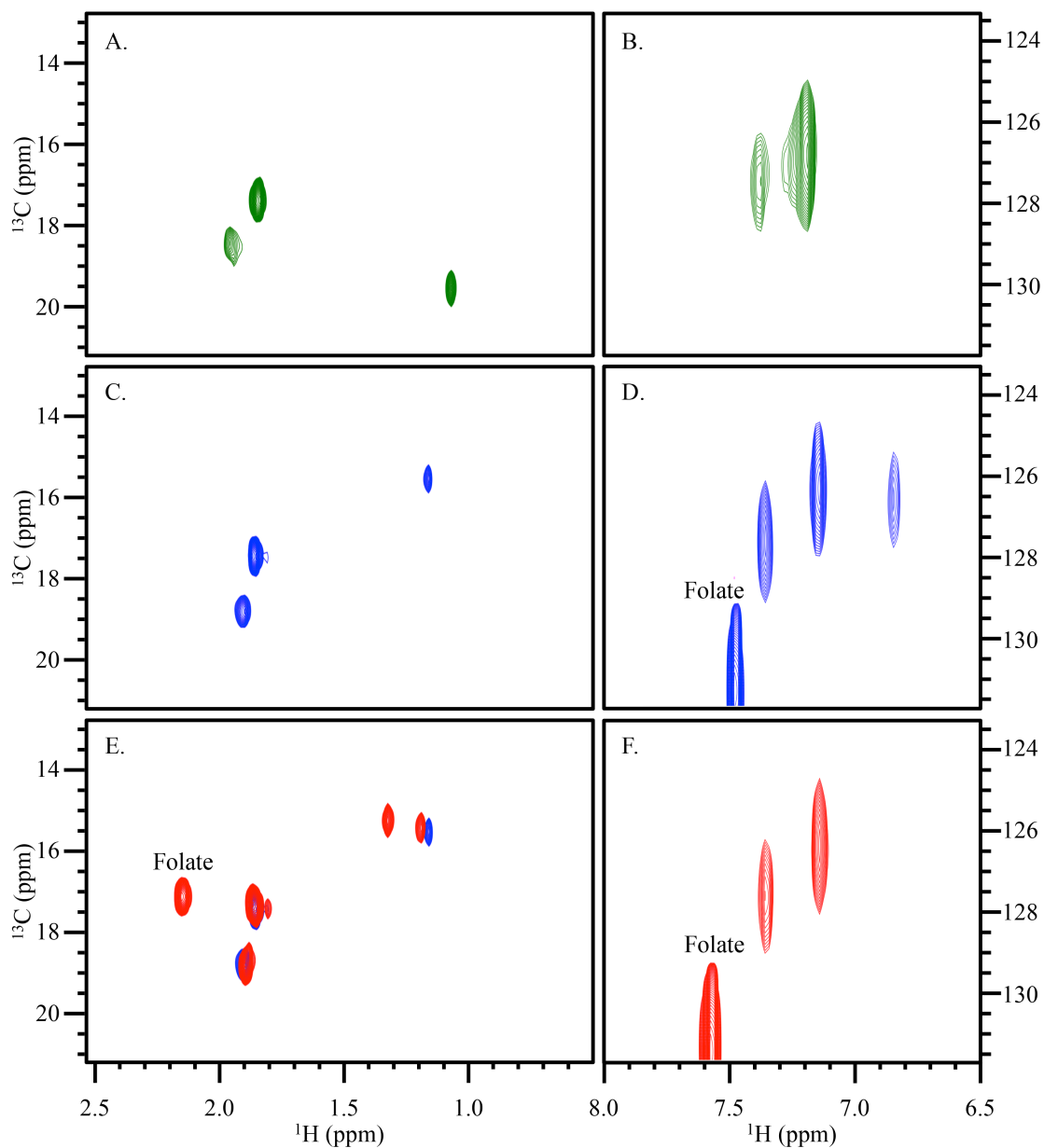


Figure 3.19: ^1H - ^{13}C HSQC spectra of ^{13}C -labelled SeDHFR complexes. (A) [*methyl*- ^{13}C]methionine-labelled SeDHFR with no ligands. (B) [δ_1 - ^{13}C] tryptophan-labelled SeDHFR with no ligands. (C) [*methyl*- ^{13}C]methionine-labelled SeDHFR in the Michaelis complex. (D) [δ_1 - ^{13}C] tryptophan-labelled SeDHFR in the Michaelis complex. (E) [*methyl*- ^{13}C]methionine-labelled SeDHFR in the product complex. (F) [δ_1 - ^{13}C] tryptophan-labelled SeDHFR in the product complex.

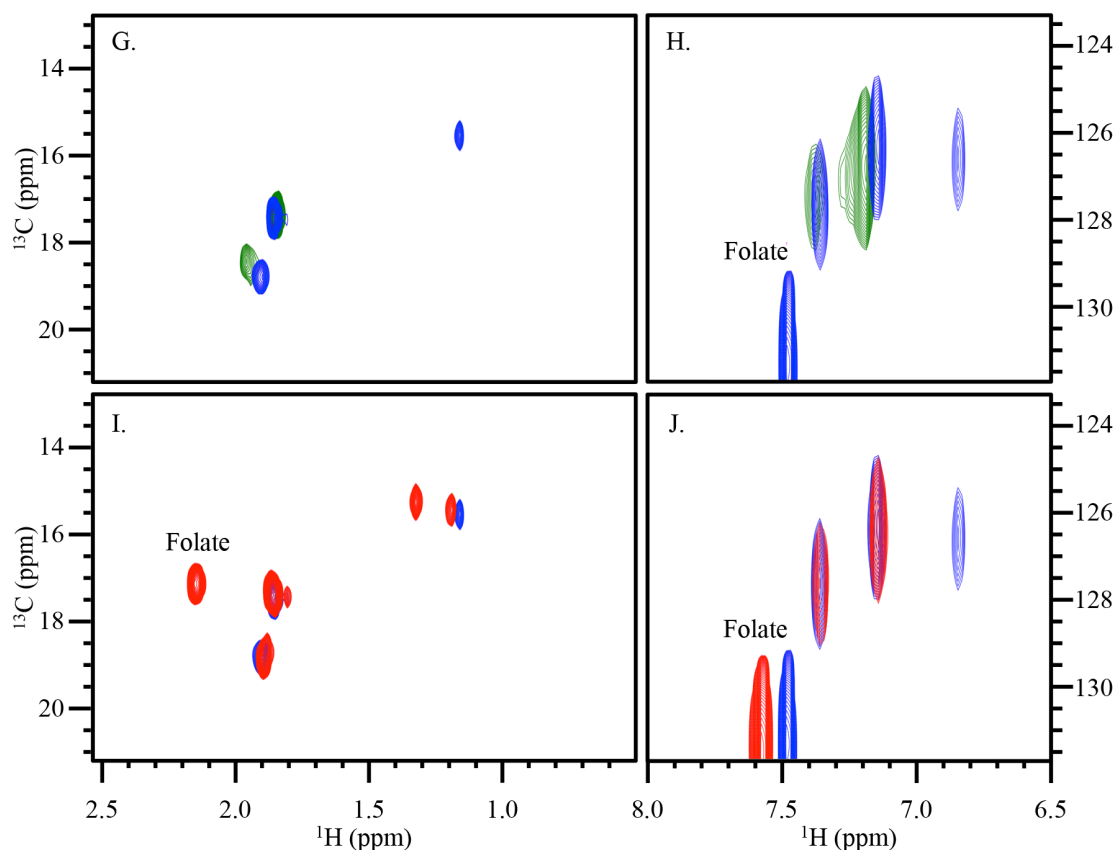


Figure 3.20: ¹H-¹³C HSQC spectra of ¹³C-labelled SeDHFR complexes, Apo (green), E:NADP⁺:folate (closed conformation in EcDHFR) (blue) and E:NADP⁺:THF (occluded conformation in EcDHFR) (red). (G and I) [*methyl*-¹³C]methionine-labelled SeDHFR (H and J) [δ_1 -¹³C] tryptophan-labelled SeDHFR.

Table 3.8: Weighted chemical shift perturbations (ppm) between ¹H-¹³C HSQC of spectra relating to [*methyl*-¹³C] methionine-labelled SeDHFR.

Residue	Apo to Michaelis complex	Michaelis to product complex
Unassigned	0.082	0.076
Unassigned	0.044	0.072
Unassigned	0.770	0.183

Table 3.9: Weighted chemical shift perturbations (ppm) between ¹H-¹³C HSQC of spectra relating to [δ_1 -¹³C] tryptophan-labelled SeDHFR.

Residue	Apo to Michaelis complex	Michaelis to product complex
Unassigned	0.105	0.062
Unassigned	0.286	0.023
Unassigned	0.244	0.000

The Ser148-Asn23 interaction is crucial for stabilisation of the occluded conformation in EcDHFR.^{53,76} To confirm whether the second conformation observed in *methyl*-¹³C spectra of methionine labelled SeDHFR is an occluded conformation the S150A-SeDHFR mutant was designed. Again in the product complex the *methyl*-¹³C spectra of methionine labelled S150A-SeDHFR exhibited evidence of two conformational states (**Figure 3.21**). However the population of the second conformation was drastically reduced, the three major cross peaks again overlapping with those in the Michaelis complex (**Figure 3.22**). It was therefore theorised that the observed second conformation may be similar the conformational change observed in EcDHFR following the chemical step. Furthermore the importance of the Ser48-Asn23 interaction in the stabilisation of an occluded conformation was reinforced. With respect to the [indole- δ_1 -¹³C] tryptophan labelled spectra for SeDHFR and the S150A-SeDHFR spectra no significant chemical shift perturbations were observed between the Michaelis and product complexes, yielding no evidence of conformational change.

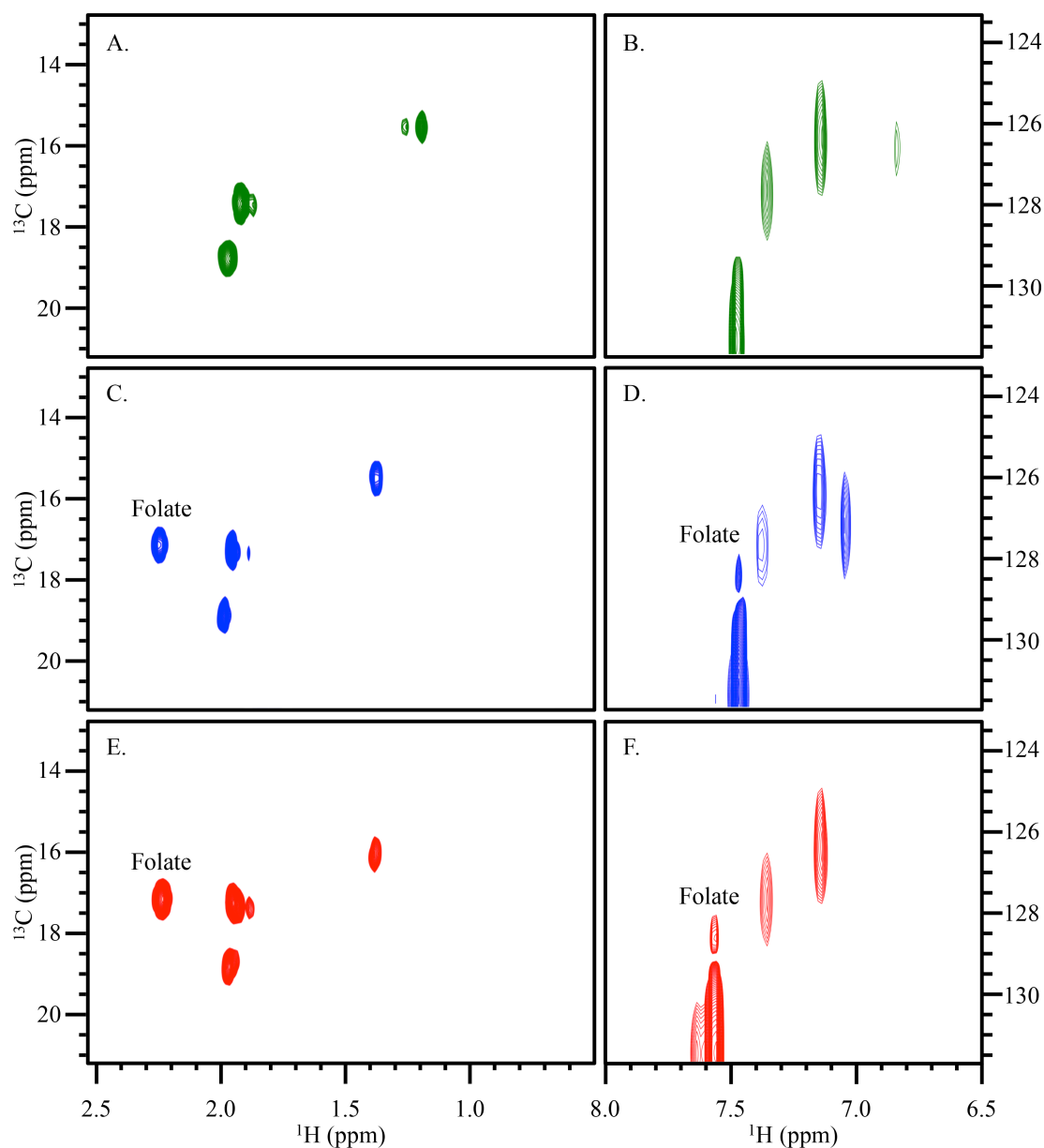


Figure 3.21: ^1H - ^{13}C HSQC spectra of ^{13}C -labelled S150A-SeDHFR complexes. (A) [*methyl*- ^{13}C]methionine-labelled S150A-SeDHFR with no ligands. (B) [δ_1 - ^{13}C] tryptophan-labelled S150A-SeDHFR with no ligands. (C) [*methyl*- ^{13}C]methionine-labelled S150A-SeDHFR in the Michaelis complex. (D) [δ_1 - ^{13}C] tryptophan-labelled S150A-SeDHFR in the Michaelis complex. (E) [*methyl*- ^{13}C]methionine-labelled S150A-SeDHFR in the product complex. (F) [δ_1 - ^{13}C] tryptophan-labelled S150A-SeDHFR in the product complex.

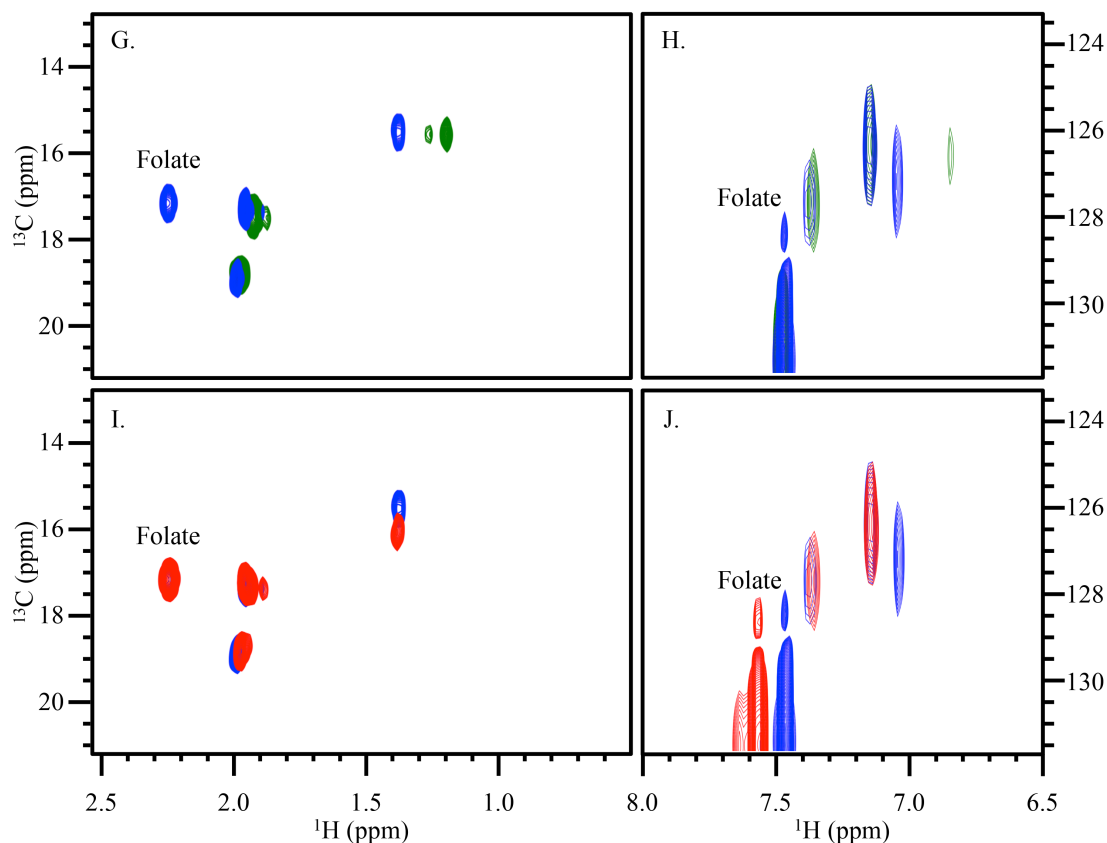


Figure 3.22: ^1H - ^{13}C HSQC spectra of ^{13}C -labelled S150A-SeDHFR complexes, Apo (green), E:NAD $^+$:folate (closed conformation in EcDHFR) (blue) and E:NAD $^+$:THF (occluded conformation in EcDHFR) (red). (G and I) [*methyl*- ^{13}C]methionine-labelled S150A-SeDHFR (H and J) [δ_1 - ^{13}C]tryptophan-labelled S150A-SeDHFR.

Table 3.10: Weighted chemical shift perturbations (ppm) between ^1H - ^{13}C HSQC of spectra relating to [<i>methyl</i> - ^{13}C] methionine-labelled SeDHFR-S150A.		
Residue	Apo to Michaelis complex	Michaelis to product complex
Unassigned	0.021	0.021
Unassigned	0.044	0.002
Unassigned	0.311	0.083

Table 3.11: Weighted chemical shift perturbations (ppm) between ^1H - ^{13}C HSQC of spectra relating to [δ_1 - ^{13}C] tryptophan-labelled SeDHFR-S150A.		
Residue	Apo to Michaelis complex	Michaelis to product complex
Unassigned	0.240	0.021
Unassigned	0.188	0.219
Unassigned	0.168	0.029

To further confirm our theory that SeDHFR adopts a second conformation following the chemical step, ^{15}N labelled SeDHFR was expressed. ^1H - ^{15}N HSQC spectra were recorded of the enzyme in both the Michaelis and product complexes (**Figure 3.23**). Like in the spectra of *methyl*- ^{13}C spectra of methionine labelled SeDHFR significant chemical shift perturbations was observed between complexes. This further suggests the second conformation observed in SeDHFR is most likely the formation of an occluded conformation. Unlike EcDHFR and MpDHFR, SeDHFR has no methionine residues located in the flexible M20 loop, although Met42 and Met92 are conserved in all three DHFR variants. Met42 and Met92 show significant chemical shift perturbations in EcDHFR and SeDHFR but not in MpDHFR. Methionine probes even when located distal to the active site therefore prove to be effective in mapping conformational behaviour.

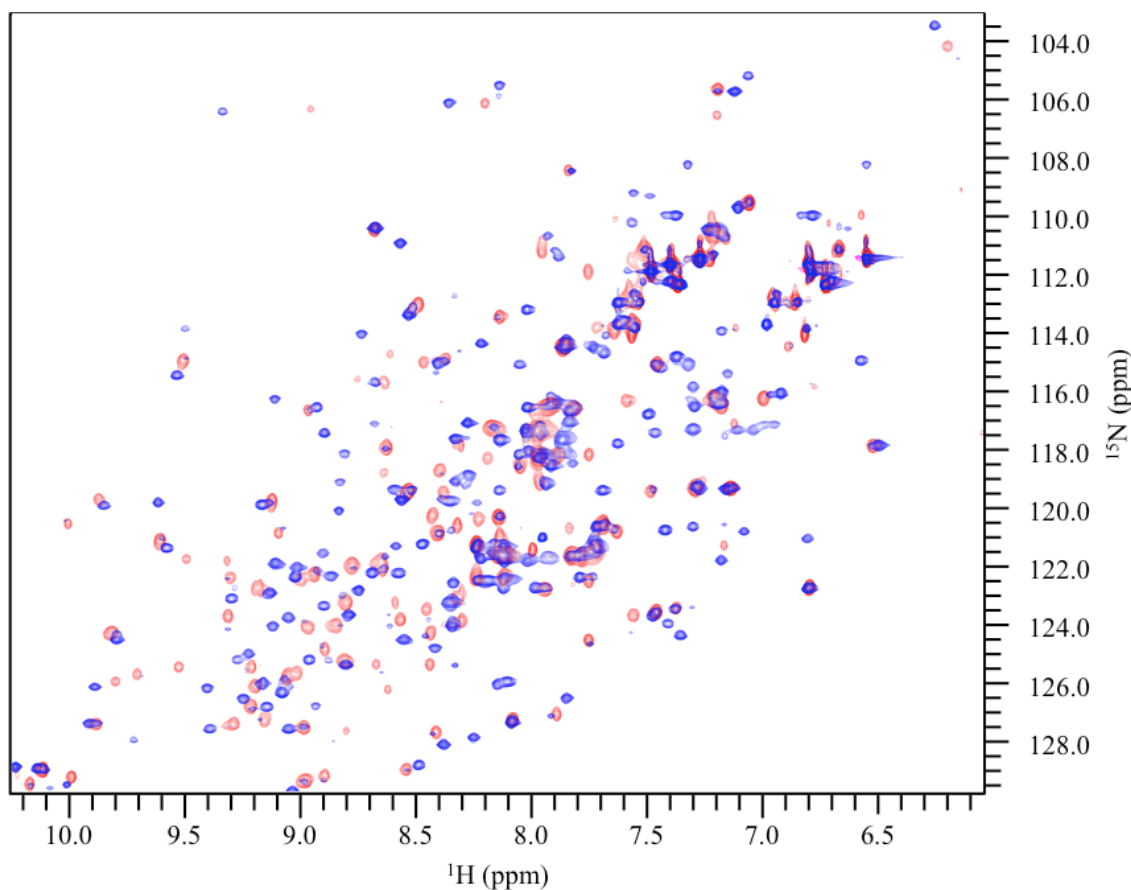


Figure 3.23: Two overlaid ^1H - ^{15}N HSQC spectra of ^{15}N labelled SeDHFR in both the Michaelis (blue) and product complexes (red).

[*methyl*- ^{13}C]-methionine labelling was found to be superior over [*indole*- δ_1 - ^{13}C] tryptophan labelling as a diagnostic tool for studying conformational behaviour in DHFR variants. Trp22 in all four DHFRs studied is found to form hydrogen bonds to bound folates in the active site, and as such is particularly susceptible to ligand binding effects.¹⁵⁰ This explains the small chemical shift perturbation observed with respect to this residue in TmDHFR and MpDHFR between each of the measured complexes. EcDHFR exhibits large chemical shift perturbations between the apo and Michaelis complex but no significant differences between the apo and product complexes. SeDHFR, on the other hand, shows no significant chemical shift perturbations at Trp22 for any of the measured complexes, highlighting how ligand-binding effects could mitigate chemical shift differences that would otherwise arise from changes in conformational behaviour. No evidence of conformational heterogeneity is also observed in apo spectra of EcDHFR, MpDHFR and SeDHFR in the [*indole*- δ_1 - ^{13}C] tryptophan labelled spectra like in the [*methyl*- ^{13}C]-methionine labelled spectra.

Although [indole- δ_1 - ^{13}C] tryptophan labelled spectra produced no chemical shift perturbations between the Michaelis and product complexes it is still evident that conformational behaviour can be tracked through tryptophan labelling as spectra relating to EcDHFR testifies. This is likely due to the increased number of tryptophan residues present in EcDHFR.

3.6 Summary and Conclusions

Although [*methyl*- ^{13}C]-methionine labelling and [indole- δ_1 - ^{13}C] tryptophan labelling were used with different protein samples they could be performed in the same protein. Spectra relating to EcDHFR and SeDHFR provided clear evidence of large-scale conformational changes following the chemical step, which had not been previously observed in any other DHFRs. The occluded conformation is stabilised by the Ser148-Asn23 interaction in EcDHFR, in MpDHFR Ser148 is replaced by Pro150, and it has previously been published that loop motions must not be critical for efficient catalysis in MpDHFR as it remains in a closed conformation during catalysis.⁷⁶ It is thought that the occluded conformation lowers the binding affinity for NADP^+ as the switch to the occluded conformation occurs immediately after hydride transfer in EcDHFR, possibly mitigating any product inhibition effects.^{76,158} At close to physiological conditions MpDHFR and EcDHFR have similar single turnover rates and it has been concluded that the ability to switch to the occluded conformation does not impact significantly on hydride transfer. It has also been shown that increased distance between reactants in the occluded conformation would effectively make hydride transfer not possible.^{76,139}

Although assignment of specific residues in TmDHFR and SeDHFR was not possible it presented no impediment to our method. Theories that TmDHFR remains in a fixed, open conformation during catalysis was based upon two crystal structures, neither of which effectively modelled either the Michaelis or product complexes.⁸⁹ Through side chain labelling described in this thesis the first direct evidence that TmDHFR does indeed remain in a fixed, open conformation during catalysis has been presented. The simplicity and low cost of the labelling strategies meant methionine or tryptophan labelled DHFR variants could be made and spectra rapidly recorded and interpreted. Again the lack of assignment data was no impediment, clear chemical shift perturbations between the Michaelis and occluded complexes indicating a definitive

change in conformational behaviour. Like in the product complex of EcDHFR evidence of an occluded conformation in SeDHFR has been observed. In SeDHFR however, equimolar concentrations of two conformations is observed, one of which is proposed to be the Michaelis complex.

Traditional NMR approaches are significantly more expensive than the side-chain labelled experiments detailed here. Evidence of conformational behaviour if observed could be expanded into crystallography or more detailed NMR study if interest warrants. The cost of [*methyl*-¹³C]-methionine labelling and [*indole- δ_1* -¹³C] tryptophan is ~£11 and ~£96 per litre of culture made respectfully, where as doubly labelled (¹³C and ¹⁵N) or triply labelled (²H, ¹³C and ¹⁵N) which is necessary for triple resonance assignment costs ~£262 or ~£622 per litre of culture respectively. The spectra produced are also much simpler than that produced by traditional methods and often allows for simple, intuitive interpretation of the data. A full ¹H-¹³C HSQC is also recorded over a spectral window of ~70 ppm, opposed to a window of 10-14 ppm in side chain experiments, drastically decreasing NMR acquisition time. In the case of [*methyl*-¹³C]-methionine labelled spectra the three equivalent protons on the methyl group also increase the sensitivity of the NMR experiment, perfect for studying systems where T_2 relaxation is poor.

Through CPMG ¹⁵N relaxation experiments EcDHFR has been shown to sample conformational states belonging to the preceding and following complex in its catalytic cycle. It would be of interest to expand on the methodology described here and observe whether sidechain labelling would be sufficient for CPMG experiments to be performed within DHFR variants.

4

Hydride Transfer and Catalysis by *Salmonella enterica* DHFR

4.1 Introduction

Enzymes utilise a multitude of motions on various timescales to efficiently catalyse reactions. Although the role of slower protein motions are somewhat established, the influence of fast femto-pico second motions on the chemical step of catalysis is still hotly debated.⁵³ A number of reports have proposed the coupling of fast femto-pico second dynamics to the chemical step of catalysis. These motions have been proposed to be long ranging, involving amino acid residues distal to the active site.^{31,48,49,79,159–165}

In the last 15 years the use of heavy isotope labelling to probe the influence of such fast motions acting upon the chemical step of catalysis has been developed. Heavy isotope labelling is achieved by expressing the enzyme in minimal media containing ²H, ¹³C & ¹⁵N labelled feedstock.⁷⁹ It is considered that heavy isotope labelling does not influence the electrostatic properties of the enzyme; instead the vibrations between bonds are slowed. Therefore differences in rate constants between heavy and natural abundance enzymes are considered to originate from a slowing of protein motions as a result of mass induced effects. The study of enzyme KIE on the chemical step of catalysis allows for an insight into how or if dynamic coupling influences the chemical step of catalysis.^{48,49,53} In this thesis the term dynamics is used to refer to fast (femto-pico second), non-stochastic motions.

A number of DHFR variants that live under a wide temperature range have been studied with respect to protein dynamics and its influence on catalysis including; EcDHFR (mesophile),^{107,113–115,166,167} MpDHFR (psychrophilic),⁴⁷ BsDHFR (Thermophile)¹²⁰ and TmDHFR (hyper-thermophile).^{53,168} The study of multiple DHFRs sourced from various physiological temperatures allows for a broader insight into the role dynamic coupling plays in catalysis. SeDHFR, like EcDHFR originates from a mesophilic bacterium and as such presents an opportunity to further investigate the relationship between dynamic coupling and catalysis in DHFRs and see if previous observations between the relationship of dynamics and catalysis holds true. Furthermore, SeDHFR is of interest, as like EcDHFR, it is believed to adopt an occluded like conformation following the chemical step.

By the study of single-turnover primary KIE and enzyme KIE and comparison of such results to other previously recorded DHFR homologues the relationship between dynamic coupling and catalysis in SeDHFR will be reported on in this chapter.

4.2 Expression and Purification of ^{13}C & ^{15}N SeDHFR

The gene encoding for SeDHFR (UniProt I.D. P12833) was purchased from GenScript in a pET-11b vector and transformed into One Shot™ BL21 Star™ (DE3) chemically competent cells. In order to grow heavy isotope (^{13}C and ^{15}N) labelled SeDHFR, protein was recombinantly overproduced in minimal media (M9) containing ^{13}C glucose and ^{15}N ammonium chloride, as described in **section 2.3.2**. Natural abundance SeDHFR was expressed in LB media.

Purification of SeDHFR largely followed previously published procedures for other DHFR variants with some adaptations to the method.¹⁵³ Unlike EcDHFR and MpDHFR it was found that SeDHFR had an insufficient interaction with anion exchange resin (Q-sepharose) at pH 7.0 causing the protein to elute immediately with multiple impurities. Adjusting the pH of the buffers to 8.0 resulted in the enzyme having a partial interaction with the column but the protein still eluted prior to the start the salt gradient (**Figure 4.1**) (section 2.3.3.2). The fractions containing SeDHFR were concentrated and further purified on a HiLoad Superdex G75 (GE Healthcare) size exclusion column and the protein eluted with an isocratic gradient (buffer C) (**Figure 4.2**) (section 2.3.3.3). The purity of the protein was evaluated with SDS-PAGE, which showed a band with a molecular weight of ~18000, coinciding with a molecular weight of 18032.6 calculated for SeDHFR (**Figure 4.3**).

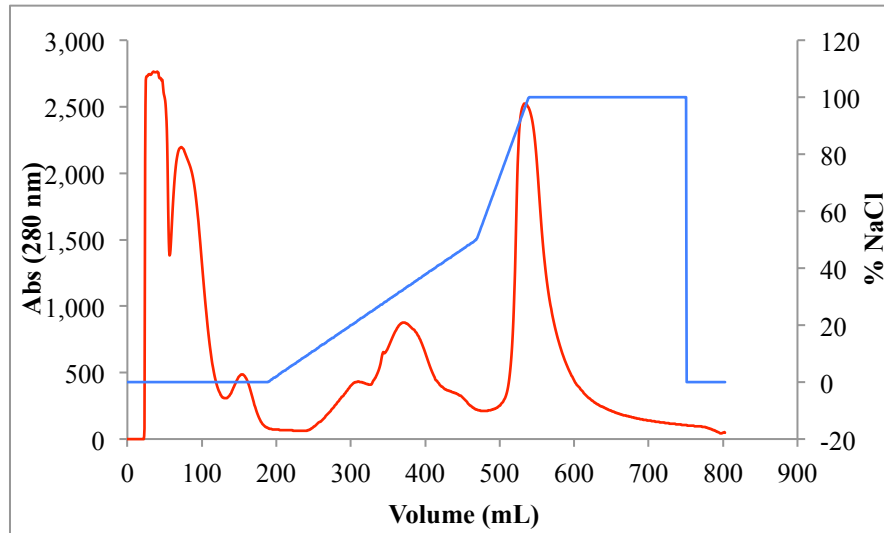


Figure 4.1: Chromatogram of the elution trace (red) of SeDHFR from the Q-Sepharose column. The salt gradient (% NaCl) is in blue. SeDHFR eluted before the salt gradient (60-120 mL).

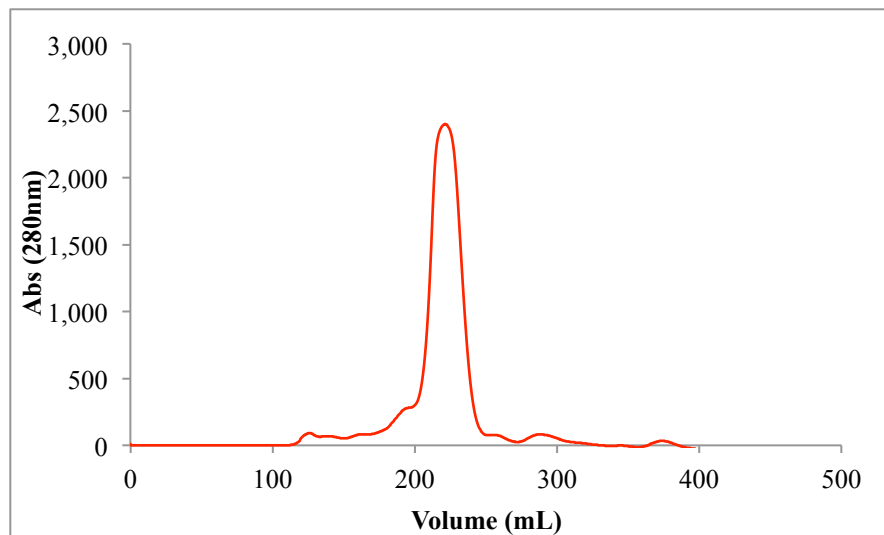


Figure 4.2: Chromatogram of the elution trace (red) of SeDHFR from the HiLoad Superdex G75 (GE Healthcare). SeDHFR elutes between 210-230 mL.

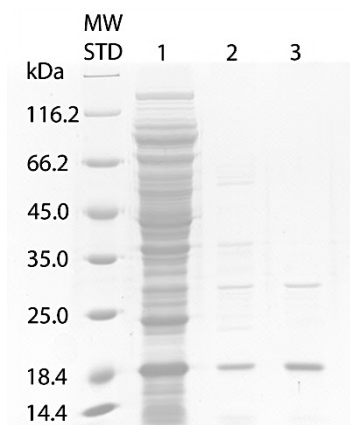


Figure 4.3: SDS-polyacrylamide gel showing; 1) Cell Lysate 2) Combined fractions from Q-Sepharose column 3) After size exclusion chromatography (BSD75). MW of SeDHFR = 18,032.

Mass spectrometry (ESI-MS) was used to measure the mass difference between heavy labelled SeDHFR and that of natural abundance SeDHFR. The calculated mass of the natural abundance enzyme was 18032.6. The mass spectrometry result was in agreement with this as the de-convoluted spectrum gave a mass of 18036.2 ± 1.6 (**Figure 4.4**). The mass of mono-isotopic SeDHFR was calculated to be 18012.00 and the weight of ^{13}C , ^{15}N labelled SeDHFR to be 19044.00. A mass spectrum of the heavy enzyme yielded a mass of 19031.6 ± 6.0 , corresponding to a mass increase of $\sim 5.5\%$, indicating $>98.7\%$ of carbon and nitrogen atoms were successfully labelled (**Figure 4.5**).

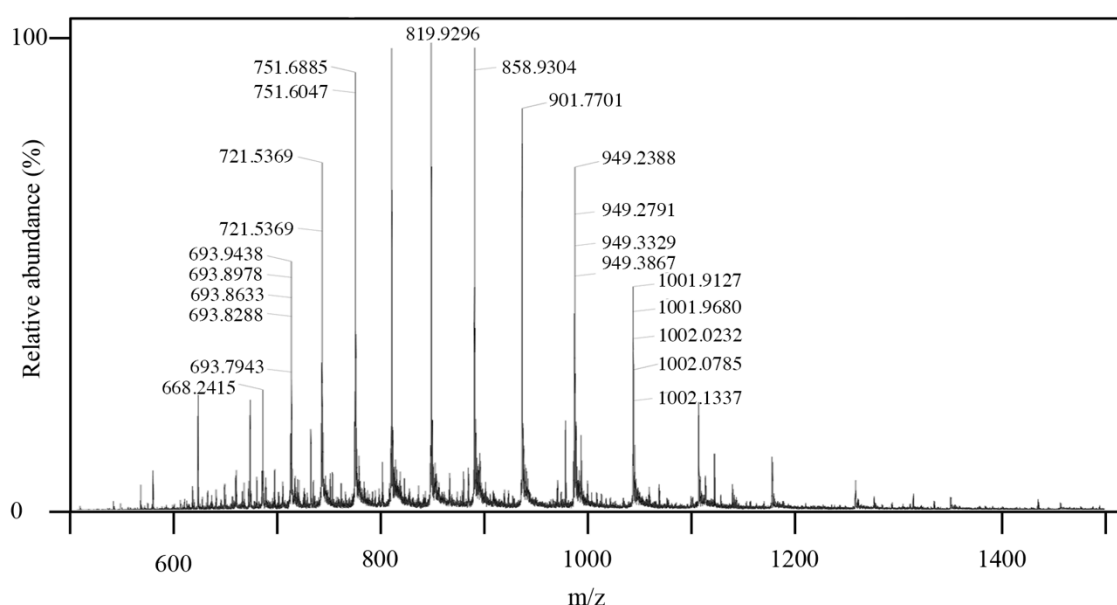


Figure 4.4: Deconvoluted ESI mass spectrum of natural abundance SeDHFR (18036.2 ± 1.6).

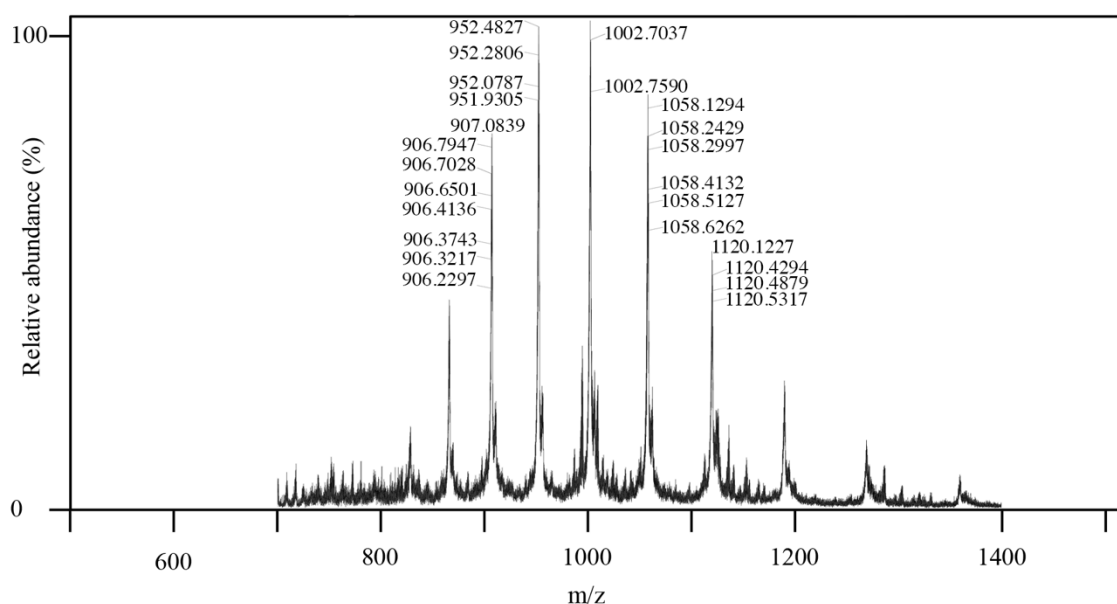


Figure 4.5: Deconvoluted ESI mass spectrum SeDHFR labelled with ^{13}C and ^{15}N (19031.6 ± 6.0).

4.3 Circular Dichroism analysis and Thermal Unfolding of SeDHFR

Circular dichroism (CD) spectra were recorded for the both the natural abundance and the heavy labelled enzyme to confirm ^{13}C and ^{15}N heavy isotope labelling had not altered structural elements of the protein (**Figure 4.6**). CD spectra for both the light and heavy enzyme were almost superimposable, indicating that isotopic labelling does not have a detrimental effect on structure. Both traces are also characteristic of folded proteins, with a broad minima between 208 and 222 nm and a peak at 193 nm corresponding to the alpha helix.¹⁶⁹

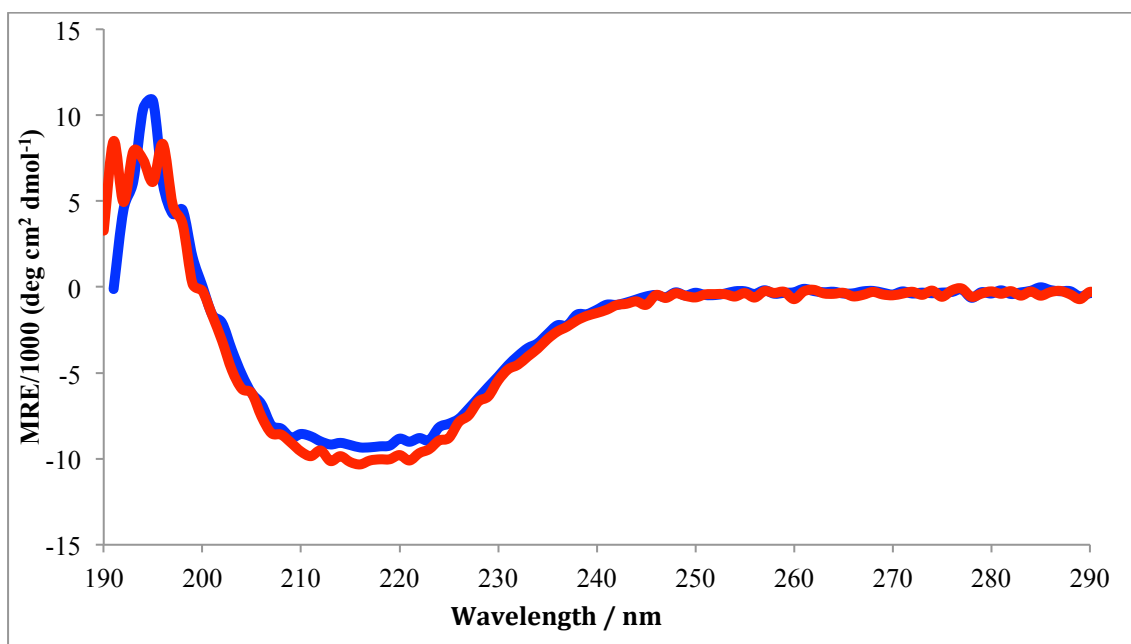


Figure 4.6: CD spectra of natural abundance (blue) and ^{13}C and ^{15}N labelled (red) SeDHFR, recorded at 20 °C.

Thermal melting temperatures (T_m) were also calculated for natural abundance and heavy labelled SeDHFR by measuring the change in mean residue ellipticity (MRE) at 208 nm over a temperature range of 5 to 80 °C. For natural abundance SeDHFR a rapid loss in secondary structure was observed between 52 and 61 °C and the T_m was calculated to be 54.3 °C (**Figure 4.7**). This is similar to the value obtained for EcDHFR ($T_m = \sim 51$ °C).¹¹⁵ No significant differences, with respect to T_m , were observed between the natural abundance and heavy labelled SeDHFR (54.7 °C) thus indicating that isotope labelling did not impact the thermal stability of the enzyme.

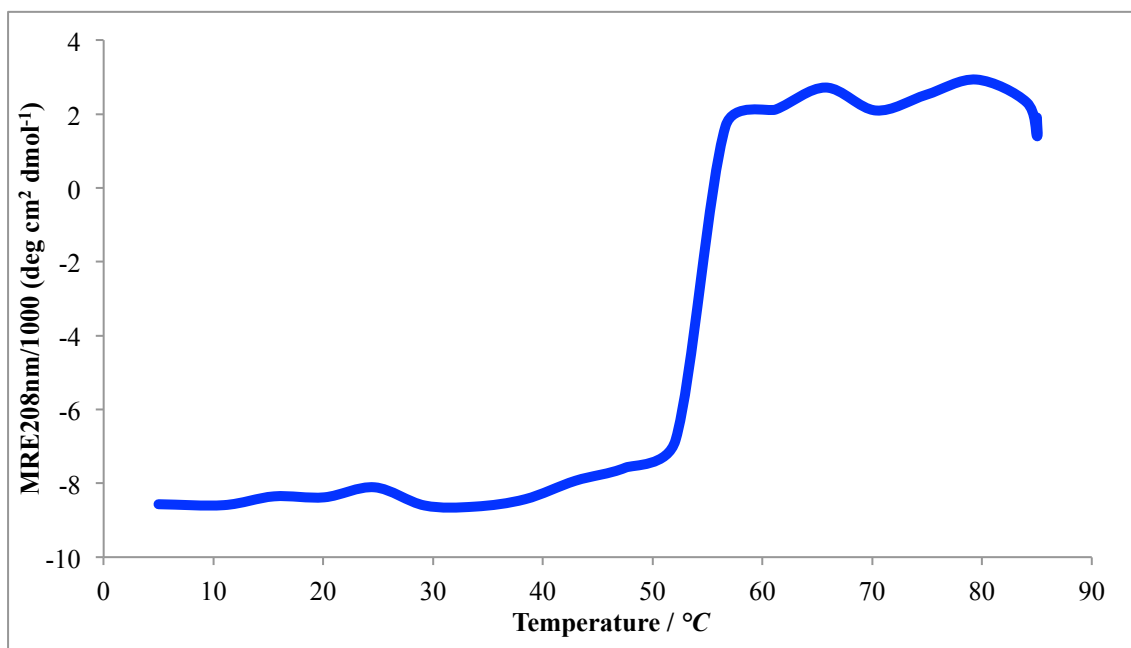


Figure 4.7: MRE recorded at 208 nm over a temperature range of 5 to 85 °C for natural abundance SeDHFR.

4.4 Steady State Kinetics of SeDHFR

The steady-state rate of the reaction catalysed by SeDHFR was measured using UV-Vis spectroscopy, monitoring the decrease in absorbance at 340 nm, corresponding to the oxidation of the nicotinamide ring of NADPH. The rate of reaction can therefore be calculated from the change in absorption using the Beer-Lambert-Bouguer law (**Equation 4.1**) with an extinction coefficient (ϵ) of $11800 \text{ M}^{-1} \text{ cm}^{-1}$, which corresponds to the enzyme-substrate complex.¹²⁹

$$A = \epsilon \times l \times c$$

Equation 4.1: The Beer-Lambert-Bouguer law, A is the change in absorbance at a measured wavelength, ϵ equates to the molar absorptivity at a specific wavelength, l refers to the path length and c refers to the concentration of the substrate.

Steady state kinetics works on the principle that rate of formation of product is in equilibrium with the rate of formation of the enzyme-substrate complex. To accomplish this the concentration of reactants are used in vast excess with respect to the

concentration of enzyme. Each measurement was taken over a period of 60 seconds and was performed in triplicate with 3 different batches of enzyme, for a total of nine measurements.

4.5 Effect of Temperature on Steady State Kinetics of SeDHFR

The kinetics of SeDHFR have not previously been characterised. The measured k_{cat} value for SeDHFR at pH 7.0 and at 20 °C ($8.6 \pm 0.3 \text{ s}^{-1}$) is similar, although slightly slower than that measured for EcDHFR ($12.6 \pm 1.4 \text{ s}^{-1}$)⁹⁰ at the same temperature and pH. MpDHFR ($14.8 \pm 0.8 \text{ s}^{-1}$)¹⁷⁰ and BsDHFR ($16.2 \pm 2.8 \text{ s}^{-1}$)¹⁴⁵ are however, almost twice as fast under the same conditions. The k_{cat} for SeDHFR is however ~72 fold faster than TmDHFR ($0.2 \pm 0.02 \text{ s}^{-1}$)⁹⁰ at pH 7.0 and 25 °C (**Table 4.1, Figures 4.8 and 4.9**). Like other DHFRs the steady state turnover rate increases exponentially with respect to temperature in accordance with expected Arrhenius behaviour.

Table 4.1: Temperature dependence of the catalytic turnover (k_{cat}) on SeDHFR and the DHFR variants EcDHFR, MpDHFR, BsDHFR and TmDHFR at pH 7.0.

Temperature (°C)	SeDHFR k_{cat} (s ⁻¹)	EcDHFR ^[a] k_{cat} (s ⁻¹)	MpDHFR ^[b] k_{cat} (s ⁻¹)	BsDHFR ^[c] k_{cat} (s ⁻¹)	TmDHFR ^[a] k_{cat} (s ⁻¹)
5	2.2 ± 0.2	N/A	5.9 ± 0.2	N/A	N/A
10	3.2 ± 0.1	N/A	8.2 ± 0.4	7.0 ± 2.0	N/A
15	6.2 ± 0.4	8.5 ± 1.2	10.8 ± 0.5	9.3 ± 2.2	N/A
20	8.6 ± 0.3	12.6 ± 1.4	14.8 ± 0.8	16.2 ± 2.8	N/A
25	14.4 ± 0.2	16.4 ± 3.6	18.7 ± 0.8	21.6 ± 1.6	0.20 ± 0.02
30	21.0 ± 0.2	24.0 ± 3.0	25.3 ± 1.1	32.7 ± 1.4	0.35 ± 0.02
35	28.1 ± 0.5	32.0 ± 5.0	32.5 ± 1.9	48.6 ± 6.8	0.47 ± 0.04
40	38.4 ± 0.2	44.9 ± 6.1	39.6 ± 1.8	66.7 ± 3.9	0.61 ± 0.04
45	N/A	53.9 ± 5.6	28.8 ± 0.8	87.3 ± 2.3	0.83 ± 0.07
50	N/A	N/A	N/A	116.0 ± 5.0	1.17 ± 0.07
55	N/A	N/A	N/A	145 ± 8	1.53 ± 0.09
60	N/A	N/A	N/A	183 ± 8	2.00 ± 0.16
65	N/A	N/A	N/A	236 ± 18	2.70 ± 0.14
70	N/A	N/A	N/A	243 ± 12	3.40 ± 0.28
75	N/A	N/A	N/A	N/A	4.05 ± 0.39
80	N/A	N/A	N/A	N/A	~4.8*

* Indicates extrapolated values, [a] data taken from reference,⁹⁰ [b] data taken from reference,¹⁷⁰ [c] data taken from reference.¹⁴⁵

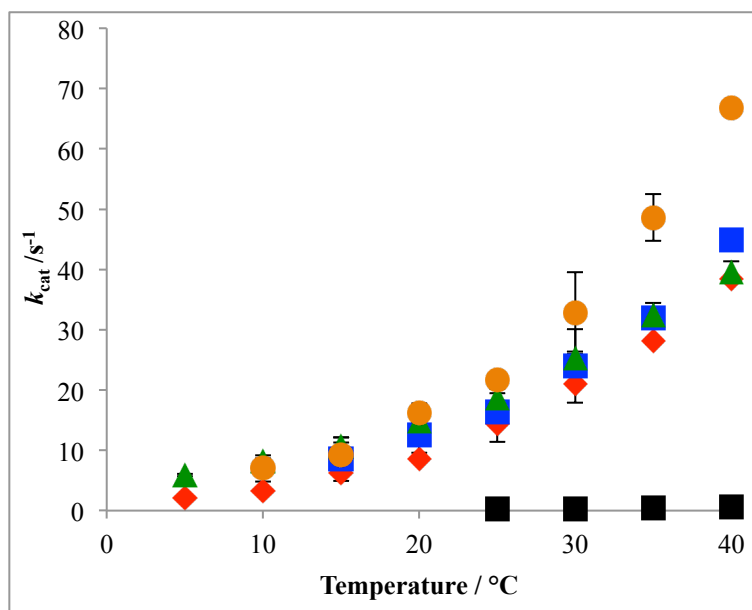


Figure 4.8: Effect of temperature (range of 5-40 °C shown only) on the steady state rate constant for five DHFR variants at pH 7.0. SeDHFR (red diamond), EcDHFR (blue square), MpDHFR (green triangle), BsDHFR (orange circle) and TmDHFR (black square).

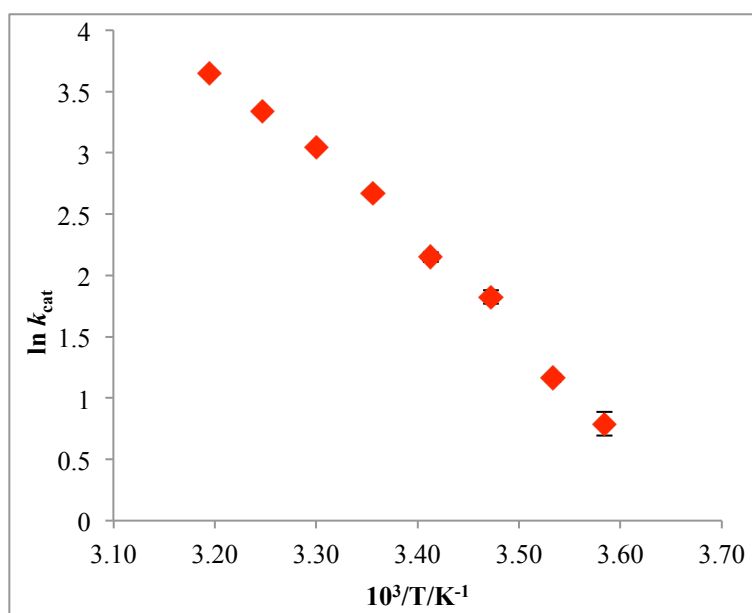


Figure 4.9: Arrhenius plot of the effect of temperature on the steady state rate of SeDHFR at pH 7.0.

The activation energy (E_a) for the SeDHFR catalysed reaction is 61.6 +/- 0.6 kJ mol⁻¹ which is slightly higher than values reported for other bacterial DHFRs including BsDHFR and TmDHFR which are thermophilic (**Table 4.2**).^{90,145} Lower E_a values are usually synonymous with psychrophilic enzymes, as is the case with MpDHFR as there is less thermal energy available to overcome the activation barrier.^{84,171,172} Like

EcDHFR and BsDHFR, SeDHFR ($27.44 \pm 0.2 \times 10^8 \text{ s}^{-1}$) has a much higher Arrhenius pre-factor than either TmDHFR or MpDHFR (**Table 4.2**).

Table 4.2: Activation parameters for SeDHFR and the DHFR variants EcDHFR, MpDHFR, BsDHFR and TmDHFR at pH 7.0.					
	SeDHFR	EcDHFR ^[a]	MpDHFR ^[b]	BsDHFR ^[c]	TmDHFR ^[a]
E_a [kJ mol ⁻¹]	61.6 ± 0.6	47.7 ± 0.8	39.9 ± 0.5	51.0 ± 3.5	51.9 ± 0.6
A_H [10^8 s^{-1}]	27.44 ± 0.2	38.4 ± 1.3	1.84 ± 0.39	88.8 ± 0.5	0.86 ± 0.02
[a] data taken from reference, ⁹⁰ [b] data taken from reference, ¹⁷⁰ [c] data taken from reference. ¹⁴⁵					

4.6 Effect of pH on Steady State Kinetics of SeDHFR

The DHFR catalysed reaction not only transfers a hydride to the C6 position of DHF from the nicotinamide ring of NADPH but also catalyses the protonation of the N5 position of DHF.^{50,51} Altering the pH of the solution will change both the ionisation state of residues in the active site as well as the number of protons available in solution. The relationship between pH and steady state rate was characterised in SeDHFR over a pH range of 5 to 9 using MTEN buffer at 20 °C (**Figure 4.10**). At low pH the k_{cat} is diminished (at pH 9.0, $k_{\text{cat}} = 2.94 \pm 0.13 \text{ s}^{-1}$), rising to a maximum of $12.05 \pm 0.08 \text{ s}^{-1}$ at pH 7.5. At higher pH values the k_{cat} decreases to $5.60 \pm 0.08 \text{ s}^{-1}$ at pH 5.0.

SeDHFR, like MpDHFR has a steady state pH dependency that forms a bell shaped curve.⁸⁴ EcDHFR on the other hand does not exhibit a significant decrease in steady state rate at lower pH and has a sigmoidal curve.¹⁷³ The mutant MpDHFR-P150S, that is postulated to allow MpDHFR to stabilise an occluded-like conformation was also found to have a sigmoidal relationship with respect to pH, similar to EcDHFR.⁷⁶ However, the mutant EcDHFR-S148P, where formation of the occluded conformation is destabilised, also exhibited a sigmoidal curve, however, the rate of k_{cat} was reduced by ~80 % across the measured pH range compared to the wild type enzyme.⁷⁶

A bell shaped pH dependency is also observed in a triple mutant of EcDHFR wherein residues from human DHFR are inserted into the α C helix.⁹⁷ A decrease in k_{cat} at low pH values was attributed to poor dissociation of THF at lower pH values.⁹⁷ These

changes with respect to pH dependency have been postulated to be a result of changes to different rate limiting steps.⁷⁶ However, release of THF from the product complex in MpDHFR was found to be independent of pH.⁷⁶ The decrease in rate at low pH values has been shown not to be a result of His24 in the active site being protonated in MpDHFR.⁸⁴ It is also unlikely that the decrease is a result of MpDHFR or SeDHFR becoming denatured as both enzymes are able to withstand pH values of 5.0 for a period of at least 30 minutes without any significant decrease in steady state rate.⁸⁴

NMR studies reported in the previous chapter of this thesis propose that SeDHFR adopts a second conformation following the chemical step, like EcDHFR. The steady state rate (k_{cat}) of TmDHFR also has a sigmoidal relationship with respect to pH.⁹⁰ It is therefore unlikely that such relationships could be indicative of conformational behaviour.

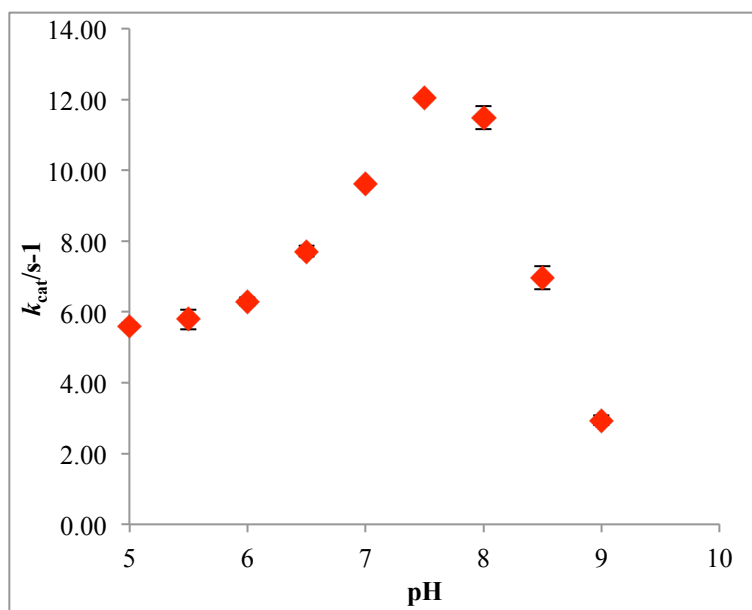


Figure 4.10: The effect of pH on the steady state rate constant in SeDHFR.

Table 4.3: pH dependency on k_{cat} for the reaction catalysed by SeDHFR.

pH	SeDHFR $k_{\text{cat}} \text{ s}^{-1}$
5.0	5.60 ± 0.08
5.5	5.79 ± 0.28
6.0	6.29 ± 0.11
6.5	7.72 ± 0.15
7.0	9.63 ± 0.02
7.5	12.05 ± 0.05
8.0	11.49 ± 0.33
8.5	6.96 ± 0.33
9.0	2.94 ± 0.13

4.7 Product inhibition in SeDHFR

Formation of the occluded conformation following the chemical step has been postulated to be important for release of NADP^+ from the active site.^{76,149} The mutant EcDHFR-S148P, where formation of the occluded conformation has been de-stabilised exhibited a massive decrease (~ 20 fold) in the IC_{50} value for inhibition by NADP^+ in comparison to wild type EcDHFR (**Table 4.4**).⁷⁶ Wild type MpdHFR has an IC_{50} value for NADP^+ which is ~ 5 fold lower than wild type EcDHFR. Interestingly, the mutant MpdHFR-P150S, wherein formation of the occluded conformation is stabilised, exhibits an almost 2-fold increase with respect to IC_{50} value. This evidence strongly suggests that formation of the occluded conformation in EcDHFR mitigates product inhibition effects.⁷⁶

To this end, IC_{50} values for NADP^+ have been measured in SeDHFR, which has been shown to adopt a second structural conformation like EcDHFR (**Table 4.4** and **Figure 4.11**). IC_{50} values for NADP^+ have also been measured for TmDHFR, which is known to remain in a fixed open conformation during catalysis (**Table 4.4**). SeDHFR exhibited an IC_{50} value almost 2 fold higher than wild type EcDHFR and ~ 12 and ~ 6 fold higher than MpdHFR and TmDHFR, which are both known not to adopt an occluded conformation following the chemical step. This evidence corroborates with earlier reports that the ability to adopt an occluded conformation following the chemical step reduces product inhibition by NADP^+ .⁷⁶

Table 4.4: IC_{50} values for $NADP^+$ for a number of DHFR variants at pH 7.0 and 20 °C.

Enzyme	IC_{50} (μM)
SeDHFR	2068 ± 300
TmDHFR	343 ± 66
EcDHFR ^[a]	820 ± 59
EcDHFR-S148A ^[a]	40 ± 1
MpDHFR ^[a]	170 ± 11
MpDHFR-P150S ^[a]	321 ± 12

[a] data taken from reference.⁷⁶

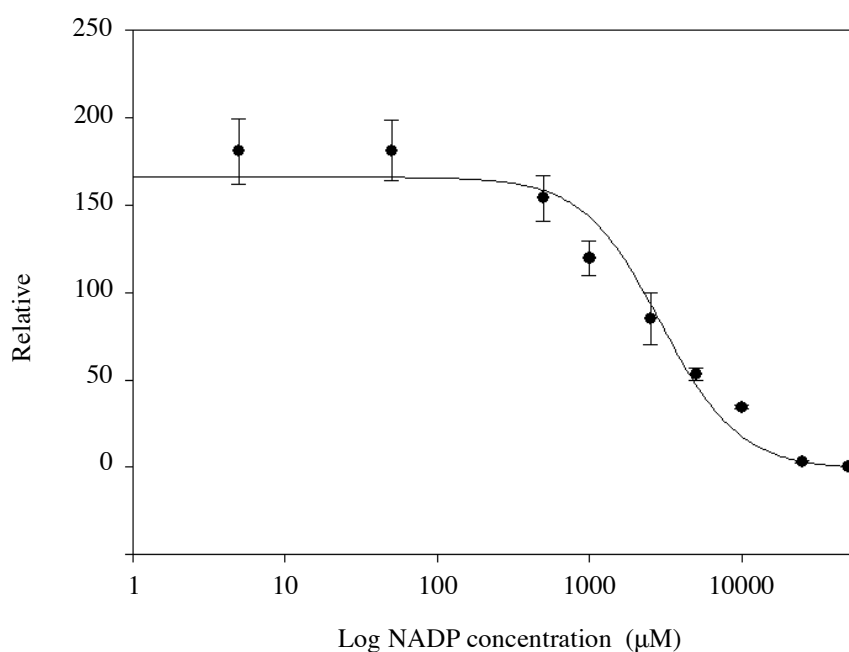


Figure 4.11: IC_{50} curve (μM) for $NADP^+$ inhibition in SeDHFR.

4.8 Hydride Transfer in SeDHFR

Hydride transfer rates were measured under single turnover conditions. The reaction was excited at 292 nm and the emission measured with a cut-off of 400 nm. Fluorescence energy transfer is observed between a tryptophan residue in the active site (Trp22) to the nicotinamide ring of NADPH *via* a mechanism known as Förster resonance energy transfer (FRET). Studying hydride transfer rate constants has been

heavily utilised in the study of DHFR variants, facilitated by Trp22 being almost ubiquitous in the DHFR active site (**Figure 4.12**).¹⁷⁴

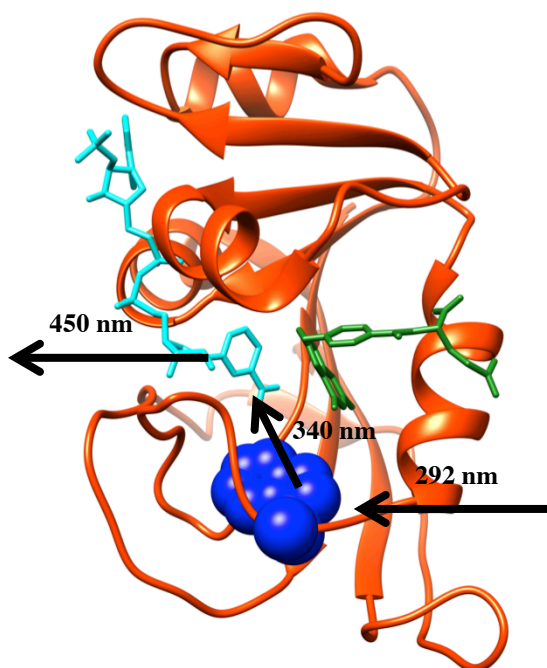


Figure 4.12: No crystal structure of SeDHFR exists. Shown is a cartoon representation of EcDHFR (1RX2),¹⁴⁹ highlighted in blue is residue Trp22 that is conserved in nearly all DHFR variants including SeDHFR.¹⁷⁴ Also highlighted is NADPH in cyan, FRET occurs between Trp22 and the nicotinamide ring of NADPH.

Previously, some stopped flow measurements have been performed at pH 9 where the rate of hydride transfer becomes rate limiting. At such high pH values the kinetics will largely report on the rate of the chemical step and contributions from other processes such as conformational behaviour will be minimised.⁵¹ However, at elevated pH values the enzyme is significantly removed from its physiological pH and, as such, the tertiary structure of the enzyme, conformational behaviour and protonation states of ionisable residues are all affected.^{111,175} Hydride transfer in SeDHFR was therefore studied at pH 7.0 over a temperature range of 5-40 °C (**Figure 4.13** and **Table 4.5**).

SeDHFR exhibited a pre-steady state rate constant of $57 \pm 0.6 \text{ s}^{-1}$ at 20 °C and at pH 7.0, which is approximately 5-fold faster than the value of k_{cat} under similar conditions. The rate constant (k_{H}) increased exponentially with temperature corresponding to expected Arrhenius behaviour (**Figure 4.14**). SeDHFR exhibited ~2.5 fold lower single turnover

rate constant than its mesophilic counterpart EcDHFR ($159 \pm 7.9 \text{ s}^{-1}$ at $20 \text{ }^\circ\text{C}$) and is also slower than MpDHFR and BsDHFR. SeDHFR, like all other measured DHFRs is still significantly faster (k_{H}) than the hyper-thermophile TmDHFR.

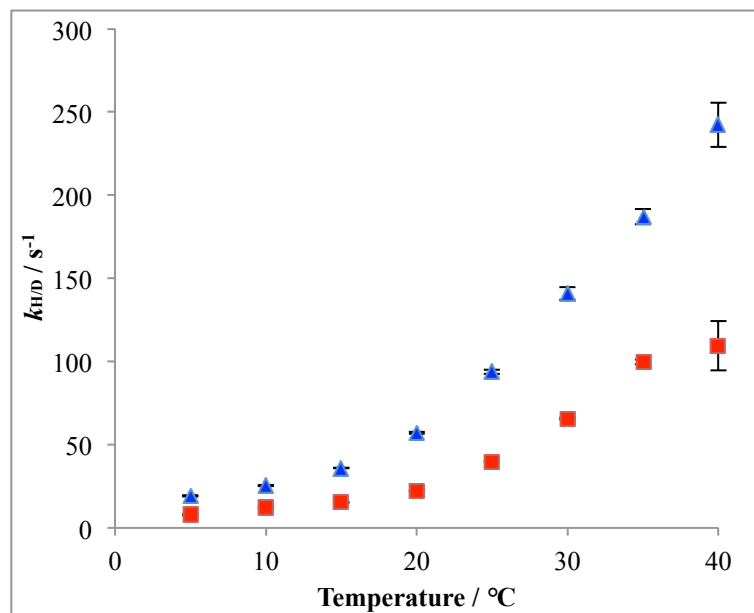


Figure 4.13: Temperature dependence of the single turnover rate constant for hydride (blue triangles) and deuteride (red squares) transfer in SeDHFR at pH 7.0.

Table 4.5: Temperature dependency of hydride transfer in SeDHFR and previously mentioned DHFR variants at pH 7.0.

Temperature (°C)	SeDHFR k_H (s ⁻¹)	EcDHFR ^[a] k_H (s ⁻¹)	MpDHFR ^[b] k_H (s ⁻¹)	BsDHFR ^[c] k_H (s ⁻¹)	TmDHFR ^[a] k_H (s ⁻¹)
5	19.2 ± 0.1	81.9 ± 1.7	267.6 ± 14.4	N/A	0.04 ± 0.01
10	25.5 ± 0.1	106.3 ± 3.1	327.2 ± 14.4	68.3 ± 8.3	0.06 ± 0.03
15	36.0 ± 0.1	135.3 ± 5.6	420.3 ± 21.3	79.2 ± 3.7	0.09 ± 0.02
20	57.0 ± 0.6	159.8 ± 7.9	484.4 ± 28.0	102.0 ± 5.0	0.12 ± 0.03
25	93.8 ± 1.2	203.7 ± 7.4	526.8 ± 23.2	131.0 ± 2.0	0.17 ± 0.02
30	140.8 ± 3.7	235.4 ± 13.8	570.5 ± 44.1	160.0 ± 8.0	0.24 ± 0.05
35	187.2 ± 4.7	287.9 ± 12.0	N/A	184.0 ± 6.0	0.34 ± 0.06
40	242.3 ± 13.4	N/A	N/A	218.0 ± 7.0	0.49 ± 0.01
45	N/A	N/A	N/A	249.0 ± 12.0	0.67 ± 0.02
50	N/A	N/A	N/A	297.0 ± 10.0	0.93 ± 0.04
55	N/A	N/A	N/A	N/A	1.25 ± 0.06
60	N/A	N/A	N/A	N/A	1.65 ± 0.09
67	N/A	N/A	N/A	N/A	2.12 ± 0.16

[a] data from ref,⁹³ [b] data from ref,¹⁷⁰ [c] data from reference.¹²⁰

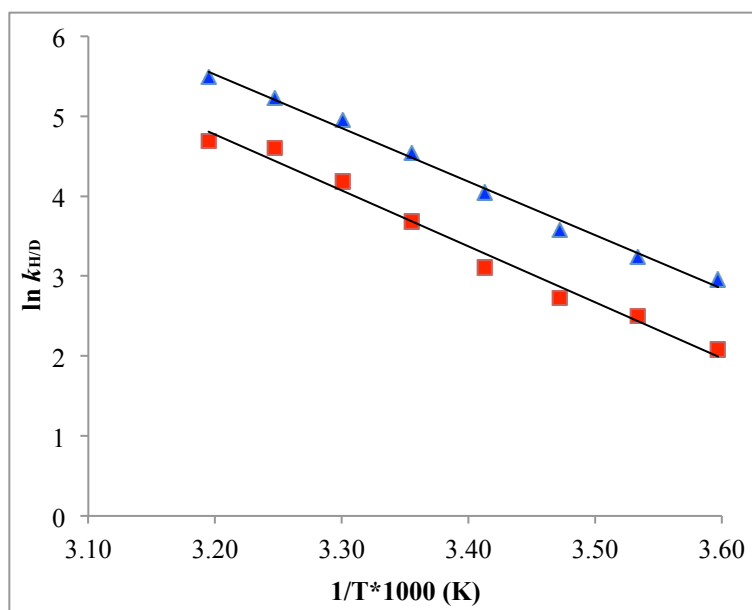


Figure 4.14: Arrhenius plots of hydride/deuteride transfer in SeDHFR at pH 7.0. Blue triangles represent hydride transfer and red squares denote deuteride transfer.

The primary KIE for the reaction catalysed by SeDHFR was determined using enzymatically prepared NADPD (section 2.3.12). The KIE being calculated using **Equation 4.1**. At 5 °C the primary KIE is $2.40 \pm 0.06 \text{ s}^{-1}$ and falls slightly to $2.22 \pm 0.02 \text{ s}^{-1}$ at 40 °C. With respect to temperature dependency of the primary KIE only a slight trend of decreasing KIE with increase of temperature can be observed (**Table 4.6** and **Figure 4.15**).

$$KIE = \frac{k_H}{k_D}$$

Equation 4.1: Primary substrate KIE is calculated as the ratio between the rate constant with NADPH and the rate constant of NADPD.

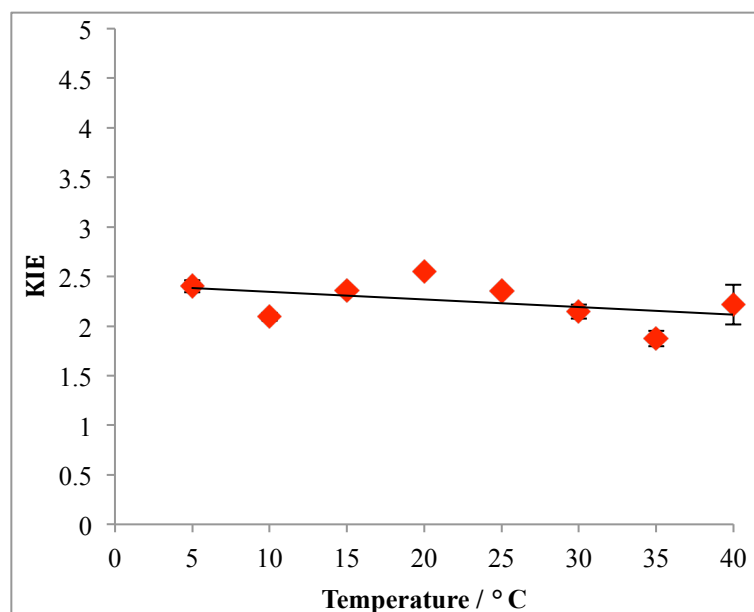


Figure 4.15: Temperature dependency of the primary KIE for SeDHFR at pH 7.0.

Table 4.6: Temperature dependency of hydride and deuteride transfer in SeDHFR and the resulting KIE at pH 7.0.

Temperature (°C)	k_H	k_D	KIE
40	242.3 ± 13.4	109.34 ± 14.8	2.22 ± 0.02
35	187.2 ± 4.7	99.9 ± 1.5	1.87 ± 0.08
30	140.8 ± 3.7	65.6 ± 0.6	2.15 ± 0.07
25	93.8 ± 1.2	39.8 ± 0.3	2.35 ± 0.02
20	57.0 ± 0.6	22.4 ± 0.2	2.55 ± 0.01
15	36.0 ± 0.1	15.3 ± 0.2	2.36 ± 0.02
10	25.5 ± 0.1	12.2 ± 0.1	2.09 ± 0.05
5	19.2 ± 0.1	8.0 ± 0.6	2.40 ± 0.06

Primary KIEs have been measured for a number of DHFR variants. Interestingly the primary KIE in EcDHFR is independent of temperature at pH 9.0 where the chemical step becomes rate determining and therefore less influenced by other events that would increase kinetic complexity.³² At pH 7.0, however the primary KIE was determined to be temperature dependant; at 5 °C the primary KIE is 3.0 ± 0.2 and decreases to 2.2 ± 0.2 at a temperature of 40 °C (**Figure 4.16**). This change in temperature dependency suggests different dynamics are at play at elevated pH values.¹²⁶ At pH 7.0 the ratio of the Arrhenius pre-factors (A_H/A_D) for the EcDHFR catalysed reaction was measured to

be 0.12 ± 0.02 , which is significantly lower than the semi-classical lower limit of 0.71.^{34,126,176} It was concluded that tunnelling is therefore involved in the hydride transfer step and computational experiments concluded that the contribution from tunnelling effectively lowers the activation energy (E_a) of the reaction catalysed by EcDHFR.^{29,110,126,177}

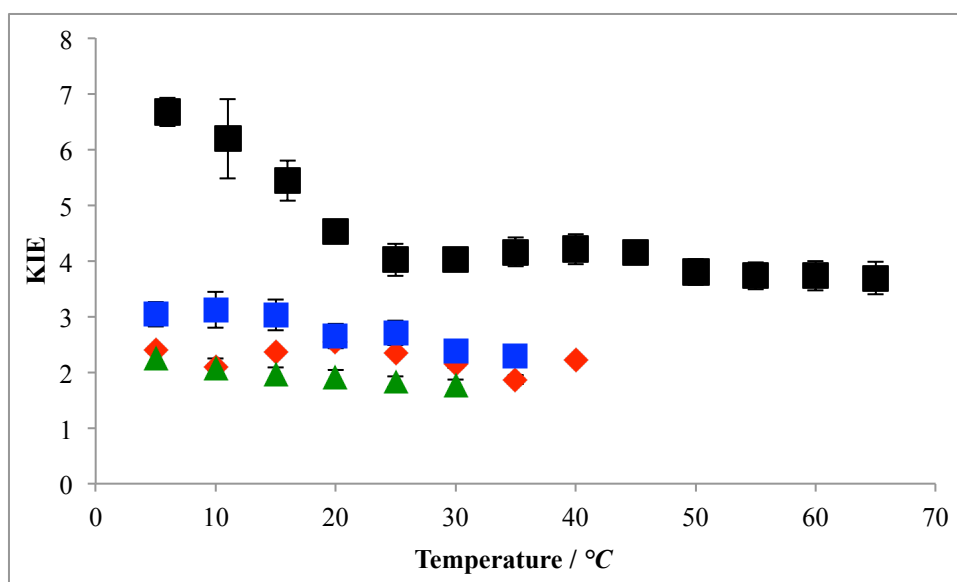


Figure 4.16: Temperature dependency of the primary KIE for SeDHFR (red diamond), EcDHFR (blue square), MpDHFR (green triangle) and TmDHFR (black square) at pH 7.0.

Like EcDHFR, the reaction catalysed by SeDHFR exhibits an Arrhenius pre-factor ratio (A_H/A_D) of 0.12 ± 0.02 for the primary KIE, which is also under the semi-classical limit of 0.71.¹⁷⁶ SeDHFR also exhibits similar $E_a^{H/D}$ values to EcDHFR and the ΔE_a between the NADPH and NADPD catalysed reactions is very similar (ΔE_a for EcDHFR = 7.60 ± 0.92 kJ mol⁻¹ and ΔE_a for SeDHFR = 7.88 kJ mol⁻¹). It therefore seems fair to apply similar conclusions about the influence of tunnelling on the reaction catalysed by EcDHFR to the reaction catalysed by SeDHFR.

The role of fast protein motions, which occur on a femto-picosecond timescale and how they influence the chemical step of catalysis, is still hotly debated. A number of models that address the role of such motions have been proposed over the past two decades.^{43,178–181} Work by Klinman and co-workers proposes that such fast dynamics can increase the tunnelling probability *via* regulation of the potential energy barrier.¹⁷⁹

DHFR has previously been reported to harbour such fast dynamics and compress the potential energy barrier, increasing the likelihood of tunnelling.¹⁸²

TmDHFR is currently the only known DHFR that forms a dimeric structure.⁸⁹ Interestingly below ~25 °C the primary KIE is strongly dependent on temperature, above ~25 °C the primary KIE shows no such strong dependency.⁹⁰ Such a breakpoint in temperature dependency of the KIE is also observed in a thermophilic alcohol dehydrogenase.³⁰ It is considered that above the breakpoint, where the KIE is independent of temperature, the enzyme adopts an active site structure that helps facilitate hydride transfer. At lower temperatures the enzyme was postulated to increasingly rely on fast dynamics, which compress the potential energy barrier.¹⁸³ For the monomeric DHFRs, EcDHFR and MpDHFR, the primary KIE becomes independent of temperature at elevated pH values, similar to the kinetics obtained for TmDHFR above 25 °C at pH 7.0.⁹⁰ It has been postulated that under such conditions all three DHFR variants rely on the enzyme adopting a reaction ready configuration before the chemical step.¹²⁶

Table 4.7: Temperature dependency of the primary KIE for hydride and deuteride transfer at pH 7.0 for SeDHFR, MpDHFR, EcDHFR and TmDHFR at pH 7.0.

Temperature (°C)	SeDHFR k_H/k_D KIE	EcDHFR ^[a] k_H/k_D KIE	MpDHFR ^[b] k_H/k_D KIE	TmDHFR ^[c] k_H/k_D KIE
5	2.40 ± 0.06	3.04 ± 0.22	2.25 ± 0.13	N/A
6	N/A	N/A	N/A	6.67 ± 0.25
10	2.09 ± 0.05	3.12 ± 0.32	2.08 ± 0.17	N/A
11	N/A	N/A	N/A	6.19 ± 0.71
15	2.36 ± 0.02	3.03 ± 0.28	1.96 ± 0.13	N/A
16	N/A	N/A	N/A	5.44 ± 0.36
20	2.55 ± 0.01	2.65 ± 0.22	1.91 ± 0.13	4.52 ± 0.20
25	2.35 ± 0.02	2.71 ± 0.22	1.83 ± 0.10	4.02 ± 0.29
30	2.15 ± 0.07	2.39 ± 0.16	1.76 ± 0.11	4.03 ± 0.16
35	1.87 ± 0.08	2.29 ± 0.11	N/A	4.16 ± 0.26
40	2.22 ± 0.02	N/A	N/A	4.21 ± 0.27
45	N/A	N/A	N/A	4.15 ± 0.12
50	N/A	N/A	N/A	3.80 ± 0.23
55	N/A	N/A	N/A	3.73 ± 0.24
60	N/A	N/A	N/A	3.73 ± 0.26
65	N/A	N/A	N/A	3.69 ± 0.29

[a] data from ref.⁹³ [b] data from ref.¹⁷⁰ [c] data from ref.⁹³

Table 4.8: Activation energies (E_a) for the single turnover rate catalysed by SeDHFR and other reported DHFR variants.

Enzyme	E_a^H (kJ mol ⁻¹)	E_a^D (kJ mol ⁻¹)	ΔE_a (kJ mol ⁻¹)
SeDHFR	32.33	40.21	7.88
EcDHFR ^[a]	29.42 ± 0.71	37.02 ± 0.58	7.60 ± 0.92
MpDHFR ^[b]	21.55 ± 2.18	28.11 ± 2.55	6.56 ± 3.35
TmDHFR(<25°C) ^[c]	49.95 ± 1.68	69.28 ± 3.69	19.32 ± 4.05
TmDHFR(>25°C) ^[c]	53.55 ± 0.44	56.03 ± 0.84	2.49 ± 0.95

[a] data from ref.⁹³ [b] data from ref.¹⁷⁰ [c] data from ref.⁹³

Table 4.9: Arrhenius pre-factors ($A_{H/D}$) for the single turnover rate catalysed by SeDHFR and other reported DHFR variants.

Enzyme	$A_H (s^{-1})$	$A_D (s^{-1})$	A_H / A_D
SeDHFR	$(3.29 \pm 0.17) \times 10^7$	$(3.27 \pm 0.05) \times 10^8$	0.10 ± 0.08
EcDHFR ^[a]	$(2.82 \pm 0.05) \times 10^7$	$(2.34 \pm 0.03) \times 10^8$	0.12 ± 0.02
MpDHFR ^[b]	$(3.17 \pm 0.19) \times 10^6$	$(2.44 \pm 0.15) \times 10^7$	0.13 ± 0.09
TmDHFR(<25°C) ^[c]	$(94.7 \pm 0.36) \times 10^7$	$(5.65 \pm 0.35) \times 10^{10}$	0.002 ± 0.001
TmDHFR(>25°C) ^[c]	$(4.11 \pm 0.03) \times 10^7$	$(2.67 \pm 0.04) \times 10^8$	1.54 ± 0.36

[a] data from ref.⁹³ [b] data from ref.¹⁷⁰ [c] data from ref.⁹³

4.9 Enzyme KIE and Dynamics in SeDHFR

Heavy isotope labelling of enzymes has recently been employed as a tool to probe the relationship between fast dynamics and catalysis in enzymes.^{48,49,79,117,119,120} Heavy isotope labelling alters the vibrational properties of bonds, and protein motions on a multitude of timescales are affected, however, it is considered that the electrostatics remain largely unaffected.^{48,49} Enzyme KIEs are calculated using **Equation 4.2**.

$$\text{enzyme KIE} = \frac{k^{LE}}{k^{HE}}$$

Equation 4.2: The KIE is calculated as a ratio between the rate constants of the light (k^{LE}) and heavy (k^{HE}) enzymes.

By measuring the rate of hydride transfer *via* stopped flow, the effect of heavy isotope labelling on the chemical step of catalysis in SeDHFR has been characterised. Hydride transfer was measured over a range of 5 to 40 °C for both natural abundance (light) and heavy SeDHFR (**Figure 4.17 and Table 4.10**). Between 5 and 35 °C the rate for hydride transfer increases exponentially for both natural abundance and heavy labelled SeDHFR. For natural abundance SeDHFR k_H ranges from $28.0 \pm 0.3 \text{ s}^{-1}$ to $216.1 \pm 17.2 \text{ s}^{-1}$ over the measured temperature range and for heavy SeDHFR k_H ranges from $28.7 \pm 0.6 \text{ s}^{-1}$ to $197.5 \pm 12.0 \text{ s}^{-1}$. The resulting enzyme KIE exhibited no significant temperature dependence increasing from 0.96 ± 0.01 at 5 °C to 0.99 ± 0.04 at 35 °C (**Figure 4.19 and Table 4.11**). This indicates that heavy isotope labelling of SeDHFR has no significant influence on the hydride transfer step of catalysis.

The effect of heavy isotope labelling was also measured on the rate of steady state turnover at pH 7.0 at 20 °C. Under these conditions the measured enzyme KIE on k_{cat} was 1.06 ± 0.08 , which is similar to the value reported for EcDHFR under similar conditions ($k_{\text{cat}}^{\text{LE}} / k_{\text{cat}}^{\text{HE}} = 1.04 \pm 0.03$). The enzyme KIE measured for EcDHFR increases from 1.01 ± 0.04 at 10 °C to 1.15 ± 0.02 at 40 °C. It is considered this temperature dependency of the enzyme KIE is a result of the conformational behaviour EcDHFR utilises for product release.⁷⁹ On the other hand, the mutant EcDHFR-N23PP/S148A which is considered to be conformationally restricted, exhibits an enzyme KIE of unity across the measured temperature range.¹¹⁹ It is therefore likely that the small enzyme KIE observed in SeDHFR is a result of conformational behaviour like that witnessed in EcDHFR.

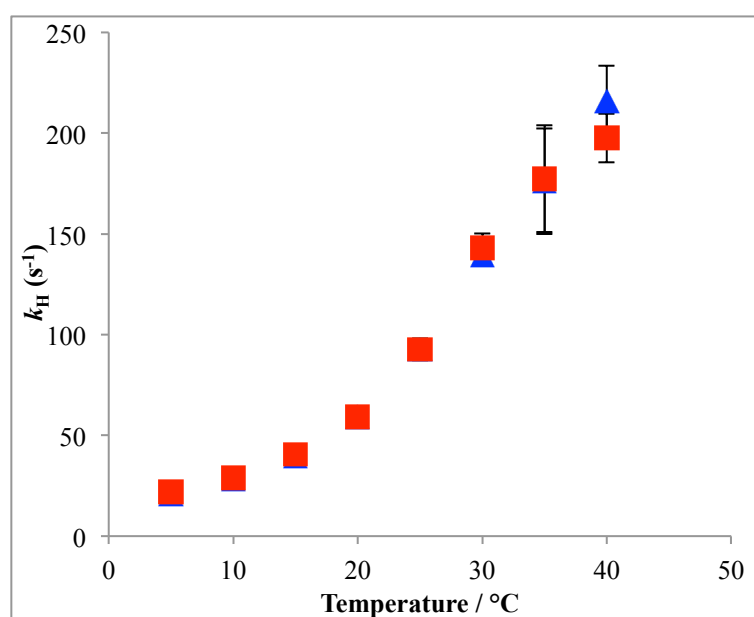


Figure 4.17: Temperature dependence of the rate constant for hydride transfer in light SeDHFR (blue triangles) and heavy SeDHFR (red squares) at pH 7.0.

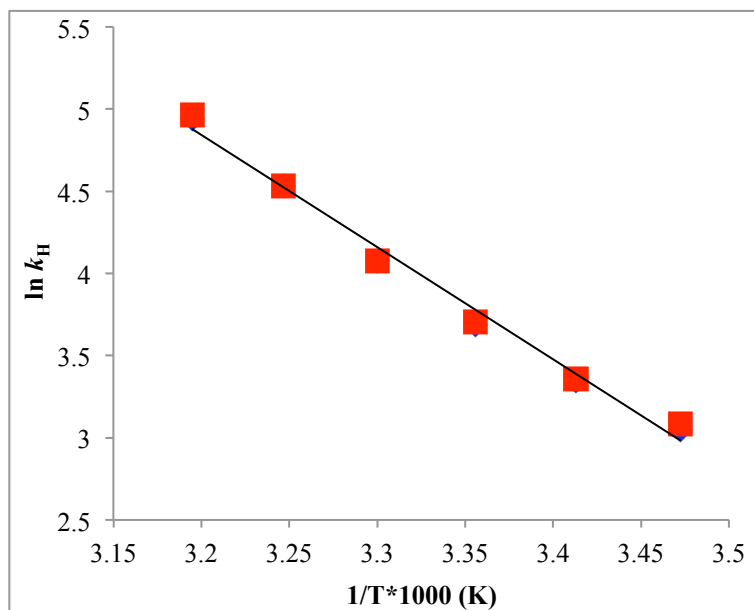


Figure 4.18: Arrhenius plots of hydride transfer in light SeDHFR (blue diamonds) and heavy SeDHFR (red diamonds) at pH 7.0.

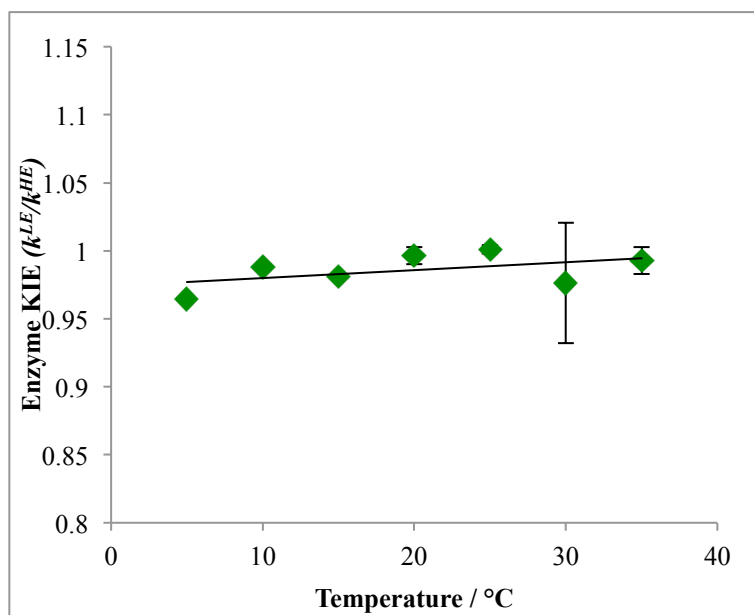


Figure 4.19: Temperature dependency of the enzyme KIE (k^{LE}/k^{HE}) at pH 7.0.

Table 4.10: Temperature dependence on the rate of hydride transfer in both light and heavy SeDHFR at pH 7.0.

Temperature (°C)	Light SeDHFR k_H (s ⁻¹)	Heavy SeDHFR k_H (s ⁻¹)
40	216.1 ± 17.2	197.5 ± 12.0
35	176.1 ± 26.2	177.4 ± 26.5
30	139.5 ± 3.1	142.9 ± 7.3
25	92.7 ± 5.1	92.6 ± 5.3
20	58.9 ± 0.8	59.1 ± 0.7
15	39.8 ± 0.3	40.6 ± 0.4
10	28.4 ± 0.3	28.7 ± 0.6
5	21.0 ± 0.4	21.8 ± 0.2

Table 4.11: Temperature dependence of the enzyme KIE ($k^{\text{LE}}/k^{\text{HE}}$) in the DHFR variants SeDHFR, EcDHFR, MpDHFR, TmDHFR and BsDHFR at pH 7.0.

Temperature (°C)	SeDHFR KIE	EcDHFR KIE ^[a]	MpDHFR KIE ^[b]	TmDHFR KIE ^[c]	BsDHFR KIE ^[d]
65	N/A	N/A	N/A	1.01 ± 0.01	N/A
60	N/A	N/A	N/A	1.03 ± 0.01	N/A
55	N/A	N/A	N/A	0.99 ± 0.01	N/A
50	N/A	N/A	N/A	1.00 ± 0.01	N/A
45	N/A	N/A	N/A	1.00 ± 0.01	1.10 ± 0.07
40	1.09 ± 0.01	1.18 ± 0.09	N/A	0.99 ± 0.01	0.99 ± 0.05
35	0.99 ± 0.04	1.07 ± 0.07	N/A	1.02 ± 0.01	1.10 ± 0.03
30	0.98 ± 0.01	1.10 ± 0.04	1.46 ± 0.06	1.01 ± 0.01	1.11 ± 0.02
25	1.00 ± 0.01	1.10 ± 0.03	1.42 ± 0.05	1.01 ± 0.01	1.21 ± 0.03
20	1.00 ± 0.01	0.92 ± 0.04	1.26 ± 0.07	1.00 ± 0.01	1.26 ± 0.03
15	0.98 ± 0.01	0.91 ± 0.03	1.09 ± 0.07	0.98 ± 0.01	1.25 ± 0.03
10	0.99 ± 0.01	0.93 ± 0.01	1.05 ± 0.07	0.99 ± 0.01	1.30 ± 0.01
5	0.96 ± 0.01	0.92 ± 0.04	1.11 ± 0.05	0.99 ± 0.01	1.24 ± 0.04

[a] data taken from ref.⁷⁹ [b] data taken from ref.⁴⁷ [c] data taken from ref.¹²¹

Experiments that utilise isotopically labelled co-factors to yield a primary KIE, such as those described in the previous section have been used as evidence for the presence of tunnelling in enzymatic reactions. Such experiments have also been used as evidence to postulate fast dynamics on the femto–picosecond timescale manipulate the properties of the potential energy barrier to increase the tunnelling probability.^{178,180,181,184,185} In the past decade protein isotope labelling has been utilised as a probe to directly study the influence of protein dynamics.^{47,53,79,120,121}

Enzyme KIEs have been studied in a range of DHFR variants.^{53,79,120} Enzyme KIE in EcDHFR showed an increase from 0.92 ± 0.04 at 5 °C to 1.18 ± 0.09 at 40 °C, therefore showing a small temperature dependency (**Figure 4.20**).⁷⁹ Computational simulations identified no significant change in the tunnelling probability for the heavy enzyme.⁷⁹ Small differences between the rate constants of the light and heavy enzyme are proposed to be a result of the heavier isotopologue being less responsive to fluctuations

in the environment. It has been proposed that the influence of any promoting motions in the reaction catalysed by EcDHFR would not have any significant impact on the overall rate of hydride transfer. In fact, it has been postulated that dynamic coupling to the reaction coordinate may be to blame for the heavier enzyme having a slower rate at lower temperatures compared to physiological temperatures. Allemann and co-workers therefore proposed protein-promoting motions, which actively decrease the width of the potential energy barrier do not play a significant role in catalysis by EcDHFR.⁷⁹

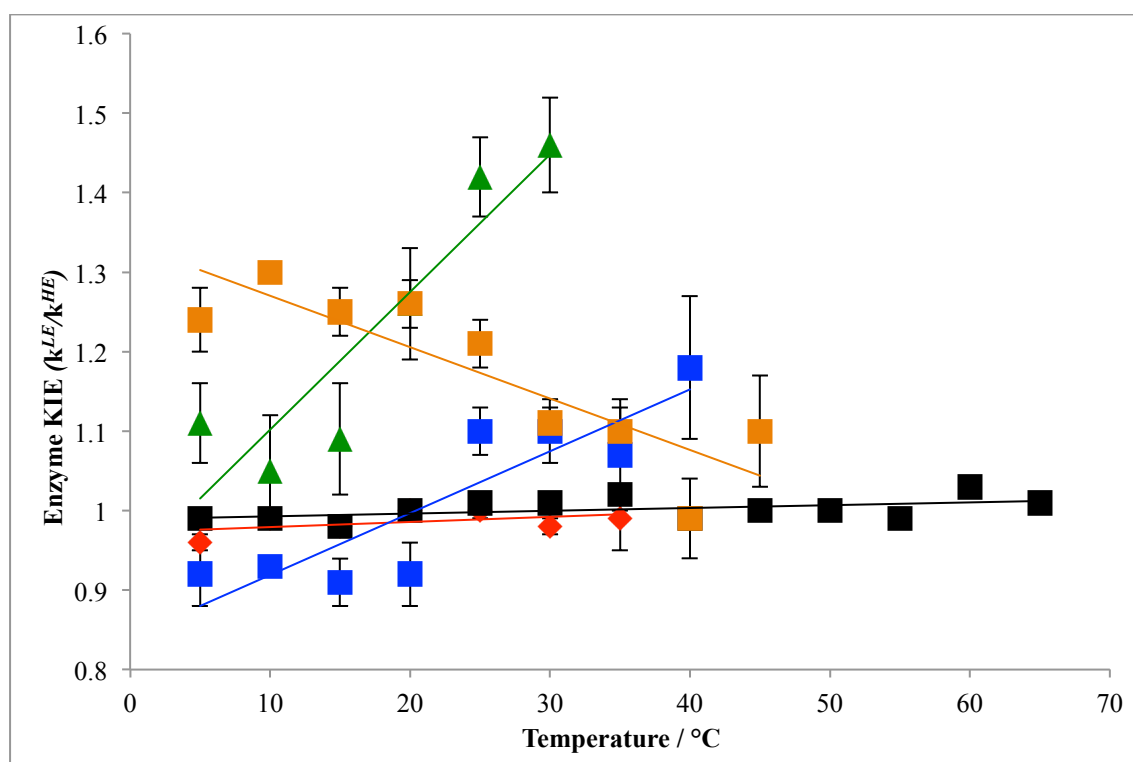


Figure 4.20: Temperature dependency of the enzyme KIE in a number of DHFR variants. SeDHFR (red diamond), EcDHFR (blue square), TmDHFR (black square), MpDHFR (green triangle) and BsDHFR (orange square) at pH 7.0.

It has been shown that the EcDHFR-N23PP/S148A mutant no longer adopts the occluded conformation following the chemical step of catalysis and has a diminished rate constant for hydride transfer. Consequently it was also proposed that the mutated residues partook in long range promoting protein motions.⁹⁸ Subsequent computational work proposed the reduction in the rate of k_H was a result of diminished electrostatic pre-organisation.¹⁸⁶ In terms of enzyme KIE the mutant exhibited a larger KIE (1.37 ± 0.03) than the wild type enzyme (1.10 ± 0.04).¹¹⁹ Computational experiments propose

that although motion is restricted on the μ s-ms timescale there is increased motion on the pico-femto second timescale. It has therefore been proposed that increased dynamical coupling of fast protein motions to the reaction coordinate has a deleterious effect on the rate of hydride transfer.¹¹⁹

TmDHFR is the only known dimeric DHFR. The structural loops, which in EcDHFR are mobile, are instead locked into the dimer interface and catalysis has to proceed through a fixed open conformation.^{83,88,89} TmDHFR exhibits drastically lower rate constants for both hydride transfer (k_H) and catalytic turnover (k_{cat}) than EcDHFR.⁸⁸⁻⁹⁰ At pH 7.0 no significant difference in the rate of hydride transfer could be observed between light and heavy TmDHFR and a KIE of ~ 1 was yielded across the measured temperature range (5 – 65 °C) (**Table 4.11** and **Figure 4.20**). The lack of any significant KIE gives strong evidence that protein dynamics do not couple to the reaction coordinate in TmDHFR.¹²¹ The inability to switch from an open conformation to a closed conformation following ligand binding means TmDHFR is unable to exclude solvent molecules from the active site like EcDHFR and this in turn prevents optimal electrostatic preorganisation.¹²¹

BsDHFR is a thermophilic DHFR with a physiological temperature of ~ 60 °C and exhibits similar catalytic properties to EcDHFR.^{187,188} BsDHFR exhibits significant enzyme KIE at low temperatures (1.24 ± 0.04 at 5 °C) that decreases to unity as the temperature increases towards its physiological temperature (0.99 ± 0.05 at 40 °C). BsDHFR therefore exhibits much larger KIE values than EcDHFR. It has been proposed that the increased flexibility of BsDHFR leads to increased effects from protein motions.¹⁸⁸ Computational simulations comparing RMSD values of the C α confirmed BsDHFR is more flexible than EcDHFR on a pico-nanosecond timescale. The drastically increased enzyme KIE at low temperatures was therefore postulated to be a result of the increased mass of the heavy enzyme having an effect on the re-crossing coefficient. In summary, it was postulated at lower temperatures light BsDHFR is better able to adopt a reaction ready conformation.¹⁸⁸

Reports on the enzyme KIE for MpDHFR showed an interesting temperature dependency. At 5 °C the KIE was 1.09 ± 0.04 which rose to 1.47 ± 0.04 at 30 °C. It was postulated that with rising temperature MpDHFR becomes more flexible and dynamic

coupling to the chemical coordinate means mass induced effects from the heavy isotope labelling have a deleterious effect on the re-crossing coefficient. Together with evidence from previously reported work it was proposed at close to physiological temperatures, effects from dynamic coupling to the chemical coordinate are minimised, resulting in Enzyme KIE that are close to unity.⁴⁷

SeDHFR exhibited an enzyme KIE that was close to unity at all measured temperatures, similar to the temperature dependency obtained for TmDHFR.¹²¹ This may mean that like TmDHFR, SeDHFR is more rigid than EcDHFR on a pico-nanosecond time domain which means mass induced effects on the re-crossing coefficient have less of an effect and thus no significant enzyme KIE is produced.

4.10 Summary and conclusions

In this chapter the recombinant overproduction and purification of SeDHFR has been detailed. Studying SeDHFR was of particular interest as it is from a mesophilic bacterium like EcDHFR and work described in the previous chapter indicated SeDHFR is likely to adopt an occluded conformation following the chemical step like EcDHFR.

The occluded conformation in EcDHFR is believed to mitigate product inhibition effects. EcDHFR has an IC_{50} value for $NADP^+$ almost ~ 5 fold higher than that observed for MpDHFR. Mutants which perturb the ability to adopt an occluded conformation in EcDHFR drastically lower the IC_{50} value for $NADP^+$. SeDHFR exhibits an IC_{50} value for $NADP^+$ almost ~ 2.5 time larger than EcDHFR and as such is not susceptible to product inhibition.⁷⁶ This is likely the result of the enzyme adopting an occluded conformation following the chemical step, evidence for which was presented in the previous chapter.

The steady state rate (k_{cat}) for SeDHFR was measured to be $8.6 \pm 0.3 \text{ s}^{-1}$ at $20 \text{ }^\circ\text{C}$ at pH 7.0, slightly lower than the value measured for EcDHFR ($12.6 \pm 1.4 \text{ s}^{-1}$) under the same pH and temperature. The steady-state rate (k_{cat}) for SeDHFR was found to be greatest at a pH of 7.5 with a recorded value of $12.05 \pm 0.08 \text{ s}^{-1}$. Similar to MpDHFR and BsDHFR, SeDHFR also exhibits a bell shaped pH dependency of the steady state rate constant. EcDHFR and TmDHFR both have pH dependencies that are sigmoidal in nature, with no significant drop in steady state turnover at low pH values. The cause of

MpDHFR having lower rate constants at low pH values is still under discussion, however it has been postulated that a change in the steady-state rate limiting step at low pH values is likely the cause.⁷⁶

The primary KIE (k_H/k_D) in SeDHFR exhibits a similar trend to that observed for EcDHFR, producing near identical Arrhenius pre-factor ratios and similar activation energies.

SeDHFR labelled with ^{13}C and ^{15}N was produced in order to measure the enzyme KIE. No significant differences were observed in CD spectra between the light and heavy enzyme, indicating labelling does not have a significant effect on stability or structure. The enzyme KIE was measured to be ~ 1 across the measured temperature range. This is in contrast to EcDHFR which exhibits a temperature dependant enzyme KIE that increases from 0.92 ± 0.04 at $7\text{ }^\circ\text{C}$ to 1.18 ± 0.09 at $40\text{ }^\circ\text{C}$.⁷⁹ TmDHFR, which is known to be conformationally restricted, exhibits a enzyme KIE that appears to be independent of temperature, maintaining a value of ~ 1 across the measured temperature range. It has been proposed this is evidence of a lack of dynamic coupling to the chemical step of catalysis in TmDHFR.¹²¹ SeDHFR also exhibits an enzyme KIE of ~ 1 across the measured temperature range and it is therefore likely dynamic coupling to the chemical step is minimised.

5

Catalysis by
Staphylococcus
aureus Lactate
Dehydrogenase

5.1 Introduction

A number of DHFR variants have been studied with respect to the influence of fast dynamics coupling to the chemical step of catalysis.^{47,79,119–121} Over the past decade, enzyme KIEs have been utilised to explore the influence of fast protein dynamics on the chemical step of catalysis in DHFR. Evidence is growing that at close to physiological conditions, the coupling of dynamics to the chemical step of catalysis in DHFR is minimised. In fact such coupling of dynamics to the chemical step could actually be detrimental to catalysis.^{45,47,189,190} It is therefore of great interest to expand the study of the role of fast dynamics to other enzyme systems and examine whether the dynamic behaviour observed in DHFR is ubiquitous or scarce.

Lactate dehydrogenase, like DHFR, catalyses a hydride transfer reaction from NADH and can be easily monitored by NADH absorbance at 340 nm. Furthermore, similar to what was proposed for DHFR, a network of residues that actively promote catalysis has been proposed to exist in human heart lactate dehydrogenase (HsLDH).^{161,191} This makes LDH an attractive enzyme for studying dynamic coupling to the chemical step of catalysis.

5.2 Lactate dehydrogenase biochemistry

Through the glycolysis pathway, glucose is ultimately catabolised into 2 units of pyruvate in a process that yields 2 ATP and 2 NADH. Under aerobic conditions pyruvate is converted to acetyl-CoA and enters the citric acid (Krebs) cycle to yield more NADH and FADH₂. These are regenerated in the electron transport chain (ECT), generating more units of ATP. However, under anaerobic conditions the ECT cannot operate so the cell requires an alternative method to regenerate NAD⁺. Lactate dehydrogenase (LDH) is ubiquitous to life and catalyses hydride transfer from the pro-*R* NADH to the C2 position of pyruvate (**Figure 5.1**), thereby regenerating NAD⁺ without the need for oxygen.⁹ Most LDH enzymes utilise a histidine residue in the active site as a proton donor, mutation of which results in enzyme inhibition.¹⁹² LDH is also able to catalyse the reverse reaction, although the equilibrium lies strongly in favour of the reduction of pyruvate. At high concentrations of lactate, LDH is susceptible to feedback inhibition and a decrease in the rate constant is observed. In

mammals, the liver takes up excess lactate where LDH converts it back to pyruvate as part of the Cori cycle.⁹

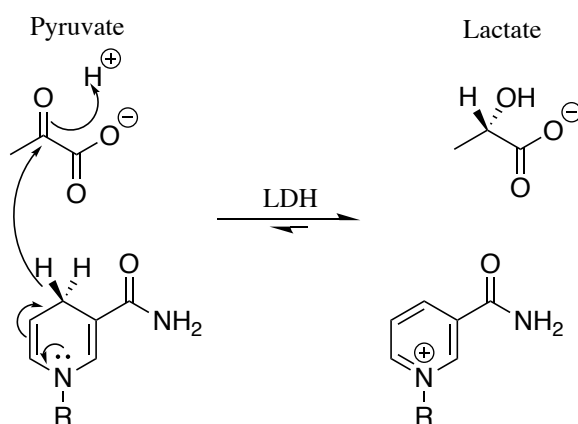


Figure 5.1: Reaction catalysed by LDH. Pyruvate is reduced to L-lactate using NADH as a cofactor.

Most LDH enzymes exist as either a homotetramer or a heterotetramer made up of different isoforms of LDH.¹⁹³ Enzyme isoforms have different amino acid sequences but catalyse the same reaction with different kinetic properties.⁴ Three LDH isoforms are found to be present in humans; LDHA, LDHB and LDHC.¹⁹⁴ LDHA favours the conversion of pyruvate to lactate and is commonly found in skeletal muscle, LDHB favours the reverse reaction and is found in aerobic tissue.^{195–197} LDHC is utilised by germ cells to produce energy during spermatogenesis and is consequently solely expressed in the testis.^{198,199}

5.3 Lactate dehydrogenase physical chemistry

LDH from *Bacillus stearothermophilus* (BsLDH), exhibits two major structural conformations (open and closed) during the catalytic cycle as defined by the position of a key flexible loop (residues 99-110). The catalytic cycle for BsLDH has been proposed to go through a number of intermediates (**Figure 5.2**). BsLDH first binds NADH (NH) and pyruvate (Pyr) to form the ternary complex E:NADH:pyruvate before transitioning to a closed conformation in which the chemical step occurs. Conformational change precedes product release from the E:NAD⁺:lactate product complex.²⁰⁰ Loop closure has been proposed to be important for efficient catalysis as it excludes the active site from bulk solvent and brings a highly conserved arginine residue into contact with the carbonyl group of pyruvate, which has been proposed to stabilise the transition

state.^{201,202} Loop closure in BsLDH, which is required to activate the reaction was found to be the rate limiting step.²⁰²

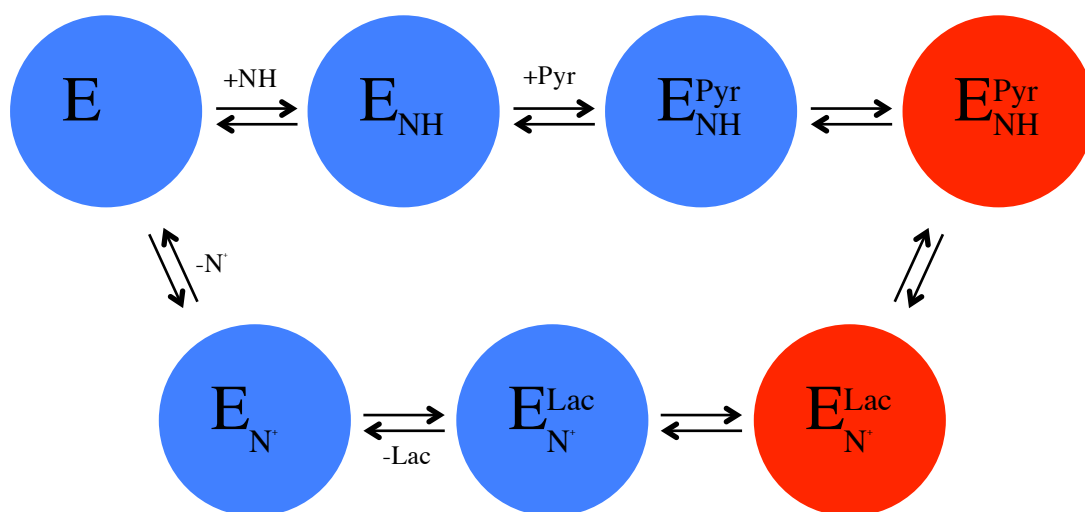


Figure 5.2: The proposed catalytic cycle of BsLDH (NH = NADH, Pyr = pyruvate, N⁺ = NAD⁺ and Lac = Lactate). A blue circle indicates the open conformation and a red circle indicates the closed conformation.

A Recent computational study, however, has provided evidence that rabbit muscle LDH is able to catalyse the chemical step in an open conformation. According to calculations the free energy barrier for the reduction of pyruvate is approximately 2 kcal/ mol lower in the open conformation than in the closed conformation in this LDH variant. It was postulated that the closure of the flexible loop in rabbit muscle LDH is more crucial for catalysing the reverse reaction. It has further been hypothesized human heart LDH is more likely able to facilitate closure of the active site loop than skeletal muscle LDH due the relative positions of the reaction equilibriums.²⁰³

The Schwartz group have presented evidence of a promoting vibration in human heart LDH.²⁰⁴ Through computational simulations, motions of a number of residues spread along a linear axis (Val31, Arg106, Gly32, Met33, Leu65 and Gln66) were proposed to couple to the reaction coordinate on a femtosecond timescale (**Figure 5.3**). It is thought that these residues act as a compressive force and move the pro-*R* hydride of NADH closer to the C2 carbon of pyruvate. It has been proposed such motions would diminish the activation barrier and further facilitate hydride transfer.²⁰⁴

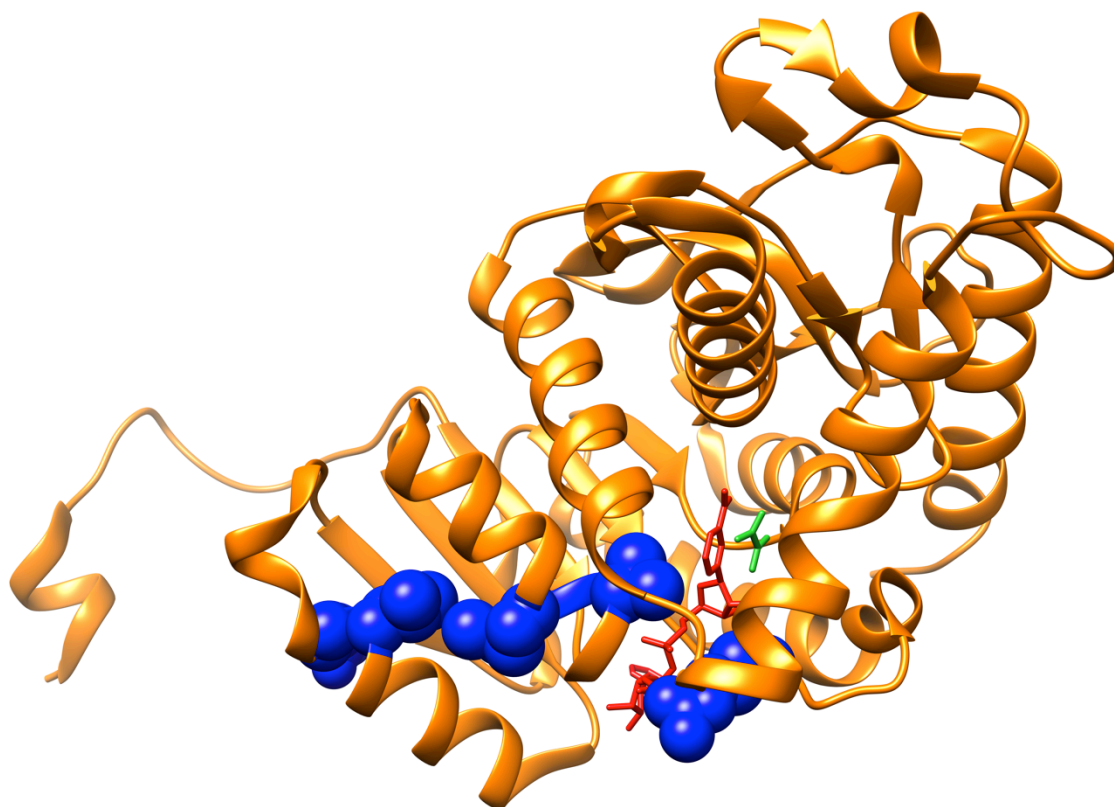


Figure 5.3: Cartoon representation of Human heart LDH (1I0Z).²⁰⁵ The residues reported to be part of the promoting protein network are highlighted in blue and are Gln66, Leu65, Met33, Gly32, Val31 and Arg106 from left to right respectively. NADH and oxamate are highlighted in red and green respectively.²⁰⁶

Recently Schramm and co-workers have expressed triply labelled (^2H , ^{13}C and ^{15}N) human heart LDH (HsLDH) and recorded the enzyme KIE. As observed with DHFR systems, the heavy labelled HsLDH enzyme exhibited a slower hydride transfer rate constant than the natural abundance enzyme. It has been claimed this is evidence of fast dynamics acting upon the chemical step of catalysis in HsLDH to promote hydride transfer.¹⁶³ Interestingly though, the enzyme KIE tends to unity as the pH nears physiological conditions (**Figure 5.4**). Such trends have also been observed in DHFR and it has been concluded that effects of dynamic coupling to the chemical step are minimised under physiological conditions.⁴⁷

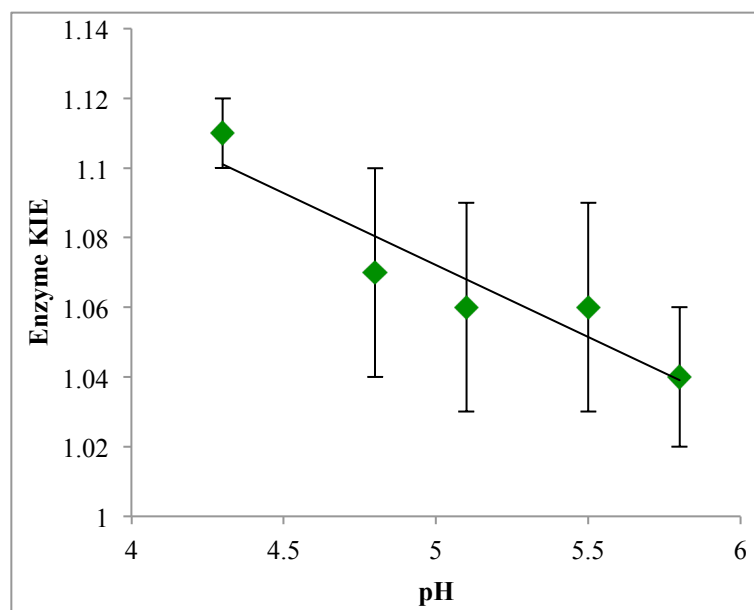


Figure 5.4: Enzyme KIE of human heart LDH against temperature. Data from reference.¹⁶³

The aim of this chapter is to further investigate the role of dynamic coupling in the chemical step of catalysis in lactate dehydrogenase (LDH).

5.4 Lactate Dehydrogenase from *Staphylococcus aureus*

One of the main goals of this chapter was to explore the influence of dynamic coupling upon the chemical step of catalysis, like the work done with DHFR enzymes.⁵³ It has previously been found however that LDH enzymes exhibit hydride transfer rates that are too fast to be studied *via* the available stopped flow methodologies, making it difficult to measure effects acting upon the chemical step.²⁰⁷ Initial reports have stated that *Staphylococcus aureus* LDH (SaLDH) exhibits a k_{cat} of $1.69 \pm 0.03 \text{ min}^{-1}$, significantly lower than steady state rates reported for other LDH enzymes.^{163,207,208} Although the chemical step may be many orders of magnitude faster than the steady state rate, it was considered that SaLDH represented a good candidate for study, allowing for the study of the chemical step of catalysis in an LDH enzyme.

Staphylococcus aureus expresses multiple isoforms of lactate dehydrogenase, called LDH-1 and LDH-2.²⁰⁹ The later is a constitutive LDH while LDH-1 is only produced under nitric oxide (NO) stress and has been shown to be important for virulence, making it a potential drug target.²¹⁰ NO inhibits the respiratory chain, leading to a build

up of NADH. LDH-1 resets the redox balance by regenerating NAD^+ . In this thesis, L-lactate dehydrogenase-1 (SaLDH) has been selected for study.

SaLDH has 37 % sequence identity with human heart LDH (HsLDH), 42 % sequence identity to rabbit muscle LDH and 65 % sequence identity to LDH from *Bacillus stearothermophilus* (BsLDH). Like other LDH's, SaLDH has a histidine residue (His179) in the active site that likely protonates the carbonyl of pyruvate.¹⁶³ The crystal structure has been solved by x-ray crystallography.²¹¹ As with other LDH's, pyruvate is bound deep within the active site (~ 10 Å) and NADH is held within a Rossmann binding fold. SaLDH, like many other LDH's, exists as a tetramer (**Figure 5.5**).^{192,211,212}

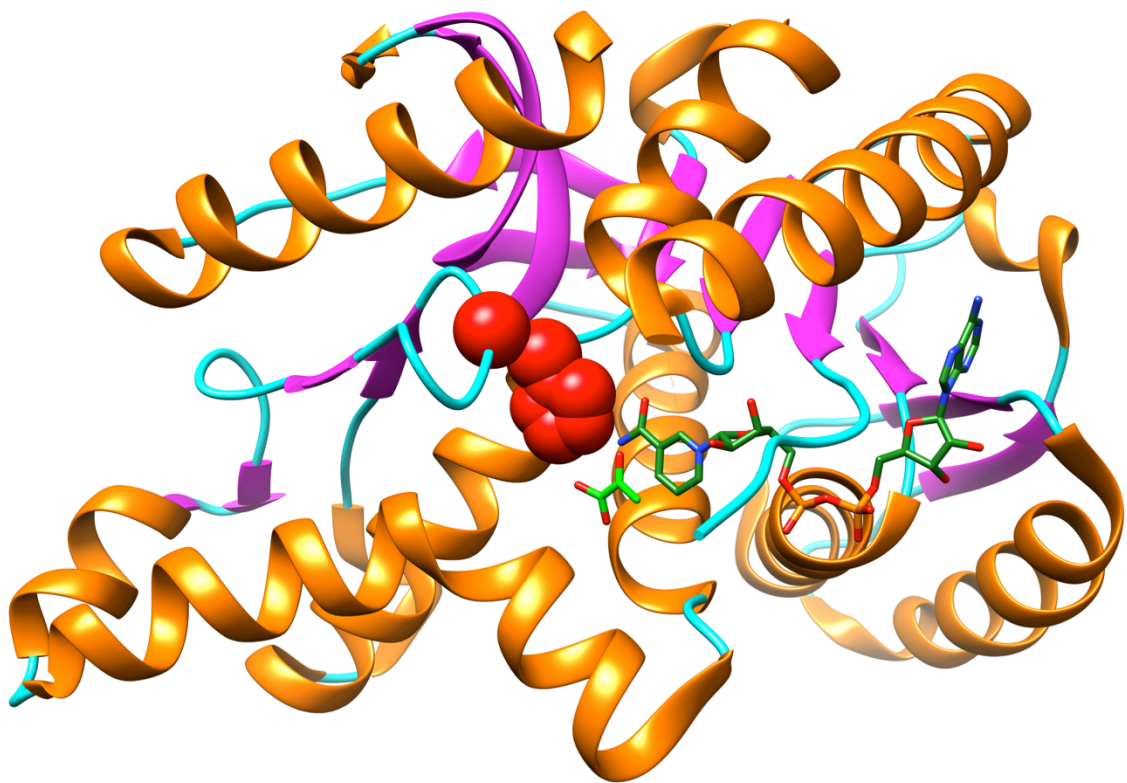


Figure 5.5: Cartoon representation of a single monomer of SaLDH (3D4P)²¹¹ complexed with NAD^+ (dark green) and pyruvate (light green). Structural elements such as coils (cyan), helix's (orange) and beta sheets (purple) are also highlighted, as well as the catalytically important His179 (red) residue.

5.5 Expression and purification of LDH from *Staphylococcus aureus*

The gene sequence for Lactate Dehydrogenase from *Staphylococcus aureus* was accessed from the American Type Culture Collection (ATCC) (ATCC®12600™) (UniProt I.D. H6UH59_STAAU) and a synthetic gene was ordered from Epoch Life Science in a pET-15b vector between *Nde*I and *Bam*HI cloning sites. The gene was codon optimised for *E.coli* expression and a poly histidine (6*) tag and a Tobacco Etch Virus endopeptidase (TEV) cleavage site were encoded upstream for simplified purification of the corresponding protein. The vector was transformed into One Shot™ BL21 Star™ (DE3) chemically competent *E.coli* cells. An overnight colony was prepared in 10 mL LB media with selection antibiotic (ampicillin) and grown at 37 °C for 16 hours. This colony was used to inoculate 1000 mL of either LB or M9 media depending on whether isotope labelling was required. The cells were grown at 37 °C to O.D.₆₀₀ 0.6 at which point gene expression was induced with IPTG and the cells left to incubate at 20 °C for a further 16 hours.

As recombinant SaLDH contained a poly histidine tag it was purified *via* Ni²⁺ nickel affinity chromatography. Pelleted cells were lysed *via* sonication in 50 mM potassium phosphate buffer at pH 8.0 containing 100 mM of NaCl and 20 mM of imidazole. The cell suspension was clarified *via* centrifuge and the supernatant loaded onto a pre-equilibrated Ni²⁺ nickel affinity column. The column was washed with 50 mM potassium phosphate buffer at pH 8.0 containing 100 mM of NaCl and 100 mM of imidazole. SaLDH was eluted from the column in 50 mM potassium phosphate buffer at pH 8.0 containing 100 mM of NaCl and 250 mM of imidazole. Fractions containing SaLDH were incubated at 4 °C with TEV protease overnight, before being sequentially dialysed into 50 mM potassium phosphate buffer at pH 8.0 containing 100 mM of NaCl and 20 mM of imidazole. Again, the protein was loaded onto a pre-equilibrated Ni²⁺ nickel affinity column. SaLDH was eluted with the wash buffer, 50 mM potassium phosphate buffer at pH 8.0 containing 100 mM of NaCl and 20 mM of imidazole, TEV protease remaining bound to the column. The quality of purified enzyme was evaluated through SDS-PAGE (**Figure 5.6**). The monomer of SaLDH was calculated to have a molecular mass of 34583.46 from the primary sequence that aligns with the single purified bands in lanes 2 to 5.

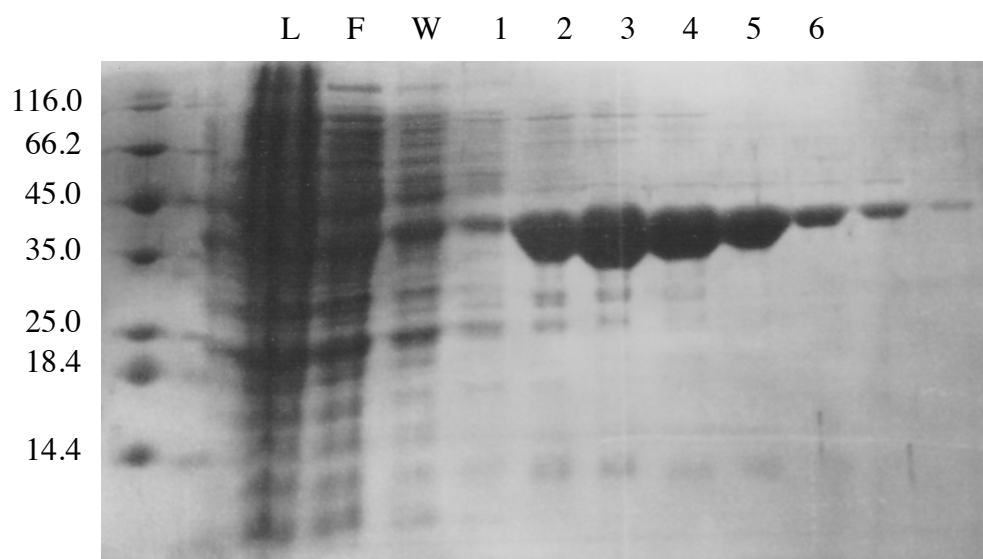


Figure 5.6: SDS-PAGE of SaLDH purification. L = lysate, F = flow through and W = wash. Fraction 1 was discarded; fractions 2-6 were combined for further use.

5.6 Pre-steady state measurements

Similar to experiments described for DHFR, characterisation of the chemical step in SaLDH was attempted using the stopped-flow methodologies described in section 2.3.14. As described in chapter 4, when measuring hydride transfer in DHFR, energy transfer (FRET) between Trp22 in the active site and the nicotinamide ring of NADPH allows the reaction to be monitored *via* FRET with an emission cut-off of 400 nm. Due to the lack of such a residue in the active site of SaLDH a decrease in absorbance at 340 nm, corresponding to the chromophore of NADH was instead monitored.

It has previously been noted in our group that single turnover rates for LDH can be very high: dogfish (*Squalus acanthias*) LDH exhibits a k_H of $>2000 \text{ s}^{-1}$ at $5 \text{ }^\circ\text{C}$.²⁰⁷ Most stopped flow instruments can only reliably measure rates of up to $600\text{-}800 \text{ s}^{-1}$. Although continuous flow apparatus can measure faster rates, cost can become inhibitive when working with isotopically labelled enzymes. L-LDH from *Staphylococcus aureus* (SaLDH) was selected for this study as a previous report had noted a k_{cat} of approximately 1.5 min^{-1} at $20 \text{ }^\circ\text{C}$, which is exceptionally low for LDH enzymes and as such it was hoped the single turnover rate would be low enough to measure using our stopped flow equipment.²⁰⁸ Initial measurements however indicated hydride transfer in SaLDH is too fast to be studied *via* stopped flow methodologies.

In order to slow down the hydride transfer step and allow observations on the rate constant to be made, it was deemed necessary to use additives, even though these move a system away from physiological conditions. Firstly, 30 % methanol was added to the buffer system to allow rates at temperatures below 0 °C to be measured as these will be significantly slower. To ensure the addition of methanol was not impacting the properties of the enzyme the k_{cat} was measured after 30 minutes incubation with 30 % methanol. No significant drop in the rate of k_{cat} was observed after this incubation time, indicating that the addition of methanol does not impact either the stability or function of the enzyme on a timescale associated with the planned experiment. However, even pre-steady state measurements recorded at -25 °C produced no valuable data from which a rate constant could be derived.

Another attempt to sufficiently slow the rate constant was to adjust the pH to 9 as this has previously been shown to reduce the single turnover rate in LDH variants.¹⁶³ 10 % glycerol was also added to buffers as this is known to increase the viscosity of the solution, slowing enzyme mobility.²¹³ Even combinations of all three changes did not lower the single turnover rate to a measurable value. Further additives would only move the system further away from physiological conditions, making any results gained hard to draw worthwhile conclusions from.

It has therefore been concluded that the single turnover rate in SaLDH is too fast to measure using our stopped flow instrument. Faster methods are therefore required to study this enzyme such as continuous flow spectroscopy or laser flash photolysis.

5.7 pH dependency of steady state kinetics in SaLDH

The pH dependency of the reaction was measured in order to investigate steady state enzyme KIE at different pH values where different events in the catalytic cycle become rate limiting depending on the pH value. The steady state rate of the reaction catalysed by SaLDH was monitored in much the same way as DHFR, a decrease in absorbance at 340 nm, due to depletion of NADH, was monitored over a period of 60 seconds. The previously reported value of k_{cat} for SaLDH was 1.69 ± 0.03 at 20 °C for the reduction

of pyruvate and 1.75 ± 0.03 at 20 °C for reverse reaction. However these measurements were performed on impure enzyme samples and consequently are estimates.²⁰⁸

The pH dependency of the steady state reaction was almost sigmoidal in nature. A maximum rate of $768 \pm 9.8 \text{ s}^{-1}$ was observed at a pH of 6.5 and a minimum of $162 \pm 5 \text{ s}^{-1}$ at pH 9.5. At a pH of 5.5 the rate only dropped to $730 \pm 6 \text{ s}^{-1}$ (**Figure 5.7 and Table 5.1**). In BsLDH the rate limiting step is attributed to motion of the active site loop at a pH of 7.0.²⁰⁰ The decrease in rate at high pH values in SaLDH is likely a consequence of a lack of protons in solution, diminishing the enzymes ability to efficiently protonate the carbonyl group of pyruvate.

The pH dependency of the reaction catalysed with NADD was also measured over the same pH range to yield a primary KIE. As the reaction catalysed with NADD instead of NADH should have a minimal impact on conformational behaviour and ligand-binding effects, obtained primary KIE values will largely report on the chemical step. The pH dependency of the primary KIE exhibited a slight downward trend with a maximum value of 1.98 ± 0.01 at pH 5.5 decreasing to 1.45 ± 0.13 at pH 9.5 (**Figure 5.8 and Table 5.2**). This indicates that the chemical step in the reaction catalysed by SaLDH is partially rate limiting, especially at lower pH values.

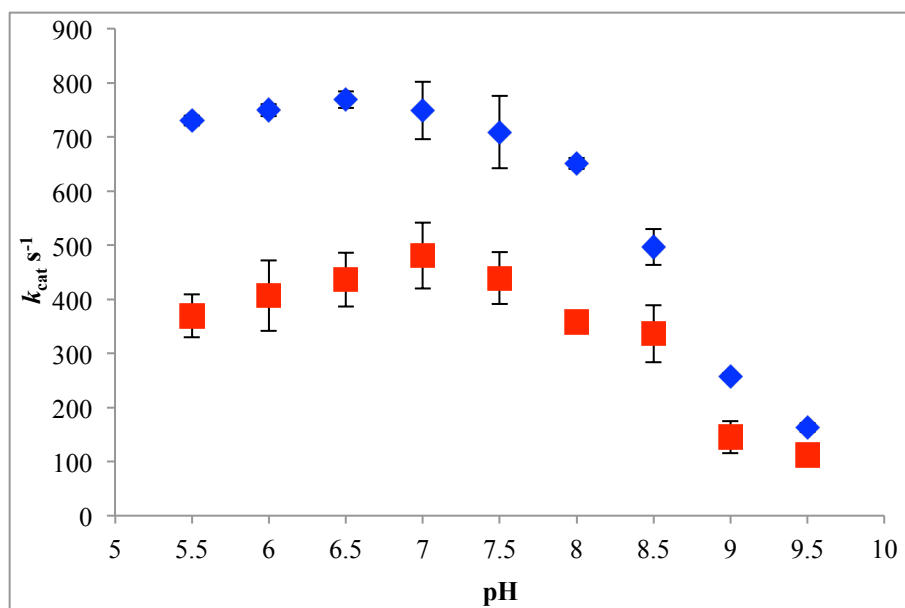


Figure 5.7: pH dependency on the steady state rate constants for hydride (blue diamond) and deuteride (red square) transfer during catalysis by SaLDH at 20 °C.

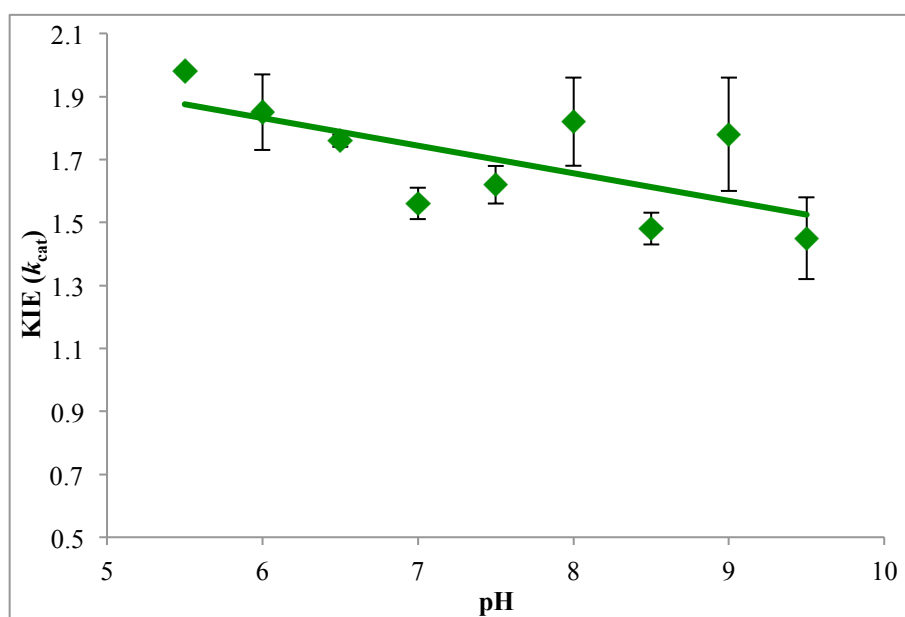


Figure 5.8: pH dependency on the steady state rate primary NADH/D KIE during catalysis by SaLDH at 20 °C.

Table 5.1: pH dependency on the steady state rate constants for hydride ($k_{\text{cat}}^{\text{H}}$) and deuteride ($k_{\text{cat}}^{\text{D}}$) transfer during catalysis by SaLDH at 20 °C.

pH	$k_{\text{cat}}^{\text{H}} \text{ s}^{-1}$	$k_{\text{cat}}^{\text{D}} \text{ s}^{-1}$
5.5	730 ± 6	369 ± 25
6.0	749 ± 74	406 ± 42
6.5	768 ± 9.8	436 ± 32
7.0	748 ± 34	480 ± 39
7.5	708 ± 43	438 ± 31
8.0	650 ± 68	358 ± 69
8.5	496 ± 21	336 ± 34
9.0	258 ± 39	145 ± 19
9.5	162 ± 5	112 ± 49

Table 5.2: pH dependency on the steady state rate primary KIE during catalysis by SaLDH at 20 °C.

pH	KIE
5.5	2.0 ± 0.1
6.0	1.9 ± 0.1
6.5	1.8 ± 0.1
7.0	1.6 ± 0.1
7.5	1.6 ± 0.2
8.0	1.8 ± 0.1
8.5	1.5 ± 0.1
9.0	1.8 ± 0.2
9.5	1.5 ± 0.1

5.8 Examination of hydride transfer through steady state kinetics.

In order to study the influence of the chemical step on catalysis in SaLDH it was deemed necessary to obtain primary NADH/D KIE measurements. The steady state rate constant in the reaction catalysed by SaLDH increased with temperature but did not have true Arrhenius behaviour, as observed by a non-linear Arrhenius plot (**Figure**

5.10). At 5 °C the primary KIE is 1.40 and at 30 °C is 1.39, meaning the KIE is largely independent of temperature.

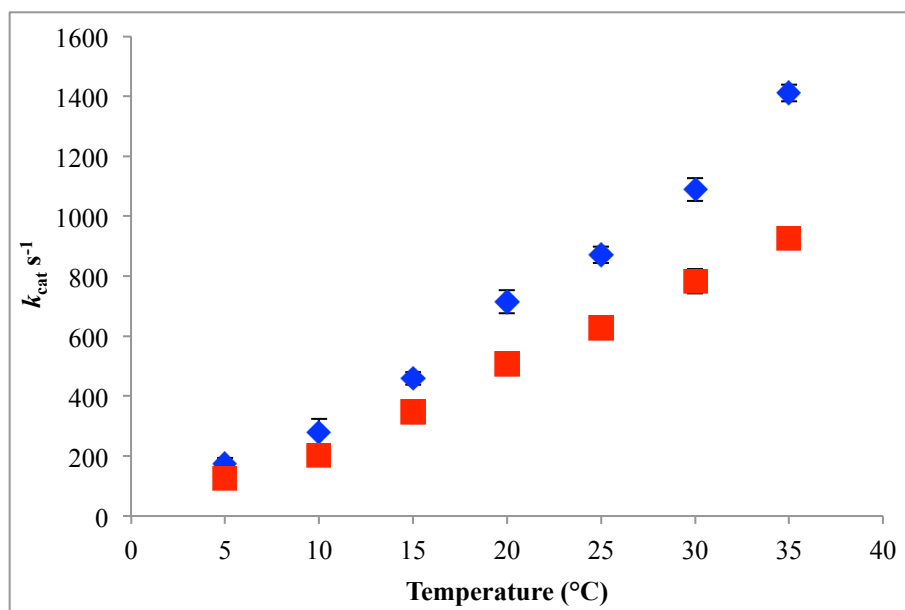


Figure 5.9: Temperature dependency on the steady state rate constants for hydride (blue diamond) and deuteride (red square) transfer during catalysis by SaLDH at pH7.0.

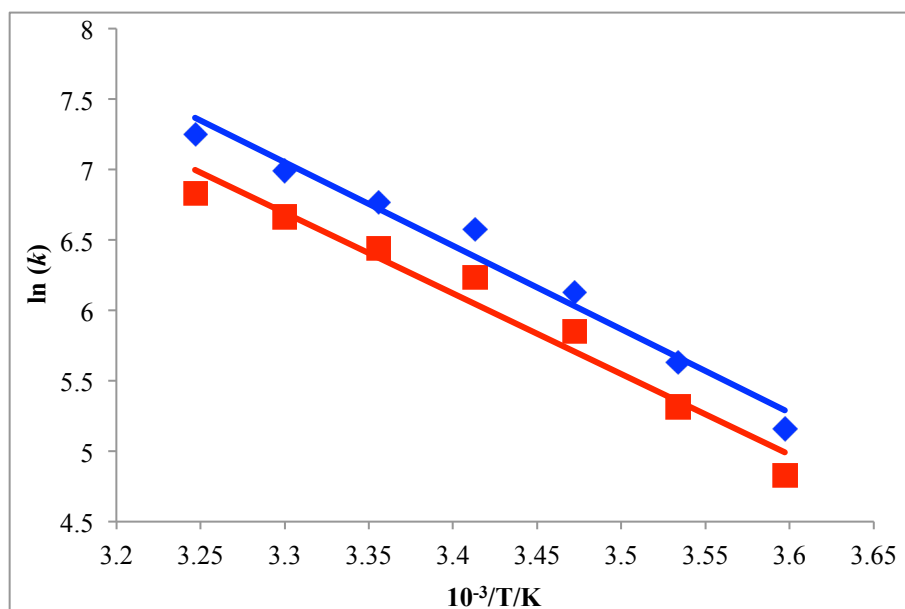


Figure 5.10: Temperature dependency on the steady state rate constants for hydride (blue diamond) and deuteride (red square) transfer during catalysis by SaLDH at pH 7.0.

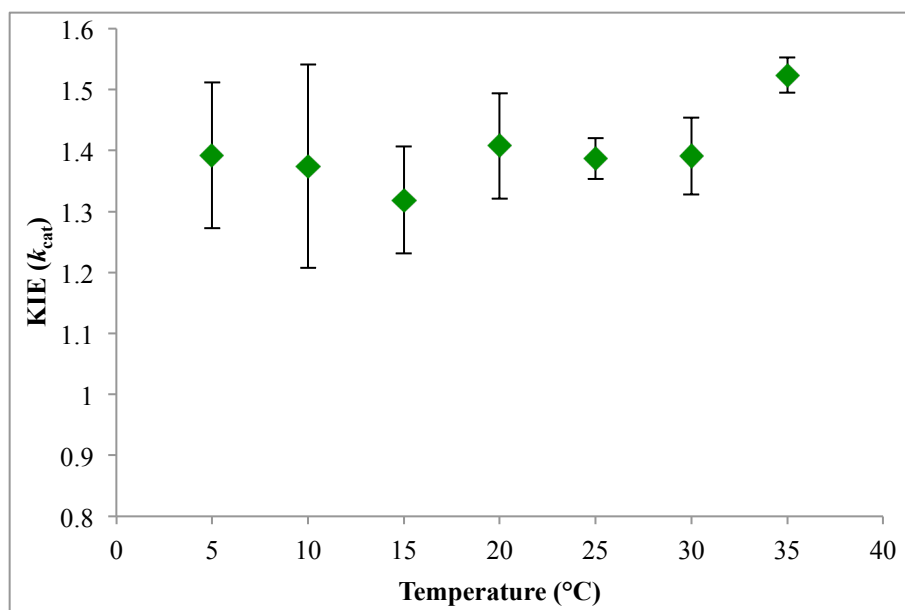


Figure 5.11: Temperature dependency on the steady state rate primary KIE during catalysis by SaLDH at pH 7.0.

Table 5.3: Temperature dependency on the steady state rate constants for hydride ($k_{\text{cat}}^{\text{H}}$) and deuteride ($k_{\text{cat}}^{\text{D}}$) transfer during catalysis by SaLDH at pH 7.0.

Temperature (°C)	$k_{\text{cat}}^{\text{H}} \text{ s}^{-1}$	$k_{\text{cat}}^{\text{D}} \text{ s}^{-1}$
5	174 ± 19	125 ± 6
10	279 ± 44	203 ± 11
15	459 ± 21	348 ± 26
20	715 ± 39	508 ± 34
25	871 ± 27	628 ± 8
30	1089 ± 38	783 ± 41
35	1411 ± 28.5	926 ± 19

Table 5.4: Temperature dependency on the steady state rate primary KIE during catalysis by SaLDH at pH 7.0.

Temperature (°C)	KIE
5	1.40
10	1.38
15	1.32
20	1.41
25	1.39
30	1.39
35	1.52

5.9 pH dependence of the steady state enzyme KIE

^{13}C and ^{15}N labelled SaLDH was prepared in a similar manor to isotopically labelled DHFRs.⁷⁹ Both the temperature (5-35 °C) and pH (5.0-9.5) dependency of the enzyme KIE has been measured under steady state conditions.

With respect to pH dependency the KIE decreased from 1.58 at pH 6.0, to a minimum of 1.27 at pH 7.5 before increasing again to 1.51 at pH 8.5. From previous experiments it is evident that the chemical step is partially rate limiting at pH 7.0 in SaLDH. Although a lot of kinetic complexity will exist under steady state conditions at this pH it seems reasonable to assign some of the observed KIE to effects from the chemical step. Therefore the influence of fast dynamics in catalysis by SaLDH can loosely be discussed.

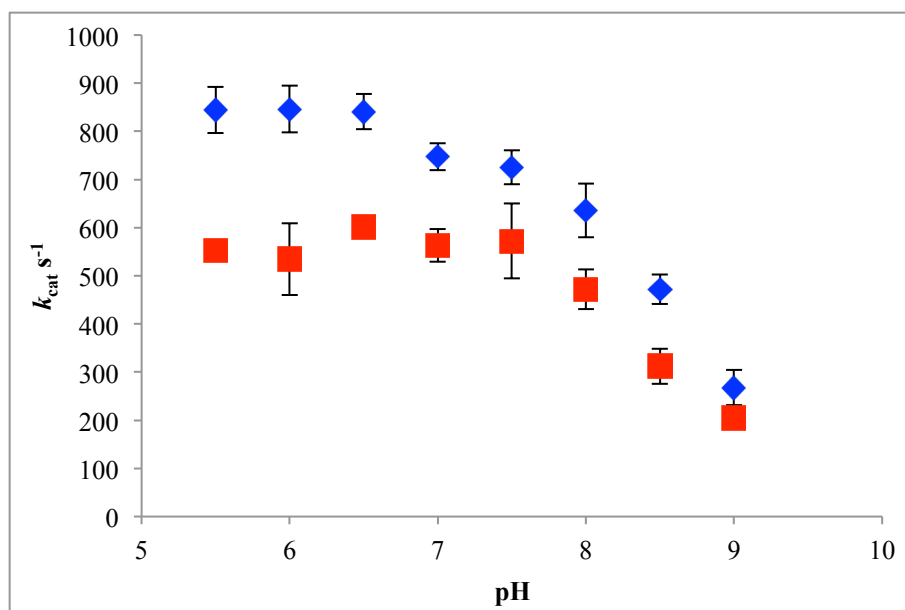


Figure 5.12: pH dependency on the steady state rate constants catalysed by light (blue diamond) and heavy (red square) SaLDH at 20 °C.

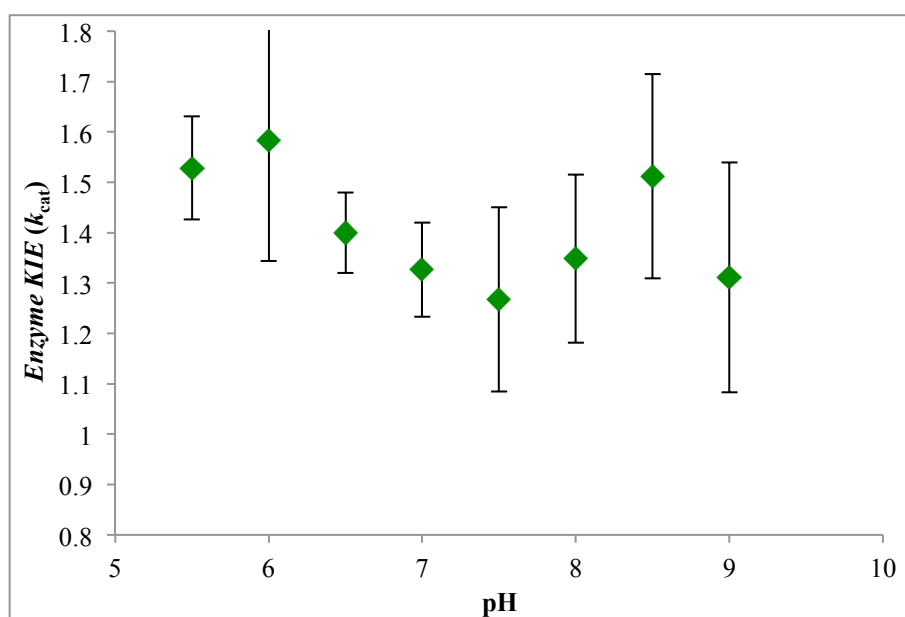


Figure 5.13: pH dependency on the steady state rate enzyme KIE during catalysis by SaLDH at 20 °C.

Table 5.5: pH dependency on the steady state rate constant for natural abundance ($k_{\text{cat}}^{\text{LE}}$) and heavy enzyme ($k_{\text{cat}}^{\text{HE}}$) catalysis by SaLDH at 20 °C.

pH	$k_{\text{cat}}^{\text{LE}} \text{ s}^{-1}$	$k_{\text{cat}}^{\text{HE}} \text{ s}^{-1}$
5.5	844	552
6.0	846	534
6.5	840	600
7.0	746	562
7.5	725	572
8.0	635	471
8.5	472	312
9.0	267	204

Table 5.6: pH dependency on the steady state enzyme KIE during catalysis by SaLDH at 20 °C.

pH	KIE
5.5	1.52
6.0	1.58
6.5	1.40
7.0	1.33
7.5	1.27
8.0	1.35
8.5	1.51
9.0	1.31

In recent work Schramm and co-workers studied the pH dependency of the hydride transfer step in the catalysis by human heart LDH. They observed a decrease in enzyme KIE from 1.11 at pH 4.3 to 1.04 at pH 5.8. They concluded that the observed KIE was evidence of protein promoting vibrations acting on the chemical step.¹⁶³ However no data has been reported for the enzyme KIE at higher pH values so an observation of the overall trend cannot be made. Interestingly though as the pH decreases to that of physiological conditions the KIE tends to unity.

Results from SaLDH show a similar trend, albeit under steady state conditions because as stated previously, the rate of hydride transfer in SaLDH could not be measured. The observed enzyme KIE is minimal under conditions close to physiological conditions in the reaction catalysed by SaLDH and raises as the pH either increases or decreases. This coupled with work by Schramm *et.al.* could be evidence that under physiological conditions the effects of dynamics coupling to the chemical step of catalysis in LDH are minimised. Multiple reports on DHFR variants show the enzyme KIE tends to unity at close to physiological temperatures.^{79,119–121,164,190}

5.10 Temperature dependence of the steady state enzyme KIE

The k_{cat} for the steady state reaction for both light and heavy (^{13}C & ^{15}N) SaLDH was measured over a temperature range of 5-35 °C. The enzyme KIE is minimal at 35 °C with a value of 1.08 ± 0.05 and increases with a decrease in temperature to a value of 1.35 ± 0.18 at 5 °C (Figure 5.15 and Table 5.8).

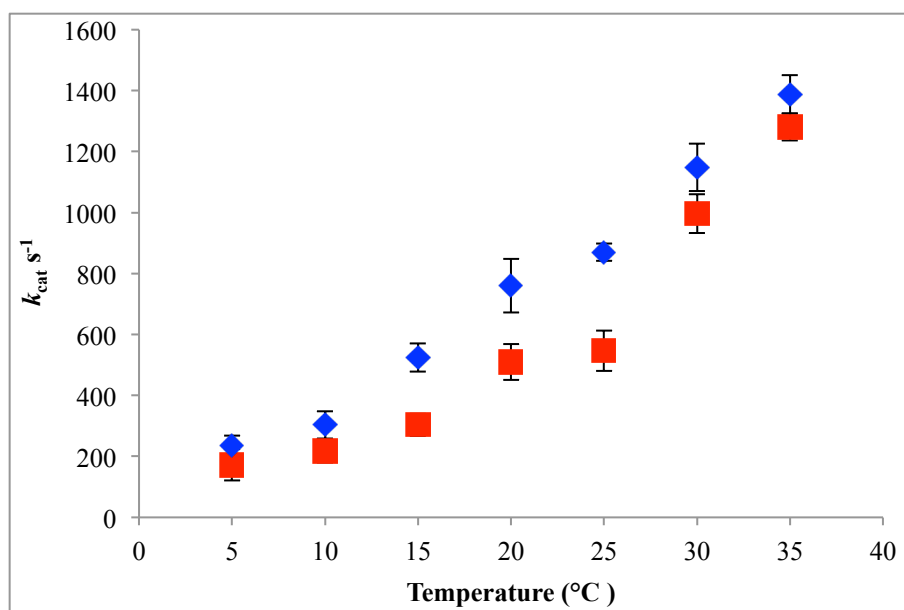


Figure 5.14: Temperature dependency on the steady state rate constants catalysed by light (blue diamond) and heavy (red square) SaLDH at pH 7.0.

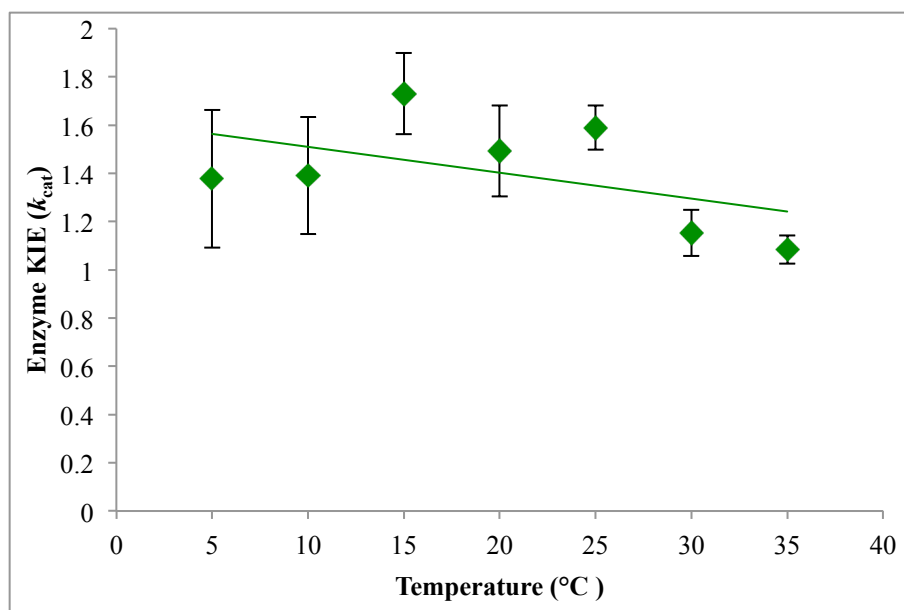


Figure 5.15: Temperature dependency on the steady state rate enzyme KIE during catalysis by SaLDH at pH 7.0.

Table 5.7: Temperature dependency on the steady state rate constant for natural abundance (k_{cat}^{LE}) and heavy enzyme (k_{cat}^{HE}) catalysis by SaLDH at pH 7.0.

Temperature (°C)	$k_{cat}^{LE} s^{-1}$	$k_{cat}^{HE} s^{-1}$
35	1388 ± 44	1281 ± 62
30	1149 ± 33	997 ± 38
25	869 ± 36	547 ± 28
20	760 ± 58	509 ± 88
15	524 ± 35	303 ± 46
10	303 ± 38	218 ± 45
5	237 ± 51	172 ± 32

Table 5.8: Temperature dependency on the steady state enzyme KIE during catalysis by SaLDH at pH 7.0.

Temperature (°C)	KIE
35	1.08 ± 0.05
30	1.15 ± 0.09
25	1.59 ± 0.18
20	1.49 ± 0.16
15	1.73 ± 0.16
10	1.39 ± 0.24
5	1.38 ± 0.18

This is in contrast to EcDHFR where the enzyme KIE under steady state conditions increases from unity at 10 °C to 1.15 ± 1.15 at 40 °C. This increase in KIE in EcDHFR is believed to be a consequence of the conformational behaviour EcDHFR utilises for product release.⁷⁹ The mutant, EcDHFR-N23PP/S148A is conformationally restricted and exhibits a temperature dependant steady state KIE.^{79,119} TmDHFR, which is also conformationally restricted, shows a similar temperature independence, exhibiting a KIE of ~ 1.3 across the measured range.¹²¹ BsDHFR exhibits a larger KIE of ~ 2.6 across the measured temperature range and it was concluded that this temperature independence of the steady state enzyme KIE shows that large scale conformational changes are not involved in catalysis. BsDHFR has been shown to be more flexible than EcDHFR and as such mass induced effects would be larger. Unlike EcDHFR, hydride transfer is also partly rate limiting in BsDHFR at pH 7.0.^{120,214}

The observed temperature dependence of the steady state KIE in SaLDH could be a result of one of two reasons, or a combination of the two. Firstly, work by Moliner *et.al.* has shown rabbit muscle LDH is able catalyse the reaction in an open conformation. Values calculated for the free energy barrier are very close for the reaction catalysed in both the closed and open conformations.²⁰³ With increasing temperature the system would gain thermal energy overcoming activation barriers. At higher temperatures it may become favourable for the enzyme to catalyse the reaction in an open conformation, resulting in conformational behaviour at higher temperatures becoming less important for efficient catalysis, explaining the observed decrease in the value of

KIE. This change in conformational behaviour at higher temperatures may also explain the observed non-Arrhenius behaviour.

Secondly as the rate of hydride transfer has been shown to be at least partially rate limiting in SaLDH, effects of isotope labelling on this step may be observed in the steady state KIE. If this were the case it would align with earlier work carried out with DHFR, showing a minimisation of dynamic effects under close to physiological conditions.^{53,79,119–121,164} Work by Schramm *et.al.* also shows a minimisation of enzyme KIE at close to physiological pH.¹⁶³ There is therefore weak circumstantial evidence to suggest that like DHFR enzymes, SaLDH may have adapted to minimise dynamic coupling acting upon the chemical step at close to physiological pH and temperature.

5.11 Promiscuity in catalysis by SaLDH

Staphylococcus aureus is a gram-positive bacterium that naturally colonizes human skin and respiratory tracts, often existing in a commensal relationship with the host. Methicillin resistant *Staphylococcus aureus* (MRSA), identified in the UK in 1962 is genetically different from the original strain, having evolved to be antibiotic resistant.^{215,216} Over the past few decades *Staphylococcus aureus* has exhibited increasing resistance to a vast number of antibiotics, resulting in medical complications. *Staphylococcus aureus* is able to form biofilms and survive under anaerobic conditions, which it is believed to utilize in order to survive antibiotics and overcome the hosts immune response.^{217,218} As such SaLDH from *Staphylococcus aureus* is a viable drug target.²¹⁰ By testing the specificity of the enzyme for different substrates insights can be gained with respect to the nature of the active site. Ultimately, it is of interest to find differences between SaLDH and human LDH that can be exploited.²¹⁹ It is established that LDH enzymes exhibit promiscuity with respect to the substrates they accept, being able to reduce a wide array of 2-ketocarboxylic acids.^{212,220} To investigate whether substrate promiscuity is similar to previously reported LDH enzymes a variety of substrates were measured with respect to k_{cat} and K_M values.

The calculated K_M for pyruvate was $253 \pm 47.54 \mu\text{M}$. SaLDH like previously studied LDH enzymes also exhibited substrate inhibition at higher concentrations of pyruvate (**Figure 5.16**), although the effect is minimal.

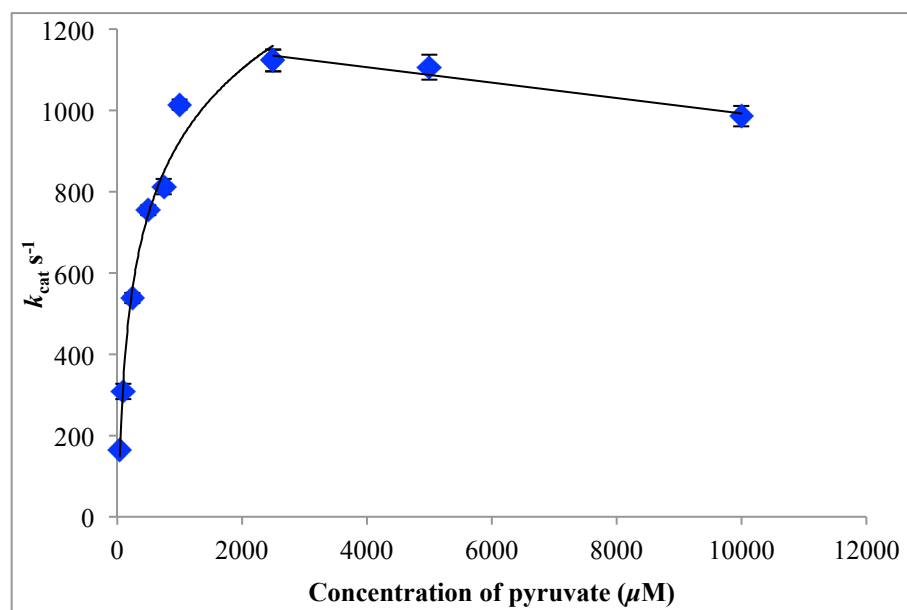


Figure 5.16: Graph of k_{cat} (s^{-1}) vs. concentration of pyruvate (μM).

Four pyruvate analogues were tested with SaLDH at 20 °C and pH 7.0 and the k_{cat} and K_{M} measured (**Figure 5.17** and **Table 5.9**). The worst substrate, as defined by its specificity constant ($k_{\text{cat}}/K_{\text{M}}$) was found to be 2,3-butanedione, which lacked a carboxylic acid moiety. This is likely a consequence of SaLDH being unable to effectively bind the substrate, evident by the high Michaelis constant ($K_{\text{M}} = 200 \pm 4$ mM) which is ~ 800 fold higher than for the natural substrate, pyruvate. The addition of a methyl group to the C3 position of pyruvate results in ~ 3.4 fold drop in the value of k_{cat} and a ~ 7 fold increase in the Michaelis constant. Addition of a carboxylic acid group to the C3 position of pyruvate only results in a ~ 5 fold reduction with respect to k_{cat} and a ~ 13 fold increase to the Michaelis constant. Only addition of a propanoic acid to the C3 position results in a significant decrease with respect to k_{cat} (~ 250 fold reduction with respect to pyruvate).

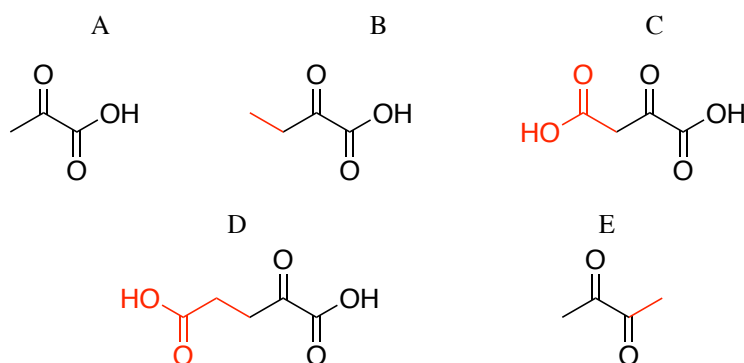


Figure 5.17: Pyruvate analogues incubated with SaLDH, differences with respect to pyruvate are highlighted in red. From left to right, top to bottom; (A) Pyruvate, (B) 2-Ketobutyric acid, (C) Oxaloacetate, (D) 2-Ketoglutaric acid and (E) 2,3-Butanedione.

Table 5.9: Kinetic constants for pyruvate analogues incubated with SaLDH at pH 7.0 and 20 °C.			
Substrate	K_M (μM)	k_{cat} (s^{-1})	k_{cat}/K_M ($\text{s}^{-1} \text{M}^{-1}$)
(A) Pyruvate	253 ± 47	1122 ± 27	4.4×10^6
(B) 2-Ketobutyric acid	1823 ± 722	327 ± 53	1.8×10^5
(C) Oxaloacetate	3452 ± 475	209 ± 14	6.1×10^4
(D) 2-Ketoglutaric acid	8806 ± 2966	4.45 ± 0.45	505
(E) 2,3-Butanedione	200618 ± 3968	3.54 ± 0.80	18

5.12 Summary and conclusions

In this chapter the expression and purification of LDH from *Staphylococcus aureus* (SaLDH) has been detailed. SaLDH was originally selected as a candidate for the study of fast dynamics acting upon the chemical step of catalysis by the study of enzyme KIE, expanding on work carried out with DHFR enzymes. Furthermore, SaLDH is of further interest as it is an essential protein that originates from a pathogenic organism and as such represents a drug target.

Like in EcdHFR, a network of residues with motions on a fs-ps timescale have been proposed to actively promote hydride transfer in human heart LDH.^{204,221} Recently, through the study of enzyme KIE Schramm and co-workers have put forward

experimental evidence for the existence of such promoting motions acting on the chemical step in catalysis by human heart LDH.¹⁶³ It was therefore desirable to apply the same heavy enzyme methodology to SaLDH to see if these results hold true for other members of the LDH family.

Unfortunately attempts to study the chemical step in SaLDH were unsuccessful, due to the rate constant for hydride transfer being too high. Attempts to lower the single turnover rate constant by reductions in temperature, addition of glycerol and pH alteration all yielded no valuable kinetic information. It was deemed the rate of hydride transfer in SaLDH was too fast to be studied *via* the available stopped flow techniques.

As pre-steady state kinetics could not be measured, steady state kinetics were investigated, with the understanding that the chemical step would likely not be rate limiting. The substrate KIE was measured with regards to NADH to assess the extent to which the chemical step was rate limiting under steady state conditions. A primary KIE (NADH/D), which decreased from 1.98 ± 0.01 at pH 5.5 to 1.45 ± 0.13 at pH 9.5, was observed and a primary KIE of ~ 1.38 was observed across the measured temperature range at pH 7.0. These results indicate that at low pH values the chemical step accounts for a larger proportion of the steady state rate constant. Dynamics acting on the chemical step can therefore loosely be studied through analysis of steady state enzyme KIE especially at lower pH values.

Interestingly the pH dependency of the enzyme KIE on the steady state turnover mirrored results obtained by Schramm and co-workers in single turnover experiments with human heart LDH. The enzyme KIE for SaLDH under steady state conditions decreased from 1.58 at pH 6.0 to 1.27 at pH 7.5 before increasing to 1.51 at pH 8.5. Although under steady state conditions there will be increased kinetic complexity it is known from primary KIE data that the rate constant k_{cat} , does in part report on the chemical step in SaLDH. The enzyme KIE under steady state conditions was found to only slightly decrease with temperature, indicating events such as conformational behaviour, which increase kinetic complexity might be minimised in SaLDH. Although results mentioned here are from steady state experiments and conclusions must be cautiously drawn, they align with work done with DHFR's in the way the effect of dynamics seem to be minimised under or near physiological conditions.

Finally, Measurements with respect to substrate specificity show SaLDH is unable to tolerate larger substrates. As such, inhibitor design based upon pyruvate analogues may be greatly limited by substrate size. Consequently, design of an specific SaLDH inhibitor may be challenging.^{219,222}

6

Summary and Conclusions

Protein motions, which occur on various time domains, are known to be central for enzyme catalysis. Conformational behaviour has been shown to be important for efficient ligand binding and product release, and in some cases facilitating catalysis through the creation of an optimal environment. However, a number of DHFR variants, which follow similar catalytic cycles, have similar primary sequences and near superimposable tertiary structures exhibit diversity with respect to conformational behaviour. It is therefore of great interest to further probe the role of such conformational behaviour to understand its overall importance in catalysis. Further to this, the influence of dynamic coupling to the chemical step of catalysis is still under great debate. Although a number of papers now agree that dynamic coupling to the chemical step is minimised in DHFR catalysis there still remains controversy on the influence of such motions in other enzymatic systems.

6.1 Probing of conformational behaviour in DHFR variants.

The initial aim of chapter 3 was to probe protein motions present in TmDHFR through an NMR based approach. Reports have given evidence that TmDHFR is a rigid enzyme considered to proceed through its catalytic cycle in a fixed, open conformation. It is therefore of interest to understand how an apparently rigid enzyme can efficiently proceed through its catalytic cycle. The initial approach relied on obtaining a fully assigned ^1H - ^{15}N HSQC spectrum, which would act as a foundation for a number of NMR based studies. This however, proved not to be possible in the given timescale. As TmDHFR has a relatively high MW it was deemed necessary to deuterate the protein in order to improve relaxation issues. During purification, deuterium present in exchangeable positions is usually back-exchanged for protons in the purification buffer, necessary for the experiment to work. In TmDHFR however, the rigidity needed for its increased thermal stability prevents this process from happening, resulting in greatly diminished signal quality in residues that are not solvent exposed. All in all, it proved very challenging to assign a ^1H - ^{15}N HSQC for TmDHFR due to fast T_2 relaxation and poor tumbling in solution. This meant just over 30% of the backbone in TmDHFR could be assigned, which was deemed insufficient for further experiments to take place.

As such, a new approach to probe conformational behaviour was needed. Selective ^{13}C labelling of the methionine and tryptophan sidechains to probe conformational

behaviour in TmDHFR allowed for a simplified, cost effective and fast solution. Moreover, labelling of sidechains yielded spectra with increased cross-peak resolution and intensity due to the improved relaxation properties.

In order to first validate our method, EcDHFR, which is known to adopt an occluded conformation following the chemical step was selectively labelled with [*methyl*-¹³C]-methionine and [*indole- δ_1* -¹³C] tryptophan. Significant chemical shift perturbations were observed between the Michaelis and product complexes, indicative of conformational change. MpDHFR, which is known to not adopt an occluded conformation following the chemical step showed no significant chemical shift perturbations between the Michaelis and product complexes. This in turn acted as a negative control for the methodology as it proved that the observed chemical shift perturbations were largely reporting on conformational behaviour and not ligand binding effects. TmDHFR, unlike EcDHFR and MpDHFR showed no significant changes in [*methyl*-¹³C]-methionine chemical shifts between the apo, Michaelis and product complexes. These results provided direct evidence for the first time that TmDHFR does indeed remain in a fixed, open like conformation throughout its catalytic cycle.

Previously, evidence of formation of an occluded conformation had only been observed for EcDHFR. Conservation of a hydrogen-bonding network between Ser148 and Asn23 has been shown as crucial for stabilising such a conformation in EcDHFR. Through amino acid sequence analysis, SeDHFR was shown to conserve the Ser148-Asn23 interaction, and therefore theorised likely to adopt an occluded conformation following the chemical step. Like EcDHFR and MpDHFR the quality of spectra for [*methyl*-¹³C]-methionine and [*indole- δ_1* -¹³C] tryptophan labelled apo-SeDHFR was of low quality, indicative of conformational heterogeneity. Like EcDHFR and MpDHFR, [*methyl*-¹³C]-methionine labelled SeDHFR exhibits three well defined cross peaks when in the Michaelis complex. However, six cross peaks are observed when SeDHFR is in the product complex, indicating the presence of two distinct conformational states. Half of the cross peaks in the product complex overlap with those present in the Michaelis complex and it was therefore proposed that in the product complex SeDHFR is in equilibrium between two species, one of which is likely to be the closed conformation and the other an occluded like state. To confirm this theory the mutant SeDHFR-S150A

was prepared, knocking out the hydrogen bonding network postulated to stabilise an occluded conformation. Like in the wild type enzyme, two species were also observed in [*methyl*-¹³C]-methionine labelled spectra for the SeDHFR-S150A mutant. There was, however, a drastic reduction in the population of the second species and the equilibrium shifted to the same species observed in the Michaelis complex. This evidence corroborated our theory that SeDHFR adopts an occluded like conformation following the chemical step. However, to provide further evidence, a ¹H-¹⁵N HSQC of SeDHFR was recorded in both the Michaelis and product complexes. Significant chemical shift differences were observed between the two sets of spectra, as observed in [*methyl*-¹³C]-methionine resonances. The evidence presented here suggests SeDHFR does indeed adopt an occluded like conformation following the chemical step.

In comparison to traditional NMR based approaches that require triple isotope labelling of the protein this methodology is significantly cheaper. Moreover, the time taken to acquire spectra is lessened due in part to increased sensitivity of the experiment and reduced spectral widths being recorded. Moreover, the spectra are drastically simplified and almost intuitive with regards to interpretation, with only a handful of cross peaks being produced. This work has shown that this methodology is sufficient to diagnose conformational behaviour in four DHFR variants and could be readily expanded to other enzyme families.

6.2 The role of dynamics in catalysis

The contribution of dynamics to the chemical step of catalysis is still a hotly debated issue. Recently evidence has been growing that at close to physiological conditions the effect of dynamic coupling to the chemical step of catalysis is minimised in DHFR variants. However much controversy still remains on the contribution of tunnelling in other enzyme families. Systematically labelling proteins with heavy isotopes (²H, ¹³C and ¹⁵N) is believed to only alter bond vibrations. Electrostatic properties are believed to be largely unaffected. Comparison of rate constants for the hydride transfer step between a heavy labelled enzyme and a natural abundance (light) enzyme yields an enzyme KIE. A number of DHFR variants have been previously studied in this way including EcDHFR, MpDHFR, BsDHFR and TmDHFR.

The temperature dependence of the enzyme KIE for SeDHFR was ~ 1 across the measured temperature range. This is similar to the trend observed in TmDHFR, which also exhibits a enzyme KIE of ~ 1 across the measured temperature range. In TmDHFR this was proposed to provide evidence for a lack of dynamic coupling to the chemical step of catalysis. EcDHFR exhibits a temperature dependant enzyme KIE that verges to unity at close to physiological temperatures, as does MpDHFR. It is therefore likely that the effect of dynamic coupling to the chemical step is likewise minimised in SeDHFR.

As evidence is growing that the effect of dynamic coupling to the chemical step is minimised in DHFR variants we looked to expand our study to other enzyme families. SaLDH was selected as it also catalysed a hydride transfer reaction that could be readily characterised using similar experiments to those used in our studies with DHFR. Similar to DHFR, a network of promoting motions have previously been proposed to actively promote catalysis in HsLDH. Furthermore, work by Schramm and co-workers has put forward experimental evidence supporting such a claim.

Attempts to study the chemical step in SaLDH proved to be unfruitful. The rate constant for the chemical step proved too great to be studied *via* the available stopped flow methodologies. Investigation of steady state kinetics revealed a substrate $KIE_{H/D}$ that decreased from 1.98 ± 0.01 at pH 5.5 to 1.45 ± 0.13 at pH 9.5. With respect to temperature dependence, measured at pH 7.0 a value of ~ 1.38 for the primary $KIE_{H/D}$ was recorded over the measured range. This suggests that in part the steady state rate constant reports on the chemical step. As such, the effect of dynamic coupling to the chemical step could be tentatively studied through enzyme KIE under steady state conditions. Although with any conclusions drawn we would have to be extremely cautious as under steady state there would be increased kinetic complexity that would perturb results.

The steady state pH dependency of the enzyme KIE decreased from ~ 1.6 at pH 6.0 to ~ 1.3 at pH 7.5, before increasing to ~ 1.5 at pH 8.5. Interestingly this was found to be a similar trend to that reported by Schramm and co-workers with human heart LDH under pre-steady state conditions. With respect to the temperature dependency of the enzyme KIE it was found to only slightly increase with temperature under steady state conditions. This suggests contributions from such things as conformational behaviour

may be minimised. Tentatively, this shows that at close to physiological pH values the contribution from dynamic coupling to the chemical step may be minimised, possibly aligning with results from DHFR variants.

6.3 Summary

In brief, we have provided further evidence that dynamic coupling to the chemical step is minimised in catalysis by DHFR and may also be minimised in catalysis by SaLDH. This thesis therefore provides further evidence that evolutionary pressure has minimised the influence of dynamic coupling to the chemical step of catalysis. We have also presented a simplified, cost-effective and intuitive approach to probe conformational behaviour in enzyme catalysis. This was utilised to provide evidence that TmDHFR does indeed remain in a fixed, open conformation during catalysis. The methodology was also used to confirm SeDHFR, like EcDHFR adopts a second structural conformation following the chemical step.

7

References

References

1. Hook, S. Vander. Louis Pasteur: Ground breaking Chemist & Biologist. (ABDO Publishing Company, 2011).
2. Manchester, K. L. Louis Pasteur (1822-1895) - chance and the prepared mind. *Trends Biotechnol.* **13**, 511–515 (1995).
3. Barnett, J. A. & Lichtenthaler, F. W. A history of research on yeasts 3: Emil Fischer Eduard Buchner and their contemporaries, 1880-1900. *Yeast* **18**, 363–388 (2001).
4. Berg, J. M., Tymoczko, John, L. & Stryer, L. Biochemistry. (W. H. Freeman and company, 2002).
5. Aebi, H. Catalase in vitro. *Methods Enzymol.* **104**, 121–126 (1984).
6. Hermanek, M., Zboril, R., Medrik, I., Pechousek, J. & Gregor, C. Catalytic efficiency of iron(III) oxides in decomposition of hydrogen peroxide: Competition between the surface area and crystallinity of nanoparticles. *J. Am. Chem. Soc.* **129**, 10929–10936 (2007).
7. Price, N. C. & Stevens, L. Fundamentals of Enzymology. (Oxford University Press, 1999).
8. Holness, M. J. & Sugden, M. C. Regulation of pyruvate dehydrogenase

- complex activity by reversible phosphorylation. *Biochem. Soc. Trans.* 1143–1151 (2003).
9. Nelson, D. L. & Cox, M. M. *Lehninger Principles of Biochemistry*. (W. H. Freeman and company, 2005).
 10. Banerjee, U. C., Sani, R. K., Azmi, W. & Soni, R. Thermostable alkaline protease from *Bacillus brevis* and its characterization as a laundry detergent additive. *Process Biochem.* **35**, 213–219 (1999).
 11. Ribeiro, D. S., Henrique, S. M. B., Oliveira, L. S., Macedo, G. A. & Fleuri, L. F. Enzymes in juice processing : a review. *Food Sci. Technol.* **45**, 635–641 (2010).
 12. Fischer, E. Einfluss der Configuration auf die Wirkung der Enzyme Influence of configuration on the action of enzymes. *Ber. Dtsch. Chem. Ges.* **27**, 2985–2993 (1894).
 13. Brown, J. XXXV1.-Enzyme. *J. Chem. Soc.* **81**, 373–388 (1902).
 14. Henri, V. Theorie Generale de l'action de Quelques Diastases. *Seances Acad. Sci.* **135**, 916–919 (1902).
 15. Henri, V. *L'Action Des Diastases*. (Universite De Gottingue, 1903).

16. Michaelis, L. & Menten, M. L. Die Kinetik der Invertinwirkung. *Biochemistry* **49**, 333–369 (1913).
17. Eyring, H. The Activated Complex in Chemical Reactions. *J. Chem. Phys.* **3**, 107–115 (1935).
18. Evans, M. G. & Polanyi, M. Some applications of the transition state method to the calculation of reaction velocities, especially in solution. *Trans. Faraday Soc.* **31**, 875–894 (1935).
19. Pauling, L. Chemical achievement and hope for the future. *Am. Sci.* **36**, 51–58 (1948).
20. Koshland, D. E. Application of a Theory of Enzyme Specificity to Protein Synthesis. *Proc. Natl. Acad. Sci. U. S. A.* **44**, 98–104 (1958).
21. Monod, J., Wyman, J. & Changeux, J.-P. On the Nature of Allosteric Transitions: A Plausible Model. *J. Mol. Biol.* **12**, 88–118 (1965).
22. Marangoni, A. G. *Enzyme Kinetics*. (John Wiley & Sons, 2003).
23. Roskoski, R. *xPharm: The Comprehensive Pharmacology Reference*. (Elsevier, 2007).
24. Arrhenius, S. *Über die Dissociationswärme und den Einfluss der Temperatur*

- auf den Dissoziationsgrad der Elektrolyte. *De Gruyter* (1889).
25. Cleland, W. W. The use of isotope effects to determine enzyme mechanisms. *Arch. Biochem. Biophys.* **433**, 2–12 (2005).
 26. Atkins, P. & Paula, J. De. *Physical Chemistry*. (Oxford University Press, 2010).
 27. Stojkovic, V. & Kohen, A. Enzymatic H Transfers: Quantum Tunneling and Coupled Motion from Kinetic Isotope Effect Studies. *Isr. J. Chem.* **49**, 163–173 (2009).
 28. Melander, L. & Saunders, W. H. *Reaction Rates of Isotopic molecules*. (Krieger, 1987).
 29. Knapp, M. J., Rickert, K. & Klinman, J. P. Temperature-dependent isotope effects in soybean Lipoxygenase-1: Correlating hydrogen tunneling with protein dynamics. *J. Am. Chem. Soc.* **124**, 3865–3874 (2002).
 30. Kohen, A., Cannio, R., Bartolucci, S. & Klinman, J. P. Enzyme dynamics and hydrogen tunnelling in a thermophilic alcohol dehydrogenase. *Nature* **399**, 496–499 (1999).
 31. Pudney, C. R. et al. Evidence to support the hypothesis that promoting vibrations enhance the rate of an enzyme catalyzed H-tunneling reaction. *J.*

- Am. Chem. Soc.* **131**, 17072–17073 (2009).
32. Sikorski, R. S. et al. Tunneling and Coupled Motion in the Escherichia coli Dihydrofolate Reductase Catalysis. *J. Am. Chem. Soc.* **126**, 4778–4779 (2004).
33. Klinman, Judith, P. & Kohen, A. Hydrogen Tunneling Links Protein Dynamics to Enzyme Catalysis. *Annu Rev. Biochem.* **82**, 471–496 (2013).
34. Bell, R. P. *The Tunnel Effect in Chemistry*. (Chapman & Hall, 1980).
35. Jonsson, T., Glickman, M. H., Sun, S. & Klinman, J. P. Experimental evidence for extensive tunneling of hydrogen in the lipoxygenase reaction: Implications for enzyme catalysis. *J. Am. Chem. Soc.* **118**, 10319–10320 (1996).
36. Wang, L., Goodey, N. M., Benkovic, S. J. & Kohen, A. Coordinated effects of distal mutations on environmentally coupled tunneling in dihydrofolate reductase. *Proc. Natl. Acad. Sci. U. S. A.* **103**, 15753–8 (2006).
37. Agrawal, N., Hong, B., Mihai, C. & Kohen, A. Vibrationally Enhanced Hydrogen Tunneling in the Escherichia coli Thymidylate Synthase Catalyzed Reaction. *Biochemistry* **43**, 1998–2006 (2004).
38. Hong, B., Maley, F. & Kohen, A. Role of Y94 in Proton and Hydride Transfers Catalyzed by Thymidylate Synthase. *Biochemistry* **46**, 14188–14197 (2007).

39. Marcus, R. A. & Sutin, N. Electron transfers in chemistry and biology. *BBA Rev. Bioenerg.* **811**, 265–322 (1985).
40. Caratzoulas, S. & Schwartz, S. D. Computational method to discover the existence of promoting vibrations for chemical reactions in condensed phases. *J. Chem. Phys.* **114**, 2910–2918 (2001).
41. Hynes, James, T., Klinman, J. P., Limbach, H.-H. & Schowen, R. L. *Hydrogen-Transfer Reactions*. (Wiley, 2006).
42. Kohen, A. & Limbach, H.-H. *Isotope effects in Chemistry and Biology*. (Taylor & Francis, 2006).
43. Nagel, Z. D. & Klinman, J. P. Tunneling and dynamics in enzymatic hydride transfer. *Chem. Rev.* **106**, 3095–3118 (2006).
44. Truhlar, D. G., Garrett, B. C. & Klippenstein, S. J. Current status of transition-state theory. *J. Phys. Chem.* **100**, 12771–12800 (1996).
45. Schramm, V. L. Transition States and Transition State Analogue Interactions with Enzymes. *Acc. Chem. Res.* **48**, 1032–1039 (2015).
46. Copeland, R. A. *Enzymes*. (VCH Publishers, 1996).
47. Ruiz-Pernía, J. J. et al. Minimization of dynamic effects in the evolution of

- dihydrofolate reductase. *Chem. Sci.* **7**, 3248–3255 (2016).
48. Silva, R. G., Murkin, A. S. & Schramm, V. L. Femtosecond dynamics coupled to chemical barrier crossing in a Born-Oppenheimer enzyme. *Proc. Natl. Acad. Sci. U. S. A.* **108**, 18661–18665 (2011).
49. Kipp, D. R., Silva, R. G. & Schramm, V. L. Mass-dependent bond vibrational dynamics influence catalysis by HIV-1 protease. *J. Am. Chem. Soc.* **133**, 19358–19361 (2011).
50. Blakley, R. L. Folates and Pterins. 191–253 (1984).
51. Fierke, C. a, Johnson, K. a & Benkovic, S. J. Construction and evaluation of the kinetic scheme associated with dihydrofolate reductase from *Escherichia coli*. *Biochemistry* **26**, 4085–4092 (1987).
52. Loveridge, E. J. et al. Reduction of Folate by Dihydrofolate Reductase from *Thermotoga maritima*. *Biochemistry* **56**, 1879–1886 (2017).
53. Luk, L. Y. P., Loveridge, E. J. & Allemann, R. K. Protein motions and dynamic effects in enzyme catalysis. *Phys. Chem. Chem. Phys.* **17**, (2015).
54. Schweitzer, B. I., Dicker, A. P. & Bertino, J. R. Dihydrofolate reductase as a therapeutic target. *FASEB J* **4**, 2441–2452 (1990).

55. Choumenkovitch, S. F. et al. Folic acid intake from fortification in United States exceeds predictions. *J. Nutr.* **132**, 2792–2798 (2002).
56. Crider, K. S., Bailey, L. B. & Berry, R. J. Folic acid food fortification-its history, effect, concerns, and future directions. *Nutrients* **3**, 370–384 (2011).
57. Vitamin B12 or folate deficiency anaemia. National Health Service (UK) (2016). at <<https://www.nhs.uk/conditions/vitamin-b12-or-folate-deficiency-anaemia/>>
58. Protein data bank. (2018). at <<http://www.rcsb.org/pdb/results/results.do?tabtoShow=Current&qrid=3E957EB9>>
59. Levitt, M. & Chothia, C. Structural patterns in globular proteins. *Nature* **261**, 552–558 (1976).
60. Filman, D. J., Bolin, J. T., Matthews, D. A. & Kraut, J. Crystal Structures of Escherichia coli and Lactobacillus casei Dihydrofolate Reductase Refined at 1.7 Å Resolution. *J. Biol. Chem.* **257**, 13663–13672 (1982).
61. Sawaya, M. R. & Kraut, J. Loop and Subdomain Movements in the Mechanism of Escherichia coli Dihydrofolate Reductase: Crystallographic Evidence, *Biochemistry* **36**, 586–603 (1997).

62. Khavrutskii, I. V, Price, D. J., Lee, J. & Brooks, C. L. Conformational change of the methionine 20 loop of Escherichia coli dihydrofolate reductase modulates pKa of the bound dihydrofolate. *Protein Sci.* **16**, 1087–1100 (2007).
63. Hecht, D., Tran, J. & Fogel, G. B. Structural-based analysis of dihydrofolate reductase evolution. *Mol. Phylogenet. Evol.* **61**, 212–230 (2011).
64. Shrimpton, P. & Allemann, R. K. Role of water in the catalytic cycle of E . coli dihydrofolate reductase. 1442–1451 (2002). doi:10.1110/ps.5060102.N5
65. Miller, G. P. & Benkovic, S. J. Stretching exercises ? flexibility in dihydrofolate reductase catalysis. *Chem. Biol.* **5**, R105–R113 (1998).
66. Lee, H., Reyes, V. M. & Kraut, J. Crystal Structures of Escherichia coli Dihydrofolate Reductase Complexed with 5-Formyltetrahydrofolate (Folinic Acid) in Two Space Groups: Evidence for Enolization of Pteridine O4. *Biochemistry* **35**, 7012–7020 (1996).
67. Chen, Y., Kraut, J., Blakley, R. & Callender, R. Determination by Raman Spectroscopy of the pKa of N5 of Dihydrofolate Bound to Dihydrofolate Reductase: Mechanistic Implications. *Biochemistry* **33**, 7021–7026 (1994).
68. Cannon, W. R., Garrison, B. J. & Benkovic, S. J. Electrostatic Characterization of Enzyme Complexes: Evaluation of the Mechanism of Catalysis of Dihydrofolate Reductase. *J. Am. Chem. Soc.* **119**, 2386–2395 (1997).

69. Cummins, P. L. & Gready, J. E. Energetically Most Likely Substrate and Active-Site Protonation Sites and Pathways in the Catalytic Mechanism of Dihydrofolate Reductase. *J. Am. Chem. Soc.* **123**, 3418–3428 (2001).
70. Shrimpton, P. & Allemann, R. K. Role of water in the catalytic cycle of E. coli dihydrofolate reductase. *Protein Sci.* **11**, 1442–1451 (2002).
71. Ferrer, S., Silla, E., Tunon, I., Martí, S. & Moliner, V. Catalytic Mechanism of Dihydrofolate Reductase Enzyme . A Combined Quantum-Mechanical / Molecular-Mechanical Characterization of the N5 Protonation Step. *J. Phys. Chem. B.* **107**, 14036–14041 (2003).
72. Wan, Q. et al. Toward resolving the catalytic mechanism of dihydrofolate reductase using neutron and ultrahigh-resolution X-ray crystallography. *Proc. Natl. Acad. Sci.* **111**, 18225–18230 (2014).
73. Angelastro, A., Dawson, W. M., Luk, L. Y. P., Loveridge, E. J. & Allemann, R. K. Chemoenzymatic Assembly of Isotopically Labeled Folates. *J. Am. Chem. Soc.* **139**, 13047–13054 (2017).
74. Henzler-Wildman, K. & Kern, D. Dynamic personalities of proteins. *Nature* **450**, 964–972 (2007).
75. Schramm, V. L. Enzymatic Transition States, Transition-State Analogs, Dynamics, Thermodynamics, and Lifetimes. *Annu. Rev. Biochem.* **80**, 703–732

- (2011).
76. Behiry, E. M., Luk, L. Y. P., Matthews, S. M., Loveridge, E. J. & Allemann, R. K. Role of the occluded conformation in bacterial dihydrofolate reductases. *Biochemistry* **53**, 4761–4768 (2014).
77. Arora, K. & Iii, C. L. B. Functionally Important Conformations of the Met20 Loop in Dihydrofolate Reductase are Populated by Rapid Thermal Fluctuations Functionally Important Conformations of the Met20 Loop in Dihydrofolate Reductase are Populated by Rapid Thermal Fluctuations. 5642–5647 (2009). doi:10.1021/ja9000135
78. Bystroff, C., Oatley, S. J. & Kraut, J. Crystal Structures of Escherichia coli Dihydrofolate Reductase: The NADP⁺ Holoenzyme and the Folate.NADP⁺ Ternary Complex. Substrate Binding and a Model for the Transition State. *Biochemistry* **29**, 3263–3277 (1990).
79. Luk, L. Y. P. et al. Unraveling the role of protein dynamics in dihydrofolate reductase catalysis. *Proc. Natl. Acad. Sci.* **110**, 16344–16349 (2013).
80. Loveridge, E. J., Behiry, E. M., Guo, J. & Allemann, R. K. Evidence that a ‘dynamic knockout’ in Escherichia coli dihydrofolate reductase does not affect the chemical step of catalysis. *Nat Chem* **4**, 292–297 (2012).
81. Boehr, D. D., McElheny, D., Dyson, H. J. & Wright, P. E. The Dynamic

- Energy Landscape of Dihydrofolate Reductase Catalysis. *Science*. **313**, 1638–1642 (2006).
82. Oyen, D. et al. Defining the Structural Basis for Allosteric Product Release from *E. coli* Dihydrofolate Reductase Using NMR Relaxation Dispersion. *J. Am. Chem. Soc.* **139**, 11233–11240 (2017).
83. Hughes, R. L., Johnson, L. A., Behiry, E. M., Loveridge, E. J. & Allemann, R. K. A rapid analysis of variations in conformational behavior during dihydrofolate reductase catalysis. *Biochemistry* **56**, 2126–2133 (2017).
84. Evans, R. M. et al. Catalysis by dihydrofolate reductase from the psychropiezophile *Moritella profunda*. *ChemBioChem* **11**, 2010–2017 (2010).
85. Gargaro, A. R. et al. The solution structure of the complex of *Lactobacillus casei* dihydrofolate reductase with methotrexate. *J Mol Biol* **277**, 119–134 (1998).
86. Feeney, J. et al. NMR structures of apo *L. casei* dihydrofolate reductase and its complexes with trimethoprim and NADPH: Contributions to positive cooperative binding from ligand-induced refolding, conformational changes, and interligand hydrophobic interactions. *Biochemistry* **50**, 3609–3620 (2011).
87. Beierlein, J. M. et al. Synthetic and crystallographic Studies of a New Inhibitor Series Targeting *Bacillus anthracis* Dihydrofolate Reductase. *J Med Chem* **51**,

- 7532–7540 (2008).
88. Dams, T. et al. Homo-dimeric recombinant dihydrofolate reductase from *Thermotoga maritima* shows extreme intrinsic stability. *Biol. Chem.* **379**, 367–371 (1998).
89. Dams, T. et al. The Crystal Structure of Dihydrofolate Reductase from *Thermotoga maritima*: Molecular Features of Thermostability. *J. Mol. Biol.* **297**, 659–672 (2000).
90. Maglia, G., Javed, M. H. & Allemann, R. K. Hydride transfer during catalysis by dihydrofolate reductase from *Thermotoga maritima*. *Biochem. J.* **374**, 529–535 (2003).
91. Guo, J., Loveridge, E. J., Luk, L. Y. P. & Allemann, R. K. Effect of dimerization on dihydrofolate reductase catalysis. *Biochemistry* **52**, 3881–3887 (2013).
92. Loveridge, E. J., Maglia, G. & Allemann, R. K. The role of arginine 28 in catalysis by dihydrofolate reductase from the hyperthermophile *Thermotoga maritima*. *ChemBioChem* **10**, 2624–2627 (2009).
93. Loveridge, E. J., Behiry, E. M., Swanwick, R. S. & Allemann, R. K. Different Reaction Mechanisms for Mesophilic and Thermophilic Dihydrofolate Reductases. 6926–6927 (2009).

94. Loveridge, E. J., Rodriguez, R. J., Swanwick, R. S. & Allemann, R. K. Effect of dimerization on the stability and catalytic activity of dihydrofolate reductase from the hyperthermophile *Thermotoga maritima*. *Biochemistry* **48**, 5922–5933 (2009).
95. Guo, J., Loveridge, E. J., Luk, L. Y. P. & Allemann, R. K. Effect of Dimerization on Dihydrofolate Reductase Catalysis. (2013).
96. Blakley, R. L. *The Biochemistry of Folic Acid and Related Pteridines*. (Elsevier, 1969).
97. Posner, B. A., Li, L., Bethell, R., Tsuji, T. & Benkovic, S. J. Engineering specificity for folate into dihydrofolate reductase from *Escherichia coli*. *Biochemistry* **35**, 1653–1663 (1996).
98. Bhabha, G. et al. A dynamic Knockout reveals that conformational fluctuations influence the chemical step of enzyme catalysis. *Science*. **332**, 234–238 (2011).
99. Bhabha, G. & Ekiert, D. Divergent evolution of protein conformational dynamics in dihydrofolate reductase. *Nat. Struct. Mol. Biol.* **20**, 1243–1249 (2013).
100. Liu, C. T. et al. Functional significance of evolving protein sequence in dihydrofolate reductase from bacteria to humans. *Proc. Natl. Acad. Sci. U. S. A.* **110**, 10159–10164 (2013).

101. Knowles, J. R. Enzyme catalysis: not different, Just better. *Nature* **350**, 121–124 (1991).
102. Bolhuis, P. G., Chandler, D., Dellago, C. & Geissler, P. L. T Throwing Ropes Over Rough Mountain Passes, in the Dark. *Annu. Rev. Phys. Chem.* **53**, 291–318 (2002).
103. Schramm, V. L. Freezing time. *TheScientist* (2012).
104. Schramm, V. L. Enzymatic Transition State Theory and Transition State Analogue Design *. *J. Biol. Chem.* **282**, 28297–28300 (2007).
105. Hammes, G. G., Benkovic, S. J. & Hammes-Schiffer, S. Flexibility, diversity, and cooperativity: Pillars of enzyme catalysis. *Biochemistry* **50**, 10422–10430 (2011).
106. Henzler-wildman, K., Lei, M., Kerns, S. J., Karplus, M. & Kern, D. A hierarchy of timescales in protein dynamics is linked to enzyme catalysis. *Nature* **450**, 913–916 (2007).
107. Agarwal, P. K., Billeter, S. R., Rajagopalan, P. T. R., Benkovic, S. J. & Hammes-Schiffer, S. Network of coupled promoting motions in enzyme catalysis. *Proc. Natl. Acad. Sci.* **99**, 2794–2799 (2002).

108. Cameron, C. E. & Benkovic, S. J. Evidence for a functional role of the dynamics of glycine-121 of Escherichia coli dihydrofolate reductase obtained from kinetic analysis of a site-directed mutant. *Biochemistry* **36**, 15792–15800 (1997).
109. Ravi Rajagopalan, P. T., Lutz, S. & Benkovic, S. J. Coupling interactions of distal residues enhance dihydrofolate reductase catalysis: Mutational effects on hydride transfer rates. *Biochemistry* **41**, 12618–12628 (2002).
110. Agarwal, P. K., Billeter, S. R. & Hammes-Schiffer, S. Nuclear quantum effects and enzyme dynamics in dihydrofolate reductase catalysis. *J. Phys. Chem. B* **106**, 3283–3293 (2002).
111. Loveridge, E. J. & Allemann, R. K. Effect of pH on Hydride Transfer by Escherichia coli Dihydrofolate Reductase. *ChemBioChem* **12**, 1258–1262 (2011).
112. Chen, Y., Kraut, J. & Callender, R. pH-Dependent Conformational Changes in Escherichia coli Dihydrofolate Reductase Revealed by Raman Difference Spectroscopy. **72**, 936–941 (1997).
113. Singh, P., Sen, A., Francis, K. & Kohen, A. Extension and limits of the network of coupled motions correlated to hydride transfer in dihydrofolate reductase. *J. Am. Chem. Soc.* **136**, 2575–2582 (2014).

114. Watney, J. B., Agarwal, P. K. & Hammes-Schiffer, S. Effect of mutation on enzyme motion in dihydrofolate reductase. *J. Am. Chem. Soc.* **125**, 3745–3750 (2003).
115. Swanwick, R. S., Shrimpton, P. J. & Allemann, R. K. Pivotal Role of Gly 121 in Dihydrofolate Reductase from *Escherichia coli*: The Altered Structure of A Mutant Enzyme May Form the Basis of Its Diminished Catalytic Performance. *Biochemistry* **43**, 4119–4127 (2004).
116. Van Den Bedem, H., Bhabha, G., Yang, K., Wright, P. E. & Fraser, J. S. Automated identification of functional dynamic contact networks from X-ray crystallography. *Nat. Methods* **10**, 896–902 (2013).
117. Luk, L. Y. P., Loveridge, E. J. & Allemann, R. K. Different Dynamical Effects in Mesophilic and Hyperthermophilic Dihydrofolate Reductases. *Biochemistry* 16–19 (2014).
118. Oppenheimer, B. M. On the quantum theory of molecules. *Ann. Phys-Berlin* **389**, 457–484 (1927).
119. Ruiz-Pernia, J. J. et al. Increased Dynamic Effects in a Catalytically Compromised Variant of *Escherichia coli* Dihydrofolate Reductase. *J. Am. Chem. Soc.* **135**, 18689–18696 (2013).
120. Luk, L. Y. P. et al. Protein isotope effects in dihydrofolate reductase from

- geobacillus stearothermophilus show entropic-enthalpic compensatory effects on the rate constant. *J. Am. Chem. Soc.* **136**, 17317–17323 (2014).
121. Luk, L. Y. P., Loveridge, E. J. & Allemann, R. K. Different dynamical effects in mesophilic and hyperthermophilic dihydrofolate reductases. *J. Am. Chem. Soc.* **136**, 6862–6865 (2014).
122. Blakley, R. L. Crystalline dihydropteroylglutamic acid. *Nature* **188**, 231–232 (1960).
123. Viola, R. E., Cook, P. F. & Cleland, W. W. Stereoselective preparation of deuterated reduced nicotinamide adenine nucleotides and substrates by enzymatic synthesis. *Anal. Biochem.* **96**, 334–340 (1979).
124. Delaglio, F. et al. NMRPipe: A multidimensional spectral processing system based on UNIX pipes. *J. Biomol. NMR* **6**, 277–293 (1995).
125. Vranken, W. F. et al. The CCPN data model for NMR spectroscopy: Development of a software pipeline. *Proteins Struct. Funct. Genet.* **59**, 687–696 (2005).
126. Swanwick, R. S., Maglia, G., Tey, L. & Allemann, R. K. Coupling of protein motions and hydrogen transfer during catalysis by *Escherichia coli* dihydrofolate reductase. *Biochem. J.* **394**, 259–265 (2006).

127. Wang, X., Chan, T. F. A. I. & Lam, V. M. S. What is the role of the second structural NADP + -binding site in human glucose 6-phosphate dehydrogenase? *Protein Sci.* **17**, 1403–1411 (2008).
128. Zakrzewski, S. F. & Sansone, A. M. A New Synthesis of Tetrahydrofolic acid. *Methods Enzymol.* 728–731 (1971).
129. Acta, B., Stone, S. R. & Morrison, J. F. Kinetic Mechanism of the Reaction Catalyzed by Dihydrofolate Reductase from *Escherichia coli*. 3757–3765 (1982). doi:10.1021/bi00259a006
130. Williamson, M. P. Using chemical shift perturbation to characterise ligand binding. *Prog. Nucl. Magn. Reson. Spectrosc.* **73**, 1–16 (2013).
131. Huber, R. et al. *Thermotoga maritima* sp. nov. represents a new genus of unique extremely thermophilic eubacteria growing up to 90 C. *Microbiol.* **144**, 324–333 (1986).
132. Dams, T., Bohm, G., Auerbach, G., Bader, G., Schurig, H. & Jaenicke, R. Homo-dimeric recombinant dihydrofolate reductase from *Thermotoga maritima* shows extreme intrinsic stability. *Biol. Chem.* **379**, 367–371 (1998).
133. Dams, T., Bohm, G., Auerbach, G., Bader, G., Schurig, H. & Jaenicke, R. The crystal structure of dihydrofolate reductase from *Thermotoga maritima*: molecular features of thermostability. *J. Mol. Biol.* **297**, 659–672 (2000).

134. Pang, J. & Allemann, R. K. Molecular dynamics simulation of thermal unfolding of *Thermatoga maritima* DHFR. *Phys. Chem. Chem. Phys.* **9**, 711–8 (2007).
135. Wilquet, V. et al. Purification and characterization of recombinant *Thermotoga maritima* dihydrofolate reductase. *Eur. J. Biochem.* **255**, 628–37 (1998).
136. Cavanagh, J., Fairbrother, W. J., Palmer, A. G., Rance, M. & Skelton, N. J. *Protein NMR Spectroscopy*. (Elsevier, 2007).
137. Protein NMR A Practical Guide. (2018). at <<http://www.protein-nmr.org.uk/>>
138. Loveridge, E. J. et al. Aliphatic ¹H, ¹³C and ¹⁵N chemical shift assignments of dihydrofolate reductase from the psychropiezophile *Moritella profunda* in complex with NADP⁺ and folate. *Biomol. NMR Assign.* **7**, 61–64 (2013).
139. Loveridge, E. J. et al. The role of large-scale motions in catalysis by dihydrofolate reductase. *J. Am. Chem. Soc.* **133**, 20561–20570 (2011).
140. Osborne, M. J., Venkitakrishnan, R. P., Dyson, H. J. & Wright, P. E. Diagnostic chemical shift markers for loop conformation and substrate and cofactor binding in dihydrofolate reductase complexes. *Protein Sci.* **12**, 2230–2238 (2003).

141. Pervushin, K., Riek, R., Wider, G. & Wuthrich, K. Attenuated T2 relaxation by mutual cancellation of dipole-dipole coupling and chemical shift anisotropy indicates an avenue to NMR structures of very large biological macromolecules in solution. *Proc. Natl. Acad. Sci.* **94**, 12366–12371 (1997).
142. Markus, M. A., Dayie, K. T., Matsudaira, P. & Wagner, G. Effect of Deuteration on the Amide Proton Relaxation Rates in Proteins. Heteronuclear NMR Experiments on Villin 14T. *Journal of Magnetic Resonance, Series B* **105**, 192–195 (1994).
143. Yamazaki, T., Lee, W., Arrowsmith, C. H., Muhandiram, D. R. & Kay, L. E. A Suite of Triple Resonance NMR Experiments for the Backbone Assignment of ¹⁵N, ¹³C, ²H Labeled Proteins with High Sensitivity. *J. Am. Chem. Soc.* **116**, 11655–11666 (1994).
144. Sattler, M. & Fesik, S. W. Use of deuterium labeling in NMR: Overcoming a sizeable problem. *Structure* **4**, 1245–1249 (1996).
145. Guo, J. Thermophilicity and Catalytic Efficiency in Dihydrofolate Reductase. (Cardiff University, 2013).
146. Burz, D. S. NMR studies of Large Protein Systems. *Methods Mol. Biol.* **278**, 133–140 (2012).
147. Rodriguez-Mias, R. A. & Pellecchia, M. Use of selective Trp side chain

- labeling to characterize protein-protein and protein-ligand interactions by NMR spectroscopy. *J. Am. Chem. Soc.* **125**, 2892–2893 (2003).
148. Williamson, M. P. Using Chemical Shift Perturbation to Characterise Ligand Binding. *Prog. Nucl. Magn. Reson. Spectrosc.* 1–16 (2013).
149. Sawaya, M. R. & Kraut, J. Loop and Subdomain Movements in the Mechanism of Escherichia coli Dihydrofolate Reductase : Crystallographic Evidence †,‡. **2960**, 586–603 (1997).
150. Ohmae, E., Sasaki, Y. & Gekko, K. Effects of five-tryptophan mutations on structure, stability and function of Escherichia coli dihydrofolate reductase. *J. Biochem.* **130**, 439–447 (2001).
151. Ohmae, E., Fukumizu, Y., Iwakura, M. & Gekko, K. Effects of Mutation at Methionine-42 of Escherichia coli Dihydrofolate Reductase on Stability and Function: Implication of Hydrophobic Interactions. *J. Biochem.* **137**, 643–652 (2005).
152. Ben-Bassat, A., Bauer, K., Chang, S. Y., Myambo, K. & Boosman, A. Processing of the initiation methionine from proteins: Properties of the Escherichia coli methionine aminopeptidase and its gene structure. *J. Bacteriol.* **169**, 751–757 (1987).
153. Hay, S. et al. Are the catalytic properties of enzymes from piezophilic

- organisms pressure adapted? *ChemBioChem* **10**, 2348–2353 (2009).
154. Miles, E. W., Bauerle, R. & Ahmed, S. A. Tryptophan synthase from *Escherichia coli* and *Salmonella typhimurium*. *Methods Enzymol.* **142**, 398–414 (1987).
155. Schnell, J. R., Dyson, H. J. & Wright, P. E. Structure, dynamics, and catalytic function of dihydrofolate reductase. *Annu. Rev. Biophys. Biomol. Struct.* **33**, 119–40 (2004).
156. Venkitakrishnan, R. P. et al. Conformational changes in the active site loops of dihydrofolate reductase during the catalytic cycle. *Biochemistry* **43**, 16046–16055 (2004).
157. Hajduk, P. J. et al. NMR-based screening of proteins containing ¹³C-labeled methyl groups. *J. Am. Chem. Soc.* **122**, 7898–7904 (2000).
158. Boehr, D. D., Dyson, H. J. & Wright, P. E. Conformational relaxation following hydride transfer plays a limiting role in dihydrofolate reductase catalysis. *Biochemistry* **47**, 9227–9233 (2008).
159. Masterson, J. E. & Schwartz, S. D. Changes in protein architecture and subpicosecond protein dynamics impact the reaction catalyzed by lactate dehydrogenase. *J. Phys. Chem. A* **117**, 7107–7113 (2013).

160. Núñez, S., Antoniou, D., Schramm, V. L. & Schwartz, S. D. Promoting vibrations in human purine nucleoside phosphorylase. A molecular dynamics and hybrid quantum mechanical/molecular mechanical study. *J. Am. Chem. Soc.* **126**, 15720–15729 (2004).
161. Basner, J. E. & Schwartz, S. D. How enzyme dynamics helps catalyze a reaction in atomic detail: A transition path sampling study. *J. Am. Chem. Soc.* **127**, 13822–13831 (2005).
162. Saen-Oon, S., Quaytman-Machleder, S., Schramm, V. L. & Schwartz, S. D. Atomic detail of chemical transformation at the transition state of an enzymatic reaction. *Proc. Natl. Acad. Sci. U. S. A.* **105**, 16543–16548 (2008).
163. Wang, Z., Chang, E. P. & Schramm, V. L. Triple Isotope Effects Support Concerted Hydride and Proton Transfer and Promoting Vibrations in Human Heart Lactate Dehydrogenase. *J. Am. Chem. Soc.* **138**, 15004–15010 (2016).
164. Luk, L. Y. P. et al. Chemical Ligation and Isotope Labeling to Locate Dynamic Effects during Catalysis by Dihydrofolate Reductase. *Angew. Chemie - Int. Ed.* **54**, 9016–9020 (2015).
165. Dametto, M., Antoniou, D. & Schwartz, S. D. Barrier crossing in Dihydrofolate Reductase does not Involve a Rate-Promoting Vibration. *Mol. Phys.* **110**, 531–536 (2012).

166. Radkiewicz, J. L. & Brooks, C. L. Protein dynamics in enzymatic catalysis: Exploration of dihydrofolate reductase. *J. Am. Chem. Soc.* **122**, 225–231 (2000).
167. Roston, D., Cheatum, C. M. & Kohen, A. Hydrogen Donor-Acceptor fluctuations from kinetic isotope effects: A phenomenological model. *Biochemistry* **51**, 6860–6870 (2012).
168. Pang, J., Pu, J., Gao, J., Truhlar, D. G. & Allemann, R. K. Hydride transfer reaction catalyzed by hyperthermophilic dihydrofolate reductase is dominated by quantum mechanical tunneling and is promoted by both inter- and intramonomeric correlated motions. *J. Am. Chem. Soc.* **128**, 8015–8023 (2006).
169. Holzwarth, G. & Doty, P. The Ultraviolet Circular Dichroism of Polypeptides. *J. Am. Chem. Soc.* **87**, 218–228 (1965).
170. Behiry, E. M. Dihydrofolate Reductase and the Physical Basis of Enzyme Catalysis. (Cardiff University, 2013).
171. Feller, G. Life at Low Temperatures: Is Disorder the Driving Force? *Extremophiles* **11**, 211–216 (2007).
172. Lonhienne, T., Gerday, C. & Feller, G. Psychrophilic Enzymes: Revisiting the Thermodynamic Parameters of Activation May Explain Local Flexibility. *Protein Struct. Mol. Enzymol.* **1543**, 1–10 (2000).

173. Stone, S. R. & Morrison, J. F. Catalytic Mechanism of the Dihydrofolate Reductase Reaction As Determined by pH Studies. *Biochemistry* **23**, 2753–2758 (1984).
174. Warren, M. S., Brown, K. A., Farnum, M. F., Kraut, J. & Howell, E. E. Investigation of the Functional Role of Tryptophan-22 in Escherichia coli Dihydrofolate Reductase by Site-Directed Mutagenesis. *Biochemistry* **30**, 11092–11103 (1991).
175. Chen, Y., Kraut, J. & Callender, R. pH-Dependent Conformational Changes in Escherichia coli Dihydrofolate Reductase Revealed by Raman Difference Spectroscopy. *Biophys. J.* **72**, 936–941 (1997).
176. Schneider, M. E. & Stern, M. J. Arrhenius Preexponential Factors for Primary Hydrogen Kinetic Isotope Effects. *J. Am. Chem. Soc.* **94**, 1517–1522 (1972).
177. Garcia-Viloca, M., Truhlar, D. G. & Gao, J. Reaction-Path Energetics and Kinetics of the Hydride Transfer Reaction Catalyzed by Dihydrofolate Reductase. *Biochemistry* **42**, 13558–13575 (2003).
178. Antoniou, D., Caratzoulas, S., Kalyanaraman, C., Mincer, J. S. & Schwartz, S. D. Barrier Passage and Protein Dynamics in Enzymatically Catalysed Reactions. *Eur. J. Biochem.* **269**, 3103–3112 (2002).

179. Knapp, M. J. & Klinman, J. P. Environmentally coupled hydrogen tunneling: Linking catalysis to dynamics. *Eur. J. Biochem.* **269**, 3113–3121 (2002).
180. Nagel, Z. D. & Klinman, J. P. A 21st century revisionist's view at a turning point in enzymology. *Nat. Chem. Biol.* **5**, 543–550 (2009).
181. Scrutton, N. S., Basran, J. & Sutcliffe, M. J. New insights into enzyme catalysis. Ground state tunnelling driven by protein dynamics. *Eur. J. Biochem.* **264**, 666–671 (1999).
182. Loveridge, E., Tey, L. & Allemann, R. Solvent effects on catalysis by *E. coli* dihydrofolate reductase. *J. Am. Chem. Soc.* **132**, 1137–1143 (2010).
183. Liang, Z.-X., Lee, T., Resing, K. A., Ahn, N. G. & Klinman, J. P. Thermal-activated protein mobility and its correlation with catalysis in thermophilic alcohol dehydrogenase. *Proc. Natl. Acad. Sci.* **101**, 9556–9561 (2004).
184. Limbach, H. H., Schowen, K. B. & Schowen, R. L. Heavy atom motions and tunneling in hydrogen transfer reactions: The importance of the pre-tunneling state. *J. Phys. Org. Chem.* **23**, 586–605 (2010).
185. Major, D. T. et al. Differential quantum tunneling contributions in nitroalkane oxidase catalyzed and the uncatalyzed proton transfer reaction. *Proc. Natl. Acad. Sci.* **106**, 20734–20739 (2009).

186. Adamczyk, A. J., Cao, J., Kamerlin, S. C. L. & Warshel, A. Catalysis by dihydrofolate reductase and other enzymes arises from electrostatic preorganization, not conformational motions. *Proc. Natl. Acad. Sci.* **108**, 14115–14120 (2011).
187. Kim, H. S., Damo, S. M., Lee, S. Y., Wemmer, D. & Klinman, J. P. Structure and hydride transfer mechanism of a moderate thermophilic dihydrofolate reductase from *Bacillus stearothermophilus* and comparison to its mesophilic and hyperthermophilic homologues. *Biochemistry* **44**, 11428–11439 (2005).
188. Guo, J., Luk, L. Y. P., Loveridge, E. J. & Allemann, R. K. Thermal adaptation of dihydrofolate reductase from the moderate thermophile *Geobacillus stearothermophilus*. *Biochemistry* **53**, 2855–2863 (2014).
189. Liu, C. T. et al. Probing the electrostatics of active site microenvironments along the catalytic cycle for *Escherichia coli* dihydrofolate reductase. *J. Am. Chem. Soc.* **136**, 10349–10360 (2014).
190. Wang, Z., Singh, P., Czekster, C. M., Kohen, A. & Schramm, V. L. Protein Mass-Modulated Effects in the Catalytic Mechanism of Dihydrofolate Reductase: Beyond Promoting Vibrations. (2014). doi:10.1021/ja501936d
191. Dzierlenga, M. W. & Schwartz, S. D. Targeting a Rate-Promoting Vibration with an Allosteric Mediator in Lactate Dehydrogenase. *J. Phys. Chem. Lett.* **7**, 2591–2596 (2016).

192. Pineda, J. R. E. T., Callender, R. & Schwartz, S. D. Ligand binding and protein dynamics in lactate dehydrogenase. *Biophys. J.* **93**, 1474–1483 (2007).
193. Adeva, M., González-Lucán, M., Seco, M. & Donapetry, C. Enzymes involved in l-lactate metabolism in humans. *Mitochondrion* **13**, 615–629 (2013).
194. Mohamed, L. A., Tachikawa, H., Gao, X. D. & Nakanishi, H. Yeast Cell-Based Analysis of Human Lactate Dehydrogenase Isoforms. *J. Biochem.* 467–476 (2015).
195. Cahn, R. D., Zwilling, E., Kaplan, N. O. & Levine, L. Nature and Development of Lactic Dehydrogenases: the Two Major Types of this Enzyme form Molecular Hybrids Which Change in Makeup During Development. *Science.* 962–969 (1962).
196. Stolzenbach, F., Cahn, R. D. & Kapi, N. The Comparative of Lactic dehydrogenase. *J. Biol. Chem.* **239**, (1964).
197. Markert, C. L., Shaklee, J. B. & Whitt, G. S. Evolution of a Gene. *Science.* **189**, 102–114 (1975).
198. Goldberg, E., Eddy, E. M., Duan, C. W. & Odet, F. The Ultimate Testis-Specific Gene. *J. Androl.* **31**, 86–94 (2010).
199. Boussouar, F. & Benahmed, M. Lactate and energy metabolism in male germ

- cells. *Trends Endocrinol. Metab.* **15**, 345–350 (2004).
200. Kedzierski, P., Moreton, K., Clarke, A. R. & Holbrook, J. J. The A245K Mutation Exposes Another Stage of the Bacterial L -Lactate Dehydrogenase Reaction Mechanism †. 7247–7252 (2001). doi:10.1021/bi0026775
201. Waldman, A. D. B. et al. The use of a Genetically Engineered Tryptophan to Identify the Movement of a domain of B.Stearothermophilus Lactate Dehydrogenase with the Process Which Limits the Steady-State Turnover of the Enzyme. *Biochem. Biophys. Res. Commun.* **150**, 752–759 (1988).
202. Holbrook, J. J. et al. Design and synthesis of new enzymes based on the lactate-dehydrogenase framework. *Philos. Trans. R. Soc. B Biol. Sci.* **332**, 177 (1991).
203. Swiderek, K., Tunon, I., Marti, S. & Moliner, V. Protein Conformational Landscapes and Catalysis. Influence of Active Site Conformations in the Reaction Catalysed by L-Lactate Dehydrogenase. *ACS Catal.* **5**, 1172–1185 (2015).
204. Antoniou, D., Basner, J., Núñez, S. & Schwartz, S. D. Computational and theoretical methods to explore the relation between enzyme dynamics and catalysis. *Chem. Rev.* **106**, 3170–3187 (2006).
205. Read, J. A., Winter, V. J., Eszes, C. M., Sessions, R. B. & Brady, R. L.

- Structural basis for altered activity of M- and H-isozyme forms of human lactate dehydrogenase. *Proteins* **43**, 175–185 (2001).
206. Quaytman, S. L. & Schwartz, S. D. Reaction coordinate of an enzymatic reaction revealed by transition path sampling. *Proc. Natl. Acad. Sci.* **104**, 12253–12258 (2007).
207. Beveridge, M. M. Phil thesis. (Cardiff University, 2015).
208. Yeswanth, S. et al. Cloning and characterization of l-lactate dehydrogenase gene of *Staphylococcus aureus*. *Anaerobe* **24**, 43–48 (2013).
209. Stockland, A. E. & San Clemente, C. L. Multiple Forms of Lactate Dehydrogenase In *Staphylococcus aureus*. *J. Bacteriol.* **100**, 347–353 (1969).
210. Richardson, A. R., Libby, S. J. & Fanf, F. C. A Nitric Oxide – Inducible Lactate Dehydrogenase enables *Staphylococcus aureus* to resist innate immunity. **319**, 1672–1676 (2008).
211. Schramm, V. L., Almo, S. C., Gutierrez, J. A. & Ho, M. Crystal Structure of Lactate Dehydrogenase from *Staphylococcus Aureus* complexed with NAD and Pyruvate. Protein Data Bank (2009).
212. Madern, D. Molecular Evolution Within the L-Malate and L-lactate Dehydrogenase Super-Family. *J. Mol. Evol.* **54**, 825–840 (2002).

213. Loveridge, E. J., Evans, R. M. & Allemann, R. K. Solvent effects on environmentally coupled hydrogen tunnelling during catalysis by dihydrofolate reductase from *Thermotoga maritima*. *Chem. A Eur. J.* **14**, 10782–10788 (2008).
214. Dawson, W. M., Prof, S. & Allemann, R. K. analysis of the transition state of a thesis submitted to Cardiff University for the degree of Doctor of Philosophy by. (2014).
215. Ventola, C. L. The antibiotic resistance crisis: part 1: causes and threats *J. Formul. Manag.* **40**, 277–83 (2015).
216. Sengupta, S., Chattopadhyay, M. K. & Grossart, H. P. The multifaceted roles of antibiotics and antibiotic resistance in nature. *Front. Microbiol.* **4**, 1–13 (2013).
217. Archer, N. K. et al. Properties , regulation and roles in human disease *Staphylococcus aureus* biofilms. 445–459 (2011).
218. De la Fuente-Núñez, C., Reffuveille, F., Fernández, L. & Hancock, R. E. W. Bacterial biofilm development as a multicellular adaptation: Antibiotic resistance and new therapeutic strategies. *Curr. Opin. Microbiol.* **16**, 580–589 (2013).

219. Shoemark, D. K., Cliff, M. J., Sessions, R. B. & Clarke, A. R. Enzymatic properties of the lactate dehydrogenase enzyme from *Plasmodium falciparum*. *FEBS J.* **274**, 2738–2748 (2007).
220. Steindel, P. A., Chen, E. H., Wirth, J. D. & Theobald, D. L. Gradual neofunctionalization in the convergent evolution of trichomonad lactate and malate dehydrogenases. *Protein Sci.* **25**, 1319–1331 (2016).
221. Davarifar, A., Antoniou, D. & Schwartz, S. D. The Promoting Vibration in Human Heart Lactate Dehydrogenase Is a Preferred Vibrational Channel. *J. Phys. Chem. B* **115**, 15439–15444 (2011).
222. Cameron, A. et al. Identification and activity of a series of azole-based compounds with lactate dehydrogenase-directed anti-malarial activity. *J. Biol. Chem.* **279**, 31429–31439 (2004).